

ICEBE
IMAGING
NATURE

Dissertation

A systematic approach to identify new thermochemical energy storage systems

carried out for the purpose of obtaining the academic degree

Doctor technicae (Dr. techn.)

submitted at TU Wien

Faculty of Mechanical and Industrial Engineering

by

Markus Deutsch

Matr.Nr.: 0725927

under the supervision of

Ao. Univ.Prof. Dr. Franz Winter

Institute of Chemical, Environmental and Biological Engineering

E166

Affidavit

I, Markus Deutsch, hereby declare

1. that I am the sole author of the present thesis, 'A systematic approach to identify new thermochemical energy storage systems', 185 pages, bound and that I have not used any source or tool other than those referenced or any other illicit aid or tool.
2. that I have not prior to this date submitted this thesis as an examination paper in any form in Austria or abroad.

Wien, 8. May 2017

Markus Deutsch

Acknowledgement

Ich möchte mich an dieser Stelle bei allen Menschen bedanken, die mir es ermöglicht haben, bis an diesen Punkt zu kommen.

Besonders möchte ich mich bei Franz Winter bedanken, der mir die Möglichkeit gegeben hat, an diesem Thema arbeiten zu können und mir alle Freiheiten gelassen hat, die Dissertation so anzugehen wie ich es wollte.

Des Weiteren möchte ich mir bei Andreas Werner und Peter Weinberger bedanken, für ihre offenen Türen bei Fragen jeglicher Art.

Mein Dank gilt auch Christian Jordan, Christian Gierl und Daniel Lager für ihre Unterstützung und ihr eingebrachte Know-How bei den unzähligen messtechnischen Problemstellungen, die im Laufe dieser Arbeit aufgekommen sind.

An dieser Stelle möchte ich auch Christian Knoll und Felix Birkelbach nennen, die mich beide vor allem in der Endphase der Dissertation, durch das unermüdliche Abarbeiten unzähliger Messreihen sowie diverse höchst wissenschaftliche Diskussionen, unterstützt haben.

Einen wesentlichen Beitrag zum Abschluss dieser Dissertation hat Matthias Kuba geleistet. Nicht nur für seinen Einsatz als unermüdlicher Korrekturleser sondern auch als wissenschaftliche Gummiwand, an die ich regelmäßig die verrücktesten Ideen werfen konnte und diese dann in einer regen Diskussion aufgegriffen und verarbeitet wurden.

An dieser Stelle möchte ich auch der Urtruppe der WTF, sowie auch allen anderen Kollegen und Exkollegen, danken, die die Zeit der Dissertation für mich unvergesslich gemacht haben. Wie immer zum Schluss, gilt der größte Dank natürlich meiner Familie und meinen Freunden, die mich durch ihren Rückhalt in schwierigen Zeiten und ihre motivierenden Worte zum Abschluss der Dissertation getragen haben. Jeder noch so kleine Motivationsschub hat mich näher dem Ziel gebracht.

Und da dies das Letzte ist was ich an meiner Dissertation ändere, kann ich nun endlich die so häufig gestellt Frage meine Vaters, wann sei denn die Dissertation endlich fertig, nun eindeutig beantworten.

Jetzt.

Markus Deutsch

Abstract

Thermochemical energy storage (TCES) is considered an emerging green technology for increased energy utilization efficiency, thereby achieving a reduction of greenhouse gases. Several reaction systems based on different substance classes (e.g. hydrates, hydroxides, oxides) were suggested and investigated so far. Nevertheless, the number of known reactions which are suitable for TCES is still limited, as the main focus lies on the investigation of a handful known substances, their further improvement or applicability.

To find novel promising candidates for TCES and also to allow for a broader view on the topic, this work presents a systematic approach to find new TCES systems. A mathematical search algorithm identifies potential reactions based on thermodynamic databases for different reactive gases. The search results are classified by their applicable temperature range and ranked by storage density.

To further assess the potential of the found systems, a novel method for the identification of temperature and pressure dependent reaction kinetics is proposed. It is an extension of the non-parametric kinetic analysis (NPK) method as it identifies the pressure dependency in addition to the temperature and conversion dependency of the reaction. This is done by analyzing kinetic data in a three-dimensional data space (conversion, temperature, pressure) and attributing the variation of the conversion rate to these independent variables. Thus, a reduction from a three-dimensional problem to three one-dimensional problems is achieved. The derivation of a kinetic model can then be performed for each dependency independently, which is easier than deriving a model directly from the data. This work presents the basic approach of the identification and combination of the three dependencies to build a full kinetic model. Also, the interpretation of the model to achieve a physically motivated model is illustrated. Then the method is applied to identify the complex reaction kinetics of the decomposition of CdCO_3 based on a set of thermogravimetric measurements. It is shown that it is possible to identify interaction terms between the dependency terms.

One promising application of TCES is its combination with concentrated solar power. Based on the search, the reaction system $\text{CuO}/\text{Cu}_2\text{O}$ has been identified as a potential candidate for such a combination. This work studies the reduction of CuO and the oxidation of Cu_2O under isothermal and isokinetic conditions. The reactions are analyzed using a simultaneous

thermal analysis (STA) and a lab scale fixed bed reactor. To develop kinetic models the NPK approach is utilized. This model free approach is expanded by the Arrhenius correlation to increase the applicable temperature range of the models. The resulting models are evaluated and compared.

Furthermore, the cycle stability of the system over 20 cycles is assessed for a small sample mass in the STA and a large sample mass in the fixed bed reactor.

Publication

Journal Publications

Markus Deutsch, Danny Müller, Christian Aumeyr, Christian Jordan, Christian Gierl-Mayer, Peter Weinberger, Franz Winter, Andreas Werner

Systematic search algorithm for potential thermochemical energy storage systems

Applied Energy, 183:113-120,2016

DOI: 10.1016/j.apenergy.2016.08.142

Markus Deutsch, Florian Horvath, Christian Knoll, Daniel Lager, Christian Gierl-Mayer, Peter Weinberger, Franz Winter

High-Temperature Energy Storage: Kinetic Investigations of the CuO/Cu₂O Reaction Cycle

Energy and Fuels, 1 (3), pp 2324-2334, 2017

DOI: 10.1021/acs.energyfuels.6b02343

Markus Deutsch, Felix Birkelbach, Christian Knoll, Michael Harasek, Andreas Werner, Franz Winter

An extension of the NPK method to include the pressure dependency of solid state reactions

submitted to *Thermochimica Acta*

Conference Publications

Markus Deutsch, Christian Aumeyr, Thomas Fellner, Johannes Widhalm, Andreas Werner, Franz Winter

Thermochemische Energiespeicherung von Niedrigtemperatur mittels Gas/Feststoff- Reaktionen

Jahrestreffen der Fachgruppe Energieverfahrenstechnik, 23. - 24. February 2015, Bonn, Germany

Markus Deutsch, Thomas Fellner, Johannes Widhalm, Christian Aumeyr, Christian Jordan, Andreas Werner, Peter Weinberger, Christian Gierl-Mayer, Franz Winter

MgO/Mg(OH)₂ as a possible thermochemical energy storage material

9th International Conference for Young Researchers and PhD students ERIN - Education, Research, Innovation 2015, 4-6 May 2015 Moninec, Czech Republic

Markus Deutsch, Christian Aumeyr, Peter Weinberger Franz Winter

Kinetic Analysis of the decomposition of H₃BO₃ and FeSO₄ · 7 H₂O for thermochemical energy storage

1st Chemistry in Energy Conference, 20 - 22 July 2015, Edinburgh, United Kingdom

Markus Deutsch, Florian Horvath, Christian Gierl-Mayer, Andreas Werner, Franz Winter

Kinetic investigations of the reaction cycle CuO/Cu₂O for thermochemical energy storage

Jahrestreffen der ProcessNet-Fachgruppe Energieverfahrenstechnik, 21-.23 März 2017, Frankfurt am Main, Germany

Christian Jordan, Markus Deutsch, Christian Aumeyr, Peter Weinberger, Thomas Fellner, Andreas Werner

Systematische Materialforschung für thermochemische Energiespeicher - "Solid-Heat Basic"

ProcessNet Jahrestagung 2014, 30. September - 2. Oktober 2014, Aachen, Germany

Johannes Widhalm, Thomas Fellner, Markus Deutsch, Andreas Werner, Franz Winter

Thermochemical energy storage as a way to increase the sustainability of energy generation

5th Asian Conference on Sustainability, Energy and the Environment, June 11 - 14, 2015 Kobe, Japan

Poster Publications

Markus Deutsch, Christian Aumeyr, Thomas Fellner, Johannes Widhalm, Peter Weinberger, Andreas Werner, Franz Winter

Systematic identification of low-temperature-energy storage materials

Vienna young Scientists Symposium, 25. - 26. Juni 2015, Vienna, Austria

Christian Aumeyr, Markus Deutsch, Thomas Fellner, Peter Weinberger, Andreas Werner

Systematic approach to identify thermochemical storage materials

30. Workshop on Novel Materials and Superconductivity, 08. - 14. February 2015, Obertraun, Austria

Markus Deutsch, Florian Horvath, Franz Winter

High temperature energy storage: Experimental investigations of the CuO/Cu₂O cycle

Adria - Danube Combustion Meeting, 07. - 08. April 2016, Wr. Neustadt, Austria

Patent

Markus Deutsch, Thomas Karel, Christian Jordan, Franz Winter, Andeas Werner

Verfahren zur thermochemischen Energiespeicherung

TU Wien, A142/2016, 16.03.2016

Contents

1	Introduction	1
1.1	Energy demand	2
1.1.1	Development of energy demand of the human race	2
1.1.2	Energy sources	3
1.2	Thermal energy storage	5
1.2.1	Potential of thermal energy storage	5
1.2.2	Thermal energy storage systems	8
1.3	Thermochemical energy storage	12
1.3.1	Principle of TCES	12
1.3.2	Comparison of TCES to other thermal energy storage systems	13
1.3.3	Requirement for TCES system	14
1.3.4	State of the art	15
1.4	Aim of this work	16
2	Fundamentals	21
2.1	Thermodynamic fundamentals	21
2.1.1	Gibbs energy G	21
2.1.2	Chemical equilibrium	24
2.2	Kinetic fundamentals	26
2.2.1	Differential rate laws	27
2.2.2	Integral rate laws	28
2.2.3	Conversion models	30
2.2.4	Pressure dependency models	41
2.3	Kinetic identification	42
2.3.1	Model-fitting methods	43
2.3.2	Model-free methods	44
3	Search for TCES systems	47
3.1	Goal of the search	47

3.2	Basis of the search	48
3.2.1	Materials	48
3.2.2	Reactive gases	48
3.3	Search algorithm	48
3.4	Search results	51
3.4.1	Reactions with H ₂ O	54
3.4.2	Reactions with CO ₂	54
3.4.3	Reactions with NH ₃	54
3.4.4	Reactions with SO ₂	54
3.4.5	Reactions with O ₂	54
4	The extended NPK method	59
4.1	Introduction	59
4.2	Method description and proof of concept	60
4.2.1	Identification of $k'(T)$ and $f(\alpha)$	61
4.2.2	Identification of $h'(p)$	65
4.2.3	Combining the dependency vectors	67
4.2.4	Interpretation of the dependency vectors	71
4.3	Decomposition of CdCO ₃	73
4.3.1	Measurements	73
4.3.2	Model identification	76
4.3.3	Investigation of the interaction effect	80
4.3.4	Validation of the identified models	81
5	The system CuO/ Cu₂O	87
5.1	CuO/ Cu ₂ O for TCES	87
5.2	Experimental setup	88
5.2.1	Material	88
5.2.2	Simultaneous thermal analysis - STA	88
5.2.3	Fixed bed reactor	93
5.2.4	X-Ray powder diffraction	94
5.2.5	BET-analyzer	95
5.3	Kinetic identification	95
5.3.1	STA measurements	95
5.3.2	Reactor measurements	95
5.3.3	Reduction	97
5.3.4	Oxidation	101
5.3.5	Cycle test	106

5.4 Discussion	106
6 Conclusion	109
Nomenclature	111
Bibliography	117
Appendix	129
A1 Asymptotic series expansion	129
A2 Schlömich series expansion	129
A3 Reaction systems found by the algorithm	129
A4 Curriculum Vitae	161

List of Figures

1.1	History of the CO ₂ concentration in the atmosphere	2
1.2	Estimated daily energy consumption per person over the evolution of the human race	3
1.3	Development of the world primary energy consumption from 1800 to 2050 . .	4
1.4	Evolution of the used primary energy sources	5
1.5	Change of the used primary energy sources in the last 40 years	6
1.6	Heat demand of the industrial sector in the EU-27 per temperature level and industrial branch	7
1.7	Net load curve of the California, US power grid for the January 11	9
1.8	Comparison of the temperature course during the energy uptake between latent and sensible heat storage	11
1.9	Schematic principle of a TCES system	13
1.10	Comparison of selected TES systems	14
2.1	Isothermal plots of $d\alpha/dt$ vs α for acceleratory conversion models	32
2.2	Isothermal plots of $d\alpha/dt$ vs α for deceleratory conversion models	34
2.3	Isothermal plots of $d\alpha/dt$ vs α for constant conversion models	35
2.4	Isothermal plots of $d\alpha/dt$ vs α for sigmoidal conversion models	35
2.5	Two different types of nuclei growth restrictions	37
2.6	Typical geometrical model assumptions about particle shapes	38
2.7	Schematic representation of the product layer buildup in diffusion models . .	42
3.1	Graphical representation of the search algorithm	50
3.2	Detailed graphical representation of loop III for the determination of ν_B . . .	52
3.3	Hit distribution maps for the different reactive gases	55
3.4	Approximated areas within the majority of reactions have been found for each reactive gas.	56
3.5	Clustering of H ₂ O-hydroxide reactions into 2 clusters	56
4.1	Reaction rate surface for the example reaction at constant pressure $p = 0.3$ bar	61

4.2	Exemplary evolution of the placement of submatrices for mixed measurements.	64
4.3	Reaction rate surface for the example at constant temperature $T = 310\text{ K}$	66
4.4	Comparison of the conversion dependency vector \mathbf{u} and $\hat{\mathbf{u}}$ identified during the identification of \mathbf{v} and \mathbf{w} , respectively	68
4.5	Visualization of two slices of the tensor \mathbf{A} at T_1 and p_1 , respectively	69
4.6	Normalized dependency vectors \mathbf{u} (left), \mathbf{v} (middle) and \mathbf{w} (right) for the example reaction	70
4.7	Identified conversion dependency vector \mathbf{u} for the example reaction with fitted conversion models	71
4.8	Identified pressure dependency vector \mathbf{w} for the example with fitted pressure models	72
4.9	Arrhenius plot of the temperature dependency of the example reaction.	74
4.10	Simulation result for isokinetic measurements of the example reaction with different heating rates β at $p = 0.3\text{ bar}$	74
4.11	Simulation result for isothermal measurements of the example reaction at different pressures at $T = 310\text{ K}$	75
4.12	Representative measurement curves in the STA for kinetic analysis. left: isokinetic measurement with $\beta = 10\text{ K/min}$ and $p_{\text{CO}_2} = 100\text{ mbar}$	76
4.13	Normalized dependency vectors \mathbf{u} (left), \mathbf{v} (middle) and \mathbf{w} (right) for the decomposition of CdCO_3	77
4.14	Conversion dependency vector \mathbf{u} of the decomposition of CdCO_3 with fitted conversion models	78
4.15	Pressure dependency vector \mathbf{w} of the decomposition of CdCO_3 with fitted conversion models	79
4.16	Temperature dependency vector \mathbf{v} for the decomposition of CdCO_3 at $p_{\text{CO}_2} = 100\text{ mbar}$	79
4.17	Arrhenius plot of the identified temperature dependency \mathbf{v} from isokinetic measurements of the CdCO_3 decomposition at $p_{\text{CO}_2} = 100\text{ mbar}$	80
4.18	Arrhenius plot of the identified temperature dependency from isokinetic measurements of the CdCO_3 decomposition at $p_{\text{CO}_2} \leq 10^{-5}\text{ bar}$	81
4.19	Identified conversion dependencies at different temperature levels and $p_{\text{CO}_2} = 100\text{ mbar}$	82
4.20	Effect of the temperature on the pressure dependency vector \mathbf{w}	82
4.21	Temperature dependency of the model parameter χ	83
4.22	Simulation result for isothermal measurements of the CdCO_3 decomposition at different temperatures with $p_{\text{CO}_2} = 100\text{ mbar}$	84

4.23	Simulation result for isobaric measurements of the CdCO_3 decomposition at different p_{CO_2} with $T = 633 \text{ K}$	84
4.24	Simulation result for measurements of the CdCO_3 decomposition outside the identified region	85
5.1	Mass based particle size distribution of the CuO granulate	90
5.2	Stability diagram for system $\text{CuO}/\text{Cu}_2\text{O}$	91
5.3	Representative measurement procedure in the STA for isokinetic analysis . .	92
5.4	Representative measurement procedure in the STA for isothermal analysis .	92
5.5	Schematic setup of the reactor used for kinetic measurements under fixed bed conditions	94
5.6	Isokinetic STA measurements at different heating/cooling rates	96
5.7	Isothermal STA measurements at different temperatures	96
5.8	Measurements in the fixed bed reactor at different starting temperatures . .	97
5.9	Temperature change in the reaction zone due to the released energy during oxidation at 950°C starting temperature	98
5.10	Conversion dependency vector \mathbf{u} derived from isokinetic measurements of the reduction of CuO in N_2	98
5.11	Temperature dependency vector \mathbf{v} derived from isokinetic measurements of the reduction of CuO in N_2	99
5.12	Arrhenius plot of \mathbf{v} derived from isokinetic measurements of the reduction of CuO in N_2	99
5.13	Simulation of the isokinetic measurements of the reduction of CuO with the identified model	100
5.14	Simulation of the isothermal measurements of the reduction of CuO with the model identified from isokinetic measurements	101
5.15	Arrhenius plot of \mathbf{v} derived from isothermal measurements of the reduction of CuO in the reactor	102
5.16	Conversion dependency vector \mathbf{u} derived from isothermal measurements of the reduction of CuO in the reactor	102
5.17	Simulation of the isothermal measurements of the reduction of CuO in the testrig	103
5.18	Arrhenius plot of \mathbf{v} derived from isothermal STA measurements of the oxidation of Cu_2O	103
5.19	Conversion dependency vector \mathbf{u} derived from isothermal STA measurements of the oxidation of Cu_2O	104
5.20	Simulation of the isothermal STA measurements of the oxidation of Cu_2O . .	104

5.21	Arrhenius plot of \mathbf{v} derived from isothermal measurements of the oxidation of Cu_2O in the reactor	105
5.22	Conversion dependency vector \mathbf{u} derived from isothermal measurements of the oxidation of Cu_2O in the reactor	105
5.23	Simulation of the isothermal measurements of the oxidation of Cu_2O in the reactor	106
5.24	CuO reaction behavior over 20 cycles in the STA at 950°C and changing N_2 /synthetic air atmosphere	107
5.25	Sintering of the granulate material in the fixed bed reactor	108

List of Tables

1.1	Comparison of different sensible storage materials	10
1.2	Comparison of different phase change materials (PCM)	12
1.3	Characteristics and comparison of the thermal energy storage systems	18
1.4	Different requirements for TCES systems	19
2.1	Different models for the temperature dependency $k(T)$ of a reaction	30
2.2	Different nucleation models for the conversion dependency $f(\alpha)$	31
2.3	Different interface models for the conversion dependency $f(\alpha)$	32
2.4	Different reaction order models for the conversion dependency $f(\alpha)$	32
2.5	Different diffusion controlled models for the conversion dependency $f(\alpha)$	33
2.6	Different models for the pressure dependency $h(p)$	42
3.1	Possible elemental compositions EC^* for reaction 3.6 found in loop III	51
3.2	Number of reactions identified with T_{equ} in the respective temperature level for each reactive gas	53
4.1	Statistical results of the five best fitting conversion models for the example reaction	72
4.2	Statistical results of the pressure dependency models for the example reaction	72
4.3	Statistical results of the five best fitting conversion models for the decomposition of $CdCO_3$	77
4.4	Statistical results of the pressure dependency fitting of the decomposition of $CdCO_3$	78
5.1	Comparison of possible O_2 based TCES systems for the application in CSP	89
5.2	Estimated raw material cost of the most promising TCES systems for CSP	90
6.1	Reactions with H_2O as reactive gas	129
6.2	Reactions with CO_2 as reactive gas	146
6.3	Reactions with NH_3 as reactive gas	147
6.4	Reactions with SO_2 as reactive gas	148

6.5	Reactions with O_2 as reactive gas	149
-----	--	-----

Chapter 1

Introduction

Energy crisis and climate change are typical subjects in today's news. Self-proclaimed experts discuss cause and effect and debate if climate change was real and/or man-made. From a scientific point of view, climate change is certain. The annual report on the state of climate of the National Centers for Environmental Information states that 2016 has been the warmest year since 1880 [1]. This makes the last three years the three hottest years on record. Looking at the warmest years on record, 16 of the top 17 have been recorded in this century. This means, every year since 2000, was warmer than all years before 2000, with the exception of 1998, which is the eighth warmest year on record [2].

The most discussed cause for climate change is the increasing concentration of CO₂ in the atmosphere. This increase can be seen in the so called Keeling curve in Figure 1.1. it shows the history of the CO₂ concentration in the atmosphere since 1958. The measurements have been conducted at Mauna Loa, Hawaii, in sufficient distance from industrial sites, so that no direct emissions could influence the measured values. The annual fluctuation in CO₂ is caused by seasonal variations in CO₂ uptake by land-based vegetation. The Keeling curve shows a distinct increase of CO₂ in the last 60 years.

With CO₂ being a greenhouse gas, a cause for climate change seemed to be found. This increase in CO₂ is mere a symptom of an underlying problem. The increase is mainly caused by to anthropogenic emissions from burning fossil fuels. They are needed to fulfill our need for energy. According to Wrangham [4] it appears that modern humans are the only species that have a need for external energy. It is believed that humans gained the ability to control fire long enough ago, that it is now necessary for our food to be cooked and the lack of fur makes us dependent on the heat provided by fire and other external heat sources. Throughout the course of history, humans have discovered many ways to convert energy from forms that are less desirable to those that are more desired; for example from grass and grain to meat, from wood to heat, and from fossil fuels to transportation and electricity [5].

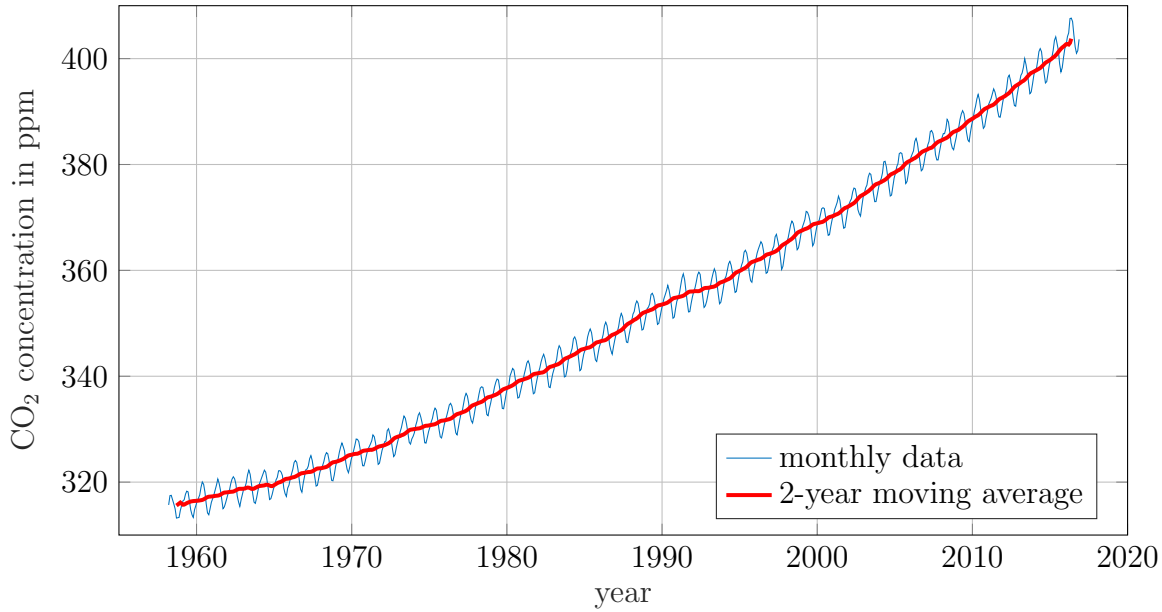


Figure 1.1: History of the CO₂ concentration in the atmosphere measured at Mauna Loa, Hawaii since 1958 [3]

1.1 Energy demand

1.1.1 Development of energy demand of the human race

The energy demand of the human race is constantly rising. Cook [6] analyzed the energy consumption from the early beginnings of mankind (Figure 1.2). The Primitive Man, who had yet to discover fire, only depended on the food he could eat, his energy consumption was approximately 8.4 MJ per day. After the discovery of fire, the energy consumption doubled to a value of 16.8 MJ/day. With the development of an agrarian society with some domestic animals, the energy consumption per capita rose to about 50.2 MJ/day. The Advanced Agricultural Man presumably doubled this value by harnessing animals for transportation and inventing devices to tap the power of wind and water. With the invention of the steam machine at the beginning of the industrial revolution, humans were no longer limited to natural energy flows. They were able to commercially use the concentrated storage deposits of solar energy such as coal, gas, and oil. At the height of the industrial revolution in the second half of the 19th century, the daily consumption of energy rose to an estimated value of 293 MJ/day. With the industrialization, the rate of consumption rose dramatically over a period of a few generations. In 1970, the average Technological Man in the U.S. consumed approximately 900 MJ/day [6]. According to the International Energy Agency (IEA) [7] the primary energy consumption per capita in 2016 in an OECD country was 477.1 MJ/day. The reduction is mainly a result of the increased population.

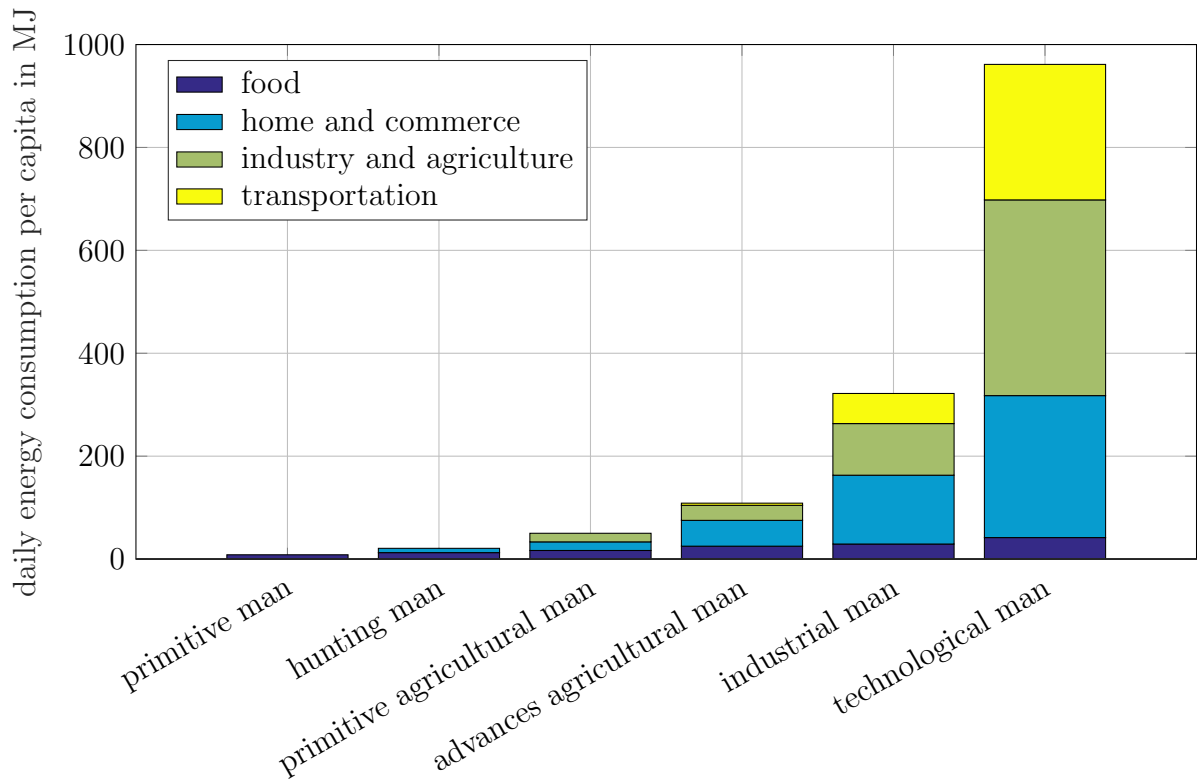


Figure 1.2: Estimated daily energy consumption per person over the evolution of the human race, adapted from [6]

1.1.2 Energy sources

The energy consumed in our daily lives comes from various primary energy sources. Those can be categorized in two groups, renewable and non-renewable energy sources. Renewable energy sources are sources that replenish on a human timescale, while non-renewable energy sources take take considerably longer (e.g. coal) or do not replenish at all (e.g. uranium) [8]. Typical types of renewable energy are solar, wind, hydro, biomass and geothermal energy [9].

Since the beginning of the industrial revolution, the mix of used primary energy sources changed constantly. As it can be seen in Figure 1.3, at the beginning of the 19th century, the energy demand was completely covered by renewable energy sources, mainly biomass and a small amount by water and wind power (mills). As a result of the industrialization, the importance of coal as energy source increased. Around 1920 only half of the globally used primary energy sources were renewable (see Figure 1.4). With the discovery of big oil reserves in the U.S. at the beginning of the 20th century, crude oil and natural gas shifted into the focus to today's energy production, which now heavily relies on oil and gas. In 2005 less than 15 % of the consumed energy was produced from renewable energy sources. Figure 1.3 also shows a projection of the primary energy demand from the year 2010 based on the

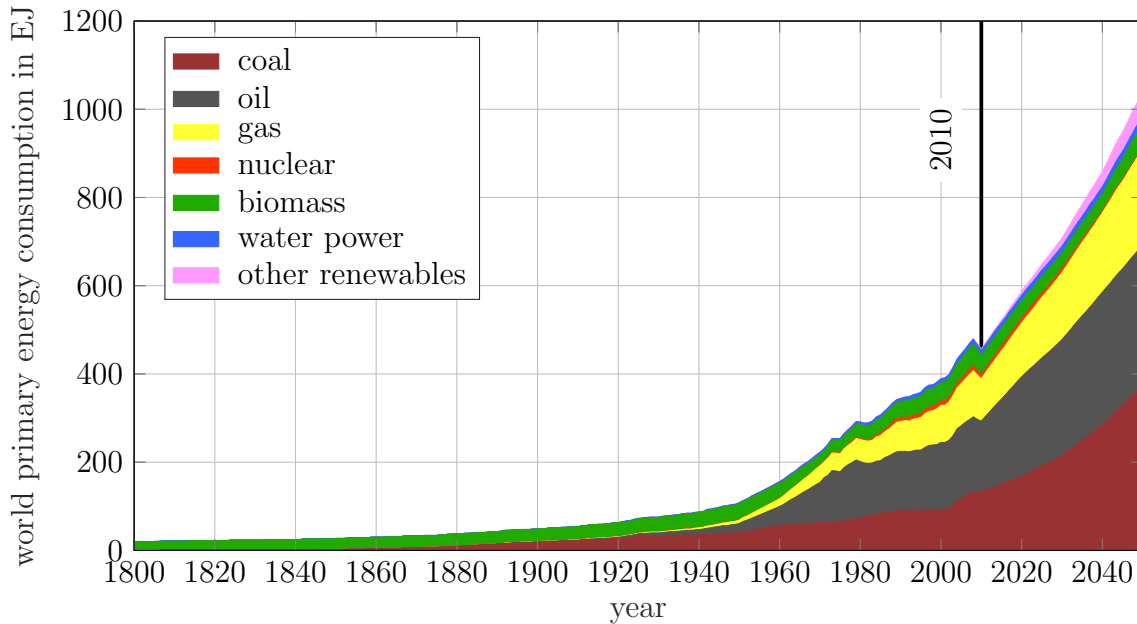


Figure 1.3: Development of the world primary energy consumption from 1800 to 2050. The period 2010 to 2050 follows the business-as-usual scenario developed by GEA [10].

GEA¹ baseline scenario. In this scenario business-as-usual is assumed and no additional actions to reduce the dependency on fossil fuels are set. If not prevented, such a scenario would result in failing the 2°C target with a probability of 99%. To reduce the emission produced in this scenario, the energy mix has to be changed. Such a high dependency on fossil fuels are not feasible in terms of climate protection. It is also comprehensible that such an increase in the energy consumption cannot be covered by renewable energy sources alone. Thus, in addition to changing the energy mix, it is also necessary to limit and reduce the primary energy demand [10].

The WBGU² issued a scenario for a global renewable energy supply until 2050 [10]. It is a vision based on a heavy expansion of the renewable capabilities. The WBGU scenario shows that to fulfill the energy demand with only renewable energy sources, it is essential to reduce the global energy consumption. The scenario assumes that this can be achieved by several measures. First, the growth of the primary energy demand of the transport sector and the electricity sector must be limited to 1% per year. Second, the global heating and cooling demand has to be reduced by 1% per year. The goal for the transport sector is assumed to be achieved by fully introducing electro-mobility. To limit primary energy demand of the electricity sector, efficiency increasing measures for the electricity generation are assumed. It is notable, that this does not mean less electricity is consumed globally, rather that the efficiency of the conversion from primary energy sources to electricity increased. Today, about

¹Global Energy Assessment, <http://www.globalenergyassessment.org/>

²Wissenschaftlicher Beirat der Bundesregierung Globale Umweltveränderungen, Germany, <http://www.wbgu.de>

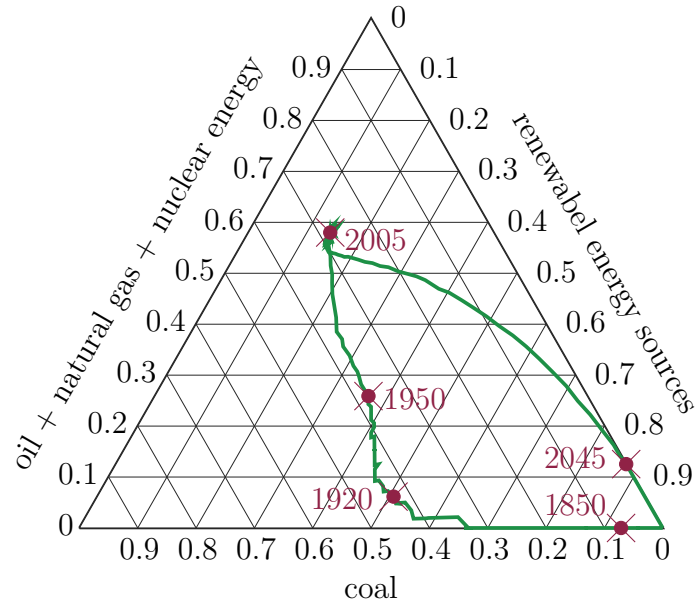


Figure 1.4: Evolution of the used primary energy sources. For the time from 1800 to 2010 the data from Figure 1.3 was used, from 2010 the WGBU scenario was used (Figure 1.5)

66% of the total primary energy input is lost during the conversion from heat to electricity in form of waste heat [11]. This value can be reduced by preventing the generation of waste heat, through direct electricity production (e.g. water or wind electricity) or repurpose the arising waste heat to a greater extent than it is done today. Repurposing would also help to reduce the global heating and cooling demand as the scenario demands. An increased utilization of waste heat is hindered by the fact that supply and demand cannot be matched temporally or the distances between producer and customer are too large [12]. To solve this discrepancy new technologies of thermal energy storages are needed.

1.2 Thermal energy storage

As outlined above, thermal energy storage (TES) plays a crucial part in protecting our climate. It does so by reducing CO₂ emission through energy savings in buildings and industrial sectors and reducing waste thermal energy on a national and continental scale [13].

1.2.1 Potential of thermal energy storage

To understand the potential of TES, the different sources of storable heat and potential consumers need to be discussed.

The IEA distinguishes three temperature levels for heat: low (< 100 °C), medium (100-400 °C) and high (> 400 °C) [14].

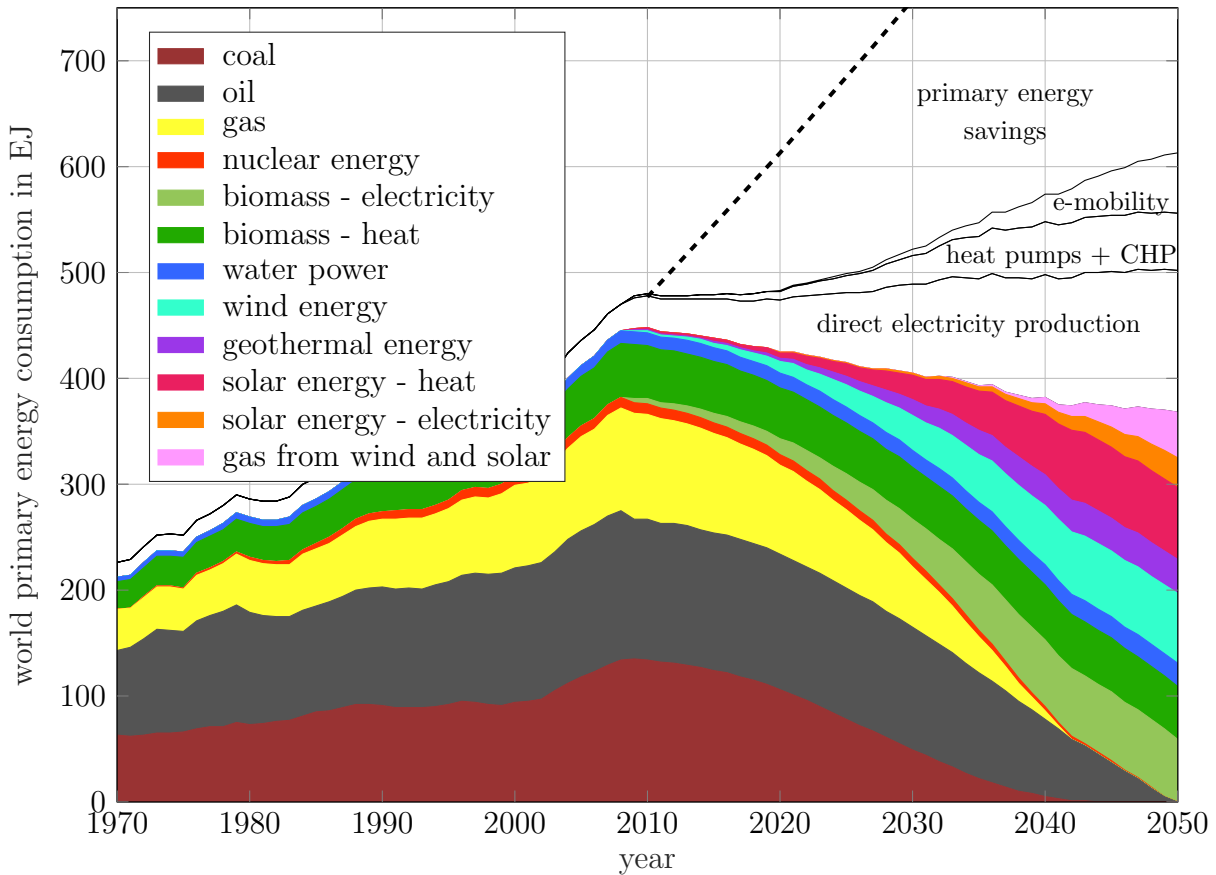


Figure 1.5: Change of the used primary energy sources in the last 40 years and the WBGU scenario for a global renewable energy supply until 2050. The dashed line shows the development of the global primary energy demand based on the GEA baseline scenario (see Figure 1.3)) [10]

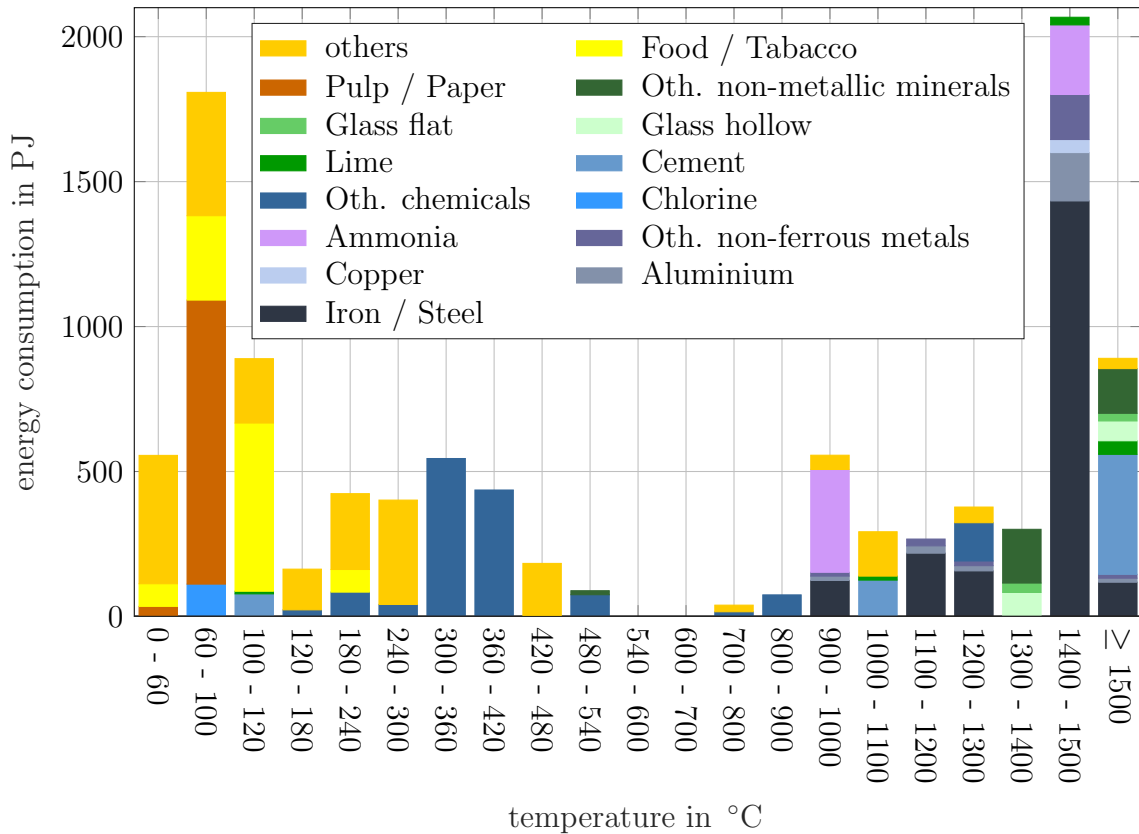


Figure 1.6: Heat demand of the industrial sector in the EU-27 per temperature level and industrial branch [20].

The low temperature level represents the typical household and building application. In Germany, more than two thirds of the energy demand of buildings are used for heating and warm water [15]. There, TES can be used to store solar energy during times of high energy availability and low demand (summer) to times of low energy and high demand (winter) [16]. The medium temperature level comprises mainly waste heat sources from industrial applications, which are a major cause of energy inefficiency [17]. Waste heat occurs when heat is used within production processes either in form of process steam or in fired furnaces [18]. In electricity production about 66 % of the total primary energy input are lost during the conversion from heat to electricity [11]. A higher conversion rate to electricity is hampered by the comparably low efficiency of the available processes (e.g. the energy efficiency of the organic rankine cycle (ORC) process at the cement plant in Lengfurt, Germany, is at only 12,8 % [19]).

The potential use for thermal energy at low and middle temperature levels is manifold. Figure 1.6 shows the heat demand of the industrial sector in the EU-27 depending on the temperature level. Heat at low temperature level is used in the pulp and paper and also in the food industry (e.g. pasteurization processes and beer industry [15]). Heat at the middle energy level is highly needed in the tobacco industry.

TES can be used to improve the energy efficiency of processes, by bridging the temporal and/or spatial gap between the producer of waste heat and potential consumer (e.g. from the heat production site to a local heating district or in a batch process, from the cool down of one cycle to the heat up of the next) [21].

In the high temperature level TES can be used for specialized applications. In cars 60% of the fuel energy are lost as heat, mostly through the exhaust at a temperature up to 800 °C [22]. TES can be used to recuperate parts of this energy and use it for minimizing the warm-up period of the exhaust track at the next cold start [23]. TES plays a vital role in the market success of solar thermal power plants as they are prone to strong fluctuations in their power output. Additionally, the highest energy output is generated at noon, while the demand is highest in the evening. This discrepancy can be seen in the net load of power grids. Conventional power plants work at a lower output during times of high solar power and have to drive steep ramps to cover the energy demand in the evening when solar power stops. Figure 1.7 shows development of the net load of the California, U.S., power grid on January 11 for the years 2014 - 2020. Due to its shape, the curve is called duck curve [24]. Predictions for the years until 2020 show that the growing penetration of renewable energy, especially solar energy, results in a worsening of this discrepancy. TES can be combined with concentrating solar power (CSP) plants to increase their production into times with low sunlight (e.g. when the sun is blocked by clouds or after sunset) [25, 26]. As a result, fluctuations in the energy production through solar power are reduced and the energy production is shifted to times of high energy demand. Thus, the load gradients on the power grid is reduced.

For this application materials for temperatures of 800 °C or higher are needed.

1.2.2 Thermal energy storage systems

TES system store energy in form of heat. A typical storage cycle consists out of three steps:

charging step During this step the energy is stored into the storage medium. To transport the heat from the waste heat source to the TES system a heat transfer medium is used. In special cases the storage medium is also used as the heat transfer medium. The charging temperature is one key parameter to choose the proper TES system.

storing step During this step, the energy is kept within the TES system. Depending on the TES system, it can be possible to transport the storage medium and, therefore, the heat between heat source and heat sink. The possible storage duration depends on the heat losses of the system, which limits possible application for each TES system.

discharging step During this step, the energy is released from the storage for further use.

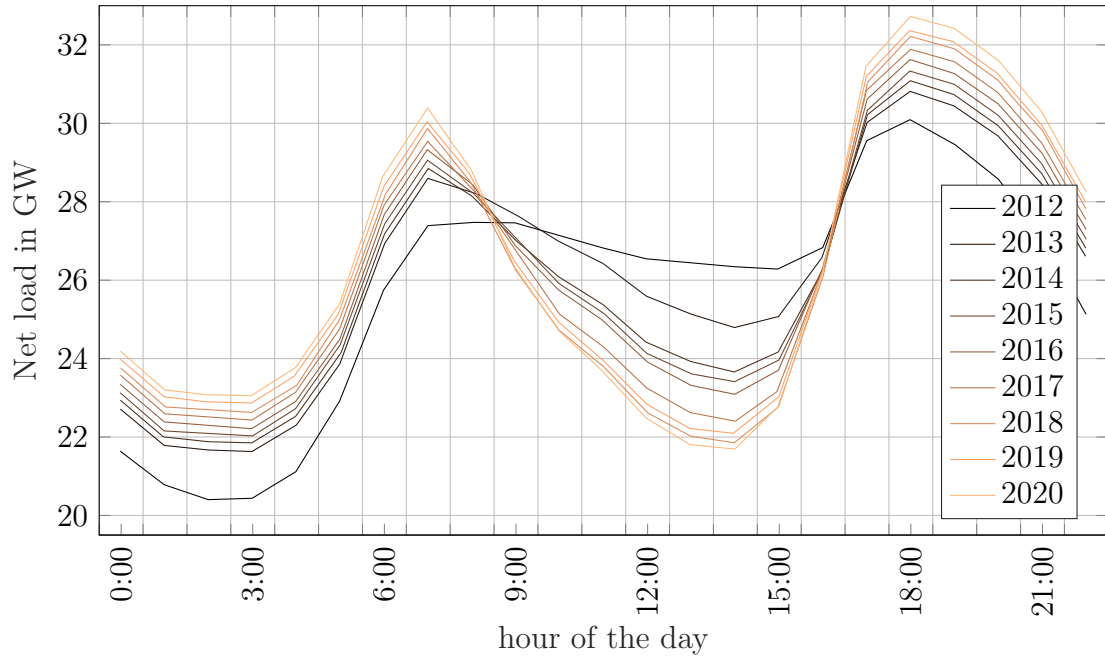


Figure 1.7: Net load curve of the California, US power grid for the January 11, years 2014 through 2020 are predictions [24].

Again, a heat transfer medium is used to transfer the heat from the TES system to the heat sink. The temperature profile of the discharged heat strongly depends on the TES system. Thus, special temperature requirements from the heat sink influence the applied TES system.

To efficiently apply TES, the storage system needs to fulfill two main requirements. First, the storage system needs to be able to store the heat close to the temperature level where it arises. Second, the energy losses during storage should be minimal. Choosing the right TES system is crucial for a successful application of TES. Generally, there are three types of storage systems.

1. sensible heat storage
2. latent heat storage
3. thermochemical heat storage

They differ in their principle method of heat storage, which results in different advantages and disadvantages as well as different fields of application. In the following all three storage types are discussed and their differences highlighted. As this work focuses on thermochemical heat storage, a more detailed discussion is given.

Table 1.1: Comparison of different sensible storage materials [28].

storage material	temperature range °C	specific heat capacity kJ/(kgK)	field of application
water	0 - 100	4.18	space heating, warm water
sand, stone	0 - 800	0.71	ground heat storage
concrete	0 - 500	0.88	thermal active structures
iron	0 - 800	0.47	solar storage applications
thermal oil	0 - 400	1.6 - 2.1	CSP
molten salt	150 - 450	1.3	CSP

Sensible heat storage

Sensible heat storage is the oldest and most common type of heat storage. There are various different materials and system, but all follow the same principle. During charging, energy is stored as a temperature difference in a storage material. The energy is used to heat up the storage material. The storage is based on retaining the temperature difference between storage material and surroundings. For discharge the temperature of the storage material is reduced and the heat is released. Eq.(1.1) shows the governing equation for sensible heat storage systems.

$$Q = m \int_{T_1}^{T_2} c_p dT \quad (1.1)$$

The stored energy Q depends on the mass of the storage material m , its heat capacity c_p and the temperature difference between the storage medium T_2 and the surrounding T_1 [27]. The maximal storage temperature depends on the used storage material, as it is not allowed to change its phase within the temperature interval T_1 to T_2 . Table 1.1 shows a comparison of different sensible storage materials, their heat capacity, applicable temperature range and field of application. A high specific heat capacity availability and its eco-friendliness makes water the most common storage material. However, its use is limited to below 100 °C under ambient pressure due to its boiling point. For higher temperatures, solid heat storage materials such as sand and gravel or molten salts are used.

Latent heat storage

Latent heat storage systems are already in the focus of researchers for quite some time. There are already working systems commercially available. They are characterized by a

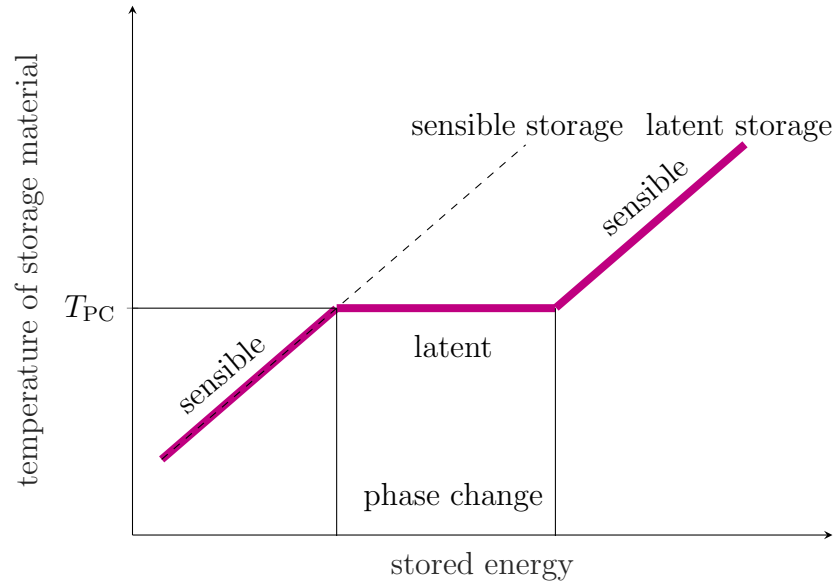


Figure 1.8: Comparison of the temperature course during the energy uptake between latent and sensible heat storage

phase change of the storage material. The energy is stored as latent heat of the phase change. Such phase changes can be solid-solid, solid-liquid or liquid-gaseous. The solid-liquid phase change is the most commonly used one, while liquid-gaseous is often avoided due to its high volume change. Storage materials used for latent heat storage are known in the literature as phase change materials (PCM). The stored energy in a latent heat storage can be described by Eq.(1.2).

$$Q = m \left(\int_{T_1}^{T_{PC}} c_{p,1} dT + \Delta H_{PC} + \int_{T_{PC}}^{T_2} c_{p,2} dT \right) \quad (1.2)$$

This equation can be seen as a combination of two sensible storage steps separated by a latent storage step. The PCM is heated up to its phase change temperature T_{PC} , thereby storing sensible heat. At T_{PC} , it then changes phase at constant temperature. The energy needed for the phase change ΔH_{PC} is stored in the PCM. This is followed by another sensible heat storage step up to T_2 .

Figure 1.8 shows a comparison of the stored energy between a sensible heat storage and a latent heat storage. The temperature of the storage material during the phase change stays constant, which results in a higher storage energy in the same temperature range. Hence, it is important to choose a PCM with an applicable phase change temperature. Table 1.2 shows different PCMs and their according phase change temperature T_{PC} as well as their according phase change enthalpy ΔH_{PC} .

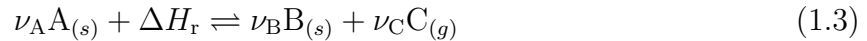
Table 1.2: Comparison of different phase change materials (PCM). All phase changes are solid-liquid [29].

storage material	phase change temperature	phase change enthalpy	specific heat capacity in kJ/(kgK)	
	T_{PC} in °C	ΔH_{PC} in kJ/kg	$c_{p,1}$	$c_{p,2}$
water	0	355	2.1	4.19
eicosane	36.6	243	1.94	2.08
laruic acid	44	183	1.8	2.16
stearic acid	69.7	221	1.83	2.3
48 NaCl / 52 MgCl ₂	450	432	0.9	1.0
67 NaF / 33 MgF ₂	832	618	1.42	1.38

1.3 Thermochemical energy storage

1.3.1 Principle of TCES

Thermochemical energy storage (TCES) is characterized by a material change of the storage material. This differentiates it to sensible and latent heat storage, where the storage material does not change its composition. It is based on a reversible chemical reaction or a reversible sorption process. The energy is stored as reaction enthalpy ΔH_r . The fundamental reaction equation is given by



Material A stores the energy while decomposing into a solid component B and a gaseous component C. This is called the charging reaction, the material B is referred to as the charged material. Through the reverse reaction or discharging reaction of B and C to A the stored energy is released again. Accordingly, the material A is referred to as discharged material. Thus, a separate storage of B and C is needed to prevent unwanted reverse reaction. It has to be noted, that, while most systems follow the reaction scheme given by Eq.(1.3), TCES is not bound to it and there are a few systems not following this scheme. The advantage of using a solid storage material which decomposes to another solid and a gaseous component is that a simple separation of both reacted materials is possible. The fundamental process for TCES is depicted in Figure 1.9. The charging reaction occurs in Reactor 1, thereby decomposing the storage material A to B following the given reaction. Depending on the reaction system it may be necessary to store the produced gas C. The heat input is generally realized using a carrier gas. It is obligatory that the carrier gas is inert in terms of the reaction system, so no side reactions occur. The charged material B reacts with C back to A in Reactor 2, releasing the previously stored energy. Again, in most processes a heat carrier

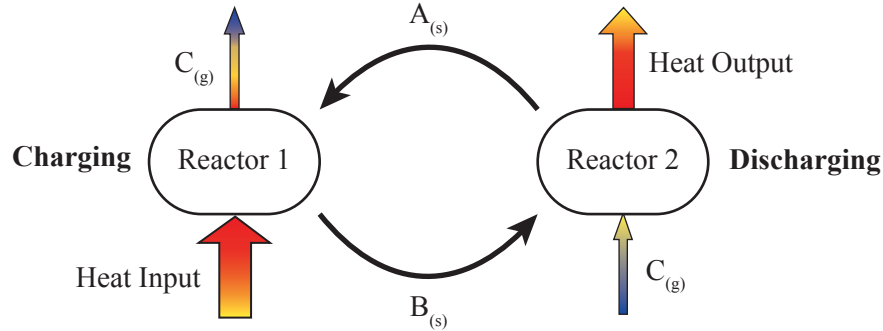


Figure 1.9: Schematic principle of a TCES system [30]

gas will be used to transport the heat out of the Reactor 2, which can be the reactive gas itself or an inert gas. Each TCES system has a specific equilibrium temperature T_{equ} (for details see section 2.1.2). Above this temperature the charging reaction occurs, below the discharging reaction. It has to be noted that the temperature in Reactor 1 T_1 has to be above T_{equ} of the reaction kinetic of the reaction system, while in Reactor 2 it has to be vice versa ($T_2 < T_{\text{equ}}$) at the given process conditions. The required temperature spread $T_2 - T_1$ strongly depends on the reaction system and the process conditions. Reactors 1 and 2 can be located at different sites with a material transport system between them, e.g. trucks transporting the material. Another possibility would be to use only one reactor for both charging and discharging at different times in a batch process. Thus, on-site material storage would be needed for this case.

1.3.2 Comparison of TCES to other thermal energy storage systems

Table 1.3 shows a comparison between sensible, latent and thermochemical energy storage. It can be seen that there are notable differences between the different technologies. First of all, TCES has a significantly higher storage density compared to the others. Figure 1.10 shows the theoretical storage capacity of selected TES systems.

Also the energy is stored at ambient temperature, thus no insulation is needed [18]. This results in a theoretically unlimited storage period, while sensible and latent energy storage systems lose energy to the surrounding [31]. Discharging effects in TCES systems are limited to sensible losses between storage temperature and reaction temperature and when the storage material reacts back, which can be prevented when separating the reaction partner. As a result of those properties, the stored energy can easily be transported over long distances. The high energy density is beneficial for a more economical transportation [32]. Depending on the used reaction system environmental hazards may arise.

Due to the simplicity of sensible heat storage systems, their development is already in in-

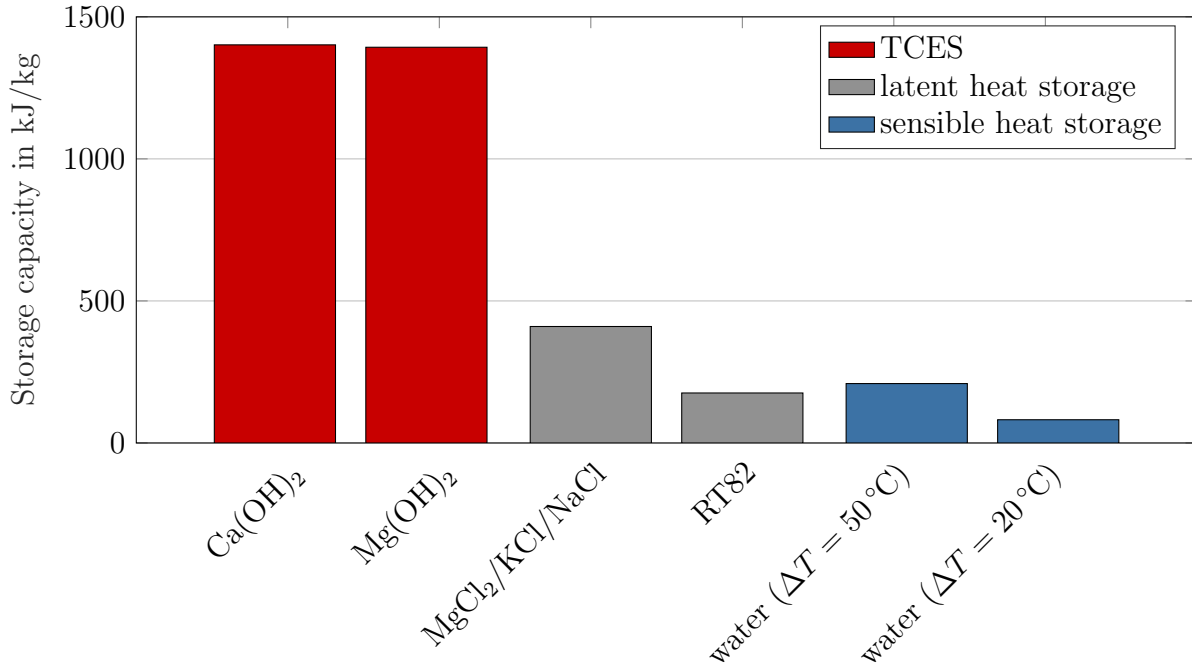


Figure 1.10: Comparison of selected TES systems

dustrial scale. Especially water based systems are widely used and commercially available. Latent heat storage systems have already been under development for some time, and pilot plants are under operation. As result of the occurring reaction and the resulting kinetics, TCES systems are complex. They moved into the focus of researchers only in the last years, therefore, they are available only on a laboratory scale [33].

1.3.3 Requirement for TCES system

In order to be successfully put to use, a TCES systems need to fulfill a set of requirements, which differ between applications. The requirement can be separated into three different groups (Figure 1.4):

reaction based These are primarily dictated by the application. They mainly determine if a reaction system can be used as TCES system for a given application. First of all the equilibrium temperature of the system has to be suitable for the application. As outlined in section 1.2.1 the possible application for TCES stretch over a wide temperature range. Thus, a proper TCES system has to be chosen individually. Second the reaction kinetic of the systems has to fit the time scale of the application on both sides, heat source as well as heat sink. If the reaction kinetics is too slow, the required dynamics of the system can not be achieved. Third the energy density has to be as high as possible. A lower energy density means, more material, more storage space and higher transport costs for the same amount of stored energy.

substance based They mainly define the handling of the substances during the process.

Key requirements are the toxicity, corrosiveness and stability of the occurring substances. Depending on the application their impact on the TCES may vary. For instance, systems designed to be placed in households have a lower tolerance for toxic materials as systems designed for industrial applications. Stability of the materials can be increased by pressurizing the storage container. This may be easier in smaller household storages as on an industrial scale.

economical These assure that the TCES system can be operated economically feasible.

They include availability and price of the materials as well as the cycle stability of the system. The operating mode of the storage influences their requirements. For small high tech storage applications the price of the material is not as important as for big commercial applications. The intended cycle duration influences the needed cycle stability. A seasonal storage that cycles only once a year has a different requirement for the cycle stability than a storage that cycles once a day.

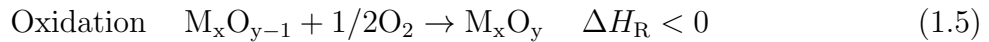
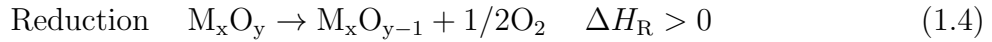
The most information needed to check if a TCES fulfills the given requirements is available in databases. Only the reaction kinetics and the cycle stability of a system are not available on a broad scale. Since both properties are crucial for a successful application of a TCES each system has to be tested individually in order to check its potential.

1.3.4 State of the art

Compared to sensible or latent heat storage, TCES is still a new technology, despite the fact that it has been already been used centuries ago. According to Thorndike the first recorded uses of TCES date back to the 10th century Persian scholar al-Razi, which used quicklime (CaO) and water to boil an egg [36]. Hieatt and Jones describe a recipe from the late 13th century on how to cook meat without fire [37]. In a technical context the first applications of TCES had been in Germany. A locomotive which runs between Aachen and Jülich in 1882 and a motorboat on the Spree in 1883, both used concentrated NaOH to generate steam which powered the machine [38].

There are various reaction systems in development at the moment. For the low and middle temperature level mainly salt hydrates [39] are currently investigated, e.g. $\text{CaCl}_2 \cdot 6 \text{H}_2\text{O}/\text{CaCl}_2$ [40, 41] and $\text{MgSO}_4 \cdot 7 \text{H}_2\text{O}/\text{MgSO}_4$ [42, 43]. Pardo et al. [34] concluded that the most promising reaction systems for the high temperature level are $\text{Ca}(\text{OH})_2/\text{CaO}$ [44] and PbCO_3/PbO [45]. For solar applications, also reactions of metal oxides are shifting into the focus of the research [46, 47]. Especially, redox systems are deemed to be suitable due to their operating temperature [30, 34]. Wong et al. [48] analyzed 16 potential metal oxide systems

following reaction equation 1.5. From these systems, only BaO, Co₃O₄, CuO, Fe₂O₃, Mn₂O₃ displayed the necessary behavior for a suitable TCES material. Co₃O₄ showed the most promising results [49] and was further analyzed in terms of reversibility and energy storage capacity [50–52]. The cycle ability of Mn₂O₃ has already been proven by Carrillo et al. [53] and compared to Co₃O₄ [47].



1.4 Aim of this work

The wide temperature range in which TCES can be utilized, the variety of applications and the resulting requirements, and the diversity of the reactions applicable for TCES create the necessity of a comprehensive database with different TCES reaction systems. Such a database would help the consumer to select an appropriate TCES system for a given application purpose. The basis for such a database is a systematic screening to find reaction systems for a wide temperature range.

So far, only one systematic approach to screen for TCES systems is known to the author. N'Tsoukpoe [54] performed a systematic evaluation of 125 salt hydrates for TCES at low temperature levels with the main focus on a household application. They first discriminated based on material safety and past experiences, then focused on thermal analysis to find suitable candidates for TCES. The 125 salt hydrates were identified using a thermochemical database, but no detailed information on how they were identified was given .

In this work, an algorithm is developed to identify TCES systems for a broad temperature range (25 °C-1000 °C). It finds possible TCES systems based on a thermodynamic database. The use of an algorithm to find reaction systems results in an objective, comprehensive list, which is not based on prior knowledge of the researcher. The found TCES systems are further analyzed in context of their equilibrium temperature and energy density.

To distinguish between possible candidates for an application it is important to identify the reaction kinetics of the system. The heat source purports the possible operating conditions (temperature, pressure) of the TCES system. To be successfully implemented, the system needs to have a sufficient reaction rate at given temperature - pressure conditions. Therefore, temperature and pressure dependent kinetic data is needed. In order to collect this necessary information, a novel kinetic method, the extended NPK method, is presented. It allows for the systematic development of a temperature and pressure dependent kinetic model based on a data-driven identification.

Based on the results of the systematic screening, the TCES system CuO/Cu₂O is investigated further for its potential solar application. The extended NPK method is applied to develop kinetic models for both, charging and discharging reaction. Additionally, the cycle stability is analyzed.

Table 1.3: Characteristics and comparison of the thermal energy storage systems [34, 35]

	Sensible heat storage	Latent heat storage	Thermochemical heat storage
Volumetric density	small $\sim 180 \text{ MJ/m}^3$ material	medium $\sim 360 \text{ MJ/m}^3$ material	high $\sim 1800 \text{ MJ/m}^3$ reactant
Gravimetric density	small $\sim 90 \text{ kJ/kg}$ material	medium $\sim 270 \text{ kJ/kg}$ material	high $\sim 270 \text{ kJ/kg}$ reactant
Storage temperature	charging step temperature	charging step temperature	ambient temperature
Storage period	limited (thermal losses)	limited (thermal losses)	theoretically unlimited
Storage life time	long	limited	limited
Transportation	small distance	small distance	distance theoretically unlimited
environmental impact	nil	little	sometimes hazardous
Maturity	industrial scale	pilot scale	laboratory scale
Technology	simple	medium	complex

Table 1.4: Different requirements for TCES systems

reaction based	substance based	economical
equilibrium temperature	toxicity	availability
reaction kinetics	corrosiveness	price
energy density	stability	cycle stability

Chapter 2

Fundamentals

To successfully describe chemical reactions as used in TCES it is necessary to analyse them on a fundamental level. Therefore, both thermodynamic and kinetic fundamentals are required. The laws of thermodynamics give the direction, in which the system reacts. The laws of reaction kinetics give the speed of the reaction. The knowledge of both is essential to successfully describe and predict the behavior of a chemical system. A good example for this is the transformation of carbon from diamond to graphite. At 25 °C and 1 atm the reaction from diamond to graphite is thermodynamically favorable, thus each diamond in jewelery should react to graphite. Luckily, the kinetic of this reaction at 25 °C is so slow, that this is not observed.

Within this chapter, necessary fundamentals are discussed to successfully describe a TCES system.

2.1 Thermodynamic fundamentals

2.1.1 Gibbs energy G

To describe the thermodynamic state and behavior of a system often the free enthalpy or Gibbs energy G is used. The Gibbs energy can be calculated with the Gibbs function (often referred to as Gibbs fundamental equation), which represents the combination of the first and second law of thermodynamics. The Gibbs function can be written as a function of the inner energy Eq.(2.1a) or the enthalpy Eq.(2.1b).

$$G(T, p, \mathbf{n}) = U(S, V, \mathbf{n}) + pV - T S \quad (2.1a)$$

$$G(T, p, \mathbf{n}) = H(S, p, \mathbf{n}) - T S \quad (2.1b)$$

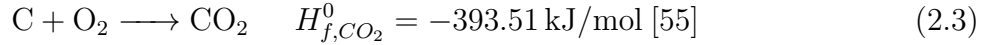
The Gibbs energy for a system at standard conditions ($T^0 = 273.15 \text{ K}$, $p^0 = 1 \text{ bar}$) is called standard Gibbs energy G^0 . The superscript 0 denotes standard conditions.

For a system with only one pure substance at standard conditions Eq.(2.1b) simplifies to

$$G_0^0(T^0, p^0) = H_f(T^0, p^0) - T^0 S_f(T^0, p^0) = H_f^0 - T^0 S_f^0 \quad (2.2)$$

where H_f^0 is the enthalpy of formation and S_f^0 the entropy of formation, both at standard conditions. G_0 is called the Gibbs energy of the pure substance. The subscript 0 denotes that the value corresponds to a pure substance.

The enthalpy of formation represents the occurring energy change when a substance is formed from the allotropic most stable form of its elements. One example is the creation of CO_2 from O_2 and C. The energy change for this reaction equals the enthalpy of formation for CO_2 H_{f,CO_2} .



The standard enthalpy of formation H_f^0 for different substances can be found in the literature and in electronic databases. The temperature dependency of H_f for isobaric conditions is given by

$$H_f(T, p_0) = H_f^0 + \int_{T^k_0}^T c_p(T) dT \quad (2.4)$$

The temperature dependency of the specific isobaric heat capacity is often described by polynomials. Given in Eq.(2.5) is one common representation, known as NASA polynomial¹.

$$c_p(T) = a_1 + a_2 T + a_3 T^{-2} + a_4 T^2 \quad (2.5)$$

With the polynomial form the integral in Eq.(2.4) can be solved, which results in

$$H_f(T, p_0) = H_f^0 + \left[a_1 T + \frac{a_2}{2} T^2 - a_3 T^{-1} + \frac{a_4}{3} T^3 \right]_{T^k_0}^T \quad (2.6)$$

The entropy of formation S_f is defined by Gmehling [56] as the change in entropy associated with the formation of one mole of a substance from its elements. The temperature dependency of S_f for isobaric conditions is given by

$$S_f(T, p_0) = S_f^0 + \int_{T_0}^T \frac{c_p(T)}{T} dT \quad (2.7)$$

Again, the standard entropy of formation S_f^0 can be found in the literature and thermo-

¹There are several different forms of th NASA polynominals

dynamic databases. With the polynomial form of the temperature dependency of the heat capacity c_p Eq.(2.5) the integral can be solved, which results in

$$S_f(T, p_0) = S_f^0 + \left[a_1 T + \frac{a_2}{2} T^2 - a_3 T^{-1} + \frac{a_4}{3} T^3 \right]_{T^0}^T \quad (2.8)$$

With Eqs.(2.4) and (2.7) the temperature dependency of the Gibbs energy of a pure substance Eq.2.2 can be written as

$$G_0(T, p^0) = H_f(T, p^0) - T S_f(T, p^0) = H_f^0 + \int_{T^0}^T c_p(T) dT - T \left(S_f^0 + \int_{T^0}^T \frac{c_p(T)}{T} dT \right) \quad (2.9)$$

The pressure dependency of the Gibbs energy can be calculated by

$$G_0(T, p) = G_0(T, p^0) + \int_{p^0}^p v_i dp \quad (2.10)$$

where v_i is the molar volume of the pure substance. The result of integral differs depending on the substance. For ideal gases Eq.2.10 can be written as

$$G_0(T, p) = G_0(T, p^0) + RT \ln \frac{p}{p^0} \quad (2.11)$$

while for incompressible substances it can be written as

$$G_0(T, p) = G_0(T, p^0) + v_i(p - p^0) \quad (2.12)$$

A system is in thermodynamical equilibrium when its Gibbs function Eq.(2.1a) is at its minimum. To find this minimum, Eq.(2.1a) needs to be derived. With the derivative of the inner energy U

$$dU(S, V, \mathbf{n}) = TdS - pdV + \sum_i \mu_i dn_i \quad (2.13)$$

the derivative of the Gibbs energy can be written as

$$\begin{aligned} dG(T, p, \mathbf{n}) &= dU(S, V, \mathbf{n}) + d(pV) - d(TS) \\ &= TdS - pdV + \sum_i \mu_i dn_i + pdV + Vdp - TdS - SdT \\ &= \sum_i \mu_i dn_i + Vdp - SdT \end{aligned} \quad (2.14)$$

where n_i is the molar amount of substance i and μ_i its chemical potential. S and V are the entropy and the volume of the considered system. A minimum in $G(T, p, \mathbf{n})$ requires $dG(T, p, \mathbf{n}) = 0$.

Therefore, the change of the Gibbs energy dG has to be negative for a process to bring the system closer to its equilibrium. In other words, a process that reduces the Gibbs energy will occur spontaneous without the need of external energy.

2.1.2 Chemical equilibrium

A system is defined to be in chemical equilibrium when the chemical potential of the products is equal to the educts Eq.(2.15).

$$\mu_{\text{educts}} = \mu_{\text{products}} \quad (2.15)$$

If an isothermal and isobaric reaction is considered ($dT = 0$ and $dp = 0$), then the definition of the chemical equilibrium stipulates that the Gibbs energy is at its minimum. This can be seen in the derivation of the Gibbs energy Eq.(2.14), which simplifies to Eq.(2.16) for the given reaction conditions.

$$dG(T, p, \mathbf{n})|_{T,p} = \sum_i \mu_i(T, p, n_i) dn_i = 0 \quad (2.16)$$

The term dn_i can be substituted by

$$dn_i = \nu_i dz \quad (2.17)$$

with ν_i being the stoichiometric coefficient of reactant i and z the general reaction progress. This leads to

$$\left. \frac{dG(T, p, \mathbf{n})}{dz} \right|_{T,p} = \sum_i \nu_i \mu_i(T, p, \mathbf{n}) = 0 \quad (2.18)$$

On a molar basis this can also be written as

$$\left. \frac{dG(T, p, \mathbf{x})}{dz} \right|_{T,p} = \sum_i \nu_i \mu_i(T, p, \mathbf{x}) = 0 \quad (2.19)$$

with $\mathbf{x} = \mathbf{n} / \sum n_i$.

To calculate the chemical equilibrium, first the chemical potential of each substance μ_i in the mixture needs to be calculated. The chemical potential of the pure substance i μ_{0i} is equal to the Gibbs energy of the pure substance i G_{0i} . The effects of an ideal mixture on the potential of substance i can be considered by

$$\mu_{i,\text{ideal}}(T, p, x_i) = \mu_{0i}(T, p) + RT \ln x_i = G_{0i}(T, p) + RT \ln x_i \quad (2.20)$$

Divergence from the behavior of the ideal mixture can be considered by adding a correction term

$$\mu_i(T, p, \mathbf{x}) = \mu_{i,\text{ideal}}(T, p) + \mu_{i,\text{real}}(T, p, \mathbf{x}) \quad (2.21)$$

Note that the chemical potential is now dependent of all substances in the mixture. The chemical equilibrium can now be calculated by introducing Eqs. (2.20) and (2.21) into (2.19) leading to

$$\begin{aligned} \sum_i \nu_i \mu_i(T, p, \mathbf{x}) &= \sum_i \nu_i G_{0i}(T, p) + RT \sum_i \nu_i \ln x_i + \sum_i \nu_i \mu_{i,\text{real}}(T, p, \mathbf{x}) \\ &= \Delta G_R(T, p) + RT \ln K(\mathbf{x}) + \sum_i \nu_i \mu_{i,\text{real}}(T, p, \mathbf{x}) \end{aligned} \quad (2.22)$$

The first sum was consolidated to the reaction Gibbs energy $\Delta G_R(T, p)$

$$\begin{aligned} \Delta G_R(T, p) &= \sum_i \nu_i G_{0i}(T, p) = \sum_i \nu_i H_{f,i}(T, p) - T \sum_i \nu_i S_{f,i}(T, p) \\ &= \Delta H_R(T, p) - T \Delta S_R(T, p) \end{aligned} \quad (2.23)$$

The terms ΔH_R and ΔS_R are known as the reaction enthalpy and the reaction entropy, respectively. Especially ΔH_R is important for TCES systems, as it gives the amount of energy that can be stored in the reaction.

The second sum in Eq.(2.22) was consolidated to the equilibrium constant $\ln K(\mathbf{x})$

$$\ln K(\mathbf{x}) = \sum_i \nu_i \ln x_i = \ln \prod_i x_i^{\nu_i} \quad (2.24)$$

The correction term in Eq.(2.21) can be included in the equilibrium constant by using a_i rather than x_i . Then, Eq.(2.22) can be written as

$$\sum_i \nu_i \mu_i(T, p, \mathbf{x}) = \sum_i \nu_i \mu_i(T, p, \mathbf{a}) = \Delta G_R(T, p) + RT \ln K(\mathbf{a}) \quad (2.25)$$

For a system in chemical equilibrium Eq.(2.22) is equal to zero.

For a typical reaction for TCES (Eq.(1.3)) the equilibrium constant can be written as

$$K(\mathbf{a}) = \frac{a_B^{\nu_B} a_C^{\nu_C}}{a_A^{\nu_A}} \quad (2.26)$$

When assuming ideal behavior of the substances the activity of the solid substances A and B are equal to 1 and the activity of the gaseous component C is equal to the partial pressure of C. Hence, the equilibrium constant K simplifies to

$$K = \frac{p_C}{p^0} \quad (2.27)$$

with p^0 being the standard pressure of 1 bar. In this case the reaction equilibrium can be calculated from

$$\sum_i \nu_i H_{f,i}(T, p) - T \sum_i \nu_i S_{f,i}(T, p) + RT \ln \frac{p_C}{p^0} = 0 \quad (2.28)$$

This equation correlates the partial pressure p_C with the equilibrium temperature of the system. For the special case of $p_C = p^0 = 1$ bar Eq.(2.28) gives

$$\Delta G_R(T, p) = \sum_i \nu_i H_{f,i}(T, p) - T \sum_i \nu_i S_{f,i}(T, p) = 0 \quad (2.29)$$

Thus the equilibrium temperature T_{equ} at $p_C = 1$ bar can be calculated by

$$T_{\text{equ}} = \left. \frac{\sum_i \nu_i H_{f,i}(T_{\text{equ}})}{\sum_i \nu_i S_{f,i}(T_{\text{equ}})} \right|_{p_C} \quad (2.30)$$

Since $H_{f,i}$ and $S_{f,i}$ are temperature dependent, Eq.(2.30) has to be solved iteratively.

2.2 Kinetic fundamentals

The kinetics of a reaction often determines its applicability and directly influences how economically feasible a process is. Knowledge of the kinetics is fundamental to choose suitable reaction conditions and to achieve satisfying conversion. Additionally, kinetic information helps to prevent unwanted side reactions.

In this work the focus lies on solid state reactions that follow Eq.(1.3). In a system with a single reaction the progress can also be described by the conversion α of the reaction. It is defined as the amount of reacted material in relation to the available material at the beginning. For the decomposition reaction it is calculated as

$$\alpha(t) = \frac{n_{A,0} - n_A(t)}{n_{A,0}} \quad (2.31)$$

where $n_{A,0}$ is the available material of A at the beginning and $n_A(t)$ the available material

at time t . The conversion for the reverse reaction can be calculated based on material B. In this work mostly thermogravimetric analysis is used to determine the conversion of a reaction. The conversion can be calculated from the measured mass signal $m(t)$ as

$$\alpha(t) = \frac{m_0 - m(t)}{m_0 - m_\infty} \quad (2.32)$$

where m_0 is the mass of the substance at the beginning of the reaction, $m(t)$ the mass at time t and m_∞ the theoretical mass after all the material has reacted.

The kinetic of such reactions is often described based on the reaction rate $d\alpha/dt$. It is generally described as a product of the contributions of three independent variables, the conversion α , the temperature T and the pressure p by the differential equation

$$\frac{d\alpha}{dt} = f(\alpha)k(T)h(p) \quad (2.33)$$

In case of reactions that follow Eq.(1.3) the pressure mainly influencing the reaction kinetics, is the partial pressure of the gaseous component C. Therefore, the absolute pressure is usually neglected.

The literature on solid state kinetic identification focuses mainly on the determination of conversion dependency $f(\alpha)$ and temperature dependency $k(T)$, while the identification of the pressure dependency $h(p)$ is often neglected [57]. Yet the pressure dependency is of great interest for reactor design since some reactor types, e. g. fluidized bed reactors, feature high concentration gradients of the reactant gas across the bed height. To take this effect into account knowledge about the pressure dependency of the reaction is absolutely necessary [58].

In the following section necessary terms and definitions for the determination of the reaction kinetics are described and derived.

2.2.1 Differential rate laws

In most cases the temperature dependency $k(T)$ is described by the Arrhenius equation [59]

$$k(T) = A e^{-E_a/(RT)} \quad (2.34)$$

which leads with Eq.(2.33) to the differential rate law

$$\frac{d\alpha}{dt} = f(\alpha)A e^{-E_a/(RT)}h(p) \quad (2.35)$$

For non isothermal experiments the following relation can be defined

$$\frac{d\alpha}{dT} = \frac{d\alpha}{dt} \frac{dt}{dT} \quad (2.36)$$

Often measurements are performed with constant heating or cooling rate β (isokinetic measurements)

$$\beta = \frac{dT}{dt} = \text{const} \quad (2.37)$$

following a linear heating or cooling program

$$T = T_{start} + \beta t \quad (2.38)$$

Substituting Eq.(2.36) and Eq.(2.37) into the differential rate law Eq.(2.35) results in the isokinetic differential rate law

$$\frac{d\alpha}{dT} = f(\alpha) \frac{A}{\beta} e^{-E_a/(RT)} h(p) \quad (2.39)$$

2.2.2 Integral rate laws

Some identification methods are based on an integral form of the rate laws. They assume isobaric conditions during the measurements. Thus the contribution of $h(p)$ can be incorporated into the pre-exponential factor as

$$A' = h(p_1)A \quad (2.40)$$

The integral form of the rate laws can be derived by integrating the differential rate law Eq.(2.35).

$$\int_0^\alpha \frac{1}{f(\alpha')} d\alpha' = \int_0^t A' e^{-E_a/(RT(\tau))} d\tau \quad (2.41)$$

The left hand side can be written as the integral form of the conversion dependency $g(\alpha)$

$$g(\alpha) = \int_0^\alpha \frac{1}{f(\alpha')} d\alpha' \quad (2.42)$$

The evaluation of the right hand side of Eq.(2.41) depends on the temperature profile of the measurements. For an isothermal measurement it can simply be integrated as every variable is time independent, resulting in the isothermal integral rate law.

$$g(\alpha) = A' e^{-E_a/(RT)} t = kt \quad (2.43)$$

For an isokinetic measurement the integral can be transformed using the substitution Eq.(2.37)

and Eq.(2.38) for the integration limits. If T_{start} lies below the temperature at which a reaction is measurable then the lower integration limit can be set to 0.

$$\int_0^t A' e^{-E_a/(RT(\tau))} d\tau = \frac{A'}{\beta} \int_0^T e^{-E_a/(RT')} dT' \quad (2.44)$$

In combination with Eq.(2.41), this transformation leads to the integral form of the isokinetic rate law.

$$g(\alpha) = \frac{A'}{\beta} \int_0^T e^{-E_a/(RT')} dT' \quad (2.45)$$

The integral is called the temperature integral [60].

Temperature integral

The so called temperature integral, as it appears in the integral form of the isokinetic rate law (Eq.(2.45)), is the result of the integration of the Arrhenius equation (Eq.(2.34)) with a time dependent temperature profile [61]. For isothermal measurement conditions the integration of the temperature integral is straight forward, as shown above. For isokinetic measurements it results in the integral in Eq.(2.45), which has no analytical solution. Several attempts have been made to implement non linear heating programs which lead to an exact analytical solution of the integral. Proposed heating programs include hyperbolic [62] and parabolic [63] heating programs. Furthermore, attempts to prevent the occurrence of the temperature integral have been made by applying non-Arrhenius temperature dependency functions [61]. Table 2.1 shows different approaches to describe the temperature dependency. However, those approaches are not well established. The most common way to resolve the problem of the temperature integral for isokinetic measurements is to apply various approximations [64]. In the literature several different approximations have been reported, varying in complexity and accuracy. [65–73]

Here only the Doyle approximation is presented [74–76], since it is used in the Ozawa, Flynn and Wall method, which is discussed later on.

In the literature, the temperature integral is generally transformed in a form which can be found in mathematical tables. With the transformation $x = E_a/(RT)$ Eq.(2.45) becomes

$$g(\alpha) = \frac{A'E_a}{\beta R} \int_x^\infty \frac{e^{-x}}{x^2} dx = \frac{A'E_a}{\beta R} q(x) \quad (2.46)$$

Doyle observed that $\log q(x)$ is linear with respect to x over a short range according to

$$\log q(x) \approx -a - bx \quad (2.47)$$

Table 2.1: Different models for the temperature dependency $k(T)$ of a reaction [61].

identifier	differential form $\frac{d(\ln(K(T)))}{dT}$	integral form $k(T)$
T1	C	$A_0 e^{CT}$
T2	B/T	$A_0 T^B$
T3	A/T^2	$A_0 e^{-A/T}$
T4	$(A + BT)/T^2$	$A_0 T^B e^{-A/T}$
T5	$(A + CT^2)/T^2$	$A_0 e^{CT} e^{-A/T}$
T6	$(BT + CT^2)/T^2$	$A_0 T^B e^{CT}$
T7	$(A + BT + CT^2)/T^2$	$A_0 T^B e^{CT} e^{-A/T}$
T8	$A/(T + B)^2$	$A_0 e^{-A/(T+B)}$

He used a three term approximation of the Schölmich series expansion (see Appendix) to calculate $a = 2.315$ and $b = 0.4567$. Hence the Doyle approximation becomes

$$\log q(x) \approx -2.315 - 0.4567x \quad (2.48)$$

Flynn and Wall reported an accuracy of $\pm 3\%$ of Eq.(2.48) within the limits of $20 \leq x \leq 60$ [77].

2.2.3 Conversion models

Conversion models are used to describe the conversion dependency $f(\alpha)$ in Eq.(2.33). These conversion models are mathematical descriptions of the measured processes during the reactions. For solid state reactions, various different models have been proposed. Some of them are based on physical processes, their mathematical description has been derived on certain mechanistic assumptions. Other models are purely empirical, with little to none mechanistic meaning. This section gives an overview of the conversion models and discussed the assumption and derivation of the most common models. The following sections are based on the work of Dickinson and Heal and the work of Khawam and Flanagan. Dickinson and Heal cover the diffusion controlled models [78], while Khawam and Flanagan discusses most of the other models [79].

Overview

Conversion models can either be classified based on their mechanistic assumption or their shape of the $d\alpha/dt$ vs α or α vs t curve. In Tables 2.2 - 2.5 they are classified based

Table 2.2: Different nucleation models for the conversion dependency $f(\alpha)$

identifier	model type	differential form $f(\alpha)$	integral form $g(\alpha)$
A1	Avrami-Erofeyev	$4(1-\alpha)[- \ln(1-\alpha)]^{3/4}$	$[- \ln((1-\alpha))]^{1/4}$
A2	Avrami-Erofeyev	$2(1-\alpha)[- \ln(1-\alpha)]^{1/2}$	$[- \ln((1-\alpha))]^{1/2}$
A3	Avrami-Erofeyev	$3(1-\alpha)[- \ln(1-\alpha)]^{2/3}$	$[- \ln((1-\alpha))]^{1/3}$
A4	Avrami-Erofeyev	$4/3(1-\alpha)[- \ln(1-\alpha)]^{1/4}$	$[- \ln((1-\alpha))]^{3/4}$
A5	Avrami-Erofeyev	$3/2(1-\alpha)[- \ln(1-\alpha)]^{1/3}$	$[- \ln((1-\alpha))]^{2/3}$
B1	Prout-Tompkins	$\alpha(1-\alpha)$	$\ln(\alpha/(1-\alpha))$
P2	Power law (n = 2)	$2\alpha^{1/2}$	$\alpha^{1/2}$
P3	Power law (n = 3)	$3\alpha^{2/3}$	$\alpha^{1/3}$
P4	Power law (n = 2)	$4\alpha^{3/4}$	$\alpha^{1/4}$

on their mechanistic assumptions. Usually four different classes of mechanistic models are distinguished: : nucleation models, geometric contraction models, reaction order models and diffusion models. Based on their shape, models are classified into acceleratory, deceleratory, constant or sigmoidal models. Acceleratory models describe an acceleration of the reaction, thus the reaction rate $d\alpha/dt$ increases with increasing α (Figure 2.1). Deceleratory models describe the opposite effect, $d\alpha/dt$ decreases with increasing α , which results in slowing down the reaction (Figure 2.2). Constant models have a reaction rate independent from the conversion (Figure 2.3). Reactions following a sigmoidal model first show an acceleration, followed by a deceleration, resulting in a bell-shaped $d\alpha/dt$ vs α curve (Figure 2.4).

Sestak and Berggren [80] proposed the following mathematical form to express the integral form $g(\alpha)$ of all reaction models with a single equation.

$$g(\alpha) = \alpha^\chi (1-\alpha)^\psi (-\ln(1-\alpha))^\omega \quad (2.49)$$

By assigning values to the constants χ , ψ and ω each model in Tables 2.2 - 2.5 can be expressed or approximated. In the following, the derivation of some commonly used models and their theoretical assumptions are discussed. All derivations assume isothermal and isobaric measurement conditions, thus the reaction can be described by the isothermal integral rate law Eq.2.43

Table 2.3: Different interface models for the conversion dependency $f(\alpha)$

identifier	model type	differential form $f(\alpha)$	integral form $g(\alpha)$
R2	contracting area	$2(1-\alpha)^{1/2}$	$1-(1-\alpha)^{1/2}$
R3	contracting volume	$3(1-\alpha)^{2/3}$	$1-(1-\alpha)^{1/3}$
R4	interface	$3/2(1-\alpha)^{1/3}$	$1-(1-\alpha)^{2/3}$

Table 2.4: Different reaction order models for the conversion dependency $f(\alpha)$

identifier	model type	differential form $f(\alpha)$	integral form $g(\alpha)$
F0	zero-order	1	α
F1	first-order	$(1-\alpha)$	$-\ln(1-\alpha)$
F2	second-order	$(1-\alpha)^2$	$[1/(1-\alpha)] - 1$
F _n	nth-order	$(1-\alpha)^n$	$\frac{1-(1-\alpha)^{1-n}}{1-n}$

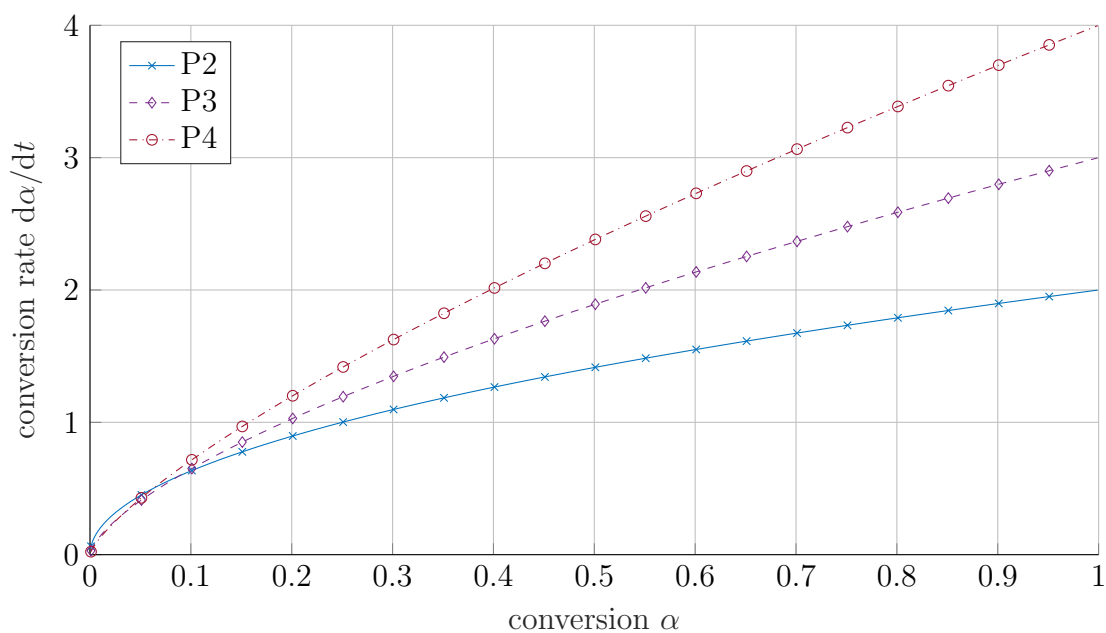
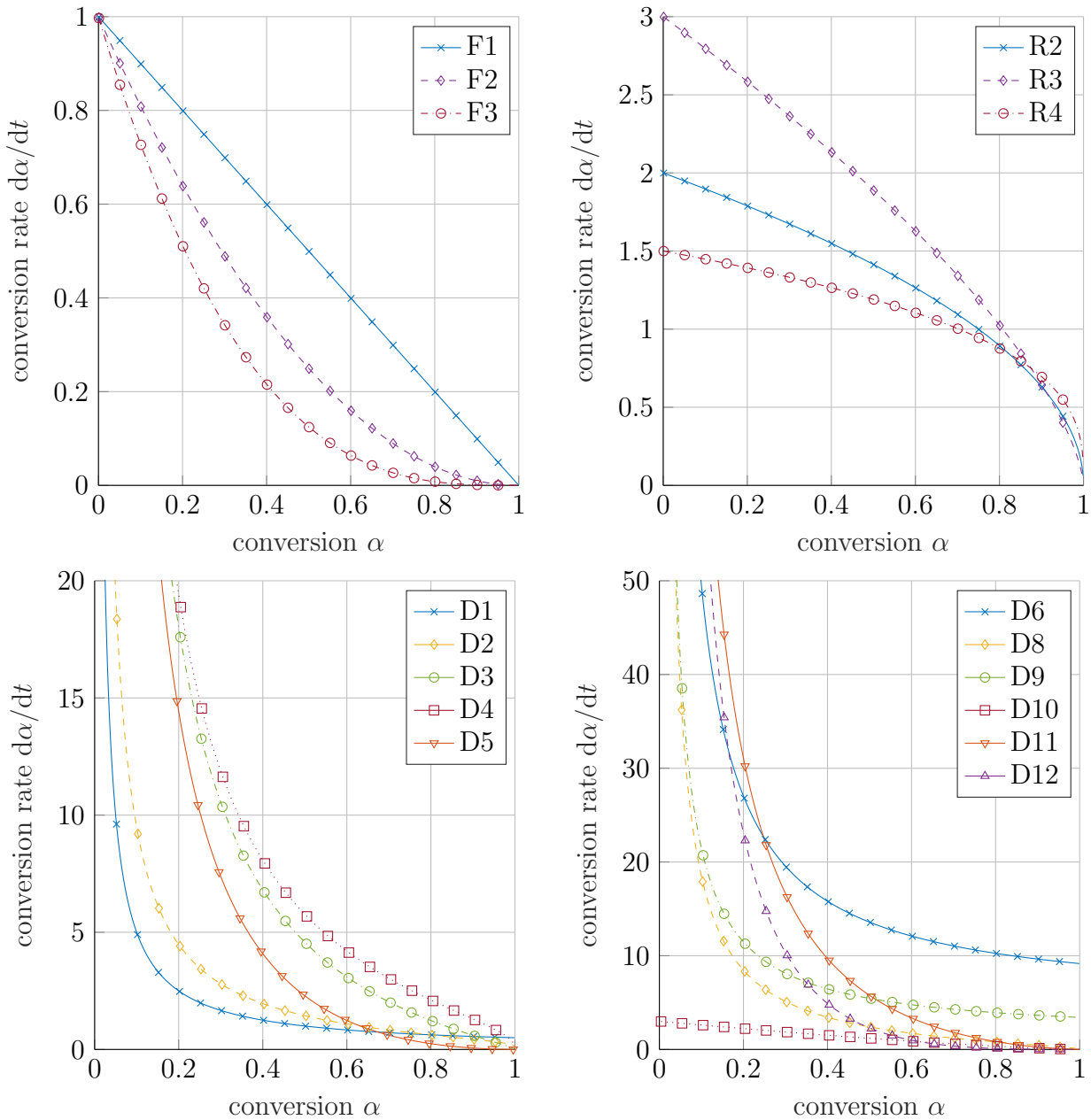
Figure 2.1: Isothermal plots of $d\alpha/dt$ vs α for acceleratory conversion models

Table 2.5: Different diffusion controlled models for the conversion dependency $f(\alpha)$

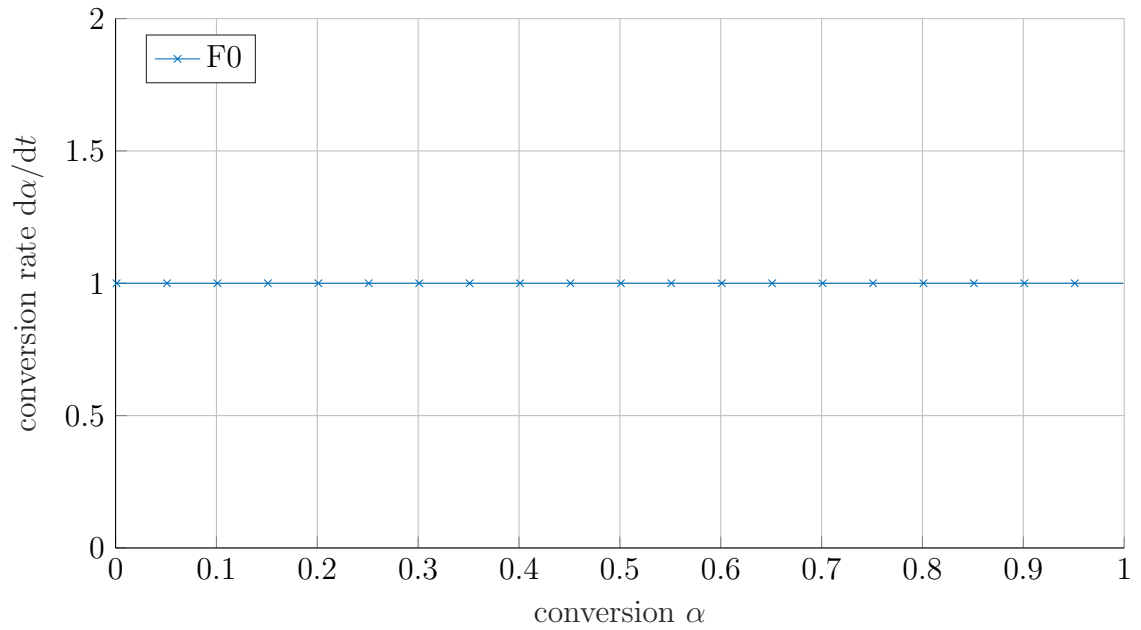
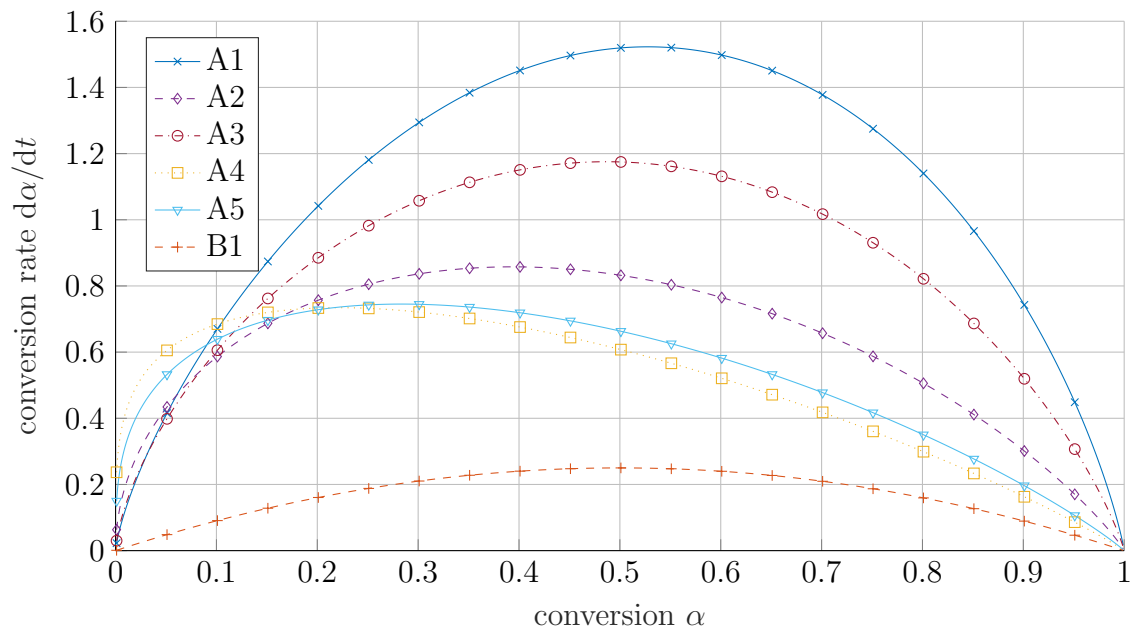
identifier	model type	differential form $f(\alpha)$	integral form $g(\alpha)$
D1	one-dimensional	$1/(2\alpha)$	α^2
D2	two-dimensional	$-\ln(1-\alpha)^{-1}$	$(1-\alpha)\ln(1-\alpha) + \alpha$
D3	Jander (three-dimensional)	$3/2(1-\alpha)^{2/3}/(1-(1-\alpha)^{1/3})$	$(1-(1-\alpha)^{1/3})^2$
D4	Ginstling-Brounshtein	$3/(2((1-\alpha)^{-1/3}-1))$	$1-2\alpha/3-(1-\alpha)^{2/3}$
D5	Zhuravlev, Lesokhin and Templeman	$(3((1-\alpha)^{4/3}))/2((1-\alpha)^{-1/3}-1))$	$(1/(1-\alpha)^{1/3}-1)^2$
D6	"Anti-Jander" (three-dimensional)	$3/2(1+\alpha)^{2/3}/((1+\alpha)^{1/3}-1)$	$((1+\alpha)^{1/3}-1)^2$
D7	Kröger and Ziegler ^a		$k \ln(t) = [1-(1-\alpha)^{1/2}]^3$
D8	Jander (cylindrical diffusion)	$1/((1-\alpha)^{-1/2}-1)$	$(1-(1-\alpha)^{1/2})^2$
D9	"Anti-Jander" (cylindrical diffusion)	$1/(1-((1+\alpha)^{-1/2}))$	$(1-(1+\alpha)^{1/2})^2$
D10	Dickinson-Heal	$3(1-\alpha)^{4/3}$	$(1-\alpha)^{-1/3}-1$
D11	Dickinson-Heal	$3(\alpha-1)/(1-(1-\alpha)^{-1/3})$	$(1-\alpha)^{-1/3}-1+1/3\ln(1-\alpha)$
D12	Dickinson-Heal	$3(1-\alpha)^{8/3}/(1-(1-\alpha)^{1/3})$	$1/5(1-\alpha)^{-5/3}-1/4(1-\alpha)^{-4/3}+1/20$

^aThis model does not follow Eq.(2.43), but is included for the sake of completeness


 Figure 2.2: Isothermal plots of $d\alpha/dt$ vs α for deceleratory conversion models

Nucleation models (P,)

Nucleation models are commonly used to describe many processes in solid-state reactions including decomposition [81, 82], adsorption [83, 84], hydration [85], desolvation [86] and crystallization [87–89]. Nucleation happens at so called nucleation sites. There, the activation energy is reduced due to imperfections of the crystal lattice, like point defects, cracks, edges or surfaces [90, 91]. In case of a decomposition following the reaction scheme given by Eq.(1.3) the new phase B is formed in the lattice of A. The volume of the new phase can be calculated by

Figure 2.3: Isothermal plots of $d\alpha/dt$ vs α for constant conversion modelsFigure 2.4: Isothermal plots of $d\alpha/dt$ vs α for sigmoidal conversion models

$$V(t) = \int_0^t v(t) \left(\frac{dN}{dt} \right)_{t=t_0} dt_0 \quad (2.50)$$

where $v(t)$ is the volume of a single nucleus at time t that was formed at t_0 and dN/dt the nucleation rate.

The volume of the single nucleus can be calculated by

$$v(t) = \sigma(r(t, t_0))^\lambda \quad (2.51)$$

where σ is the shape factor (e.g. $4\pi/3$ for a sphere) and λ is the growth dimension (i.e. $\lambda = 1, 2$ or 3) and $r(t, t_0)$ the radius at time t of a nucleus, that was formed at time t_0 . The radius $r(t, t_0)$ can be calculated from the rate of nucleus growth given by Eq.(2.52).

$$r(t, t_0) = \int_{t_0}^t \Theta(\tau) d\tau \quad (2.52)$$

Inserting Eqs.(2.51) and (2.52) into Eq.(2.50) leads to

$$V(t) = \int_0^t \sigma \left(\int_{t_0}^t \Theta(\tau) d\tau \right)^\lambda \left(\frac{dN}{dt} \right)_{t=t_0} dt_0 \quad (2.53)$$

Assuming a simple case, where the nucleation rate follows a power law

$$\frac{dN}{dt} = D\gamma t^{\gamma-1} \quad (2.54)$$

and the nucleation growth rate is constant

$$\Theta(t) = k_\Theta \quad (2.55)$$

the volume of all nuclei can be calculated by

$$V(t) = \int_0^t \sigma (k_\Theta(t - t_0))^\lambda D\gamma t_0^{\gamma-1} dt_0 \quad (2.56)$$

Solving the integral [92] leads to

$$V(t) = \underbrace{\sigma k_\Theta^\lambda t^{\gamma+\lambda} D\gamma \left(1 - \frac{\lambda\gamma}{\gamma+1} + \frac{\lambda(\lambda-1)\gamma}{2!(\gamma+2)} \dots \right)}_{D'} = \sigma k_\Theta^\lambda t^{\gamma+\lambda} D' \quad \lambda \leq 3 \quad (2.57)$$

The volume $V(t)$ is directly proportional to the conversion given by

$$\alpha = \frac{V(t)}{V_0} \quad (2.58)$$

where V_0 is the initial volume. With $n = \lambda + \gamma$ and inserting Eq.(2.57) into Eq.(2.58) results



Figure 2.5: Two different types of nuclei growth restrictions: ingestion (a), coalescence (b) Black dots represent nucleation sites, gray areas the build up phase.

in

$$\alpha = \frac{\sigma k_{\Theta}^{\lambda} D'}{V_0} t^n = \left(\underbrace{\left(\frac{\sigma k_{\Theta}^{\lambda} D'}{V_0} \right)^{1/n}}_k t \right)^n = (kt)^n \quad (2.59)$$

Rearranging Eq.(2.59) leads to the integral form of the different P-models Eq.(2.60)

$$\alpha^{1/n} = kt \quad (2.60)$$

These models assume constant nuclei growth without any growth restrictions. Nevertheless, two restrictions for solid-state decompositions have been identified: ingestion and coalescence (Figure 2.5) [93]. Ingestion describes the reduction of possible nucleation sites by growth of an existing nucleus (Figure 2.5a). Coalescence is the loss of reactant interface when reaction zones of two growing nuclei merge.

The number of possible nucleation sites $N(t)$ can be calculated by [94]

$$N(t) = N_0 - N_1(t) - N_2(t) \quad (2.61)$$

where N_0 are the possible nuclei forming sites, N_1 the number of already activated nuclei and N_2 the ingested nuclei. Developing a nucleation rate dN/dt from Eq.(2.61) and substituting into Eq.(2.53) results in an expression without analytical solution [92]. Avrami [95] proposed an extended conversion α' to overcome this problem. The extended conversion α' ignores ingestion of nucleation sites and follows Eq.(2.59). Avrami related the actual conversion α to α' by

$$d\alpha' = \frac{d\alpha}{1 - \alpha} \quad (2.62)$$

Integration of Eq.(2.62) gives

$$\alpha' = -\ln(1 - \alpha) \quad (2.63)$$

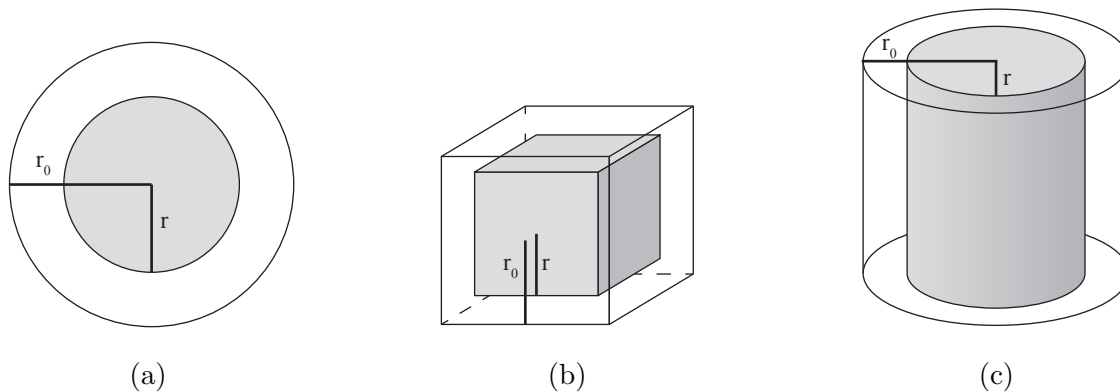


Figure 2.6: Typical geometrical model assumptions about particle shapes: sphere (a), cube (b), cylinder (c)

Inserting Eq.(2.59) into Eq.(2.63) and rearranging leads to

$$(-\ln(1-\alpha))^{1/n} = kt \quad (2.64)$$

This is the general form of the Avrami-Erofeyev models. Erofeyev [96] derived Eq.(2.64) for $n = 3$ on a different way, and was therefore also attributed to the models.

Interface models (R)

Interface models (also known as geometrical contraction models) model the availability of reactive sites on the surface of the reacting particle. Thus the reaction progress is directly dependent on the available surface of the particle. Depending on particle shape different mathematical descriptions can be derived (Table 2.3). The first assumption necessary is the shape of the reacting particle. Figure 2.6 shows the most commonly applied shapes and their characteristic radii. Furthermore, it is assumed that the characteristic radius of the particle decreases linearly with time [97], following

$$r = r_0 - k_1 t \quad (2.65)$$

where r is the radius of the particle at time t , r_0 is the radius at t_0 and k_1 a reaction rate constant.

Contracting volume model - R3 If a spherical particle with constant density is assumed, then the unreacted mass m at time t can be written as

$$m = \frac{4}{3}\rho\pi r^3 \quad (2.66)$$

With Eq.(2.66), the definition of the conversion α Eq.(2.31) can be written as

$$\alpha = \frac{m_0 - m}{m_0} = \frac{\frac{4}{3}\rho\pi r_0^3 - \frac{4}{3}\rho\pi r^3}{\frac{4}{3}\rho\pi r_0^3} \quad (2.67)$$

and simplified to

$$\alpha = \frac{r_0^3 - r^3}{r_0^3} = 1 - \frac{r^3}{r_0^3} \quad (2.68)$$

Note, the assumption of a cubic particle also leads to Eq.(2.68), as in both cases $m \propto r^3$. After inserting Eq.(2.65) into Eq.(2.68) and rearranging Eq.(2.69) can be found.

$$1 - \alpha = \left(1 - \frac{k_1}{r_0}t\right)^3 \quad (2.69)$$

With $k = k_1/r_0$ the integral form of the contracting sphere model is found as

$$1 - (1 - \alpha)^{1/3} = kt = g(\alpha) \quad (2.70)$$

Contracting area model - R2 The model is derived in the same way as the contracting volume model R3. The only difference is that the particle form is assumed to be cylindrical with only the jacket reacting, hence $m \propto r^2$. This leads to

$$\alpha = \frac{r_0^2 - r^2}{r_0^2} = 1 - \frac{r^2}{r_0^2} \quad (2.71)$$

Thus, following the derivation of the contracting volume model, the integral form of the contraction area model is found

$$1 - (1 - \alpha)^{1/2} = kt = g(\alpha) \quad (2.72)$$

Order based models (F)

Order based models originate from homogeneous kinetics. There, the reaction rate is proportional to the concentration of the reacting substance raised to a power of n , which is called the reaction order. For an elementary reaction the reaction order n is equal to the sum of all involved molecules. For heterogenic reactions the elementary steps are often not measurable, thus the reaction order has little meaning. Nevertheless, order based models are often used to describe measurement data mathematically since they are easy to fit. They are based on the n^{th} order equation (Fn)

$$\frac{d\alpha}{dt} = k(1 - \alpha)^n \quad (2.73)$$

If a first order model (F1) is assumed, then $n = 1$ which leads to

$$\frac{d\alpha}{dt} = k(1 - \alpha) \quad (2.74)$$

Solving this differential equation leads to the integral form of the first order model

$$-\ln(1 - \alpha) = kt \quad (2.75)$$

This model is also called a Maple model, and represents a special case of the Avrami-Erofeyev with $n = 1$.

For order based models with $n \neq 1$ solving the differential problem Eq.(2.73) leads to the integral form of the n^{th} order model

$$\frac{1 - (1 - \alpha)^{1-n}}{1 - n} = kt \quad (2.76)$$

Diffusion controlled models (D)

Diffusion models focus on one of the biggest difference between homogeneous and heterogeneous reactions, the immobility of certain phases. In a homogeneous system the reaction products are homogeneously distributed throughout the system, while in a heterogeneous system the products can form a layer around the reacting educt phase. The formed layer can impede further reaction progress. In diffusion controlled reactions, the reaction rate decreases proportionally to the thickness of the built-up product layer. The simplest diffusion model D1 assumes an one-dimensional diffusion between two planes as depicted in Figure 2.7a. This derivation assumes the formation of component A according to reaction equation Eq.(1.3). There B and C are the reactants and A is the formed product layer. Since the diffusion is assumed to be the rate limiting step, the build-up of the product layer is proportional to the transported mass of gaseous reactant C given by

$$\frac{dl}{dt} = -D \frac{M_A}{M_C \rho} \frac{dc}{dx} \quad (2.77)$$

where l is the thickness of the product layer, D the diffusion coefficient, M_A and M_C the molar masses of A and C, respectively, ρ the density of A, c the concentration of C in the product layer and x the distance from the interface Ψ . When a linear concentration gradient of C between the interfaces Ψ and Φ (see Figure 2.7a) is assumed then Eq.(2.77) becomes

$$\frac{ds}{dt} = -D \frac{M_A}{M_C \rho} \frac{c_\Phi - c_\Psi}{l} \quad (2.78)$$

where c_Φ and c_Ψ are the concentrations of C at the interfaces Φ and Ψ . Solving the differential equation given by Eq.(2.78) results in

$$l^2 = -D \frac{M_A}{M_C \rho} (c_\Phi - c_\Psi) t \quad (2.79)$$

When substituting $k' = -D (c_\Phi - c_\Psi) M_A / (M_C \rho)$ Eq.(2.79) becomes what is known as the parabolic law of diffusion

$$l^2 = k' t \quad (2.80)$$

For an one dimensional problem the conversion is proportional to the thickness of the formed product layer ($\alpha \propto l$), thus from Eq.(2.80) follows

$$\alpha^2 = k t \quad (2.81)$$

This is the one-dimensional diffusion model 'D1'. In this model no geometric shape factors are included. For a spherical particle (Figure 2.7b) the three-dimensional diffusion model 'D3' can be derived. Starting by formulating the correlation between the conversion and the thickness of the product layer l

$$\alpha = \frac{\frac{4}{3}\rho\pi r_0^3 - \frac{4}{3}\rho\pi(r_0 - l)^3}{\frac{4}{3}\rho\pi r_0^3} \quad (2.82)$$

which can be simplified and rearranged to

$$l = r_0(1 - (1 - \alpha)^{1/3}) \quad (2.83)$$

Jander [98] used the parabolic law Eq.(2.80) to describe the progression of l . Combining the Eq.(2.80) and Eq.(2.83) leads to the three-dimensional diffusion model 'D3' or Jander model

$$(1 - (1 - \alpha)^{1/3})^2 = k t \quad (2.84)$$

with $k = k' / r_0^2$.

Other models assume different concentration gradients (e.g. the concentration c depends on α) and/or geometric shapes (e.g. cylindrical models). Their detailed derivation can be found in the literature [78] [79].

2.2.4 Pressure dependency models

In contrast to conversion dependency models are pressure dependency models not very well developed. The models used to describe the pressure dependency $h(p)$ are generally empirical and allow only limited physical interpretation. The models considered in this work are given in Table 2.6. They were commonly found in the literature. Since none of these pressure

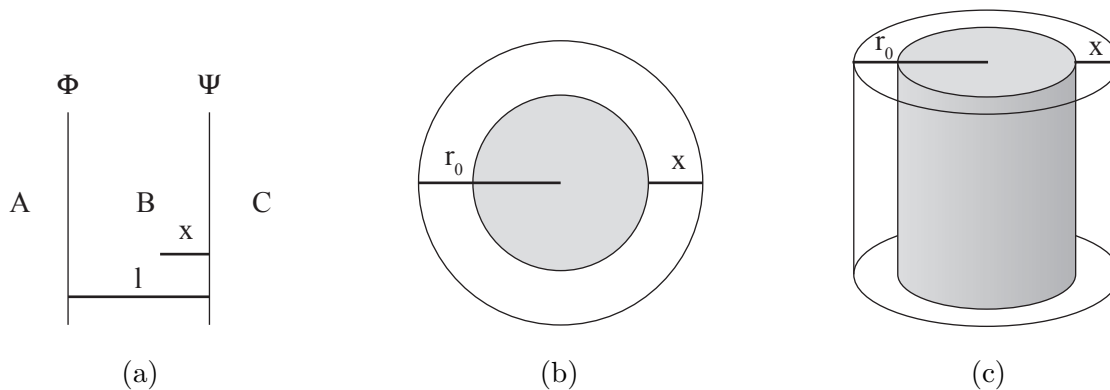


Figure 2.7: Schematic representation of the product layer buildup in diffusion models: 1-D plane (a), spherical particle (b), cylinder (c)

Table 2.6: Different models for the pressure dependency $h(p)$ (greek symbols are model parameters)

identifier	$h(p)$	Literature
p1	p^x	[100]
p2	$(\omega - p)^\psi$	[101]
p3	$p^x(\omega - p)^\psi$	
p4	$\exp(\chi p)$	[102]

dependency models have a sound physical foundation the resulting equations should be considered mathematical expressions rather than physical models. Model p2 is sometimes used to include the effect of the chemical equilibrium on the reaction kinetic. Then the model parameter ω represents the equilibrium pressure at given the temperature [99].

2.3 Kinetic identification

Most methods assume that the temperature dependency $k(T)$ follows the Arrhenius equation Eq.(2.34) and identify a so called kinetic triplet. It consists out of the conversion dependency $f(\alpha)$, the activation energy E_a and the pre exponential factor A . The pressure dependency $h(p)$ is normally incorporated in the identified Arrhenius parameter and can only be detected by the identified variation of the E_a and A at different pressure levels. The presented methods assume isobaric conditions ($p = p_1$), thus Eq.(2.40) holds. A direct identification of $h(p)$ is not described in the literature. Most methods can be divided into four different groups. First, a distinction according to the analyzed measurement data can be made. Most methods are developed for either isothermal or isokinetic measurements. In the literature isokinetic measurements are often referred to as non isothermal measurements, which technically is correct. Since non isothermal measurements also include measurements with an arbitrary

temperature profile, which most identification methods can not handle, the more specific term isokinetic is used here. Second, the methods can be divided into model-based and model-free² methods.

2.3.1 Model-fitting methods

Model-fitting methods are performed in two steps. First, fit a conversion model onto the data. In most cases the conversion model is distinguished by the goodness of fit of the respective model. Second, based on this fit E_a and A' are determined. Thus the accuracy of E_a and A' directly depends on whether the correct conversion model has been found.

Direct differential method

The direct differential method uses the logarithmic form of the isokinetic rate law Eq.(2.39) [103] on one isokinetic measurement.

$$\ln \frac{\frac{d\alpha}{dt}}{f(\alpha)} = \frac{-E_a}{RT} + \ln \frac{A'}{\beta} \quad (2.85)$$

The left hand side of Eq.(2.85) is plotted for different conversion dependencies $f(\alpha)$ against $1/T$. The model which gives the best linear fit is chosen as the conversion dependency model and the activation energy E_a calculated from its slope. From its intercept the product A' can be calculated.

Coats-Redfern method

Coats and Redfern developed an isokinetic identification method based on the integral form of the isokinetic rate law Eq.(2.45) [65, 104]. They used the asymptotic series expansion (see Appendix) and truncated it after the second term, to approximate $q(x)$. This leads to

$$\ln \frac{g(\alpha)}{T^2} = \ln \left(\frac{A'R}{\beta E_a} \left[1 - 2 \frac{RT_{mean}}{E_a} \right] \right) - \frac{E_a}{RT} \quad (2.86)$$

where T_{mean} is the mean temperature of the measurement. This linearization is used to plot its left-hand side against $1/T$ to calculate the activation energy E_a and the product A' . Since the left-hand side depends on the chosen model $g(\alpha)$, the quality of the linear fit changes with the model. The one, resulting in the best linear fit is assumed to be the correct one.

²Sometimes the term "isoconversional" is used instead of "model-free", however not all model-free methods are isoconversional methods

Kissinger method

The Kissinger method calculates kinetic parameters based on different isokinetic DTA measurements. It analyses the change in position of the peak maxima as result of different heating rates β . For reaction-order models (Fn), it was proposed by Kissinger [105, 106] and generalized by Chen et al. for any reaction model [107].

At the position of the peak maxima the second differential of Eq.(2.35) should be equal to 0.

$$\frac{d^2\alpha}{dt^2} = A' f(\alpha) e^{-E_a/(RT)} \frac{E_a}{RT^2} \frac{dT}{dt} + A' e^{-E_a/(RT)} f'(\alpha) \frac{d\alpha}{dt} = 0 \quad (2.87)$$

with $f'(\alpha) = df(\alpha)/d\alpha$. Rearranging Eq.(2.87) and substituting Eq.(2.37) gives

$$f(\alpha_m) \frac{E_a \beta}{RT_m^2} = f'(\alpha_m) \left. \frac{d\alpha}{dt} \right|_m \quad (2.88)$$

where the index m denotes the respective values at peak maximum. All necessary information can be obtained by DTA. The activation energy E_a can be calculated from Eq.(2.88) when a conversion dependency model is known or assumed. The product A' is calculated from Eq.(2.35) subsequently.

2.3.2 Model-free methods

Model-free (isoconversional) methods allow the determination of E_a without prior assumptions about the conversion model. E_a is identified at different values of α . The identification requires multiple kinetic curves. [108–110]

Standard isoconversional method

The standard isoconversional method is based on the logarithmic form of the isothermal integral rate law Eq.(2.43).

$$\ln g(\alpha) = \ln(A') - \frac{E_a}{RT} + \ln t \quad (2.89)$$

Rearranging Eq.(2.89) results in

$$-\ln t = \ln \frac{A'}{g(\alpha)} - \frac{E_a}{RT} \quad (2.90)$$

The left hand side of Eq.(2.90) can be plotted against $1/T$ for each α . From the resulting slope E_a can be calculated with

$$-\ln t_\alpha = \ln \frac{A'}{g(\alpha)} \Big|_\alpha - \frac{E_{a\alpha}}{RT_\alpha} \quad (2.91)$$

Friedman's isoconversional method

Friedman's isoconversional method was one of the first isoconversional methods [111]. The method uses multiple isothermal measurements to calculate the activation energy E_a of a reaction based on the logarithm of the differential rate law Eq.(2.35)

$$\ln \frac{d\alpha}{dt} = \ln(A'f(\alpha)) - \frac{E_a}{RT} \quad (2.92)$$

The left hand side of Eq.(2.92) can be plotted against $1/T$ for a constant α in different measurements following

$$\ln \frac{d\alpha}{dt} \Big|_\alpha = \ln(A'f(\alpha_\alpha)) - \frac{E_{a\alpha}}{RT_\alpha} \quad (2.93)$$

The slope of such plots gives the activation energy E_a with respect to the conversion α .

Ozawa, Flynn and Wall (OFW) method

This method was developed by Flynn and Wall [62, 77] and Ozawa [112] for the calculation of the activation energy E_a based on isokinetic data. By taking the decadic logarithm of Eq.(2.46) the following equation is obtained

$$\log g(\alpha) = \log \frac{A'E_a}{\beta R} + \log q(x) \quad (2.94)$$

Inserting the Doyle approximation (Eq.(2.48)) and substitution the temperature integral transformation $x = E_a/(RT)$ leads to

$$\log g(\alpha) = \log \frac{A'E_a}{\beta R} - 2.315 - 0.4567 \frac{E_a}{RT} \quad (2.95)$$

Rearranging Eq.(2.95) gives a linear correlation between $\log \beta$ and $1/T$.

$$\log \beta = \log \frac{A'E_a}{g(\alpha)R} - 2.315 - 0.4567 \frac{E_a}{RT} \quad (2.96)$$

Plotting $\log \beta$ against $1/T$ for different isokinetic measurements at constant α yields the activation energy E_a independent of the conversion model $g(\alpha)$ according to

$$\log \beta = \log \frac{A'E_a}{g(\alpha)R} \Big|_\alpha - 2.315 - 0.4567 \frac{E_{a\alpha}}{RT_\alpha} \quad (2.97)$$

Modified Coats-Redfern method

This is a modification of the model-fitting Coats-Redfern method, done by Burnham and Braun [113]. They rearranged the original model fitting method Eq.(2.86) to an isoconversional method

$$\ln \frac{\beta}{T^2} = \ln \left(\frac{A'R}{g(\alpha)E_a} \left[1 - 2 \frac{RT_{mean}}{E_a} \right] \right) - \frac{E_a}{RT} \quad (2.98)$$

Plotting $\ln(\beta/T^2)$ against $1/T$ for multiple isokinetic measurements at constant α yields the activation energy E_a independent of the reaction model according to

$$\ln \frac{\beta}{T^2} \Big|_{\alpha} = \ln \left(\frac{A'R}{g(\alpha)E_a} \left[1 - 2 \frac{RT_{mean}}{E_a} \right] \right) \Big|_{\alpha} - \frac{E_{a\alpha}}{RT_{\alpha}} \quad (2.99)$$

Chapter 3

Search for TCES systems

This chapter is a modification of:

Markus Deutsch, Danny Müller, Christian Aumeyr, Christian Jordan, Christian Gierl-Mayer, Peter Weinberger, Franz Winter and Andreas Werner

Systematic search algorithm for potential thermochemical energy storage systems

Applied Energy, 183:113-120,2016

DOI: 10.1016/j.apenergy.2016.08.142

3.1 Goal of the search

Section 1.2 shows that there is a multitude of different application for TCES, each with its own set of requirements. Most critical are the various temperature levels of the heat source. Due to thermodynamic limitations each TCES system is efficiently applicable only in a specific temperature range. For maximum storage efficiency, it is mandatory that a TCES system fits to the required temperature level. So far only a limited number of TCES systems are under development making it hard to find a proper system. In this section an algorithm is presented, to systematically search for new principally suitable TCES system. Those will be stored in a TCES database, where they are listed and assessed regarding their potential applicability. The entries in the database include products and educts of the reaction, equilibrium temperatures and, for selected promising candidates, also experimental data regarding material properties, reversibility of the TCES reaction, cycle stability and storage density.

3.2 Basis of the search

The focus of this search algorithm lies on reactions of solid inorganic substances with a reactive gas, following general reaction



This focus on gas/solid reaction was done since the separation of solid components from gaseous components can be achieved easily. In contrast, for solid/liquid systems the separation is more energy consuming, resulting in a reduced storage capacity. Additionally, solid/liquid systems are contend with solubility of the solid reactants [114]. Furthermore, only one gaseous component is allowed avoiding the need of sophisticated gas separation systems.

The focus on inorganic substances was necessary due to the limitations of the search algorithm. While inorganic reactions can be identified by comparison of molecular formulas, for most organic reactions the structural formula of each reactant has to be considered. This would result in a steep increase in the complexity of the search algorithm and was therefore neglected in this approach.

3.2.1 Materials

In this first approach, building the basis of our database, a sum of 4528 different materials was taken into account as possible TCES materials. The thermodynamic data was gathered from HSC Chemistry data base [115].

3.2.2 Reactive gases

As outlined before, the investigated reactions were limited to gas-solid reactions. The reactive gases in this work were narrowed down to H₂O, CO₂, O₂, NH₃ and SO₂, as those are all commercially used reactive gases used on industrial scales. Additionally, risks and safety issues regarding handling and storage are known. Due to intrinsic problems on storage and handling, H₂ was excluded as a reactive gas.

3.3 Search algorithm

To find reaction systems suitable for TCES, an algorithm was designed to find all possible reactions for a given set of materials. The algorithm identifies all possible decomposition reactions within the selected boundary conditions (maximal allowed stoichiometric coefficient) represented by reaction 3.1.

Figure 3.1 shows a graphical visualization of the algorithm. It consists of three intertwined loops to determine the stoichiometric indices ν_A (loop I), ν_B (loop III) and ν_C (loop II). In the following, the methodology is discussed and the determination of ν_A , ν_B and ν_C is explained based on examples.

The concept behind the search algorithm is the rearrangement of a stoichiometric equation. From a mathematical point of view reaction 3.1 is identical to reaction 3.2.



Hence, a stoichiometric correct reaction is obtained, if the subtraction of reactive gas C from substance A results in an elemental composition EC , for which a substance B can be found in the database.

In case of reaction 3.3, the subtraction of the elemental composition of H_2O (2 H, 1 O with 1 and 2 being the elemental indices) from the elemental composition of $Mg(OH)_2$ (1 Mg, 2 O, 2 H) results in a composition (1 Mg, 1 O) which correlates to the database entry of magnesia oxide MgO .



To identify reactions which require multiple subtractions of C, (see reaction 3.4) the stoichiometric coefficient ν_C is increased incrementally until the subtraction is no longer possible (loop II). During each iteration, the resulting EC is checked against the database. A positive hit in the database is followed by the output of the corresponding substances as suitable TCES reaction. Subsequently or on a negative database request, the loop is repeated until the calculation of EC is no longer possible.



If a subtraction of ν_C -times of C is not possible for the current ν_C , the algorithm increases the stoichiometric coefficient ν_A incrementally and starts again to subtract one C (loop I). This is necessary to find reactions like reaction 3.5, where more than 1 molecule of A is needed to obtain a balanced reaction equation with integers. Loop I is repeated until $\nu_A > \nu_{A,max}$ ($\nu_{A,max}$ is given by the user).



To identify reactions with $\nu_B \neq 1$, like reaction 3.6, the calculated EC of each subtraction is further analyzed in loop III (Figure 3.2).

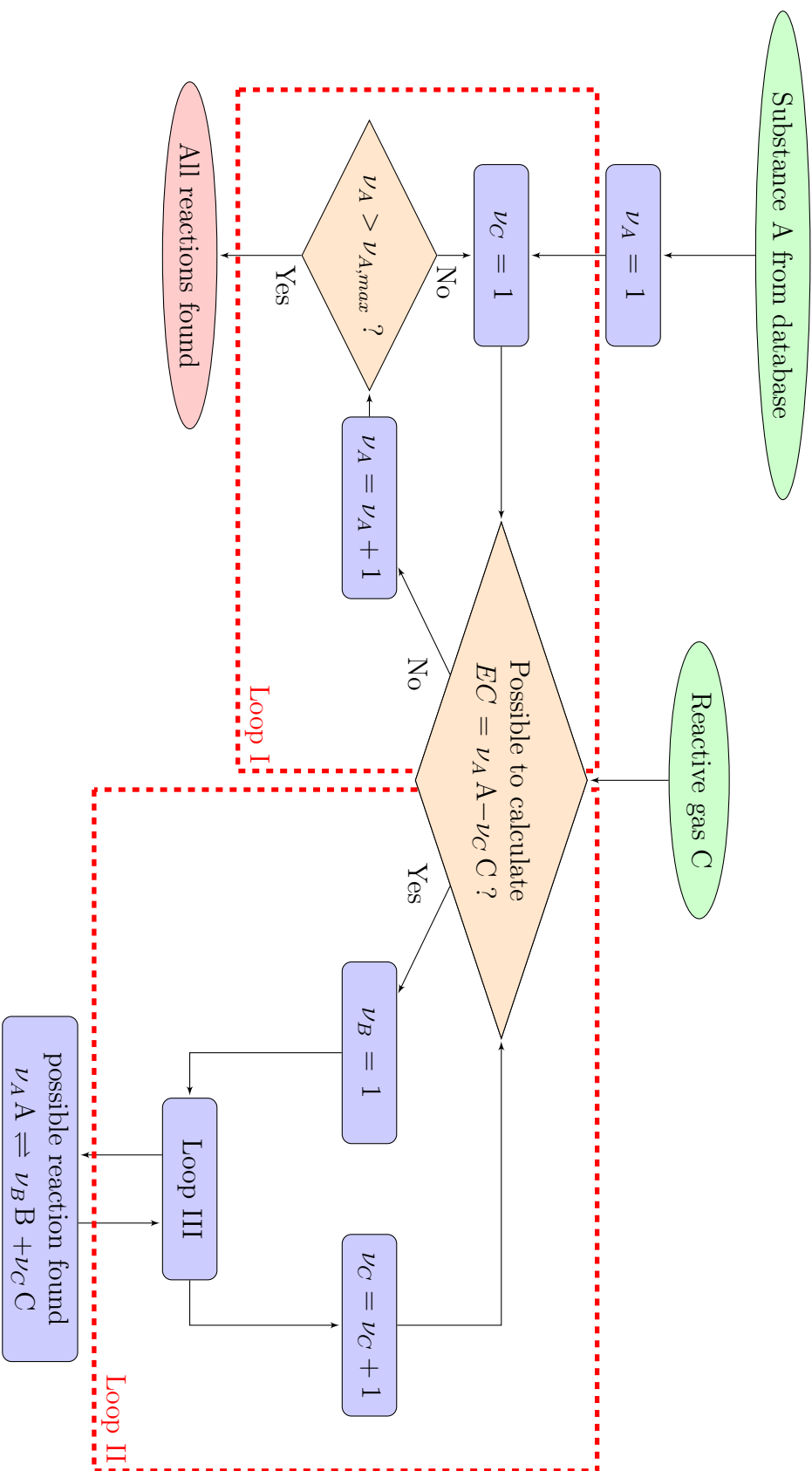


Figure 3.1: Graphical representation of the search algorithm

element	ν_B		
	1	2	4
Mn	12	6	3
O	16	8	4

Table 3.1: Possible elemental compositions EC^* for reaction 3.6 found in loop III

Therefore, the highest possible value for ν_B , $\nu_{B,max}$, is determined based on the calculated elemental composition EC . In case of reaction 3.6 EC is 12 Mn and 16 O based on Eq.(3.2) with $\nu_A = 6$ and $\nu_C = 1$. $\nu_{B,max}$ is calculated as the lowest elemental index of EC , since it is the highest integer still able to divide EC without remainder. In this case $\nu_{B,max} = 12$ due to Mn.

To find all possible combinations, at first, a reaction with $\nu_B = 1$ is assumed. An intermediary elemental composition is calculated as $EC^* = EC/\nu_B$. EC^* is checked against the database to find a substance with a matching elemental composition. Then ν_B is increased by one. If the division of all elemental indices of EC with the new ν_B is possible without a remainder ($EC \bmod \nu_B = 0$), another possible elemental composition $EC^* = EC/\nu_B$ is found and subsequently checked against the database. This is repeated until $\nu_B > \nu_{B,max}$. For reaction 3.6 all possible ν_B and the corresponding elemental compositions EC^* are given in Table 3.1. Only for $\nu_B = 4$ can a substance with a matching elemental composition (Mn_3O_4) be found in the database.

It should be noted, that this approach identifies all numerically possible reactions. The further discrimination of these hits regarding their chemical significance is given in section 3.4.5.

3.4 Search results

The search for each reactive gas was performed with $\nu_{A,max} = 6$ to cover reactions like reaction 3.6. For the five reactive gases (H_2O , CO_2 , NH_3 , SO_2 , O_2) more than 1700 unique reactions were found. A comprehensive list of all reactions can be found on the project's homepage solidheat.project.tuwien.ac.at and in the appendix. For each reaction the equilibrium temperature T_{equ} has been calculated following Eq.(2.29) based on the thermodynamic data from HSC database and assuming a pressure of the reactive gas of 1 bar.

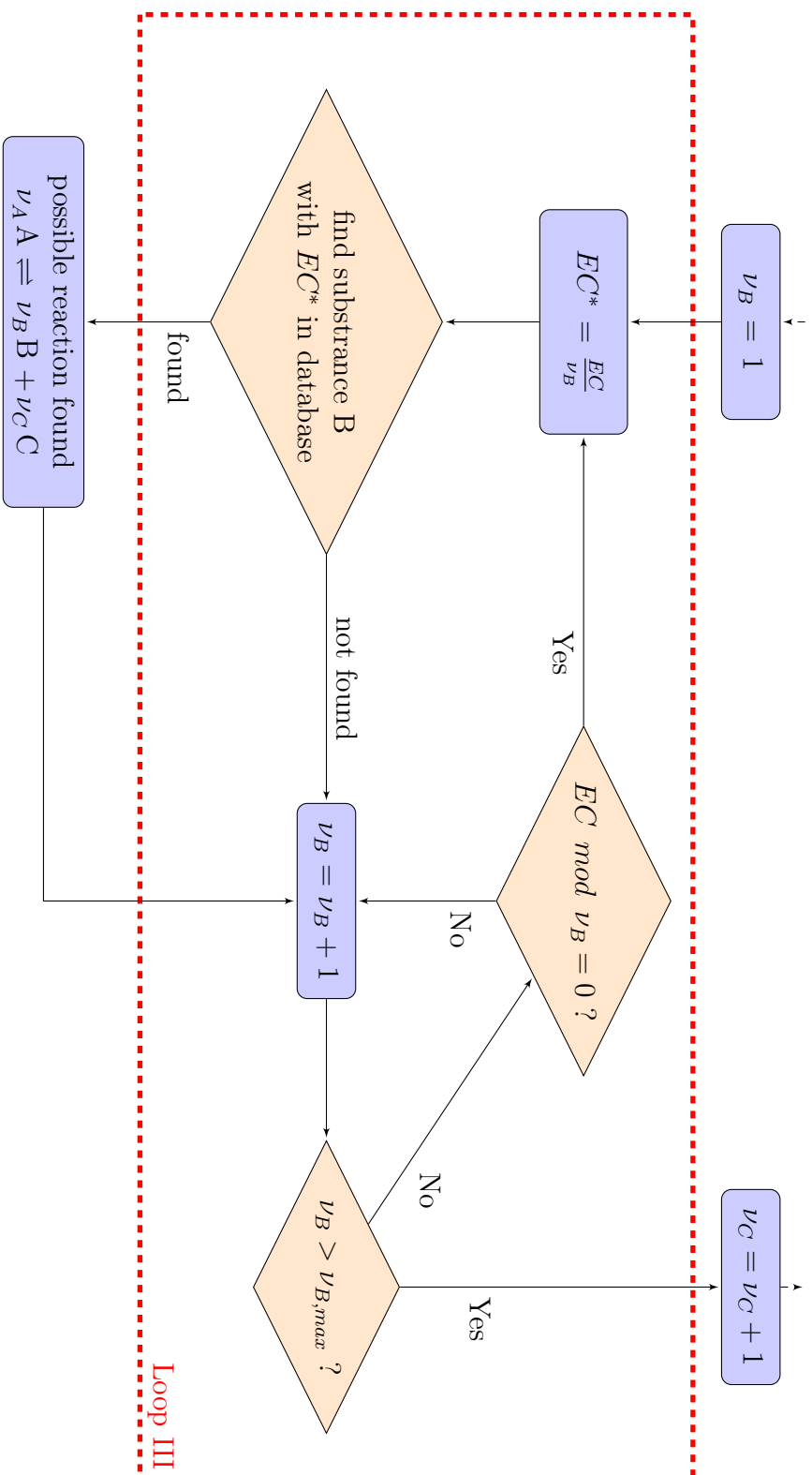


Figure 3.2: Detailed graphical representation of loop III for the determination of ν_B

reactive gas	Temperature level of T_{equ}			Σ
	<100 °C	100-400 °C	>400 °C	
H ₂ O	203	321	29	553
CO ₂	1	22	17	40
NH ₃	15	20	4	39
SO ₂	0	2	26	28
O ₂	12	70	443	525
Σ	231	435	519	1185

Table 3.2: Number of reactions identified with T_{equ} in the respective temperature level for each reactive gas

For a reaction principally suitable as TCES system two criteria have to be met:

$$\Delta G_R(25\text{ °C}, 1\text{ bar}) > 0 \quad (3.7a)$$

$$\Delta H_R(T_{equ}, 1\text{ bar}) > 0 \quad (3.7b)$$

Criterion 1 Eq.(3.7a) defines the decomposition reaction for 25 °C as disfavored (based on Eq.(2.29)), thus non-spontaneous. Therefore, at room temperature no decomposition will occur, which is obligatory for storage without energy loss. Criterion 2 Eq.(3.7b) follows the requirement that the reaction is endothermic at T_{equ} and therefore capable of storing energy while it decomposes.

Additionally, at this point only reactions with T_{equ} within the range of 25-2000 °C are considered relevant.

Thereby, the number of potential TCES systems is reduced to 1185 reactions. Table 3.2 gives the number of identified reactions per temperature level for each reactive gas based on T_{equ} . In Figure 3.3 the distribution of the identified reactions is shown. The energy content is calculated as ΔH_R at T_{equ} for one kilogram of substance A of each reaction, therefore, representing the theoretical energy amount stored in 1 kg material in its discharged state. Due to the high number of identified reactions with H₂O, those reactions are separated into reactions of hydroxides and metal hydrates.

A comparison of the different reactive gases is given in Figure 3.4. The area for each gas marks the range where the majority of reactions are identified. To take into account that reactions with a higher T_{equ} are more sparse than with lower T_{equ} , as seen in Figure 3.3, the reactions identified for each reactive gas were clustered. Figure 3.5 shows the clustering exemplary for the reactions of hydroxides. First two clusters were calculated, utilizing *k-means* clustering

based on the normed euclidean distances [116]. Then, from each cluster 80% of the reactions closest to the corresponding cluster centre are together surrounded by one convex hull. The line in Figure 3.5 is equivalent to the line for H₂O-hydroxides in Figure 3.4. In the following the identified reactions for different reactive gases are discussed further.

3.4.1 Reactions with H₂O

The search with H₂O as reactive gas resulted in 553 identified reactions. They consist of reactions of metal hydroxides (47 reactions) and metal salt hydrates (506 reactions). The metal salt hydrates can be reduced to 206 decomposition reactions of different materials, excluding changes between different hydrate contents. As shown in Figure 3.4, the reactions of metal salt hydrates mostly occur in a temperature range from room temperature to 500 °C, while the decomposition reactions of metal hydroxides can be found up to 1000 °C. All found reaction are listed in Table 6.1.

3.4.2 Reactions with CO₂

In total 40 reactions of CO₂ as reactive gas were identified. This class consists mainly of carbonates and a few oxalates, having equilibrium temperatures distributed over the whole temperature range. All found reaction are listed in Table 6.2.

3.4.3 Reactions with NH₃

NH₃ as reactive gas yielded 39 decomposition reactions of 12 different metal salts, all of them having various coordination numbers of ammonia. The equilibrium temperatures are found between room temperature and 600 °C. All found reaction are listed in Table 6.3.

3.4.4 Reactions with SO₂

The search for reactions with SO₂ found 28 possible reactions, all reactions of metal oxides forming sulfates or sulfites. They are found in a temperature range between 400 °C-1500 °C. All found reaction are listed in Table 6.4.

3.4.5 Reactions with O₂

Looking at reaction 3.8a it is evident that due to the approach of the search algorithm reactions are identified which are stoichiometrically correct, but chemically they will not occur. For example, the oxidation of FeS with O₂ occurs according to reaction 3.8b, rather

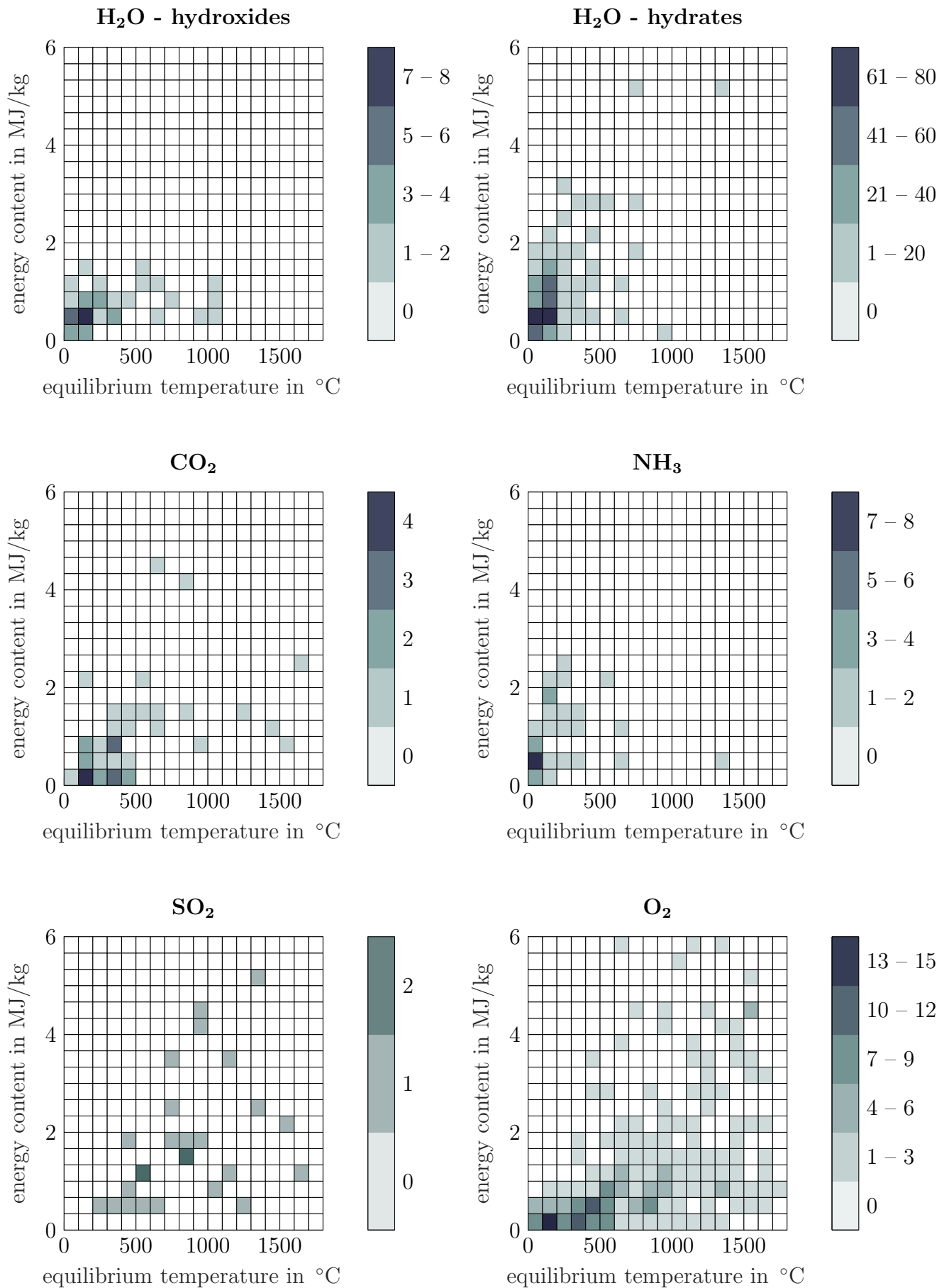


Figure 3.3: Hit distribution maps for the different reactive gases. The color corresponds to the number of reactions identified in the cell. Each cell has a width of 100 °C and a height of 0.33 MJ/kg.

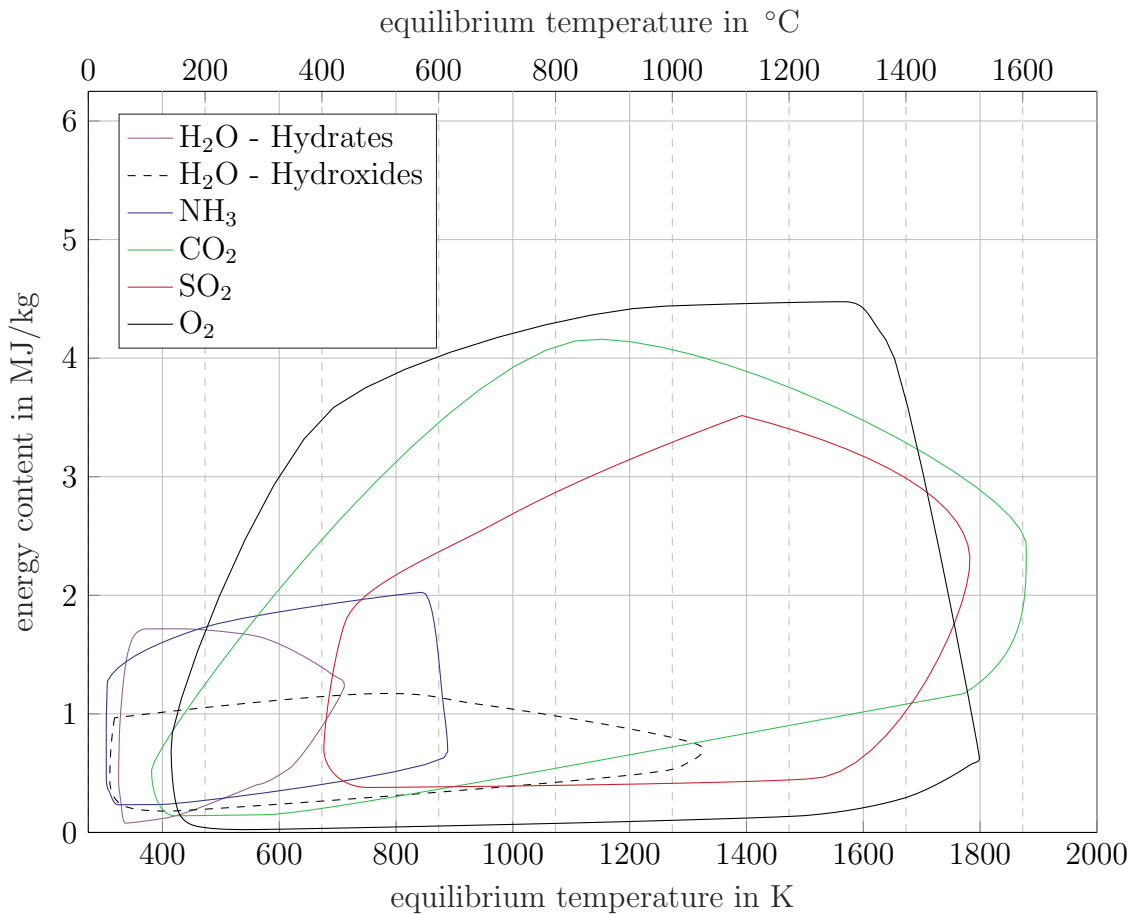


Figure 3.4: Approximated areas within the majority of reactions have been found for each reactive gas.

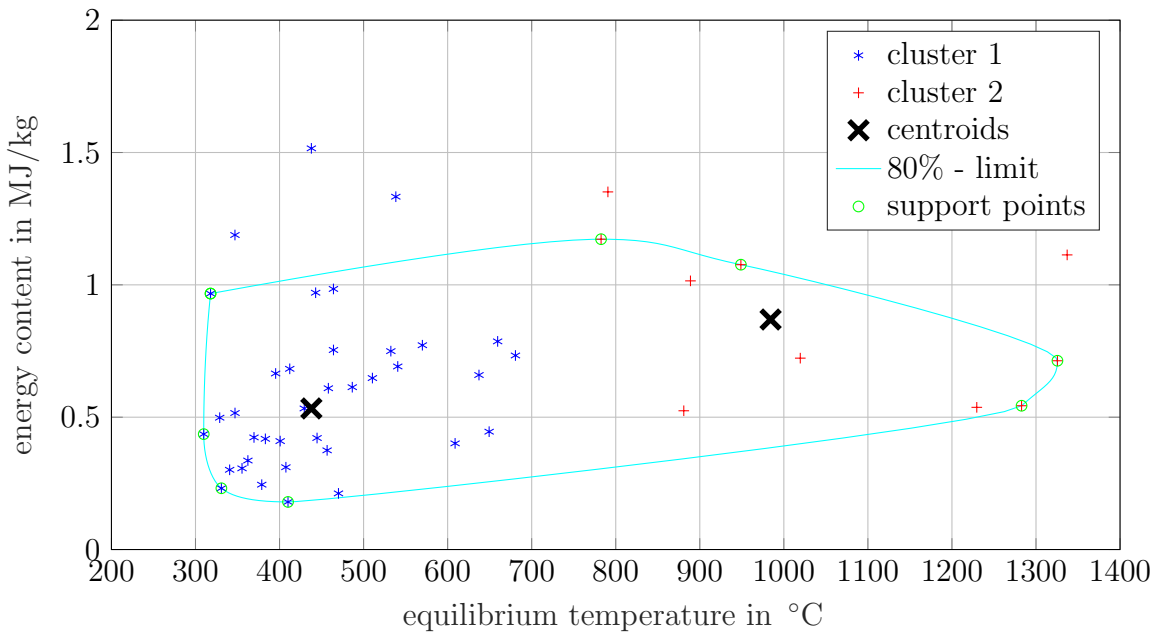


Figure 3.5: Clustering of H_2O -hydroxide reactions into 2 clusters utilizing k - means clustering on normed euclidean distances. The blue line surrounds 80% of the reactions of each cluster and is calculated on the support points (\circ)

than reaction 3.8a. But as reaction 3.8b cannot be generalized via the approach of reaction 3.2, 3.8b is not identified by the algorithm.



In order to reduce the number of reactions, which are stoichiometrically correct but chemically nonsense, they were separated into two classes. The first class included reactions where only O_2 and a metal are involved. This resulted in 248 reactions, which can be further divided into reactions involving an elemental metal (65 reactions) and reactions, where the solid components are both metal oxides, undergoing a change in the oxidation stage of metal (oxides) or the oxygen (peroxides) (overall 183 reactions). All these reactions are assumed to be chemically meaningful.

The second class includes reactions where oxygen, a metal and a non-metal element are involved (like 3.9). It can be assumed that reactions where the oxidation number of the non-metal element changes from positive to negative can be eliminated for a first approach as they are more unlikely to occur. Reactions 3.9 illustrate this, as reaction 3.9b is eliminated while reaction 3.9a is kept. This leads to additional 104 reactions with O_2 for further investigation (173 reactions where removed). All found reaction are listed in Table 6.5.



Chapter 4

The extended NPK method

A modified version of this chapter has been submitted to *Thermochimica Acta* as :
Markus Deutsch, Felix Birkelbach, Christian Knoll, Michael Harasek, Andreas Werner
and Franz Winter

**An extension of the NPK method to include the pressure dependency of
solid state reactions**

4.1 Introduction

To further assess the potential of a TCES system and distinguish between potential candidates for an application, kinetic information about the system is necessary. It is crucial that the time frame in which energy can be stored and released is acceptable, in order to efficiently store and release energy. As the application purpots the operating conditions (temperature, pressure), the TCES system must have an acceptable conversion rate within the given parameters. Furthermore, development of a proper reactor design and a storage concept depend on a reliable kinetic model for the TCES system. Thus, gathering temperature and pressure dependent kinetic information is critical.

Since the literature only provides insufficient methods to identify temperature and pressure dependency, a new method is presented, which allows the combined identification of both dependencies. It is an extension of the NPK method, which was developed by Serra et al. and Sempere et al. [117–120] to identify the temperature and conversion dependency for isokinetic measurements. It was then generalized by Heal [121, 122] for isothermal measurements.

The NPK method does not rely on a priori established models and avoids explicit kinetic models as well as the Arrhenius law. From a mathematical point of view, the only assumptions are the choice of the independent variables and the multiplicativity of the contributions of each factor. In principle, the method separates the effect of conversion α , temperature T

and partial pressure p of the gaseous component C on the conversion rate $d\alpha/dt$. This is done according to the general kinetic equation Eq.(2.33).

Typically, measurements are performed at constant pressure to determine the temperature dependency $k(T)$ and the conversion dependency $f(\alpha)$. This simplifies Eq.(2.33) to the well known expression

$$\left. \frac{d\alpha}{dt} \right|_{p_1} = f(\alpha)k(T)h(p_1) = f(\alpha)k'(T) \quad (4.1)$$

It can be seen that the effect of $h(p_1)$ results in a factor which would usually be incorporated in the temperature dependency when no pressure dependency is considered. This attribution is a result of the common assumption that the temperature dependency follows the Arrhenius equation Eq.(2.34).

Thus, the value of $h(p_1)$ is incorporated in the pre-exponential factor during the identification as $A = A_{Arr}h(p_1)$. Note, that this is always the case for other identification methods (e.g. Ozawa, Flynn and Wall (OFW) method [62, 77, 112], Kissinger method [105, 106]), when the pressure dependency is neglected.

To identify the pressure dependency it is necessary to vary the pressure affecting the reaction. In this work this is the partial pressure of the gaseous component. If the temperature is kept constant during the measurements then Eq.(2.33) can be reduced to

$$\left. \frac{d\alpha}{dt} \right|_{T_1} = f(\alpha)k(T_1)h(p) = f(\alpha)h'(p) \quad (4.2)$$

In this case the contribution of $k(T_1)$ is incorporated into $h'(p)$.

In the following section the identification of $f(\alpha)$, $k'(T)$ and $h'(p)$ from measurement data is described and a novel method is introduced to combine these results to find the full model with $k(T)$ and $h(p)$. Then the method is applied to real data to analyze the decomposition of CdCO_3 .

4.2 Method description and proof of concept

For better understanding and as a proof of concept of the presented method, a single step decomposition reaction based on Eq.(1.3) is assumed. The example reaction follows conversion model 'A1' (see table 2.2), the Arrhenius temperature dependency with $A = 10^9 \text{ s}^{-1}$ and $E_a = 60 \text{ kJ/mol}$ and the pressure dependency 'p2' (see table 2.6) with $\omega = 1$ and $\psi = 4$. This results in the following dependencies:

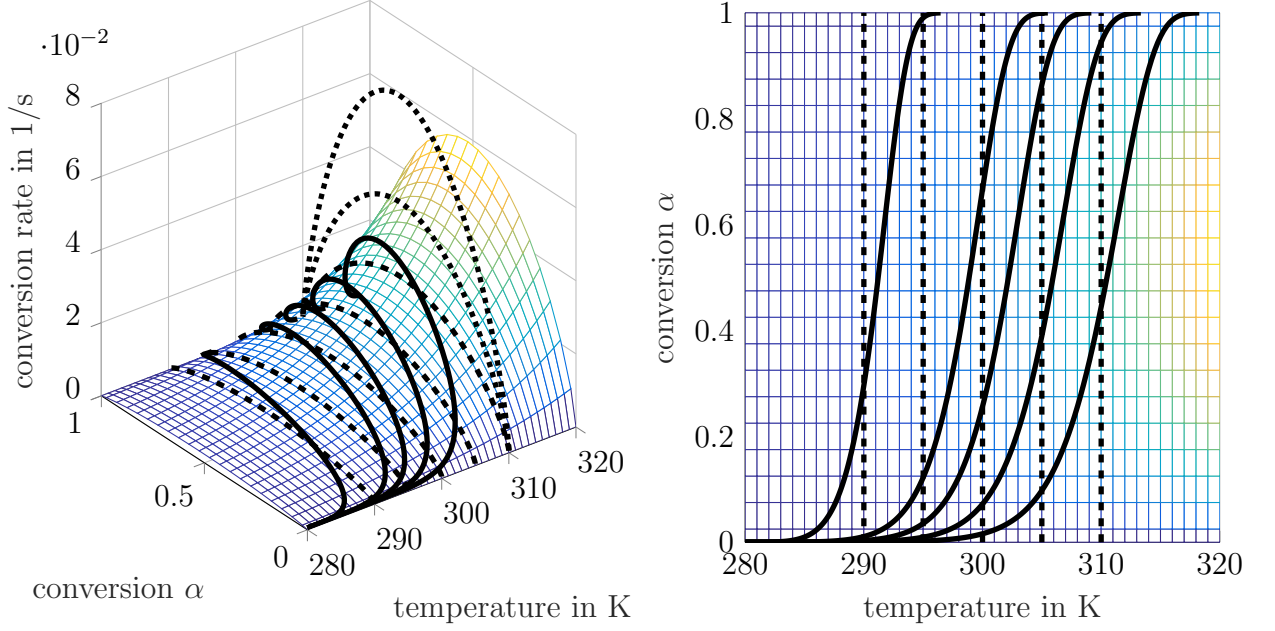


Figure 4.1: Reaction rate surface for the example reaction at constant pressure $p = 0.3$ bar. Solid lines (—) represent isokinetic experiments, dashed lines (---) isothermal experiments, dotted lines (···) the change of the surface with decreasing pressure.

$$f(\alpha) = 4(1 - \alpha)[- \ln(1 - \alpha)]^{3/4} \quad (4.3)$$

$$k(T) = 10^9 \exp\left(\frac{-6 \cdot 10^4}{8.314T}\right) \quad (4.4)$$

$$h(p) = (1 - p)^4 \quad (4.5)$$

The input for the method is generated by simulating measurements based on the example reaction. For the identification of the temperature dependency, isokinetic measurements with a heating rate β of 2, 5, 7, 10 and 15 K/min at $p = 0.3$ bar are simulated. To identify the pressure dependency isothermal measurements at 310 K and different pressure levels (0.1, 0.2, 0.3, 0.4 and 0.5 bar) are simulated.

4.2.1 Identification of $k'(T)$ and $f(\alpha)$

For isobaric conditions, the conversion rate $d\alpha/dt$ in Eq.(4.1) can be visualized as a continuous three dimensional surface in the α - T -space.

Figure 4.1 shows this surface for the example reaction. The lines in Figure 4.1 represent the trajectory of isokinetic measurements (solid) and isothermal measurements (dashed). The dotted lines visualize the change of the surface for isothermal measurements with decreasing pressure.

This surface can be discretized for fixed values of $\boldsymbol{\alpha} = [\alpha_1 \cdots \alpha_l]^T$ and $\mathbf{T} = [T_1 \cdots T_m]^T$ and written in a $(l \times m)$ matrix \mathbf{A}_T ¹ so that the matrix element (i, j) gives the conversion rate at α_i and T_j , as shown in Eq.(4.6).

$$\mathbf{A}_T = \begin{bmatrix} f(\alpha_1)k'(T_1) & f(\alpha_1)k'(T_2) & \cdots & f(\alpha_1)k'(T_m) \\ f(\alpha_2)k'(T_1) & f(\alpha_2)k'(T_2) & \cdots & f(\alpha_2)k'(T_m) \\ \vdots & \vdots & \ddots & \vdots \\ f(\alpha_l)k'(T_1) & f(\alpha_l)k'(T_2) & \cdots & f(\alpha_l)k'(T_m) \end{bmatrix} \quad (4.6)$$

Each element in matrix \mathbf{A}_T corresponds to one grid point of the surface in Figure 4.1. Grid points on an isothermal line correspond to columns in \mathbf{A}_T , while grid points on an isoconversional line correspond to rows.

The matrix \mathbf{A}_T can be written as matrix product

$$\mathbf{A}_T = \mathbf{f}\mathbf{k}'^T = \mathbf{f} \otimes \mathbf{k}' \quad (4.7)$$

with the vectors \mathbf{f} and \mathbf{k}' defined as:

$$\mathbf{f} = \left[f(\alpha_1) \quad f(\alpha_2) \quad \cdots \quad f(\alpha_l) \right]^T \quad (4.8)$$

$$\mathbf{k}' = \left[k'(T_1) \quad k'(T_2) \quad \cdots \quad k'(T_m) \right]^T \quad (4.9)$$

Thus, matrix \mathbf{A}_T is by definition a rank-1 matrix.

Utilizing the singular value decomposition (SVD) [123], the matrix \mathbf{A}_T is decomposed according to Eq.(4.10).

$$\mathbf{A}_T = \sum_{i=1}^n s_i \mathbf{u}_i \otimes \mathbf{v}_i = s_1 \mathbf{u}_1 \otimes \mathbf{v}_1 + \sum_{i=2}^n s_i \mathbf{u}_i \otimes \mathbf{v}_i \quad (4.10)$$

where \mathbf{u} and \mathbf{v} are normalized row and column vectors, respectively and s is the norm of the submatrix.

The SVD returns a successive best first order approximation of the matrix \mathbf{A}_T . Thus, if the assumption of multiplicativity in Eq.(4.1) holds, all but the first singular value will be zero. Since real data contain measurement errors, all singular values will differ from zero. If the reaction follows Eq.(4.1), the first singular value will be bigger than the others. Then the SVD can be truncated after the first term since it is safe to assume that the remaining terms only contain noise.

This simplifies Eq.(4.10) to

¹bold upper-case letters symbolize matrices or tensors, bold lower-case letter vectors

$$\mathbf{A}_T = s_1 \mathbf{u}_1 \otimes \mathbf{v}_1 = s_T \mathbf{u} \otimes \mathbf{v} \quad (4.11)$$

The SVD attributes the variation of the conversion rate to the independent variables α and T .

Comparing Eq.(4.11) to Eq.(4.7) the following correlations can be found:

$$\mathbf{f} = c_1 \mathbf{u} \quad (4.12)$$

$$\mathbf{k}' = c_2 \mathbf{v} \quad (4.13)$$

$$s_T = c_1 c_2 \quad (4.14)$$

with c_1 and c_2 being scaling factors. These are needed, since the scales of the quantities are lost during the matrix decomposition process [121]. This can be seen by means of Eq.(4.14). When c_1 is multiplied by an arbitrary factor and c_2 is divided by the same factor, the result of Eq.(4.11) would not change, but the vectors \mathbf{u} and \mathbf{v} would be scaled. Since the scaling is arbitrary all vectors are normalized so that their maximum value is 1. The normalization factors are included in singular value s_T .

To summarize, by applying a SVD analysis to \mathbf{A}_T , two independent vectors \mathbf{u} and \mathbf{v} are found, which are proportional to the conversion dependency \mathbf{f} and the temperature dependency \mathbf{k}' of the reaction. Since $k'(T)$ is also only a scaled version of $k(T)$, as given by (4.1), the following can be written

$$\mathbf{k} = c_3 \mathbf{v} \quad \text{with} \quad c_3 = \frac{c_2}{h(p_1)} \quad (4.15)$$

Hence, vector \mathbf{v} is also proportional to \mathbf{k} . Figure 4.6 shows the identified conversion dependency vector \mathbf{u} (left) and the identified temperature dependency vector \mathbf{v} (middle).

The biggest problem lies in building matrix \mathbf{A}_T . For the SVD analysis a fully populated matrix is needed. This can be achieved by using isothermal measurement data. Then, each column of matrix \mathbf{A}_T represents one isothermal measurement, resulting in a fully populated matrix. There are two major drawbacks to use only isothermal experiments. First, the information about the temperature dependency $k'(T)$ is only known at the measured temperatures. Thus, this results in a temperature dependency vector \mathbf{v} , which contains only a few points, at the measured temperatures. A more dense vector would require a higher measurement effort. Second, it is hard to measure the full reaction under isothermal conditions. For example, when measuring a decomposition of a material in a TGA or DSC, the sample starts to decompose as soon as the equilibriums temperature is exceeded. Therefore,

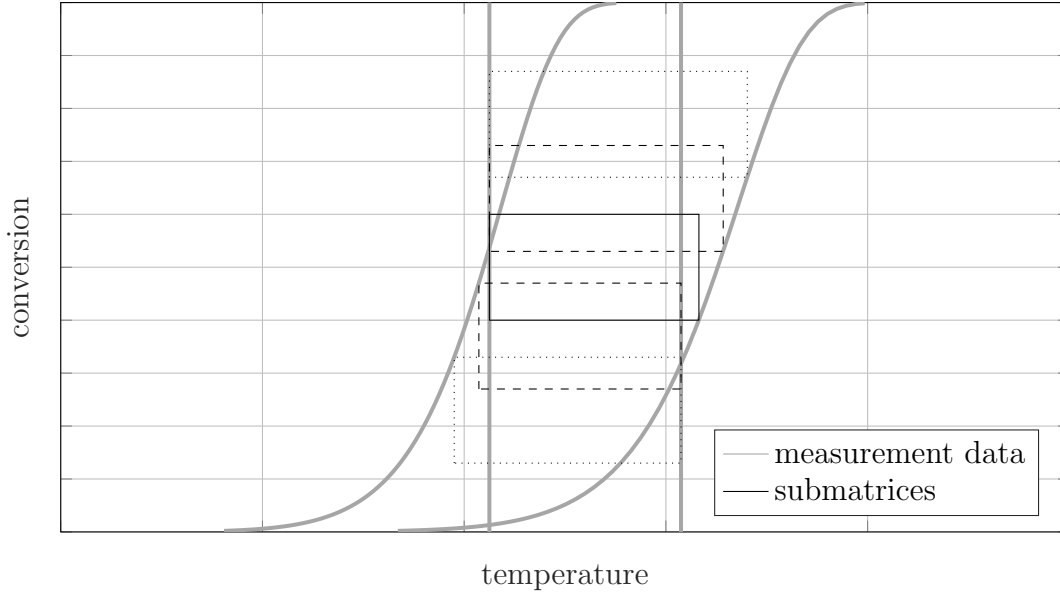


Figure 4.2: Exemplary evolution of the placement of submatrices for mixed measurements.

the beginning of a reaction is not measured at isothermal conditions. This can be avoided by influencing the equilibriums temperature via the partial pressure of the reaction gas, as described by Eq.(2.28), which is the preferred method in this work, but this is not always possible. A different approach to building matrix \mathbf{A}_T is by using isokinetic measurements. Their advantage over isothermal measurements are that continuous information over a wide temperature range is recorded and the start of the reaction is measured at well-defined conditions. This results in a very dense temperature dependency vector \mathbf{v} with only a few necessary measurements. Their downside is that use of isokinetic data results in a sparse band matrix \mathbf{A}_T , preventing the use of a direct SVD analysis. Sempere et al. [120] proposed a method to split matrix \mathbf{A}_T into fully populated submatrices $\mathbf{A}_{T,s}$. In this work the method is expanded so that a combination of isokinetic and isothermal measurements can be analyzed simultaneous to increase the quality of the identified models. Figure 4.2 shows an example for the placement of such submatrices. To fully populate the submatrices, the missing information between the measurement data is interpolated. Normally linear interpolation is used, although different interpolation methods can be applied. The general expression of these submatrices is given by (4.16).

$$\mathbf{A}_{T,s} = \begin{bmatrix} f(\alpha_i)k'(T_j) & f(\alpha_i)k'(T_{j+1}) & \cdots & f(\alpha_i)k'(T_{j+p}) \\ f(\alpha_{i+1})k'(T_j) & f(\alpha_{i+1})k'(T_{j+1}) & \cdots & f(\alpha_{i+1})k'(T_{j+p}) \\ \vdots & \vdots & \ddots & \vdots \\ f(\alpha_{i+q})k'(T_j) & f(\alpha_{i+q})k'(T_{j+1}) & \cdots & f(\alpha_{i+q})k'(T_{j+p}) \end{bmatrix} \quad (4.16)$$

Since each submatrix $\mathbf{A}_{T,s}$ is fully populated, a SVD can be calculated for each individually.

The result are different conversion and temperature dependency vectors \mathbf{u}_s and \mathbf{v}_s , one pair for each submatrix.

$$\mathbf{A}_{T,s} = \mathbf{u}_i s_i \mathbf{v}_i^T \quad (4.17)$$

Each vector is valid within the range of the analyzed submatrix. The scales of the quantities of each vector are lost during the matrix decomposition process, thus the vectors of different submatrices are not properly scaled with respect to each other. To achieve continuous progression of the dependency vectors \mathbf{u} and \mathbf{v} , each vector \mathbf{u}_i and \mathbf{v}_i needs to be scaled properly. To be able to calculate the correct scaling factor, it is necessary to place the submatrices, in such a way, that they overlap, as it is depicted in figure 4.2. Since the dependencies are continuous functions, both dependency vectors of two adjacent submatrices must be equal within the overlapping region. Thus, the scaling factor ϕ_i for each submatrix after the first can be calculated by

$$\phi_i = \frac{\mathbf{u}_i}{\mathbf{u}_{i-1}} \Big|_{\alpha^*} \quad (4.18)$$

where α^* are the conversion values where \mathbf{u}_i and \mathbf{u}_{i-1} overlap.

With the calculated scaling factors the conversion dependency vector of each submatrix can be scaled to the level of the first submatrix with

$$\mathbf{u}_{i,\text{scaled}} = \mathbf{u}_i \prod_{n=2}^i \phi_n \quad (4.19)$$

Since the product of both dependency vectors needs to fulfill (4.17), the temperature dependency vector needs to be scaled according to

$$\mathbf{v}_{i,\text{scaled}} = \mathbf{v}_i \prod_{n=2}^i \frac{1}{\phi_n} \quad (4.20)$$

4.2.2 Identification of $h'(p)$

To identify the pressure dependency of a reaction $h'(p)$ information about the reaction rate at different pressure levels is needed. Due to limitations of the analytical equipment, measurements with continuously changing pressure are usually not possible. This is especially true for TGA (thermogravimetric analysis) measurements, where each pressure change results in oscillations and errors in the weight signal due to pressure surges. Thus the most promising approach is to measure under isobaric conditions at different pressure levels. Nevertheless, the proposed method can handle measurements with continuously changing pressure in the same way as isokinetic temperature ramp measurements during the temperature dependency

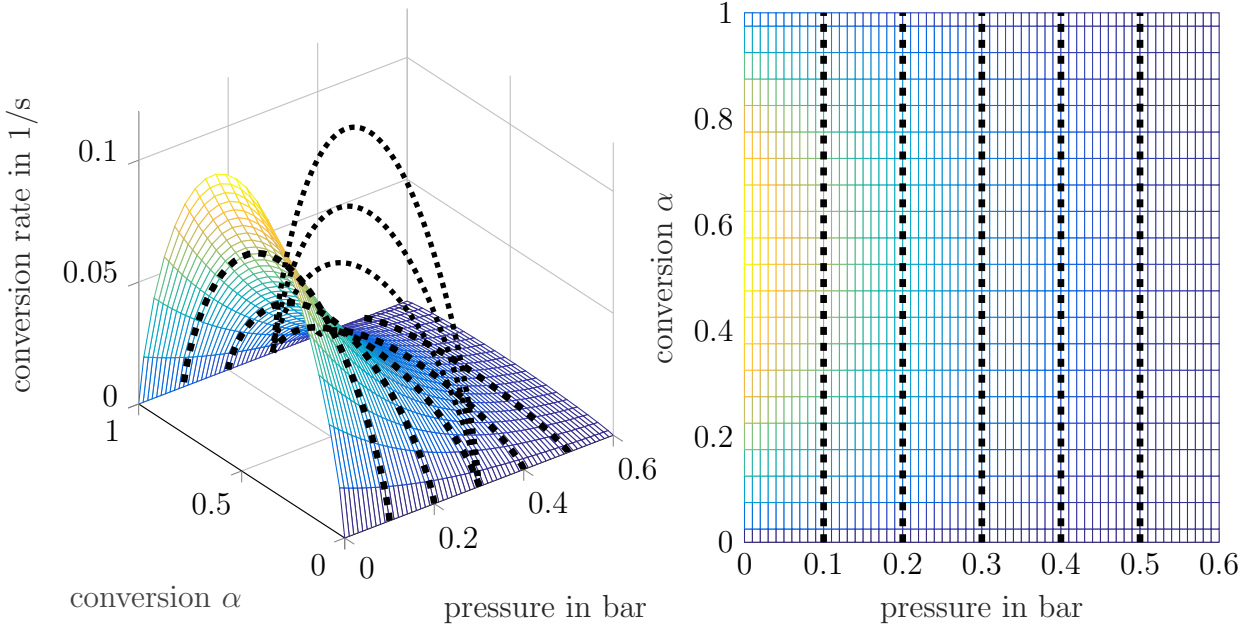


Figure 4.3: Reaction rate surface for the example at constant temperature $T = 310$ K. Dashed lines (–) represent isobaric experiments, dotted lines (..) the change of the surface with increasing temperature.

identification.

The identification of the pressure dependency $h'(p)$ is accomplished in the same way as the identification of the temperature dependency $k'(T)$ described in the previous section.

The information about the conversion rate, as given by Eq.(4.2), can again be visualized as a surface, now, in the α - p -space. Figure 4.3 shows this surface for the example reaction at $T = 310$ K.

The discretization of the surface at a specific temperature T_1 given by Eq.(4.2) results in the $(l \times n)$ data matrix \mathbf{A}_p .

$$\mathbf{A}_p = \begin{bmatrix} f(\alpha_1)h'(p_1) & f(\alpha_1)h'(p_2) & \cdots & f(\alpha_1)h'(p_n) \\ f(\alpha_2)h'(p_1) & f(\alpha_2)h'(p_2) & \cdots & f(\alpha_2)h'(p_n) \\ \vdots & \vdots & \ddots & \vdots \\ f(\alpha_l)h'(p_1) & f(\alpha_l)h'(p_2) & \cdots & f(\alpha_l)h'(p_n) \end{bmatrix} = \mathbf{f}\mathbf{h}^T = \mathbf{f} \otimes \mathbf{h}' \quad (4.21)$$

with

$$\mathbf{h}' = \left[h'(p_1) \quad h'(p_2) \quad \cdots \quad h'(p_n) \right]^T \quad (4.22)$$

Resulting from a SVD analysis of matrix \mathbf{A}_p the following decomposition can be obtained

$$\mathbf{A}_p = s_p \hat{\mathbf{u}} \otimes \mathbf{w} \quad (4.23)$$

with s_p representing the scaling factor of this decomposition, $\hat{\mathbf{u}}$ the conversion dependency

vector and \mathbf{w} the pressure dependency vector. From comparison of Eqs. (4.21) and (4.23) follows

$$\mathbf{f} = \hat{c}_1 \hat{\mathbf{u}} \quad (4.24)$$

$$\mathbf{h}' = c_4 \mathbf{w} \quad (4.25)$$

$$s_p = \hat{c}_1 c_4 \quad (4.26)$$

$$\mathbf{g} = c_5 \mathbf{w} \quad \text{with} \quad c_5 = \frac{c_4}{k(T_1)} \quad (4.27)$$

The right curve in Figure 4.6 shows the calculated pressure dependency vector \mathbf{w} for the given example.

As the conversion dependency \mathbf{f} is identical for both identifications, the identified conversion dependency vectors \mathbf{u} and $\hat{\mathbf{u}}$ must be proportional to each other. Also, since the vectors are scaled in such way that the maximum value is equal to 1 the ratio c_1/\hat{c}_1 will be approximately 1 and the two vectors should be identical:

$$\mathbf{u} = \frac{\hat{c}_1}{c_1} \hat{\mathbf{u}} \approx \hat{\mathbf{u}} \quad (4.28)$$

Figure 4.4 shows the comparison between the identified conversion dependencies \mathbf{u} and $\hat{\mathbf{u}}$. The deviation between both identifications originates from numerical errors in the decomposition algorithm. The difference is negligible though. When applying the extended NPK method it should always be confirmed that the conversion vectors of each identification step coincide.

4.2.3 Combining the dependency vectors

To create a numerical representation of the full model according to Eq.(2.33) the identified dependency vectors \mathbf{u} , \mathbf{v} and \mathbf{w} have to be combined correctly. Similarly to the matrices \mathbf{A}_T and \mathbf{A}_p , a three dimensional ($l \times m \times n$) tensor \mathbf{A} can be built, which represents a discretization of Eq.(2.33) in the α - T - p -space.

$$\mathbf{A} = \mathbf{f} \otimes \mathbf{k} \otimes \mathbf{h} \quad (4.29)$$

By inserting Eqs.(4.12), (4.15) and (4.27) into Eq.(4.29) the identified dependency vectors can be related to the tensor \mathbf{A} as

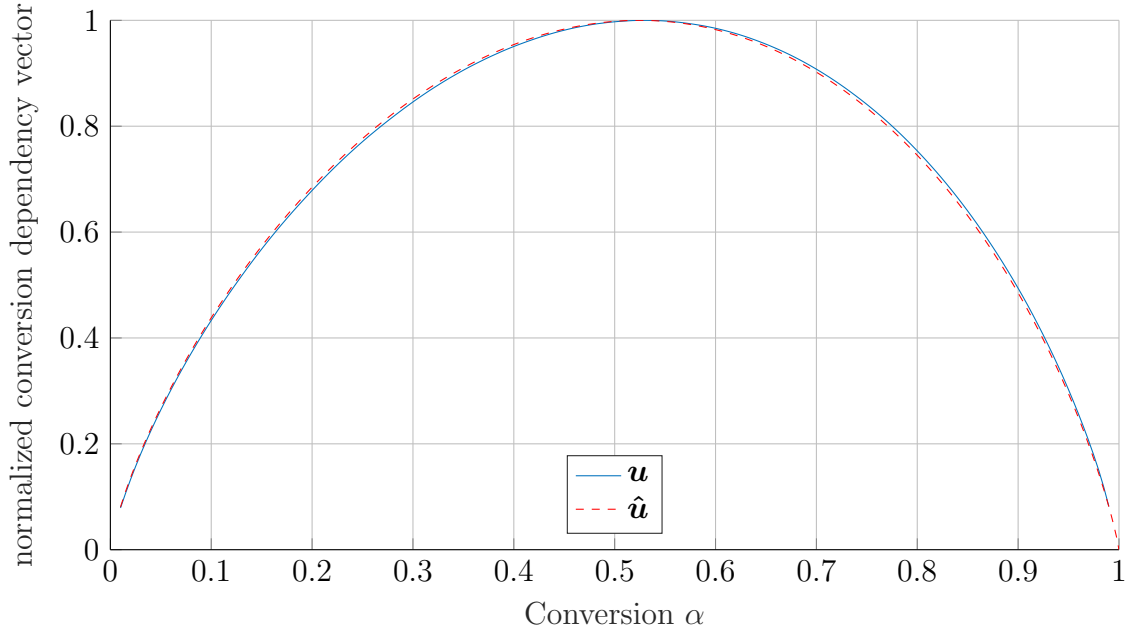


Figure 4.4: Comparison of the conversion dependency vector \mathbf{u} and $\hat{\mathbf{u}}$ identified during the identification of \mathbf{v} and \mathbf{w} , respectively

$$\mathbf{A} = s \mathbf{u} \otimes \mathbf{v} \otimes \mathbf{w} \quad \text{with} \quad s = c_1 c_3 c_5 \quad (4.30)$$

The difficulty of combining the identified dependency vectors \mathbf{u} , \mathbf{v} and \mathbf{w} lies in finding the residual scaling factor s as the factors c_1 , c_3 and c_5 are unknown.

The matrix \mathbf{A}_T for the identification of the temperature dependency represents a slices of \mathbf{A} at a specific pressure. Similarly, \mathbf{A}_p for the identification of the pressure dependency represents a slices of \mathbf{A} at a specific temperature. This is visualized in Figure 4.5. The axes span the tensor \mathbf{A} , while the red and the blue panes symbolize the matrices \mathbf{A}_T and \mathbf{A}_p . The contour lines represent the conversion rate $d\alpha/dt$ as shown in Figures 4.1 and 4.3, the solid black lines represent various measurements used for the identification and the black dashed line is the intersection line of the two panes.

In mathematical terms this can be written as

$$\mathbf{A}|_{p_1} = \mathbf{A}_T = s_T \mathbf{u} \otimes \mathbf{v} \quad (4.31)$$

Here, the notation $\mathbf{A}|_{T_1}$ means that the tensor \mathbf{A} is evaluated at T_1 reducing its dimensions to a matrix. If T_1 lies between the discretization points, then the values are interpolated. Similarly, $\mathbf{v}|_{T_1}$ denotes an evaluation of \mathbf{v} at T_1 which results in a scalar value.

To find the value of s , the intersection vector of the slices \mathbf{A}_T and \mathbf{A}_p at $T = T_1$ and $p = p_1$ has to be considered (dashed line in Figure 4.5). At this intersection the following equation holds

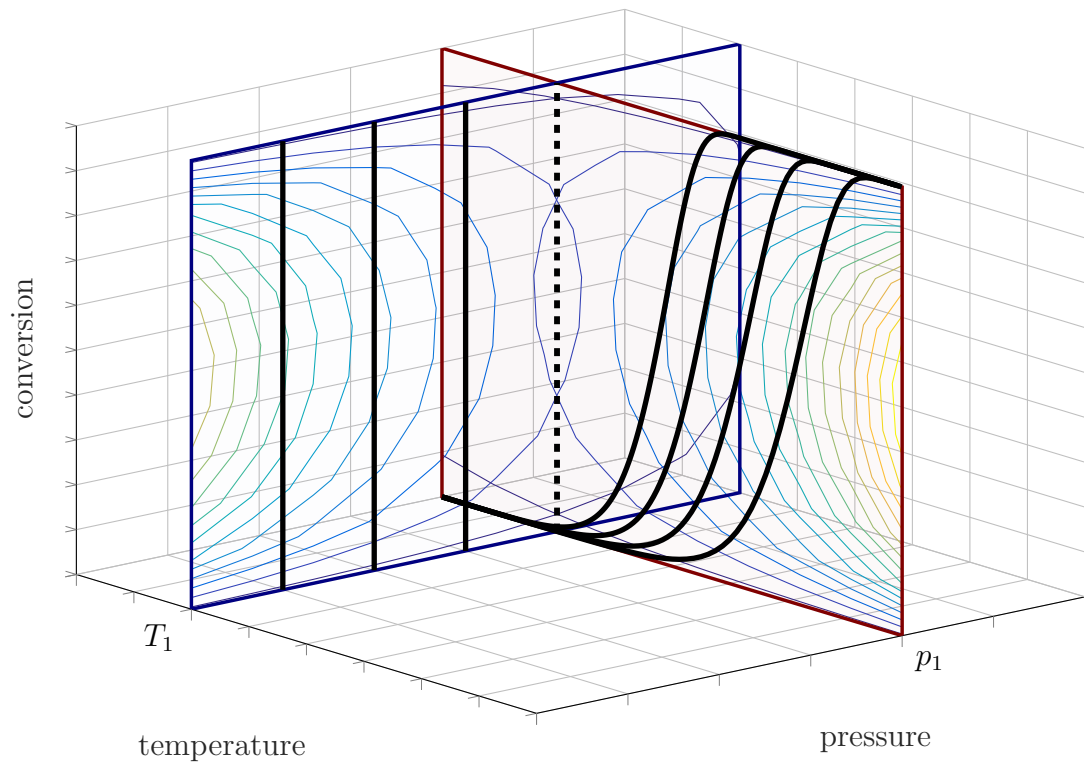


Figure 4.5: Visualization of two slices of the tensor \mathbf{A} at T_1 and p_1 , respectively. The contour lines represent the change of the conversion rate $d\alpha/dt$, the solid black line represent various measurements used for the identification and the black dashed line is the intersection line between the two panes.

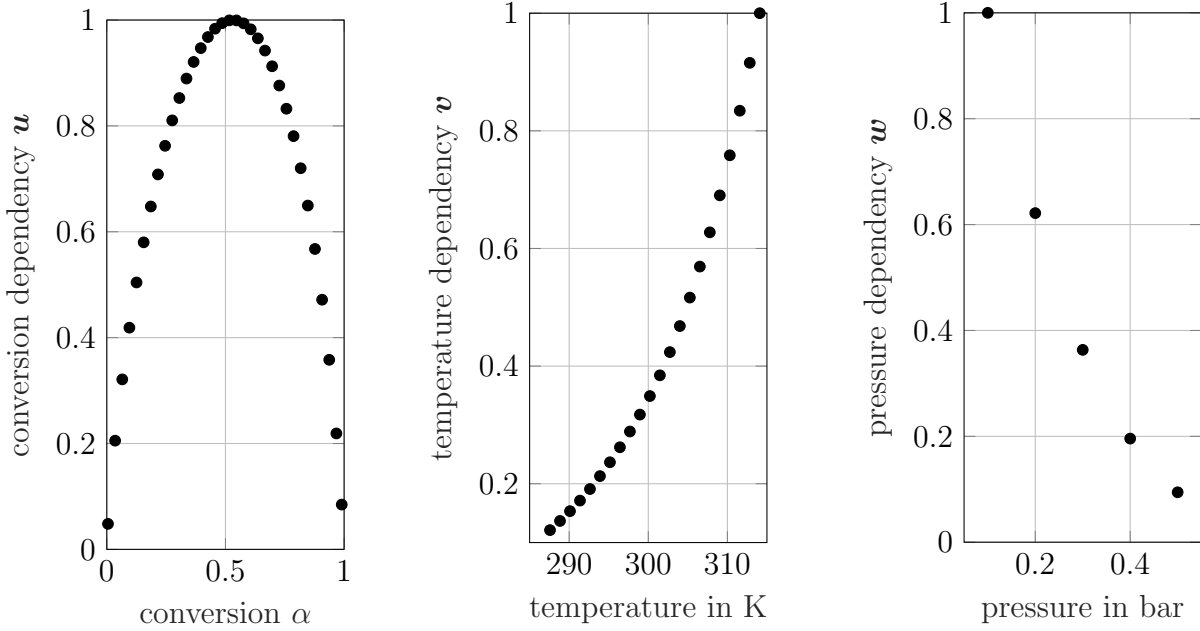


Figure 4.6: Normalized dependency vectors \mathbf{u} (left), \mathbf{v} (middle) and \mathbf{w} (right) for the example reaction ($s = 0.1008$)

$$\mathbf{A}|_{T_1, p_1} = \mathbf{A}_T|_{T_1} \quad (4.32)$$

Substituting Eqs.(4.30) and (4.31) into (4.32) results in

$$s \mathbf{u} \mathbf{v}|_{T_1} \mathbf{w}|_{p_1} = s_T \mathbf{u} \mathbf{v}|_{T_1} \quad (4.33)$$

which yields

$$s = \frac{s_T}{\mathbf{w}|_{p_1}} \quad (4.34)$$

It is also possible to calculate the scaling factor s by considering the pressure identification matrix $\mathbf{A}|_{T_1, p_1} = \mathbf{A}_p|_{p_1}$. Then $\hat{s} = s_p / \mathbf{v}|_{T_1}$.

Incorporating this into (4.30) yields

$$\mathbf{A} = s_T \mathbf{u} \otimes \mathbf{v} \otimes \frac{\mathbf{w}}{\mathbf{w}|_{p_1}} = s_p \hat{\mathbf{u}} \otimes \frac{\mathbf{v}}{\mathbf{v}|_{T_1}} \otimes \mathbf{w} \quad (4.35)$$

Provided that (4.28) holds the two scaling factors s and \hat{s} should have the same value. The deviation can be used to assess the quality of the decomposition procedure. In case of the example reaction the relative difference between the values is 0.53 %.

Figure 4.6 shows all identified dependency vectors. With the scaling factor $s = 0.1008$ they represent the full numeric model.

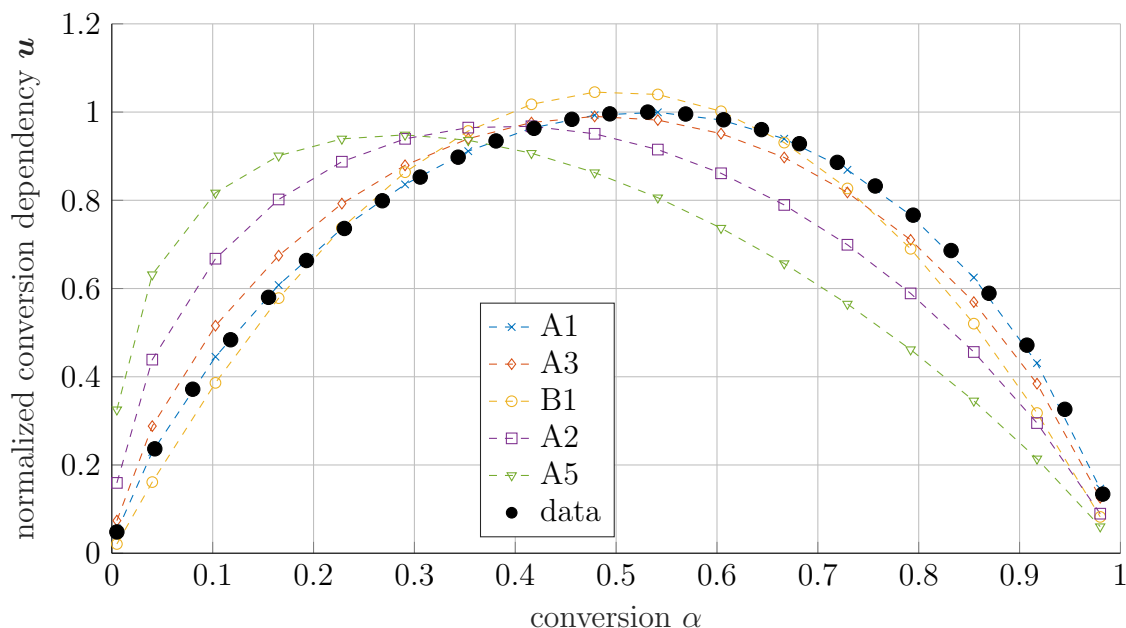


Figure 4.7: Identified conversion dependency vector \mathbf{u} for the example reaction with fitted conversion models. Only the five models with the best fit are shown.

4.2.4 Interpretation of the dependency vectors

Now that the effect of each dependency vector has been identified, the next step is to arrive at a physical interpretation of the identified dependency vectors. To do that model functions are fitted to each vector.

To describe the conversion dependency vector \mathbf{u} , the conversion models $f(\alpha)$ described in Section 2.2.3 are considered. Since none of the models has extra parameters the only fitting parameter is the scaling constant c_1 from Eq.(4.12).

First all models are fitted to the conversion dependency vector \mathbf{u} with the least-squares-method. Based on the R^2 -value (see Table 4.1) the five best fitting models are selected and plotted (Figure 4.7).

Since the resulting R^2 values are often very similar a pairwise F-test is performed to discriminate between the models. The best fitting model is compared to each of the other models. Then the result of the F-test is a p -value that reflects the statistical probability of the first model being an improvement over the other model. The result is deemed to be statistically significant if the p -value is greater than 0.95. The results in Table 4.1 show that model A1 is a significantly better fit than all the other considered models. Hence the proposed method successfully identified the conversion model that was used to simulate the example data.

To identify the best fitting model for the pressure dependency the same procedure as above is used. In addition to the model parameters the scaling factor c_5 from Eq.(4.27) is fitted with each model. The fitted models are plotted in Figure 4.8 and the statistical results are provided in Table 4.2. The two highest scoring models, p2 and p3, result in almost identical

Table 4.1: Statistical results of the five best fitting conversion models for the example reaction

Model ID	R^2	p
A1	0.9998	
A3	0.9648	1.000
B1	0.9468	1.000
A2	0.6914	1.000
A5	0.1042	1.000

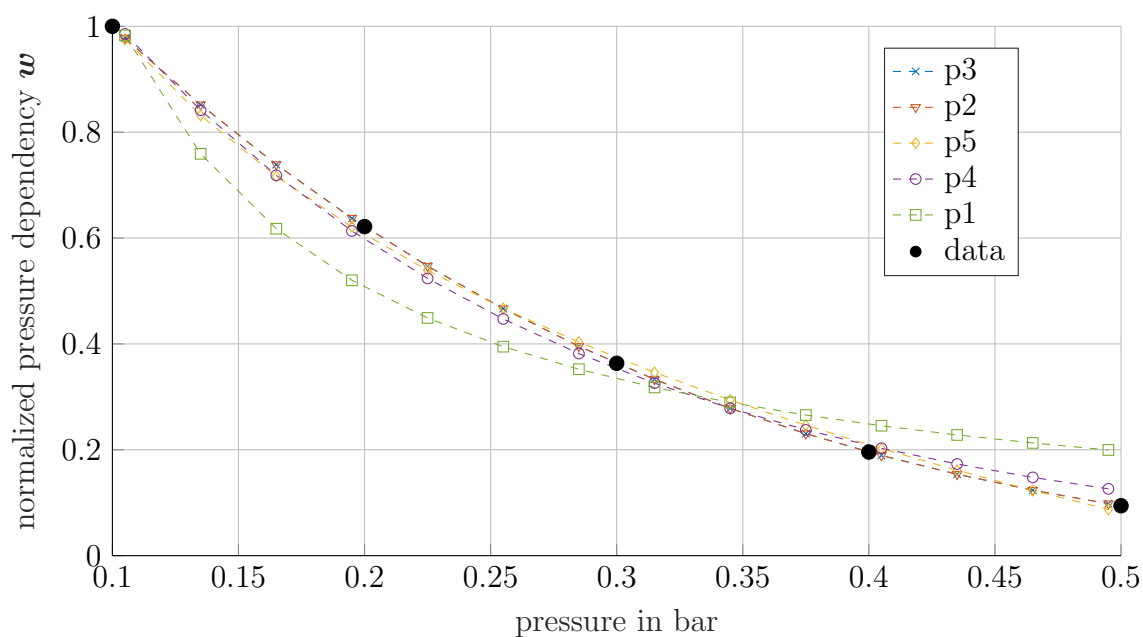


Figure 4.8: Identified pressure dependency vector \mathbf{w} for the example with fitted pressure models. The difference of models p2 and p3 is within the range of numerical error, therefore they can not be distinguished in this plot.

Table 4.2: Statistical results of the pressure dependency models for the example reaction

Model ID	R^2	p
p3	1.0000	
p2	1.0000	0.066
p5	0.9987	0.999
p4	0.9966	0.999
p1	0.9460	1.000

R^2 -values. This comes as no surprise since p3 is an extension of p2. Here, the F-test allows us to discriminate between the two models: Only with a probability of 7% is the model p3 an improvement over the second best model p2. Since this value is far below the significance threshold of 0.95 the simpler model with less parameters, p2, is chosen.

Again the presented method identified the correct model and with $\omega = 1.014$ and $\chi = 4.102$ also the recovered values of the model parameters are very accurate.

With the two fitted scaling factors c_1 and c_5 the missing scaling factor c_3 can be calculated from Eq.(4.35). Assuming that the temperature dependency follows the Arrhenius equation in Eq.(2.34), Eq.(4.15) can be written as

$$c_3 \mathbf{v}|_T = A \exp\left(\frac{-E_a}{RT}\right) \quad (4.36)$$

By transforming this equation to

$$\ln(c_3 \mathbf{v}|_T) = \ln(A) - \frac{E_a}{RT} \quad (4.37)$$

a linear fit can be used to calculate the Arrhenius parameters (see Figure 4.9) as $A = 7.44 \times 10^8$ 1/s and $E_a = 59.2$ kJ/mol. As with the results of the two prior identification steps these values are very accurate. Even though the difference between the identified and the original Arrhenius parameter might seem quite big, it has to be kept in mind that the parameters have been identified in a logarithmic fit, where a 30% difference of the Arrhenius parameter results in only a slight shift of the line.

As a final verification step the simulated measurements that have been used as input for the method will be reproduced. First, to demonstrate the efficacy of combined pressure-temperature NPK decomposition only the identified dependency vectors given in Figure 4.6 are used. Second, the derived model equations from this section are used to show that the method is an useful tool for kinetic model identification. Figures 4.10 and 4.11 show the simulated measurements with the initial model (blue), the dependency vectors (green) and the identified model (red). Both, the vector based and the model based simulations fit the initial data very well.

4.3 Decomposition of CdCO₃

4.3.1 Measurements

To test the proposed method on real data the decomposition of CdCO₃ was analyzed. This reaction follows the equation

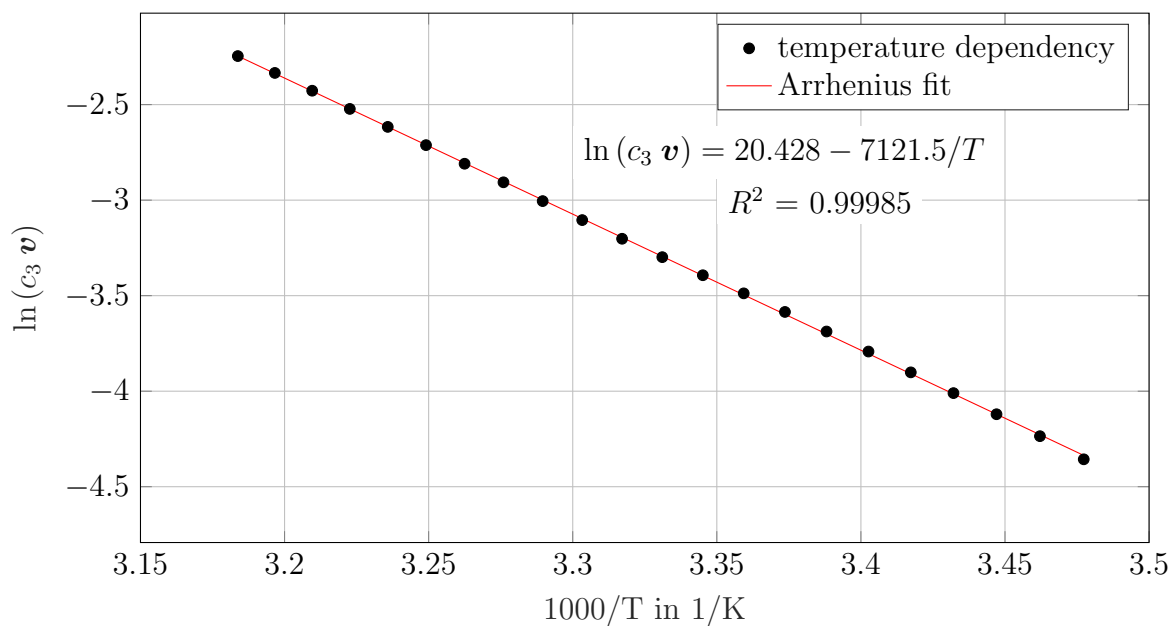
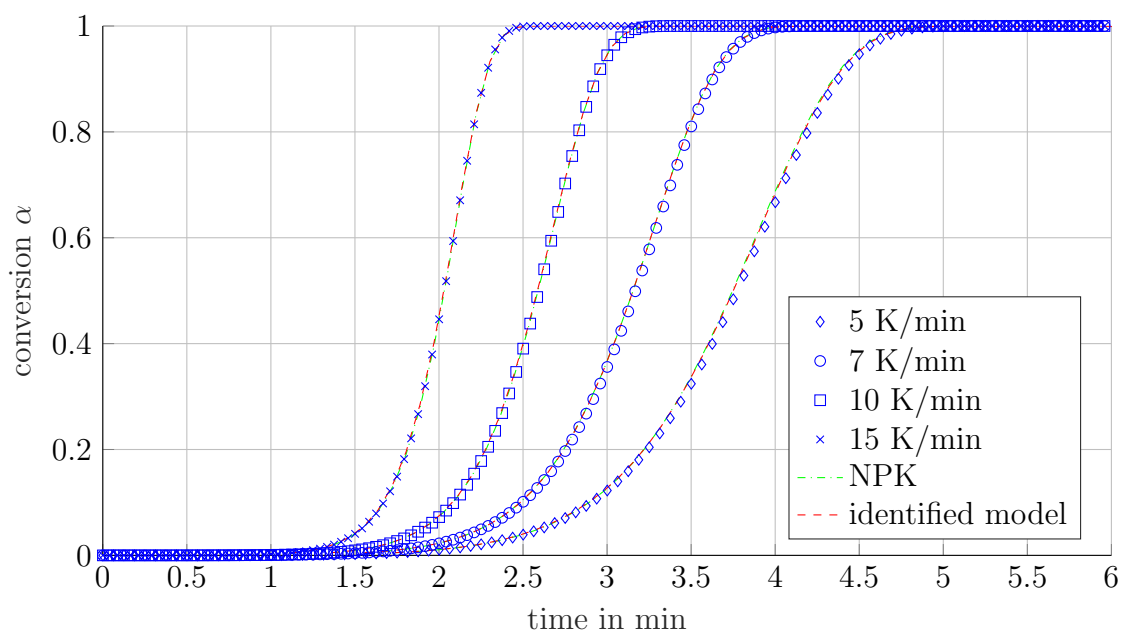


Figure 4.9: Arrhenius plot of the temperature dependency of the example reaction.

Figure 4.10: Simulation result for isokinetic measurements of the example reaction with different heating rates β at $p = 0.3$ bar

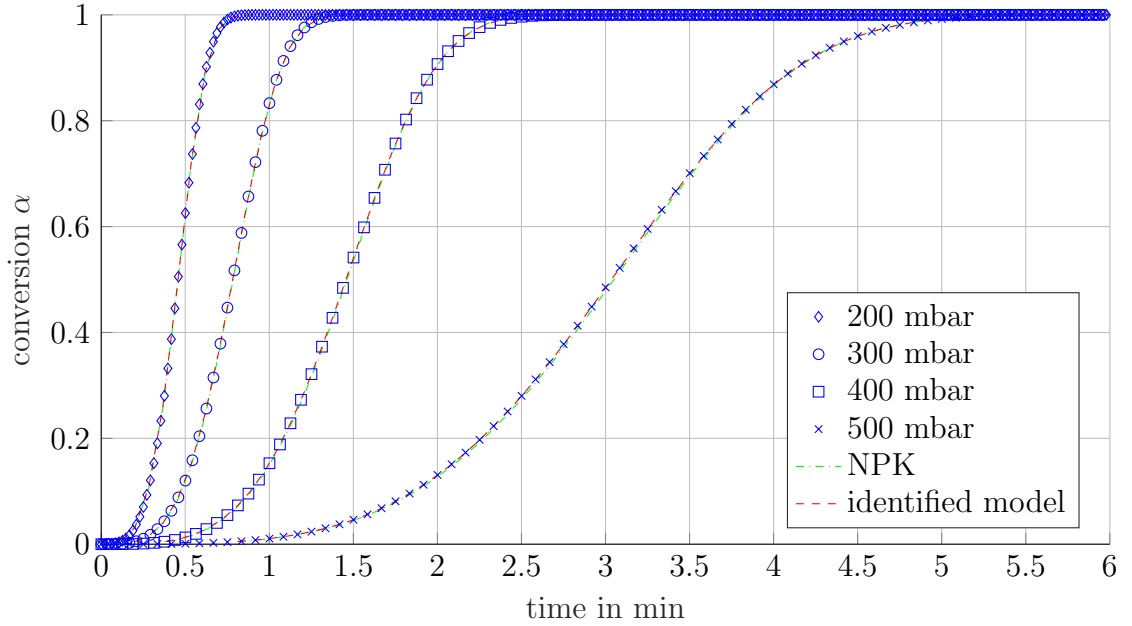
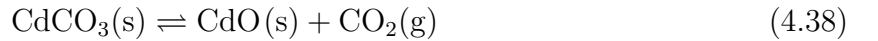


Figure 4.11: Simulation result for isothermal measurements of the example reaction at different pressures at $T = 310$ K



The material used for all decomposition experiments was CdCO₃ purissimum from Merck. For the STA measurements a fraction with a particle size between 180 μm -250 μm was used. The STA measurements were done in a Netzsch STA 449 F1 Jupiter with a differential thermal analysis (TGA-DTA) measurement setup in open Al-crucibles. The sample mass in all STA measurements was 5 ± 0.05 mg CdCO₃.

To identify the temperature dependency $k(T)$ isokinetic measurements with different heating rates ($\beta = 2, 5, 7, 10$ and 15 K/min) at a constant CO₂ partial pressure $p_{\text{CO}_2} = 100$ mbar were performed. To identify the pressure dependency $h(p)$ isothermal experiments were performed: The sample was heated under CO₂ atmosphere ($p_{\text{CO}_2} = 1$ bar) at a rate of 10 K/min up to the measurement temperature. When a constant sample temperature was reached, the atmosphere was switched to a CO₂/N₂ mixture to induce the decomposition. The measurements were performed at 633 K with CO₂ partial pressures of 25, 50, 100, 150 and 200 mbar. The partial pressure of N₂ was chosen in a way that the total pressure was always 1 bar. Figure 4.12 shows typical measurement curves for isokinetic and isothermal measurements.

The conversion α can be calculated from the mass signal $m(t)$ as

$$\alpha(t) = \frac{m_0 - m(t)}{m_0 - m_\infty} \quad (4.39)$$

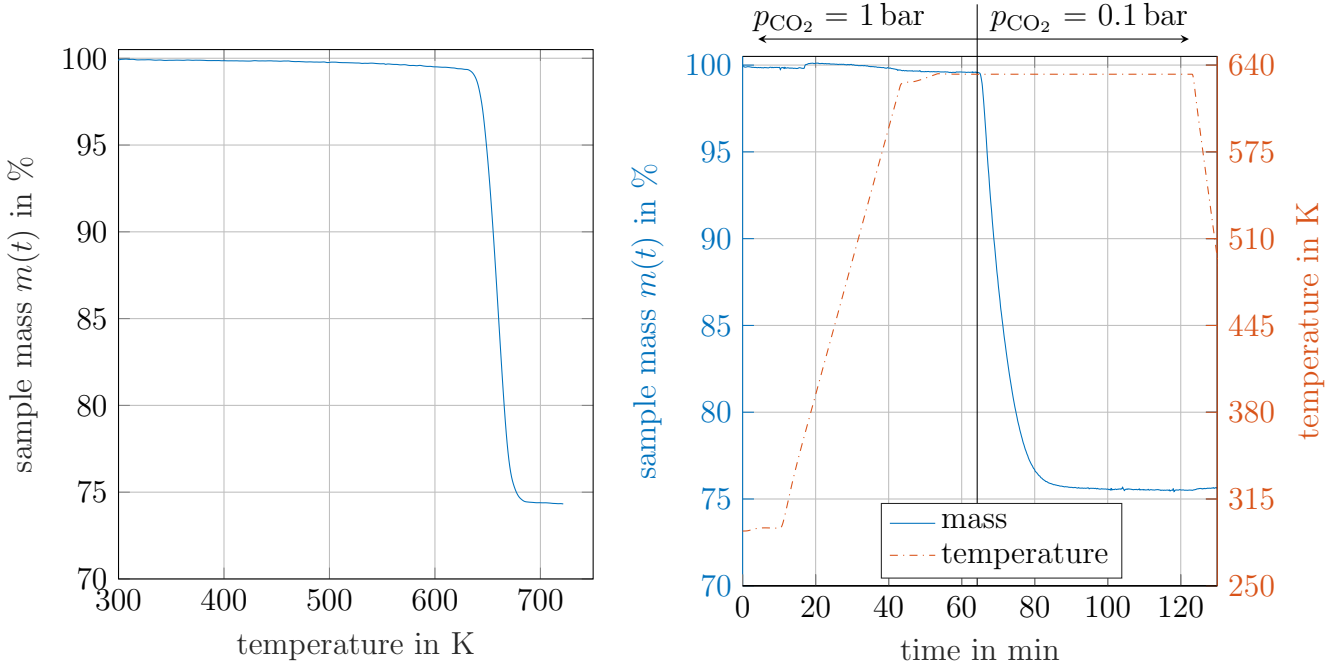


Figure 4.12: Representative measurement curves in the STA for kinetic analysis. left: isokinetic measurement with $\beta = 10 \text{ K/min}$ and $p_{\text{CO}_2} = 100 \text{ mbar}$, right: isothermal measurement with $T = 633 \text{ K}$ and atmosphere change from $p_{\text{CO}_2} = 1 \text{ bar}$ to $p_{\text{CO}_2} = 100 \text{ mbar}$

where m_0 is the initial sample mass, $m(t)$ is the sample mass at time t and m_∞ is the sample mass at the end of the decomposition. XRD analyses of the material after STA measurements were performed to confirm full conversion.

4.3.2 Model identification

The procedure to decompose the measurement data into dependency vectors is the same as described in the previous section. The data lie in the T - p_{CO_2} - α -space. Within this space, the measurements to identify the temperature dependency lie on an isobaric pane and the measurements to identify the pressure dependency lie on an isothermal pane. The measurements were performed in such a way that the panes intersect at $T = 633 \text{ K}$ and $p_{\text{CO}_2} = 100 \text{ mbar}$ (see Figure 4.5).

The identified dependency vectors are shown in Figure 4.13. Their combination resulted in a scaling factor $s = 0.455$.

The conversion dependency vector \mathbf{u} was taken from the pressure dependency identification step. This was done, because the measurements for the pressure dependency are performed under isothermal conditions. Thus, reducing possible error sources, due to heat transfer effects within the sample at isokinetic measurements.

To derive model equations, the fitting procedure described in Section 4.2.4 has been applied to the identified dependency vectors.

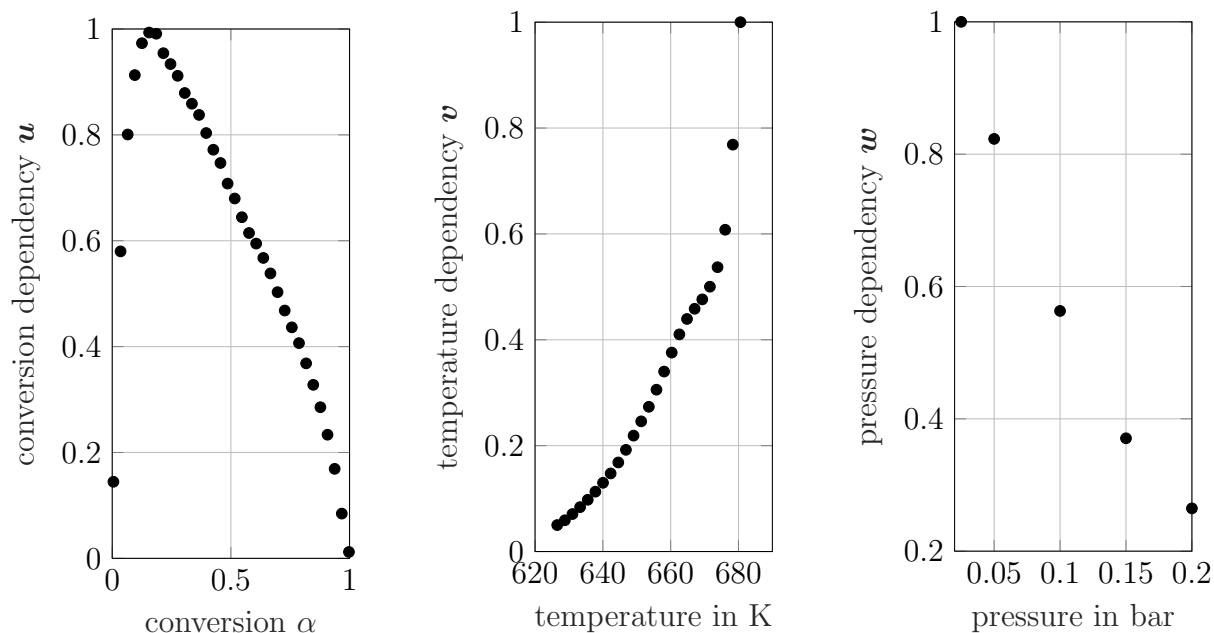


Figure 4.13: Normalized dependency vectors \mathbf{u} (left), \mathbf{v} (middle) and \mathbf{w} (right) for the decomposition of CdCO_3 ($s = 0.455$)

Table 4.3: Statistical results of the five best fitting conversion models for the decomposition of CdCO_3

Model ID	R^2	p
A4	0.9484	
A5	0.9045	1.000
R2	0.7722	1.000
R3	0.7320	1.000
R4	0.7101	1.000

The conversion dependency vector \mathbf{u} and the five best fitting models are plotted in Figure 4.14. Table 4.3 shows the corresponding statistical results. Based on the p-values it can be seen that the F-test unambiguously identifies the model A4 as the best fitting one. The Avrami-Erofeyev nucleation models are often found to describe various decomposition reactions [81, 82]. Criado et al. found that the reaction follows most likely a first order decomposition, but based on provided data the fit of the model R3 is not significantly worse [124]. Authors of both works used isothermal experiments without atmosphere change. Thus it is likely that the beginning of the reaction is not properly considered in the identification. If the fitting of the conversion models is only done for a range of α between 0.2 and 1, than the R-models would result in a good fit. Mu et al. also stated that the reaction follows model R3 but did not include A-models in the identification [125].

Figure 4.15 shows the identified pressure dependency vector \mathbf{w} alongside the fitted pressure models from Table 2.6. The fitting results show that all models fit the data well. Yet, from

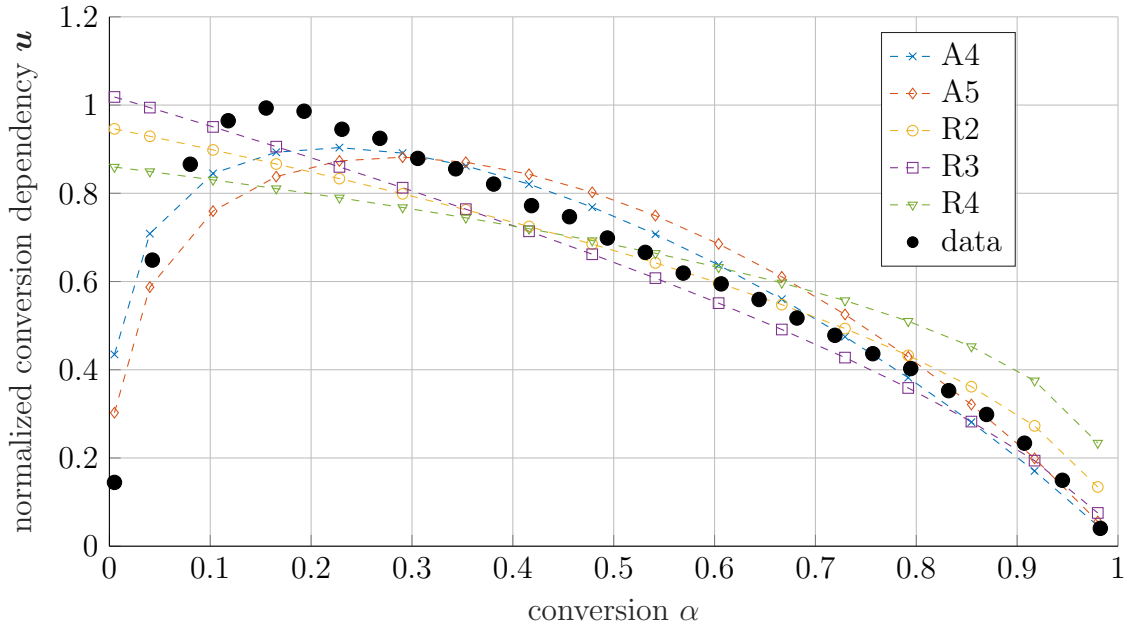


Figure 4.14: Conversion dependency vector \mathbf{u} of the decomposition of CdCO_3 with fitted conversion models. Only the five best fitting models are shown.

Table 4.4: Statistical results of the pressure dependency fitting of the decomposition of CdCO_3

Model ID	R^2	p
p4	0.9996	
p3	0.9995	1.000
p2	0.9937	1.000
p1	0.9373	0.999

a mathematical point of view, the model p4 is to be preferred, not only because it produces the smallest error, but also because it only has one parameter. The models p3 and p2 fit the data almost equally well, but this might just be due to the higher number of degrees of freedom. This fact is taken into account by the F-test resulting in a probability of almost 100% on p4 being better than p2 or p3. It has to be noted, that model p4 has no direct physically motivated derivation, despite being used in the literature [102]. Thus we strive to present a mathematical representation of the data rather than a physically bullet proof model.

The temperature dependency vector was identified based on isokinetic measurements at $p_{\text{CO}_2} = 100 \text{ mbar}$. The result is shown in Figure 4.16. It can be seen that there is a clear deviation from the typical Arrhenius form of the temperature dependency. Thus, an interaction effect between the temperature and another factor is expected.

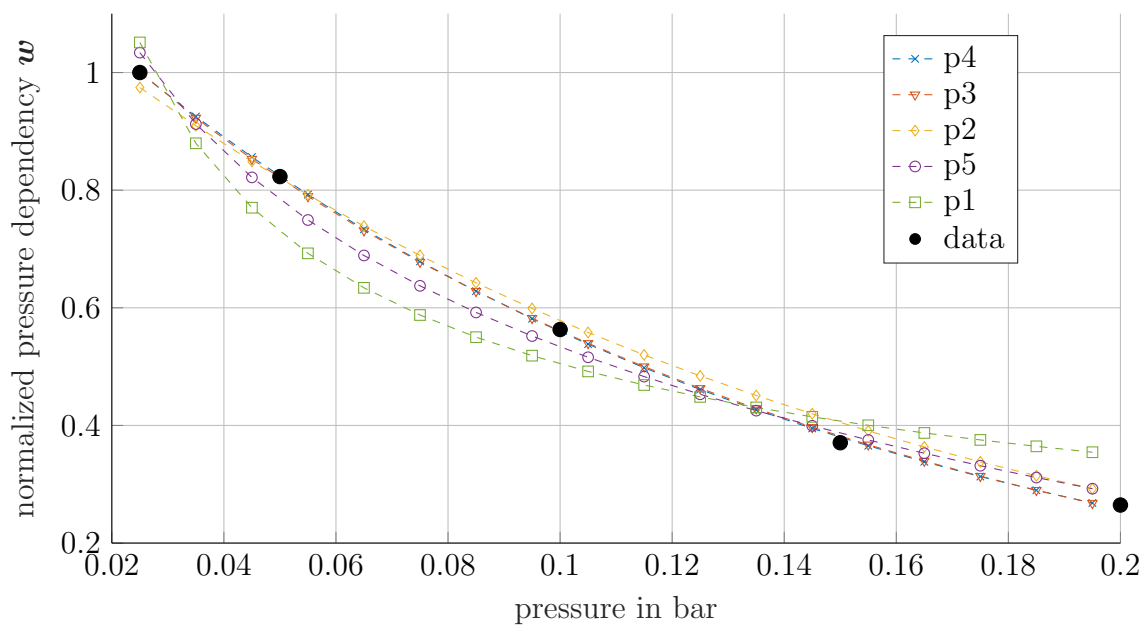


Figure 4.15: Pressure dependency vector \boldsymbol{w} of the decomposition of CdCO_3 with fitted conversion models according to Table 2.6

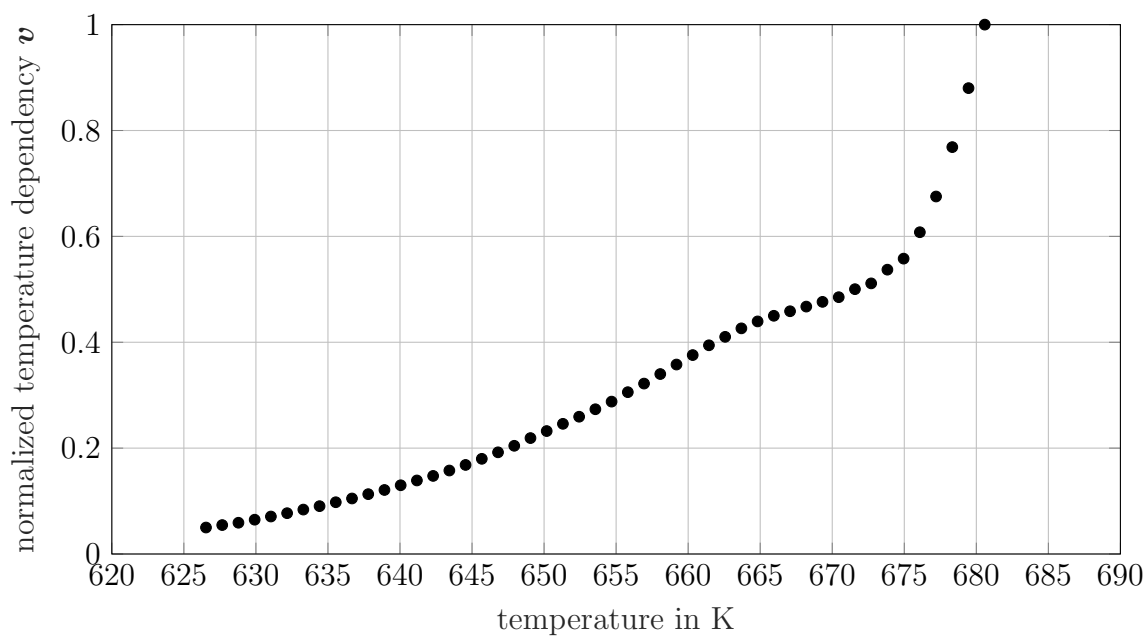


Figure 4.16: Temperature dependency vector \boldsymbol{v} for the decomposition of CdCO_3 at $p_{\text{CO}_2} = 100$ mbar

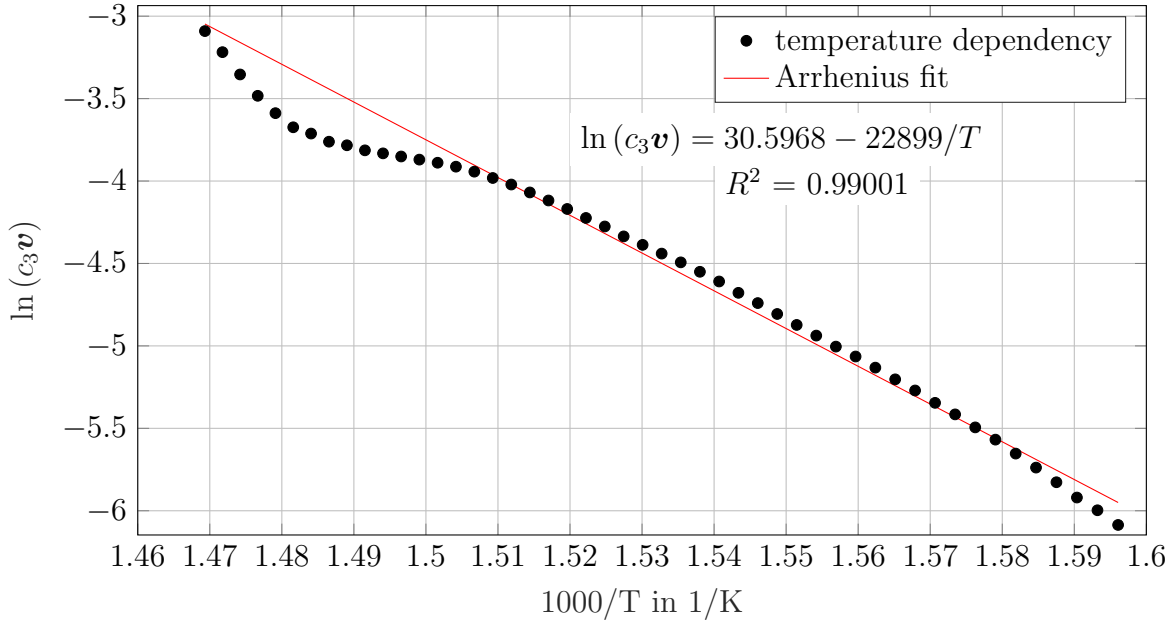


Figure 4.17: Arrhenius plot of the identified temperature dependency \mathbf{v} from isokinetic measurements of the CdCO_3 decomposition at $p_{\text{CO}_2} = 100$ mbar

4.3.3 Investigation of the interaction effect

Analyzing the Arrhenius plot of the found temperature dependency vector shows a strong deviation from the expected linear form (Figure 4.17). To further investigate, the isokinetic experiments for determination of the temperature dependency were repeated in inert N_2 atmosphere ($p_{\text{CO}_2} \leq 10^{-5}$ bar). From comparing the resulting Arrhenius plot (Figure 4.18) with the one at $p_{\text{CO}_2} \leq 100$ mbar two observations can be made. First, the absence of CO_2 changed the temperature dependency vector \mathbf{w} . As a result the quality of the linear fit increased significantly. Second, a change in the slope of the fitted linear equation is detectable. Thus, the activation energy changes as a result of the pressure change. This was also observed by Criado et al. [124]. Both observations led to the conclusion that an interaction effect between pressure and temperature exists.

To describe this effect the pressure dependency vector \mathbf{w} was identified at different temperatures. At each temperature level the data was decomposed into a conversion dependency vector and a pressure dependency vector as described in section 4.2.2. The identified conversion dependency vectors agree extremely well as can be seen in Figure 4.19. Thus an interaction effect with the conversion α can be ruled out. Figure 4.20 shows the identified pressure dependency vectors. It can be seen that the pressure dependency vector gets steeper at lower temperature. This can be taken into account by making the χ parameter temperature dependent. In this work a linear temperature dependency of χ is assumed, which is mathematically justifiable as it can be seen in Figure 4.21. With this temperature dependency of χ the pressure dependency $h(p_{\text{CO}_2}, T)$ is given by

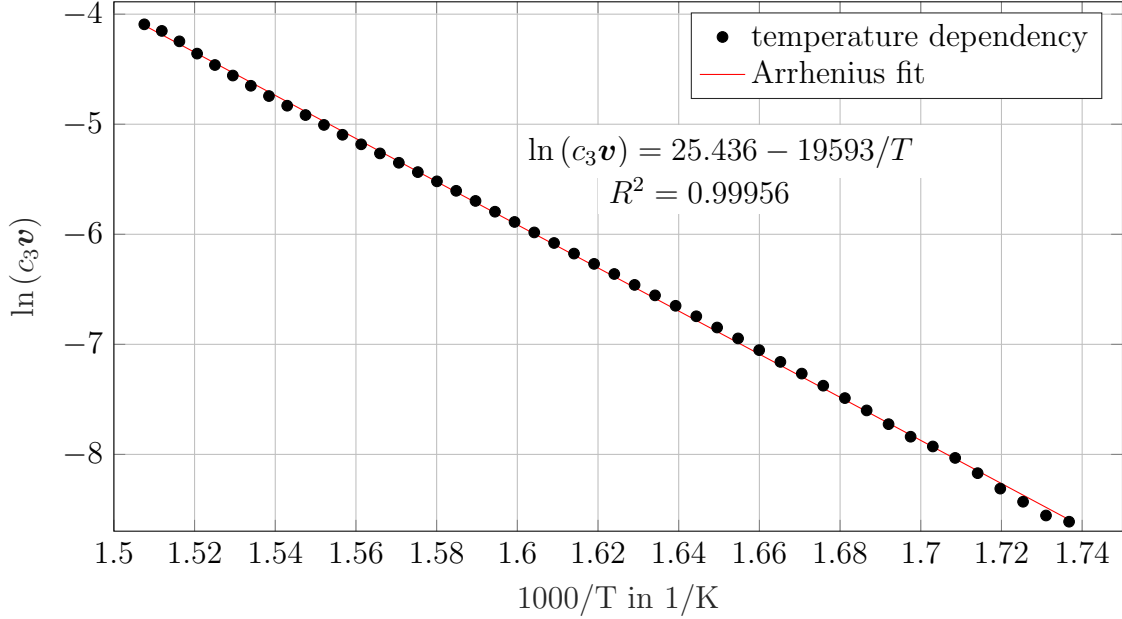


Figure 4.18: Arrhenius plot of the identified temperature dependency from isokinetic measurements of the CdCO_3 decomposition at $p_{\text{CO}_2} \leq 10^{-5}$ bar

$$h(p_{\text{CO}_2}, T) = \exp((0.3216 T + 211.7) p_{\text{CO}_2}) \quad (4.40)$$

T is in K, p_{CO_2} in bar.

To determine the Arrhenius parameters E_a and A , the temperature dependency vector identified in inert atmosphere is used. From this vector E_a and A can be directly determined by Eq.(4.37), since the pressure dependency does not contribute. This is a result of $h(p_{\text{CO}_2} \leq 10^{-5} \text{ bar}, T) \approx 1$ regardless of the temperature T . This results in an activation energy $E_a = 162.9 \text{ kJ/mol}$ and a pre exponential factor $A = 1.11 \times 10^{11} \text{ 1/s}$ for the decomposition of CdCO_3 . L'vov et al. calculated for E_a a value of 135 kJ/mol for the decomposition of CdCO_3 [126], while Mu et al. measured a value of 135 kJ/mol [125]. For the pre exponential factor A they determined a value of $6.67 \times 10^9 \text{ 1/s}$, but they identified a different conversion model, the values are hardly comparable.

4.3.4 Validation of the identified models

In this work two models have been derived. The first model was the combination of the dependency vectors of the extended NPK method (Figure 4.13). The derivation of this model was purely data driven with the only modelling assumption being the multiplicativity of the contribution of the factors. The second model is a further development of the first by identifying underlining functions in the dependency vectors. This resulted in the following function based model:

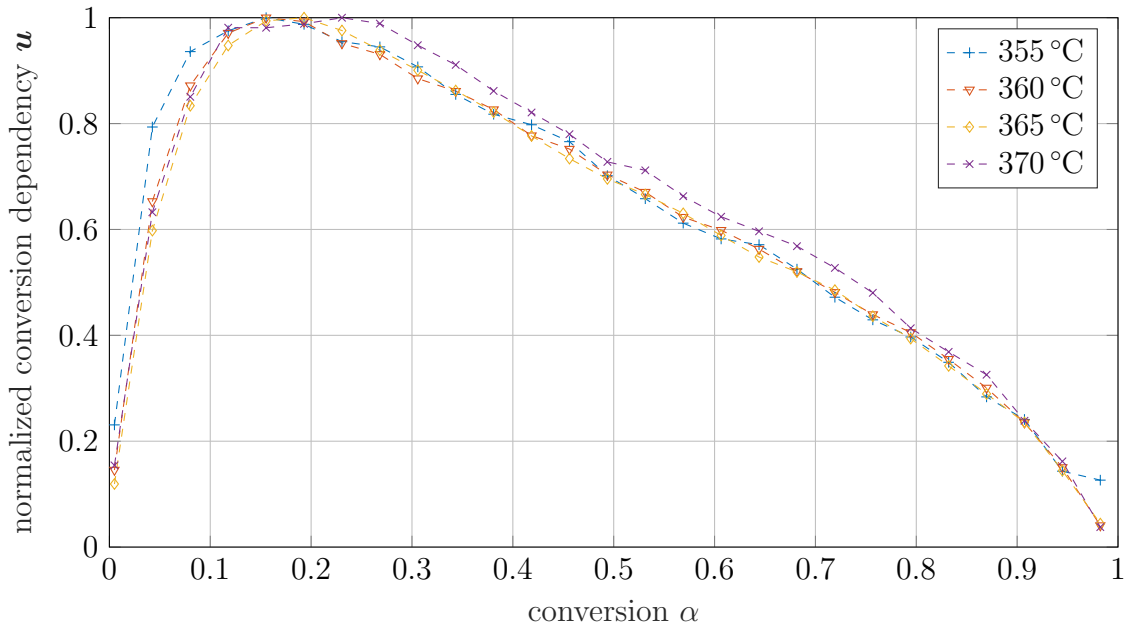


Figure 4.19: Identified conversion dependencies at different temperature levels and $p_{\text{CO}_2} = 100 \text{ mbar}$

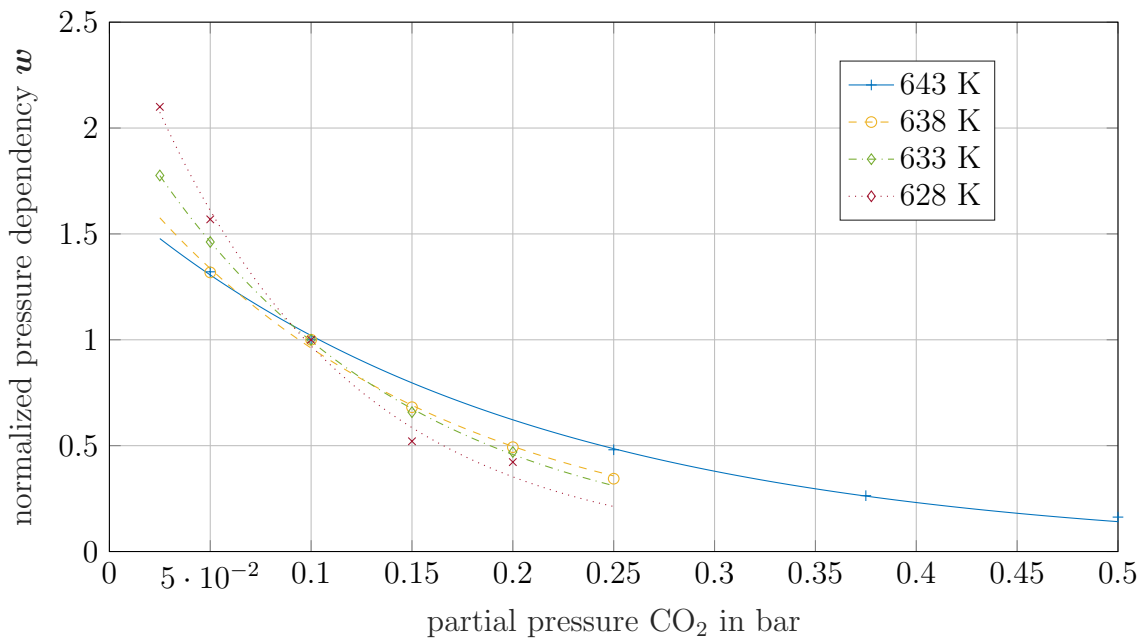


Figure 4.20: Effect of the temperature on the pressure dependency vector w . All vectors were normalized at $p_{\text{CO}_2} = 100 \text{ mbar}$ for comparison. The lines are the best fit using pressure model p4.

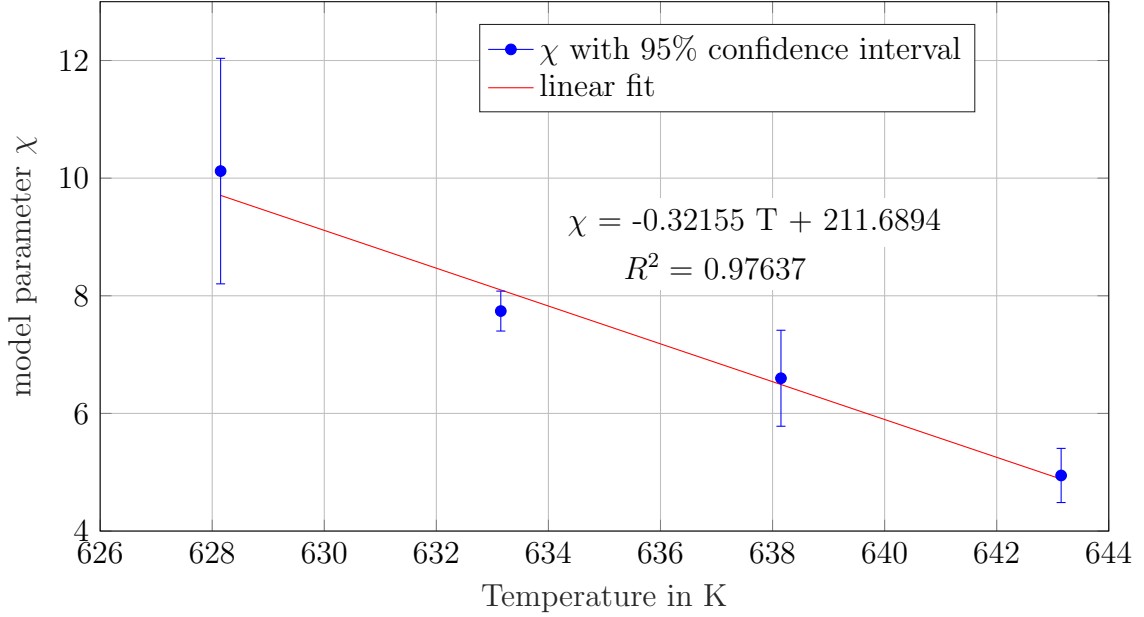


Figure 4.21: Temperature dependency of the model parameter χ . The error bars shows the 95 % confidence interval of χ as a result of the optimization.

$$\frac{d\alpha}{dt} = f(\alpha) k(T) h(p_{\text{CO}_2}, T) \quad (4.41)$$

$$f(\alpha) = 4/3(1 - \alpha)[- \ln(1 - \alpha)]^{1/4} \quad (4.42)$$

$$k(T) = 1.11 \times 10^{11} \exp\left(\frac{-1.629 \times 10^5}{8.314T}\right) \quad (4.43)$$

$$h(p_{\text{CO}_2}, T) = \exp((0.3216 T + 211.7) p_{\text{CO}_2}) \quad (4.44)$$

The temperature T is in K, the pressure p_{CO_2} in bar.

For validation of both identified models isothermal measurements at $p_{\text{CO}_2} = 100$ mbar and isobaric measurements at $T = 633$ K were simulated and compared to measured data. Figures 4.22 and 4.23 show that both the vector based model (NPK) and the function based model (function based) fit the measured data for measurements that lie on the panes of the T - p_{CO_2} - α -space, used for the identification. The simulation results for measurements outside the temperature and pressure region used for the identification show a difference between the two models (Figure 4.24). The vector based model is not capable to reproduce the measurement, as the found interaction between temperature and pressure is not described by the model. The function based model shows a good agreement between the measurements and the simulation. This implies that the functions chosen to describe the dependencies and the interaction are reasonable.

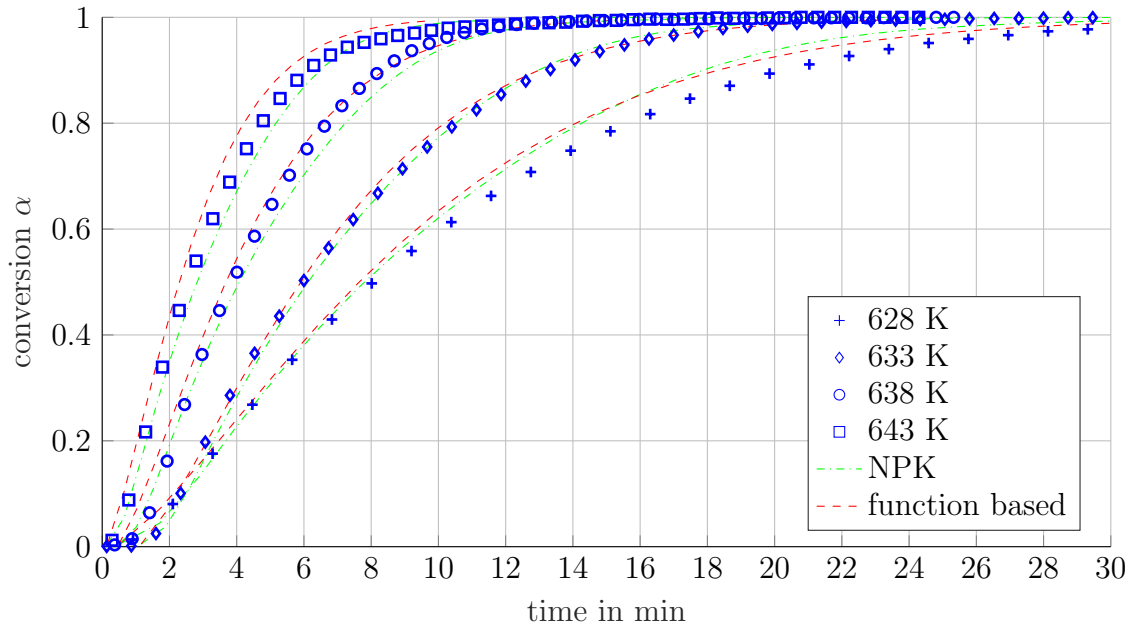


Figure 4.22: Simulation result for isothermal measurements of the CdCO_3 decomposition at different temperatures with $p_{\text{CO}_2} = 100$ mbar

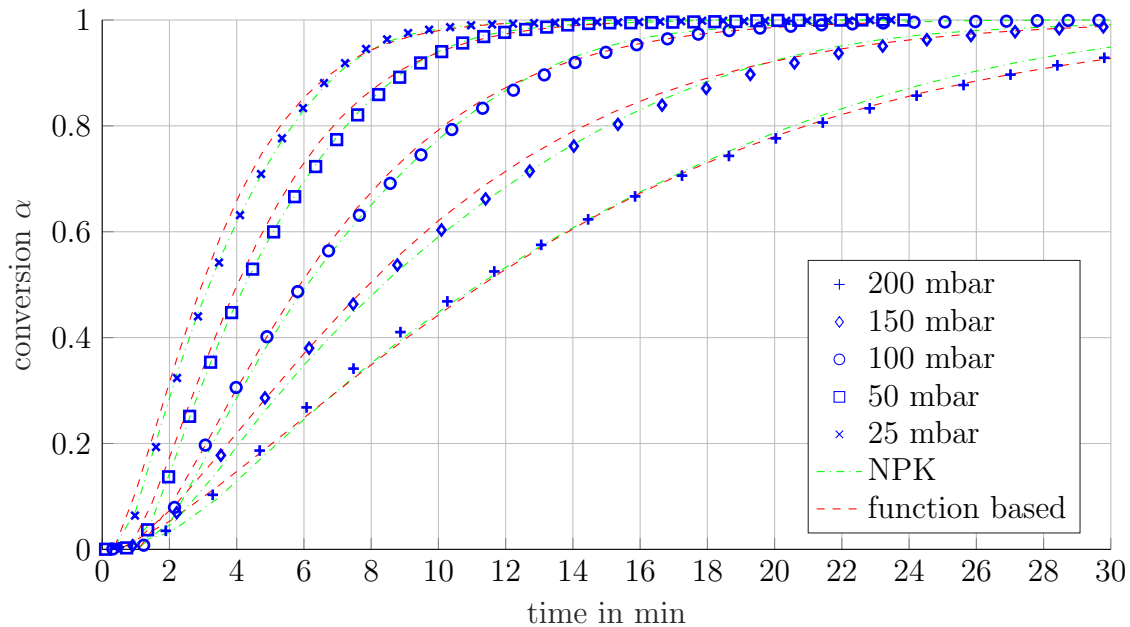


Figure 4.23: Simulation result for isobaric measurements of the CdCO_3 decomposition at different p_{CO_2} with $T = 633$ K

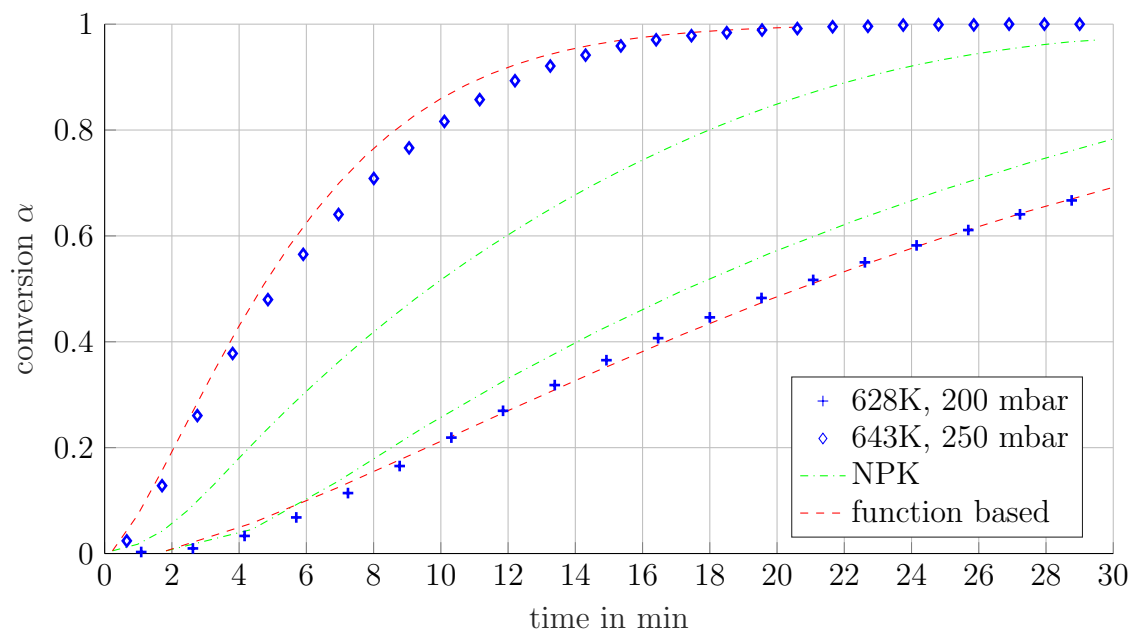


Figure 4.24: Simulation result for measurements of the CdCO_3 decomposition outside the identified region

Chapter 5

The system CuO/ Cu₂O

This chapter is a modification of:

Markus Deutsch, Florian Horvath, Christian Knoll, Daniel Lager, Christian Gierl-Mayer, Peter Weinberger and Franz Winter

High-Temperature Energy Storage: Kinetic Investigations of the CuO/Cu₂O Reaction Cycle

Energy and Fuels, 31 (3), pp 2324-2334, 2017

DOI: 10.1021/acs.energyfuels.6b02343

5.1 CuO/ Cu₂O for TCES

TCES is a promising technology to increase the efficiency of high-temperature applications. Especially, the combination with CSP is advantageous. TCES can help to increase the productivity of the CSP plant and reduce power grid fluctuations (see Section 1.2.1). For such an application, storage materials for temperatures between 800 °C-1200 °C are needed. The conducted search showed, that reactions with O₂ are most suitable for this temperature range. This result is in accordance with results from the literature [34]. Additionally, using O₂ as reactive gas is favorable as O₂ is highly available. Table 5.1 lists the 20 reaction systems with the highest energy storage capacity found in the desired temperature range. Oxides based on rare earth elements and radioactive elements are considered not practicable and, therefore, have been removed. For further discrimination the cost for the storage material has been considered. Table 5.2 shows estimated raw material costs for storing 1 kWh of the most promising TCES systems[49]. As pointed out by Alonso et al. [127], copper oxide is highly available in emerging CSP markets like Mexico and Chile, which results in a further reduction of the material price compared to other metal oxides. Both facts, the high energy

storage capacity and the low price, consolidate the potential of CuO as TCES candidate. The kinetics of the system CuO/Cu₂O has been investigated as possible oxygen carrier for chemical looping combustion (CLC). Several groups reported a reduction of the oxidation rate in air at higher temperatures [128, 129]. Clayton et al. [101, 130] studied the oxidation and reduction kinetics of Cu-based carrier materials with a CuO loading of up to 50%. Their work focused on the development of kinetic expressions aimed at better describing the observed oxidation profiles of cuprous oxide-based oxygen carriers. Zhu et al. [131] investigated the oxidation of Cu₂O in a temperature range of 600 °C-1050 °C during the copper oxidation with and without an initial thin CuO layer.

The goal of this work is the development of reliable kinetic models for the reaction system CuO/ Cu₂O as it occurs in a TCES application. Previous works investigated the system only for CLC application, in which copper based carriers with CuO loading up to 64% are used [101, 130]. For TCES applications, this would result in a reduced energy density of at least 37%. Therefore, it is important to measure kinetics, without possible effects of a carrier material. The kinetic analysis was performed in a simultaneous thermal analysis (STA) and in a lab scale fixed bed reactor. The cycle stability of the system is analyzed on a chemical reaction level in a STA and on a macroscopic level in a lab scale fixed bed reactor to further investigate the applicability for TCES.

5.2 Experimental setup

5.2.1 Material

The material used for all experiments was a granular CuO from Merck Emsure[®]. The particle size distribution of the granulate material can be seen in Figure 5.1. For further analysis the granulate was ground with a Retsch planetary ball mill PM 100 and afterwards sieved. For the analysis the fraction with a particle size between 32 μm-45 μm was used. A BET surface analysis resulted in a specific surface of the milled material of 3.1 m²/g. The phase composition yielding >99.9% pure CuO phase was determined by X-Ray powder diffraction.

5.2.2 Simultaneous thermal analysis - STA

The STA measurements were done in a Netzsch STA 449 F1 Jupiter with a differential thermal analysis (DTA) measurement setup. The sample mass in all STA measurements was 151.2 ± 0.6 mg CuO. The measurements were performed according to Figures 5.3 and 5.4. It shows the stability diagram of the system. The equilibrium curve is calculated based

Table 5.1: Comparison of possible O₂ based TCES systems for the application in CSP sorted by storage capacity. Based only on thermodynamic considerations. Storage capacity is based on 1 kg charged material at room temperature

#	reaction system	equilibrium temperature °C	storage capacity kJ/kg
1	$4\text{V}_2\text{O}_5 \rightleftharpoons 3\text{O}_2 + 2\text{V}_4\text{O}_7$	950	2540
2	$4\text{CuO} \rightleftharpoons \text{O}_2 + 2\text{Cu}_2\text{O}$	1119	1773
3	$2\text{MnO}_2 \rightleftharpoons \text{O}_2 + 2\text{MnO}$	1000	1574
4	$4\text{SbO}_2 \rightleftharpoons \text{O}_2 + 2\text{Sb}_2\text{O}_3$	1172	1294
5	$4\text{V}_2\text{O}_4 \rightleftharpoons \text{O}_2 + 2\text{V}_4\text{O}_7$	939	1292
6	$2\text{Na}_2\text{O}_2 \rightleftharpoons \text{O}_2 + 2\text{Na}_2\text{O}$	1160	1258
7	$\text{Rh}_2\text{O}_3 \rightleftharpoons \text{O}_2 + \text{Rh}_2\text{O}$	835	1027
8	$\text{Sb}_2\text{O}_5 \rightleftharpoons \text{O}_2 + \text{Sb}_2\text{O}_3$	911	881
9	$2\text{OsO}_4 \rightleftharpoons \text{O}_2 + 2\text{OsO}_3$	833	801
10	$4\text{AgO}_2 \rightleftharpoons \text{O}_2 + 2\text{Ag}_2\text{O}_3$	861	672
11	$2\text{Sb}_2\text{O}_4 \rightleftharpoons \text{O}_2 + 2\text{Sb}_2\text{O}_3$	1136	647
12	$4\text{KO}_2 \rightleftharpoons \text{O}_2 + 2\text{K}_2\text{O}_3$	988	622
13	$4\text{RbO}_2 \rightleftharpoons \text{O}_2 + 2\text{Rb}_2\text{O}_3$	1054	595
14	$\text{V}_6\text{O}_{13} \rightleftharpoons 2\text{O}_2 + 3\text{V}_2\text{O}_3$	956	519
15	$2\text{BaO}_2 \rightleftharpoons \text{O}_2 + 2\text{BaO}$	884	510
16	$2\text{Rb}_2\text{O}_2 \rightleftharpoons \text{O}_2 + 2\text{Rb}_2\text{O}$	805	355
17	$2\text{Rh}_2\text{O}_3 \rightleftharpoons \text{O}_2 + 4\text{RhO}$	974	343
18	$6\text{Mn}_2\text{O}_3 \rightleftharpoons \text{O}_2 + 4\text{Mn}_3\text{O}_4$	1000	321
19	$\text{V}_6\text{O}_{11} \rightleftharpoons \text{O}_2 + 3\text{V}_2\text{O}_3$	819	303
20	$4\text{V}_7\text{O}_{13} \rightleftharpoons 5\text{O}_2 + 14\text{V}_2\text{O}_3$	801	275

Table 5.2: Estimated raw material cost of the most promising TCES systems for CSP [49]

#	reaction system	raw material costs \$/kWh
1	$4\text{V}_2\text{O}_5 \rightleftharpoons 3\text{O}_2 + 2\text{V}_4\text{O}_7$	72
2	$4\text{CuO} \rightleftharpoons \text{O}_2 + 2\text{Cu}_2\text{O}$	8
3	$2\text{MnO}_2 \rightleftharpoons \text{O}_2 + 2\text{MnO}$	13
4	$4\text{SbO}_2 \rightleftharpoons \text{O}_2 + 2\text{Sb}_2\text{O}_3$	27

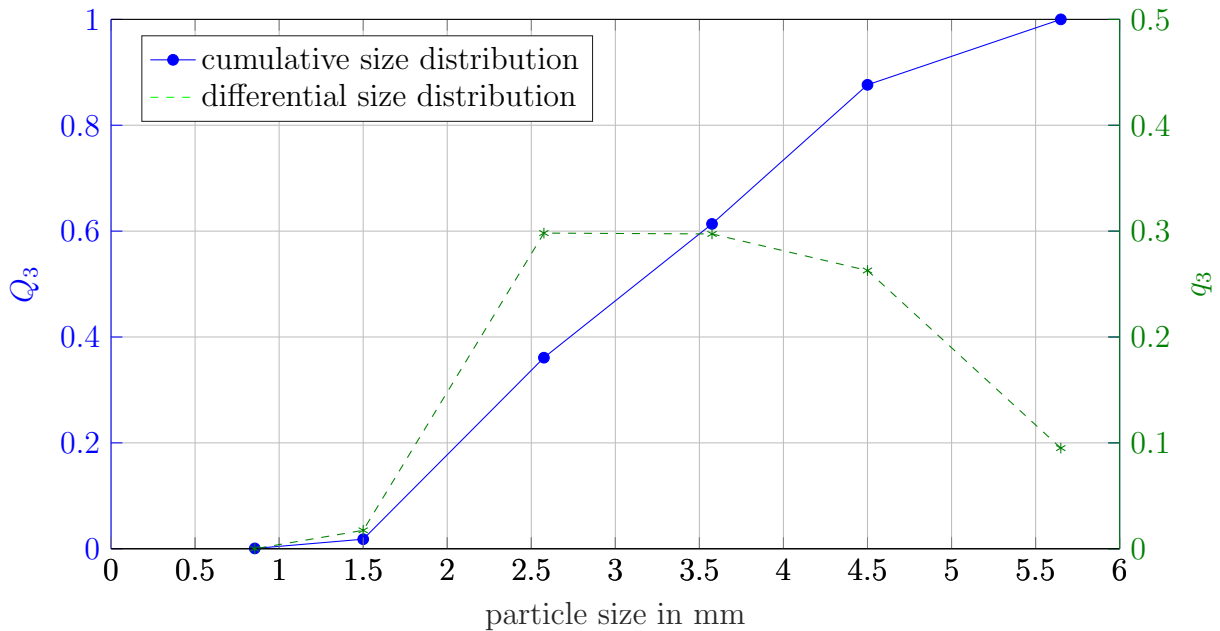


Figure 5.1: Mass based particle size distribution of the CuO granulate. Drawn points represent mean value of mesh size.

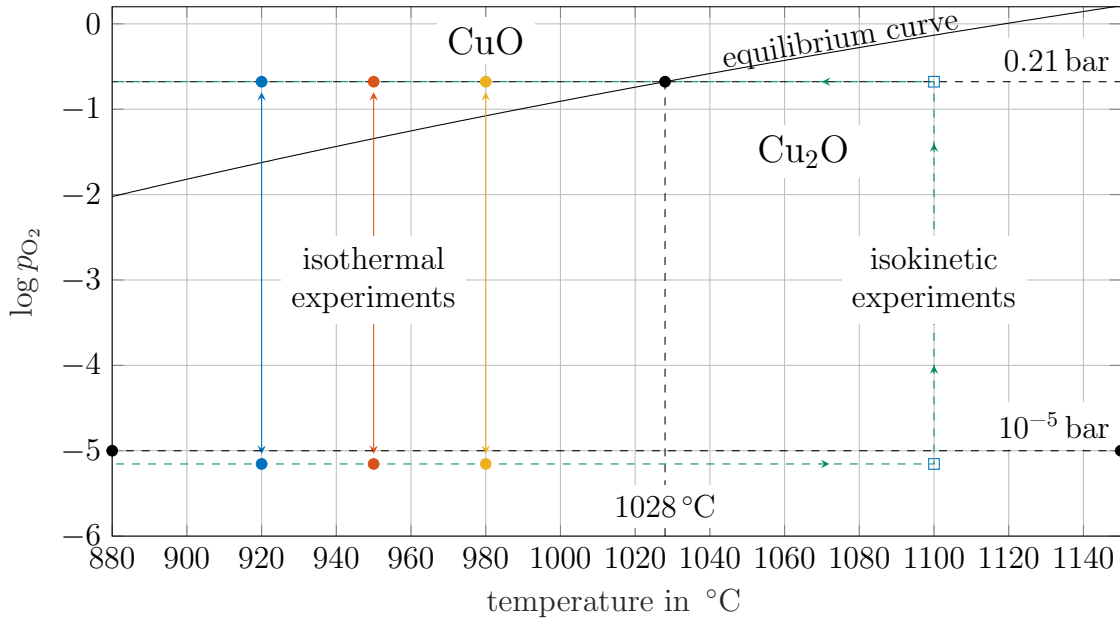


Figure 5.2: Stability diagram for system CuO/Cu₂O based on data from HSC Database [115] shown with the investigated experimental conditions

on data from HSC Database [115] according to Eq.(2.28). As shown there, CuO reacts to Cu₂O in air ($p_{\text{O}_2} = 0.21$ bar) at temperatures over 1028 °C [115].

For isokinetic STA measurements the sample was heated up with a constant heating rate β up to 1100 °C in N₂ atmosphere ($p_{\text{O}_2} < 10^{-5}$ bar). Then the atmosphere was switched to synthetic air ($p_{\text{O}_2} = 0.21$ bar) and the sample was cooled down with a cooling rate equal to the heating rate. In this work heating rates of 2, 5 and 10 K/min were applied.

For isothermal STA measurements, the sample was heated up under synthetic air atmosphere with 10 K/min up to the measurement temperature. When a constant sample temperature was achieved, the atmosphere was switched to N₂ inducing the reduction. After the reduction was completed, the atmosphere was switched back to synthetic air to start the oxidation. At the end of the oxidation the sample was cooled down with 10 K/min. In this work, isothermal STA measurements were performed at 920, 950 and 980 °C.

The cycle test was performed at 950 °C. The sample was heated up with 10 K/min in synthetic air atmosphere. When isothermal conditions were reached, the cycle was started. The cycle consisted of two segments:

1. reduction under N₂ atmosphere for 60 min
2. oxidation under synthetic air atmosphere for 75 min

The cycle was repeated 20 times. Then the sample was cooled down with 10 K/min to room temperature.

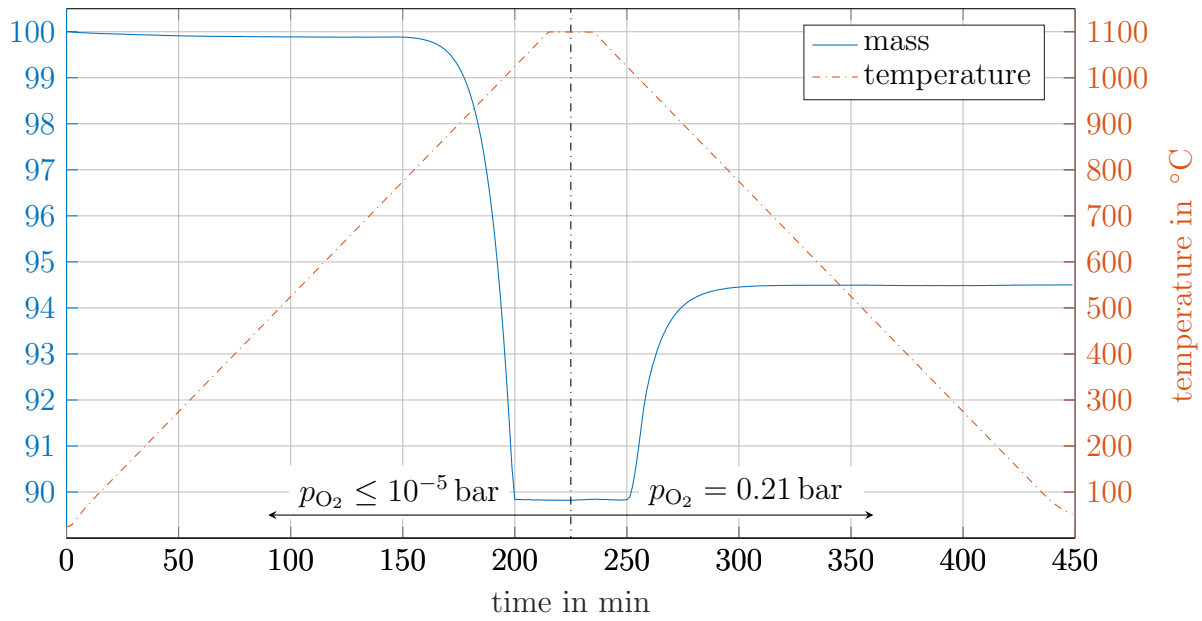


Figure 5.3: Representative measurement procedure in the STA for isokinetic analysis with $\beta = 5 \text{ K/min}$

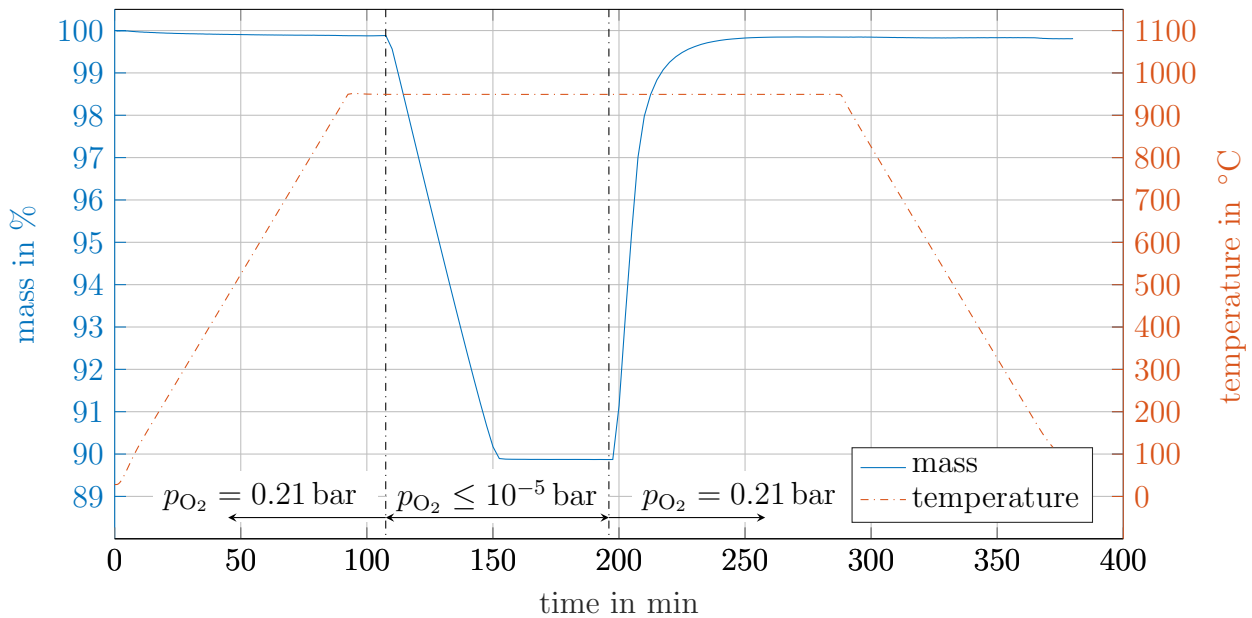


Figure 5.4: Representative measurement procedure in the STA for isothermal analysis with $T = 950 \text{ }^\circ\text{C}$

From the mass signal $m(t)$ of each measurement, the mass content of CuO $w(t)$ can be calculated based on

$$w(t) = \frac{m(t) - m_0 \nu}{m_0 (1 - \nu)} \quad \text{with } \nu = \frac{M_{CuO}}{2 M_{Cu_2O}} \quad (5.1)$$

with M_{CuO} and M_{Cu_2O} are the molar masses of CuO and Cu_2O , respectively, and m_0 the sample mass at the beginning. The conversion α in case of the oxidation is equal to $w(t)$, in case of the reduction $\alpha = 1 - w(t)$ is valid.

5.2.3 Fixed bed reactor

A reactor was used to investigate the reaction under macroscopic conditions. Its schematic setup is shown in Figure 5.5. It consists of two tubes on top of each other with an inner diameter of 40 mm. The lower tube is the preheating zone and is filled with sand for better heat transfer onto the reaction gas. In the reaction chamber the material was placed on a glass frit. The quartz glass frit with a pore size between 160 μm -250 μm is used to evenly distribute the reaction gas over the cross section of the reactor. The reactor is heated with resistance heating shells up to 1100 °C. The temperature control is done based on the temperature inside the reactor, which is measured with a thermocouple type K within the CuO bulk. To achieve different gas atmospheres, N_2 and O_2 can be mixed via two mass flow controllers. After passing the reactor the reactive gas passes a gas cooling system into a gas analyzer which measures the O_2 concentration c_{O_2} . Compressed air is used for outer cooling of the reactor and better temperature control. In the reactor isothermal tests at 930, 950 and 980 °C with 50 g of CuO granulate material were performed. The material was heated up with a gas flow of 2.5 L/min N_2/O_2 mixture with $p_{O_2} = 0.21$ bar to simulate air. When isothermal conditions were reached in the reactor the reaction atmosphere was switched to 2.5 L/min N_2 ($p_{O_2} \leq 10^{-5}$ bar) to induce the reduction (see Figure 5.2). When the O_2 concentration reached zero in the off-gas the reduction was assumed to be completed and the oxidation was started. This was done by switching back to the starting reaction atmosphere of 2.5 L/min N_2/O_2 mixture ($p_{O_2} = 0.21$ bar).

The cycle test was similar to the test in the STA. The test used 50.8267 g CuO. The sample was heated up in mixed gas flow of 2 L/min N_2 and 0.5 L/min O_2 . When isothermal conditions at 950 °C were reached the cycle was started. The cycle consisted of two segments:

1. reduction under 2.5 L/min N_2 for 200 min
2. oxidation under 2 L/min N_2 and 0.5 L/min O_2 for 130 min

The cycle was repeated 23 times.

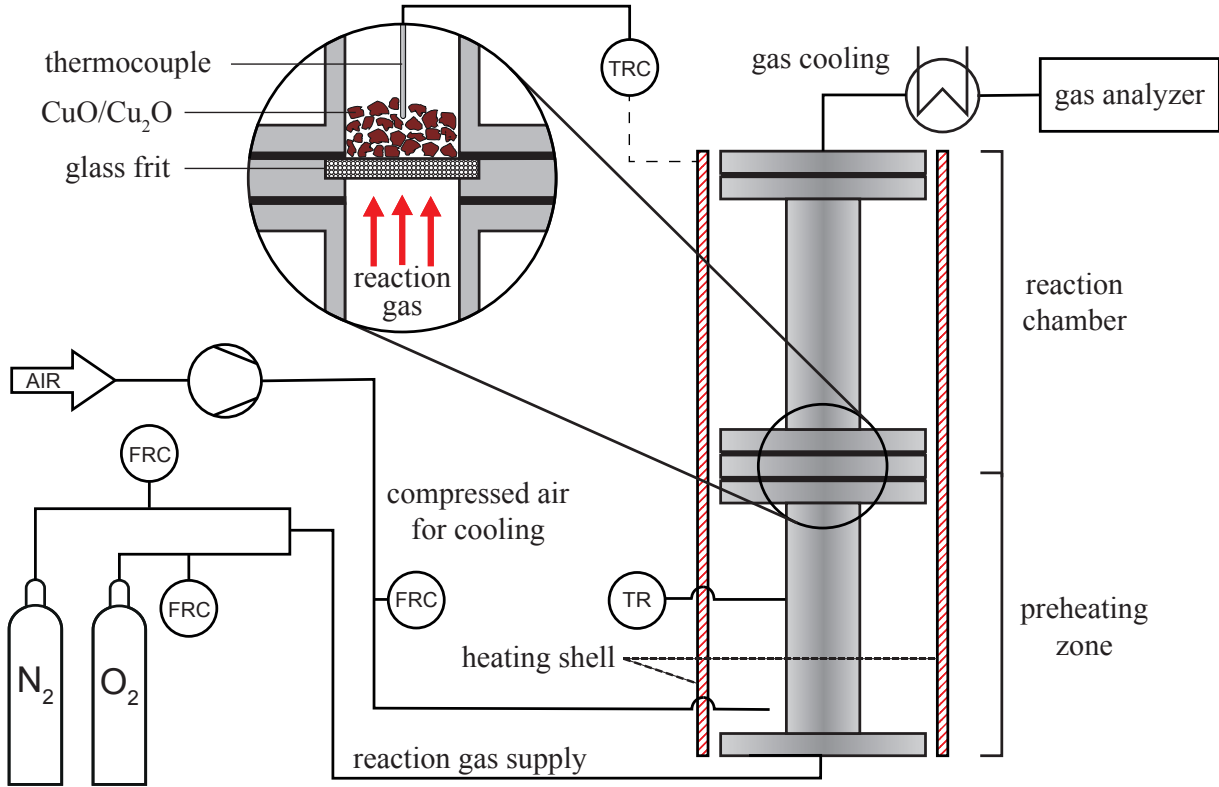


Figure 5.5: Schematic setup of the reactor used for kinetic measurements under fixed bed conditions

The conversion α in this case is calculated on the O_2 concentration c_{O_2} following

$$\alpha(t) = \frac{\int_0^t \dot{V} \Delta c_{O_2}(t) dt}{\int_0^{t_{end}} \dot{V} \Delta c_{O_2}(t) dt} \quad (5.2)$$

where \dot{V} is the volumetric gas flow through the reactor, t_{end} the duration of the reaction and $\Delta c_{O_2}(t)$ the difference in c_{O_2} between an empty reactor and a reactor filled with reactive material. The change of \dot{V} due to the released or consumed O_2 is negligible.

5.2.4 X-Ray powder diffraction

The powder X-ray diffraction measurements were carried out using a PANalytical X'Pert diffractometer in Bragg Brentano geometry using $Cu K_{\alpha 1,2}$ radiation, a X'Celerator linear detector with a Ni filter, sample spinning with back loading zero background sample holders and $2\Theta = 4-90^\circ$ ($T = 25^\circ C$). The diffractograms were evaluated using the PANalytical program suite HighScorePlus v3.0d. A background correction and a $K_{\alpha 2}$ strip were performed.

5.2.5 BET-analyzer

The analysis of the specific surface of the samples was determined with nitrogen sorption measurements on an ASAP 2020 (Micromeritics) instrument. The samples (amounts between 100-200 mg) were degassed under vacuum at 80 °C overnight prior to the measurement. The surface area was calculated according to the method of Brunauer, Emmett and Teller (BET) [132].

5.3 Kinetic identification

5.3.1 STA measurements

The results of the isokinetic STA measurements are shown in Figure 5.6. In the left diagram the reduction of CuO in N₂ atmosphere during heating can be seen for different heating rates. It reveals that the system reacts completely regardless of the heating rate with the typical shift of the conversion curve to higher temperatures for higher heating rates. The right diagram shows the oxidation of Cu₂O during cooling in synthetic air atmosphere. There, the reached content of CuO strongly depends on the cooling rate, with the slowest rate reaching the highest CuO content. The reaction stops as the temperature falls below 800 °C. This behavior is similar for all investigated cooling rates, therefore, it can be concluded that the available energy at temperature levels below 800 °C is not enough to promote the reaction. Hence the reaction is kinetically limited by the temperature. This also explains the difference in final conversions, as the sample in a measurement with a slower cooling rate remains longer in a temperature range above 800 °C where the reaction occurs. Due to this, the temperatures 920, 950 and 980 °C were chosen for the isothermal measurements, as the reaction has a relevant reaction rate in this temperature range.

The isothermal measurements are shown in Figure 5.7. The left diagram shows the reduction of CuO in N₂ atmosphere, the right diagram shows the oxidation of Cu₂O in synthetic air atmosphere. In both cases the conversion is complete. On one hand, it can be seen that higher temperature results in faster reduction. On the other hand the oxidation is slowed down with increased temperature as it has been reported in the literature [130].

5.3.2 Reactor measurements

The results of the measurements in the test reactor are presented in Figure 5.8. All measurements reached full conversion, which was verified by X-ray powder diffraction analysis. The major difference between the STA measurements and the reactor measurements is that the oxidation does not slow down with the increasing temperature. This is most likely con-

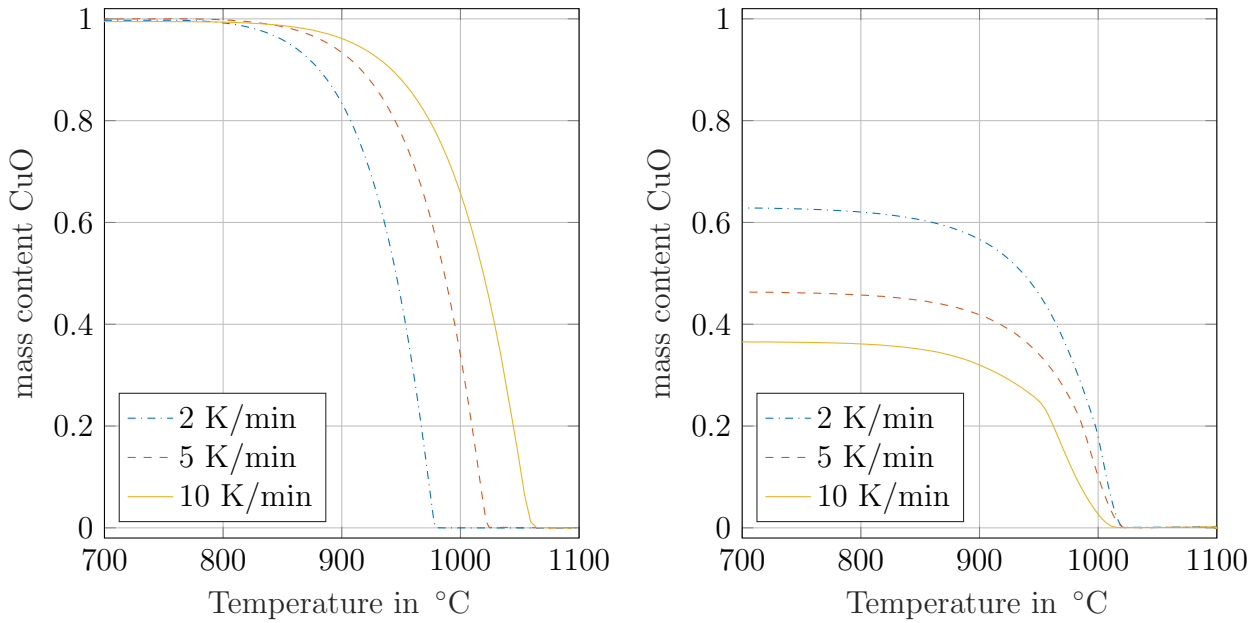


Figure 5.6: Isokinetic STA measurements at different heating/cooling rates - left: reduction in N₂ during heating, right: oxidation in synthetic air during cooling

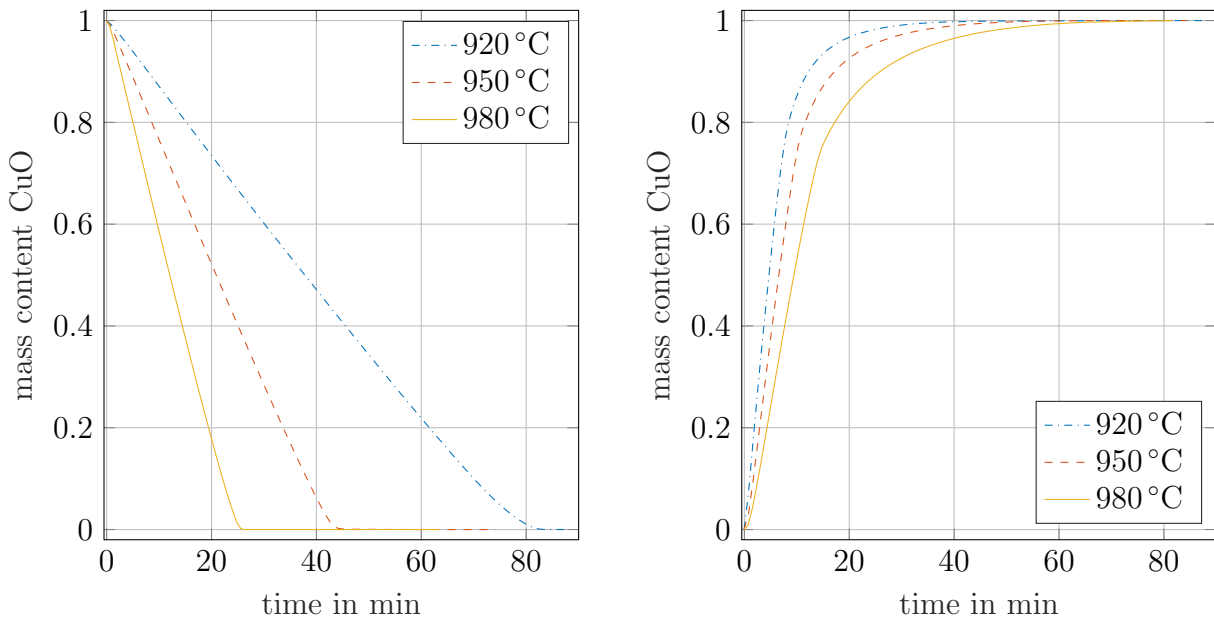


Figure 5.7: Isothermal STA measurements at different temperatures - left: reduction in N₂, right: oxidation in synthetic air

nected to a better mass transport inside the bulk due to the flow through of the reactive gas compared to the laminar transport in the STA crucible.

Additionally, it has to be noted that the temperature inside the reactor for the oxidation is not constant. As a result of the big sample mass in the reactor (50 g), the released energy influences the local sample temperature inside the reactor. Due to the thermal inertia of the system, the released energy results in non-isothermal measurement conditions, which are

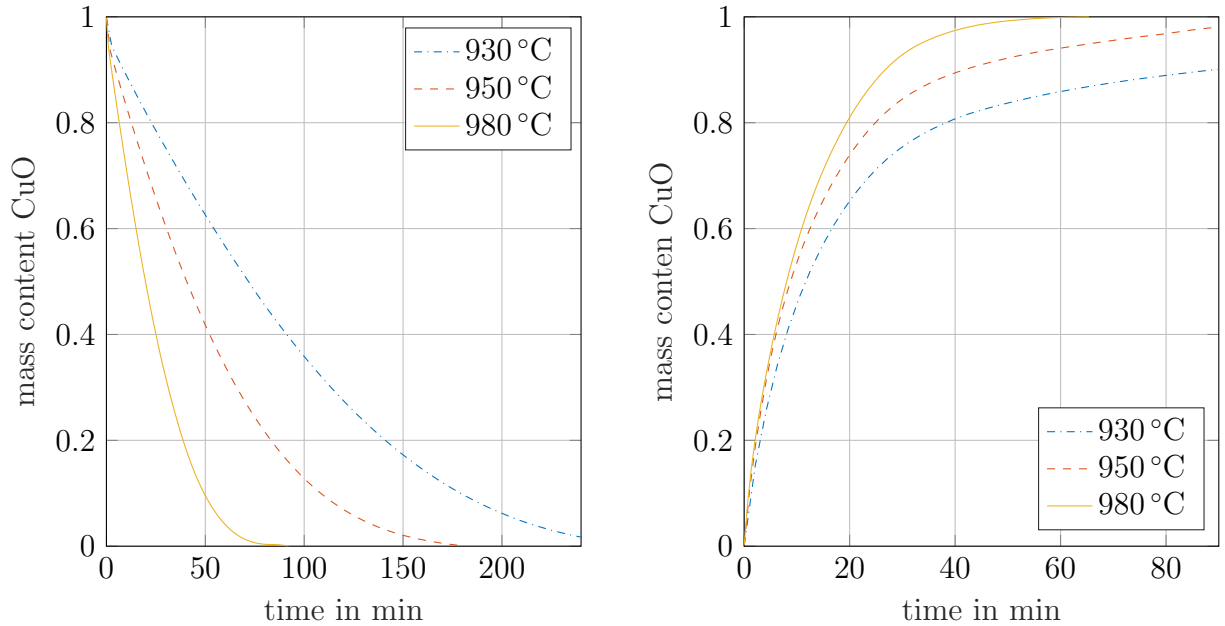


Figure 5.8: Measurements in the fixed bed reactor at different starting temperatures - left: reduction in N_2 , right: oxidation in synthetic air

recorded by the thermocouple within the bulk material. Figure 5.9 shows representatively the deviation of the isothermal temperature of $950\text{ }^\circ\text{C}$ during the oxidation. The released energy can hardly be compensated by the cooling of the reactor. This further consolidates the system $\text{CuO}/\text{Cu}_2\text{O}$ as a promising CSP-TCES system.

5.3.3 Reduction

The kinetic identification of the reduction was performed on the isokinetic STA measurements (Figure 5.6). Utilizing the NPK method, this resulted in a model based on (4.11), with $s = 2.949 \cdot 10^{-3} \text{ s}^{-1}$ and the vectors \mathbf{u} and \mathbf{v} as shown in Figures 5.10 and 5.11. Linearization of \mathbf{v} based on (4.37) results in the Arrhenius plot in Figure 5.12. From the slope of the fitted linear equation the apparent activation energy E_a for the reduction can be calculated as 255.68 kJ/mol .

Therefore, both the isokinetic measurements as well as the isothermal measurements were simulated based on the model derived from the isokinetic data. Additionally, the simulation was performed in two different ways.

With the kinetic information calculated with the NPK method, the reduction was simulated in two ways. Once, with the result of the NPK method used directly to simulate the conversion ('full NPK') and once with the temperature dependency described by the identified Arrhenius equation ('NPK + Arrhenius'). Often the conversion dependency found by the NPK method is valid in a sufficient range, but the temperature dependency is limited. By fitting the Arrhenius equation an extrapolation is possible and, therefore, the temperature

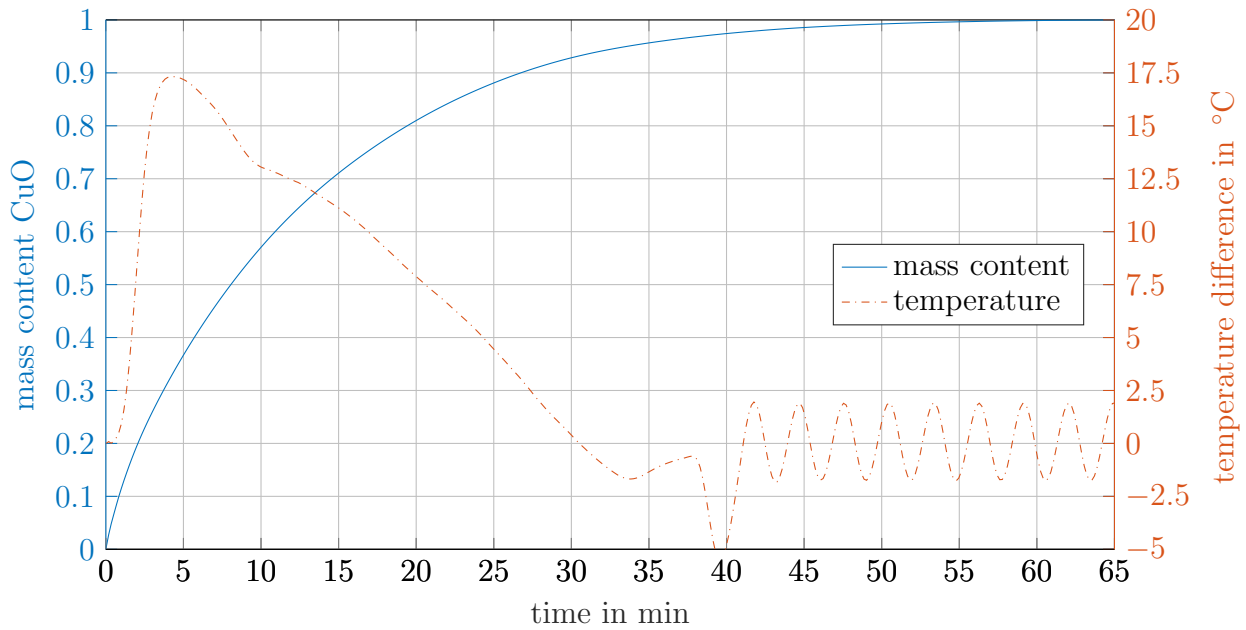


Figure 5.9: Temperature change in the reaction zone due to the released energy during oxidation at 950°C starting temperature

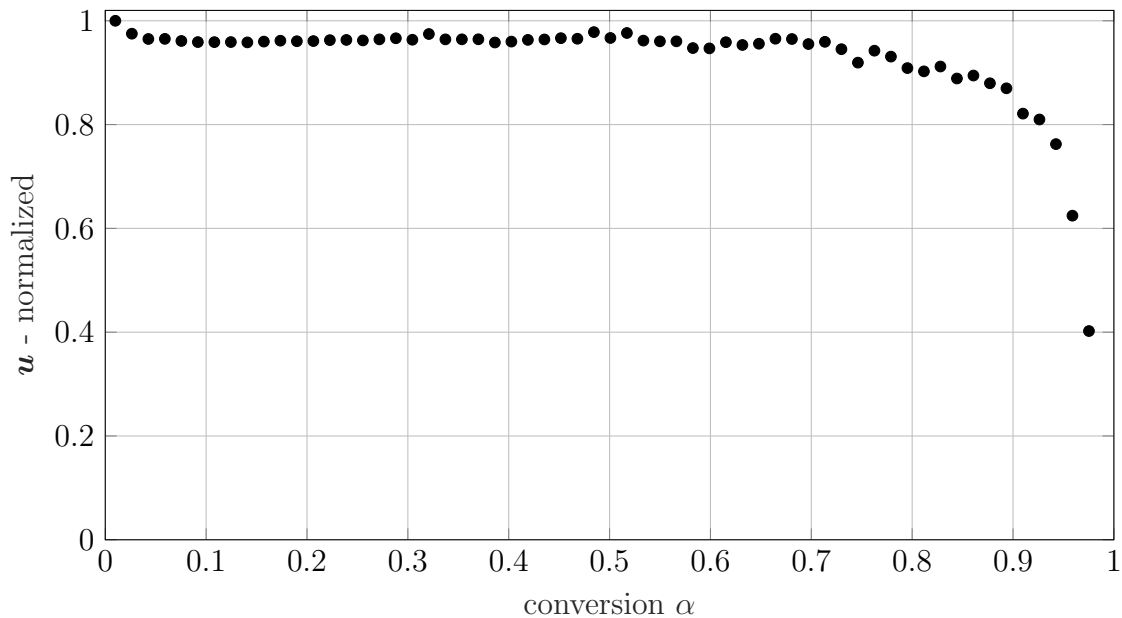


Figure 5.10: Conversion dependency vector \mathbf{u} derived from isokinetic measurements of the reduction of CuO in N_2

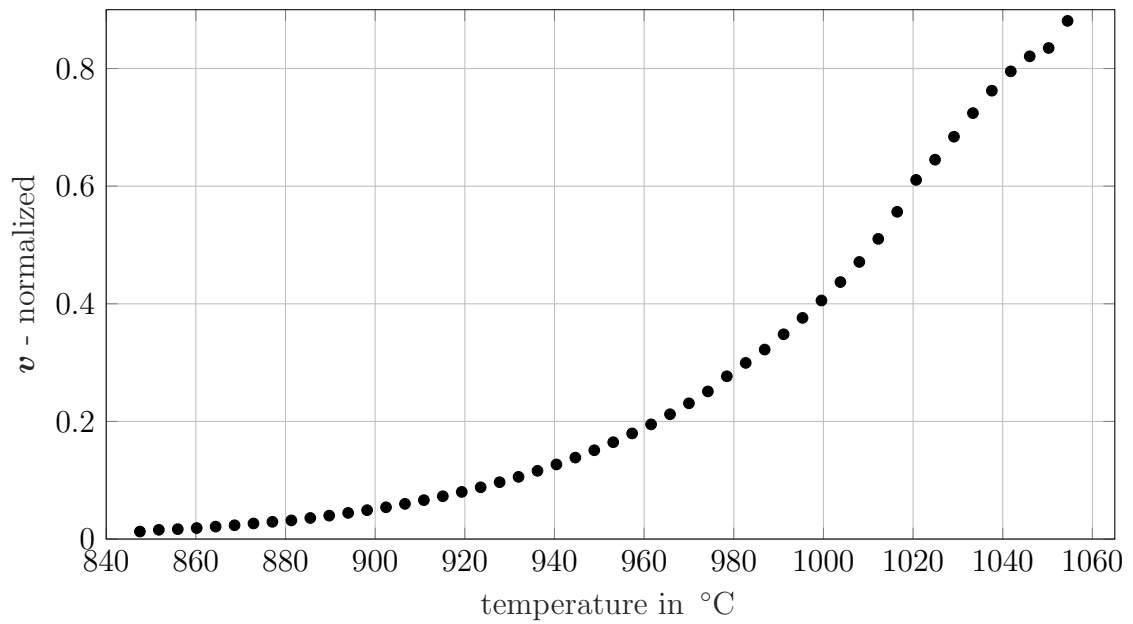


Figure 5.11: Temperature dependency vector \boldsymbol{v} derived from isokinetic measurements of the reduction of CuO in N_2

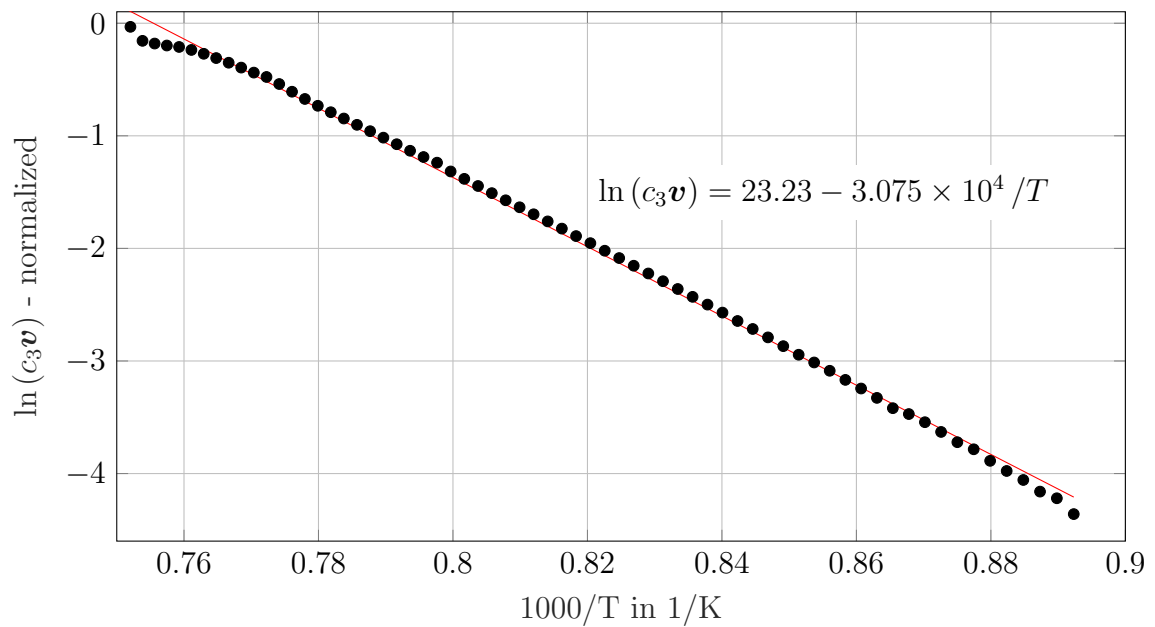


Figure 5.12: Arrhenius plot of \boldsymbol{v} derived from isokinetic measurements of the reduction of CuO in N_2

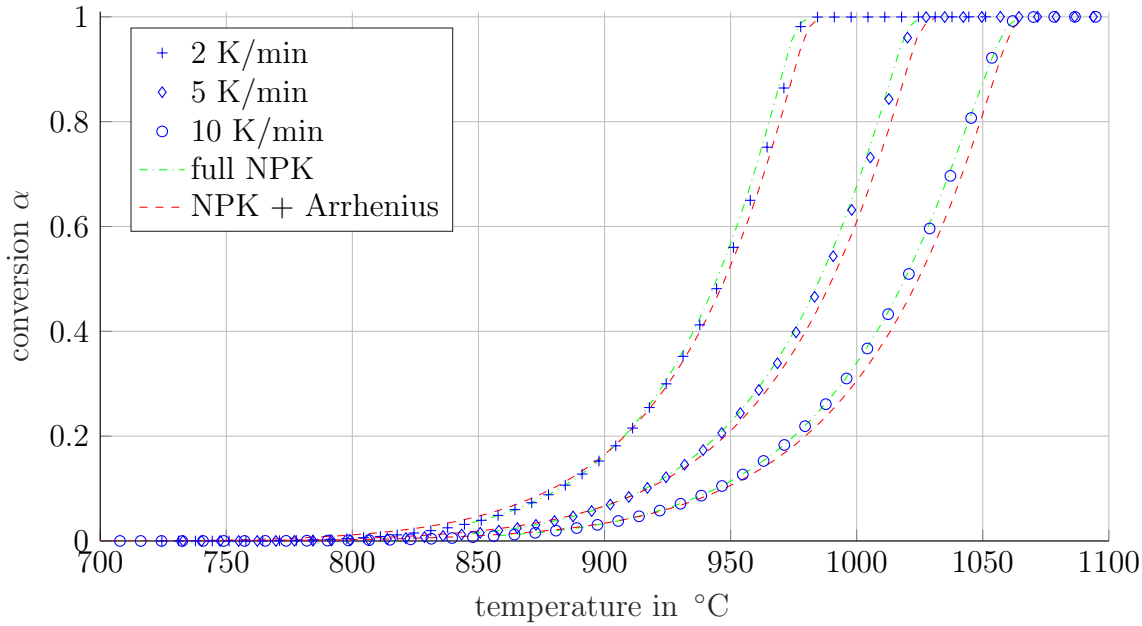


Figure 5.13: Simulation of the isokinetic measurements of the reduction of CuO with the identified model

range in which the model is applicable is increased. Note that the apparent pre-exponential factor is only correct in combination with the vector \mathbf{u} , identified by the NPK method. Figure 5.13 shows the fit of the simulated isokinetic measurements to the actual measurements for conversion and conversion rate. Both methods reproduce the measurements well and while the full NPK method is limited to temperatures above 850 °C due to \mathbf{u} (Figure 5.11), the combination of NPK and Arrhenius equation is capable of giving the behavior of the reaction below 850 °C.

The results of the simulation of the isothermal experiments are shown in Figure 5.14. There it can be seen that the models fit the measurements reasonably well, especially, since the model was identified from isokinetic data.

Additionally, the reduction in the reactor is analyzed. Since only three temperature levels are available, vector \mathbf{v} consists of only 3 points. The activation energy E_a based on the corresponding Arrhenius plot (Figure 5.15) was calculated as 316.9 kJ/mol. The difference between E_a in the STA and the fixed bed reactor leads to the conclusion that the reaction in the STA is not only governed by the intrinsic reaction kinetics but also by mass transfer [133]. One can also see that the conversion dependency \mathbf{u} (Figure 5.16) differs from the dependency found in the STA measurements. Note, the dead volume in the reactor smears out the change of the O₂ concentration in the off gas. This is especially significant at the beginning of the reduction, when the atmosphere in the reactor is changed from synthetic air to N₂. This causes the steep drop at the beginning of \mathbf{u} . Thus, it is assumed that the conversion dependency is only valid for $\alpha > 0.1$. With the identified model for the reactor,

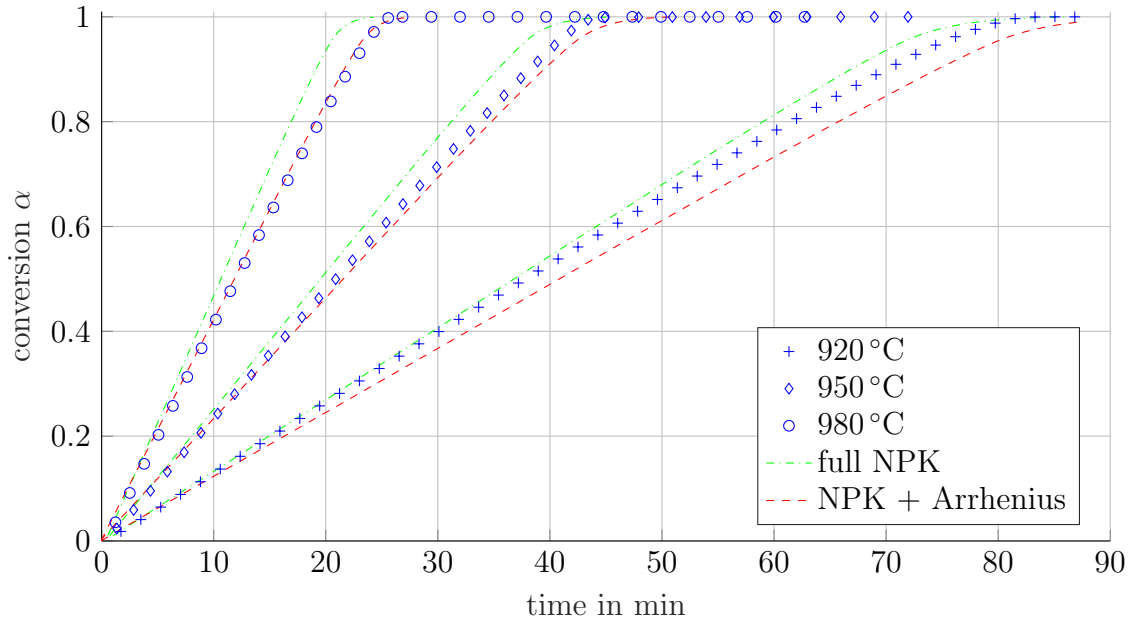


Figure 5.14: Simulation of the isothermal measurements of the reduction of CuO with the model identified from isokinetic measurements

it was also possible to reproduce the measurement results satisfactory (Figure 5.17).

5.3.4 Oxidation

Since the isokinetic STA measurements of the oxidation reaction (see Figure 5.6) do not reach full conversion, it is not possible to calculate the conversion dependency for a satisfying conversion range. Therefore, the NPK method was performed on the isothermal STA experiments. The identified vectors \mathbf{u} and \mathbf{v} are shown in Figures 5.19 and 5.18. The shape of \mathbf{u} in the oxidation differs from the reduction, thus, it can be concluded that the conversion mechanism differs between reduction and oxidation. Again, vector \mathbf{v} consists only of three points. Also, as expected from the isothermal measurement data, the fitted linear equation in the Arrhenius plot of \mathbf{v} has a positive slope, resulting in an apparent activation energy E_a of -137.10 kJ/mol. Nevertheless, the simulation can reproduce the measurement with good accuracy (Figure 5.20).

The result of the kinetic identification of the oxidation in the reactor is shown in Figures 5.21 and 5.22. In contrast to the other isothermal measurements, vector \mathbf{v} consists of more than 3 points. This is due to the non-isothermal condition described in chapter 5.3.2. This can be considered in the kinetic identification by the NPK method and, therefore, additional temperature information is extracted from the data. As a downside, a non-isotropic temperature field occurs, reducing the quality of the identified model and leading to a higher deviation of the simulation from the measurement (Figure 5.17).

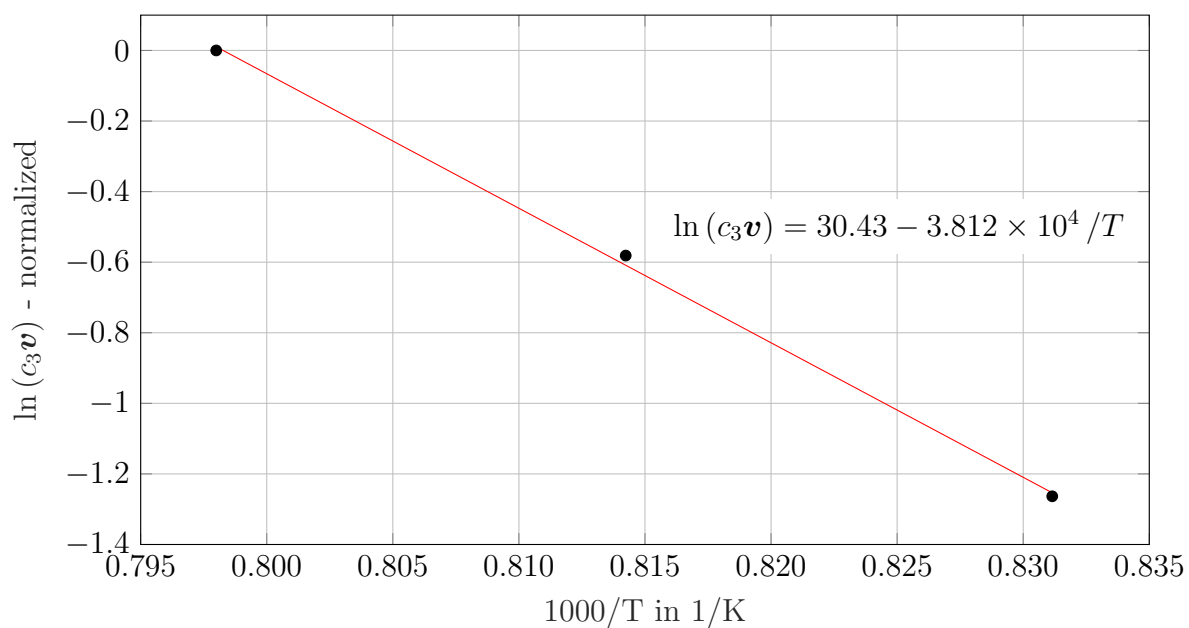


Figure 5.15: Arrhenius plot of v derived from isothermal measurements of the reduction of CuO in the reactor

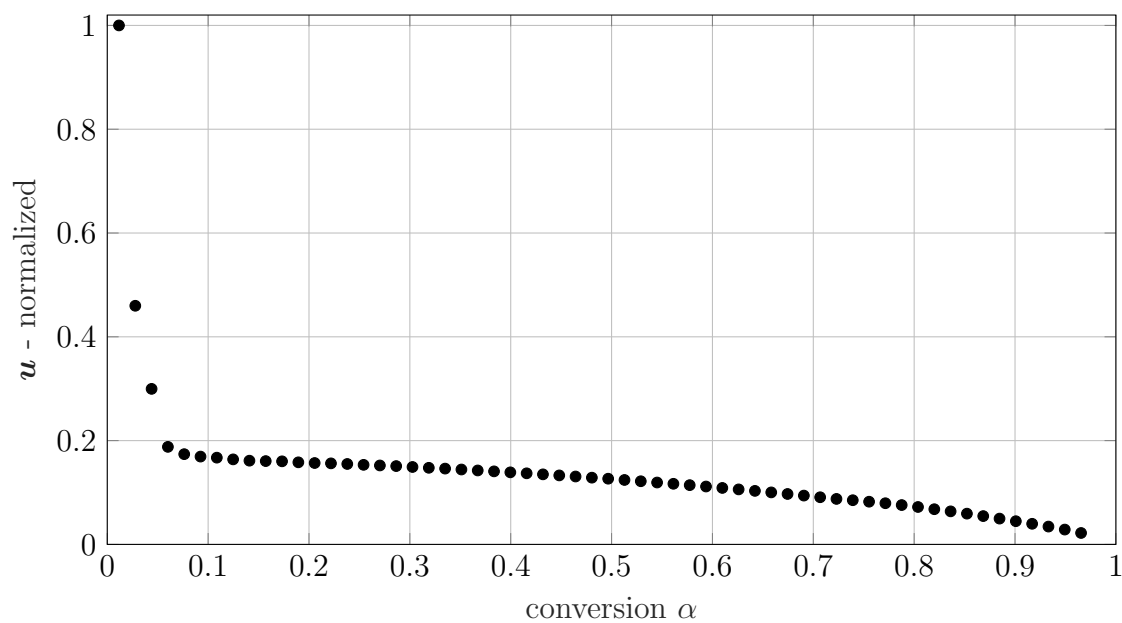


Figure 5.16: Conversion dependency vector u derived from isothermal measurements of the reduction of CuO in the reactor

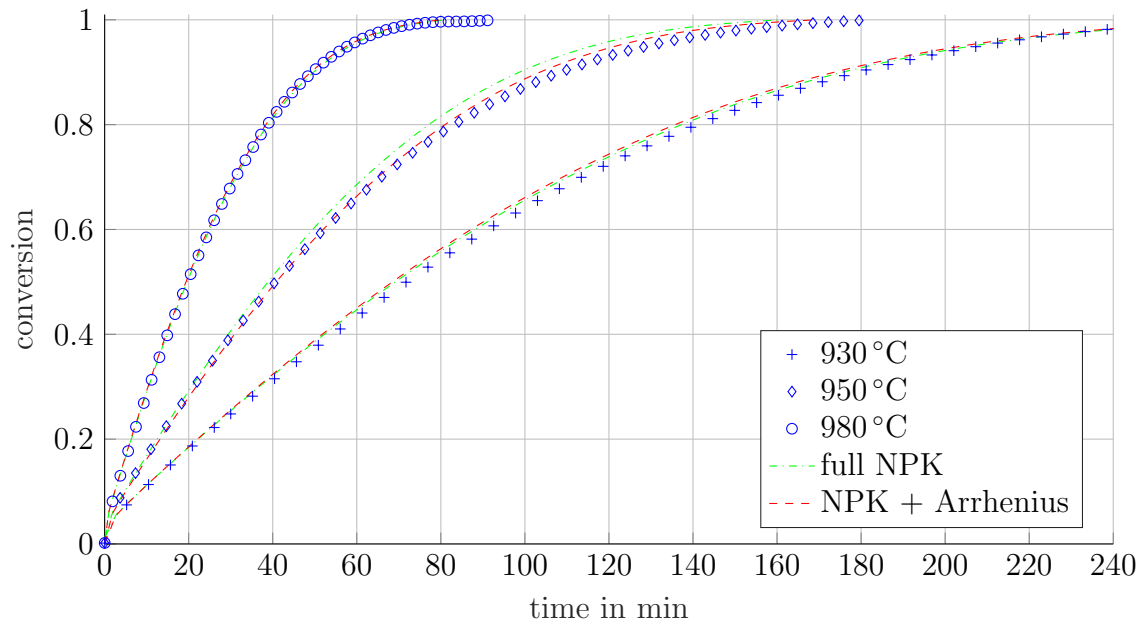


Figure 5.17: Simulation of the isothermal measurements of the reduction of CuO in the testrig

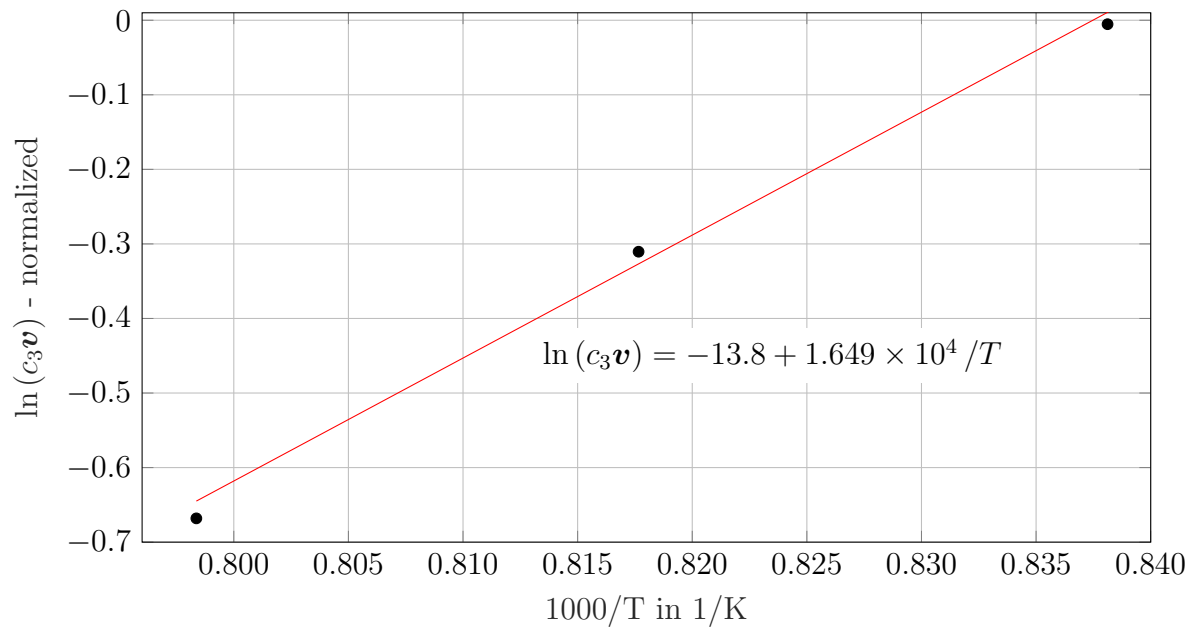


Figure 5.18: Arrhenius plot of v derived from isothermal STA measurements of the oxidation of Cu_2O

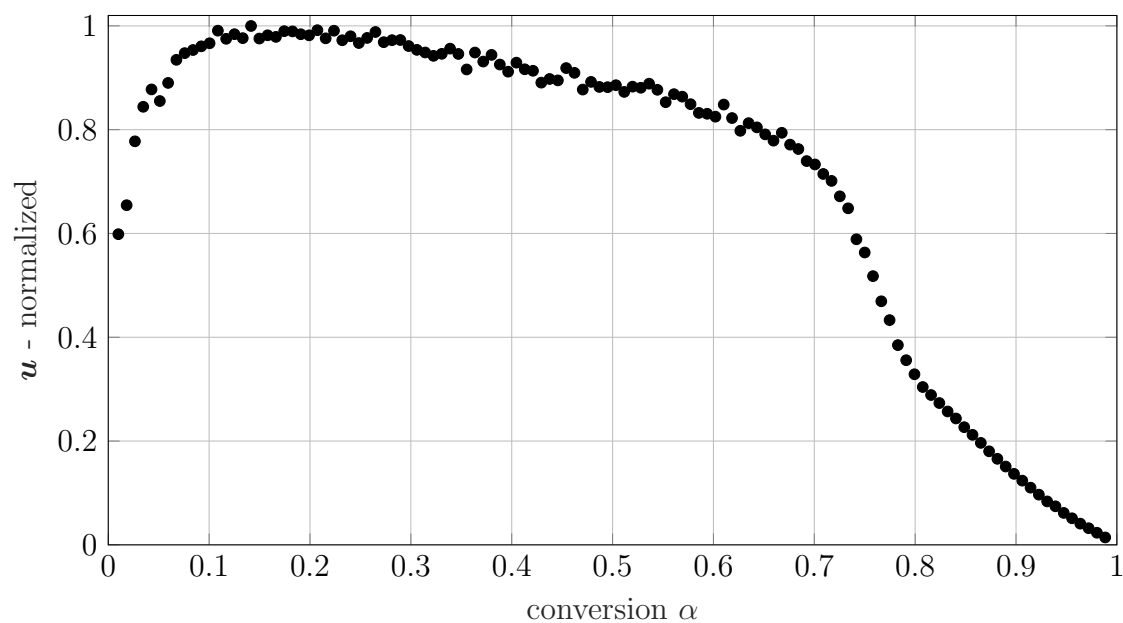


Figure 5.19: Conversion dependency vector u derived from isothermal STA measurements of the oxidation of Cu_2O

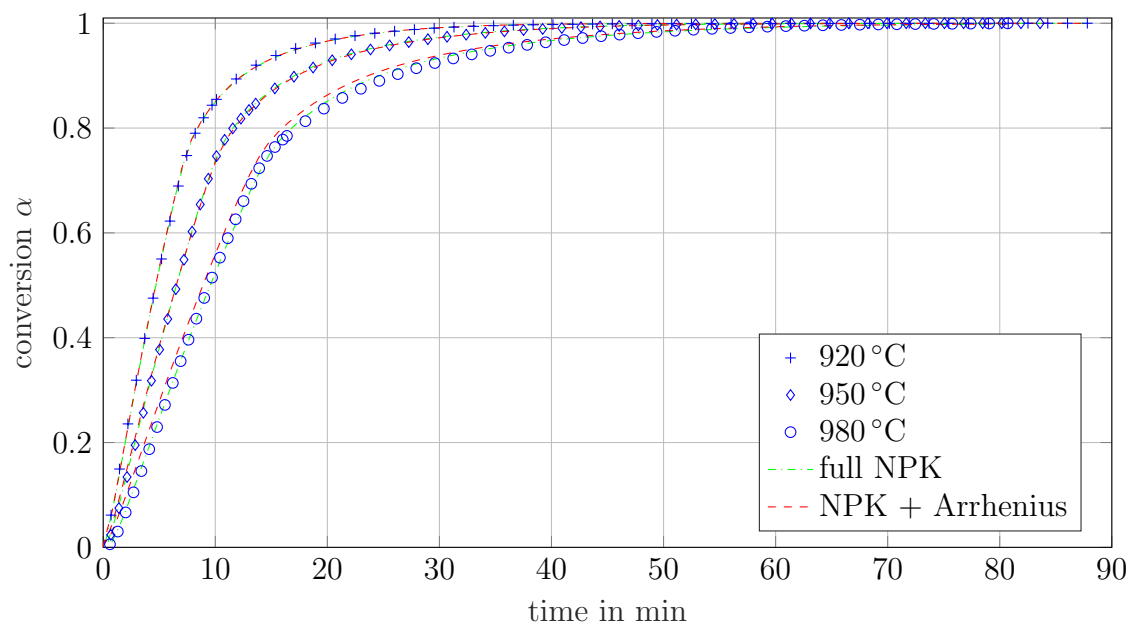


Figure 5.20: Simulation of the isothermal STA measurements of the oxidation of Cu_2O

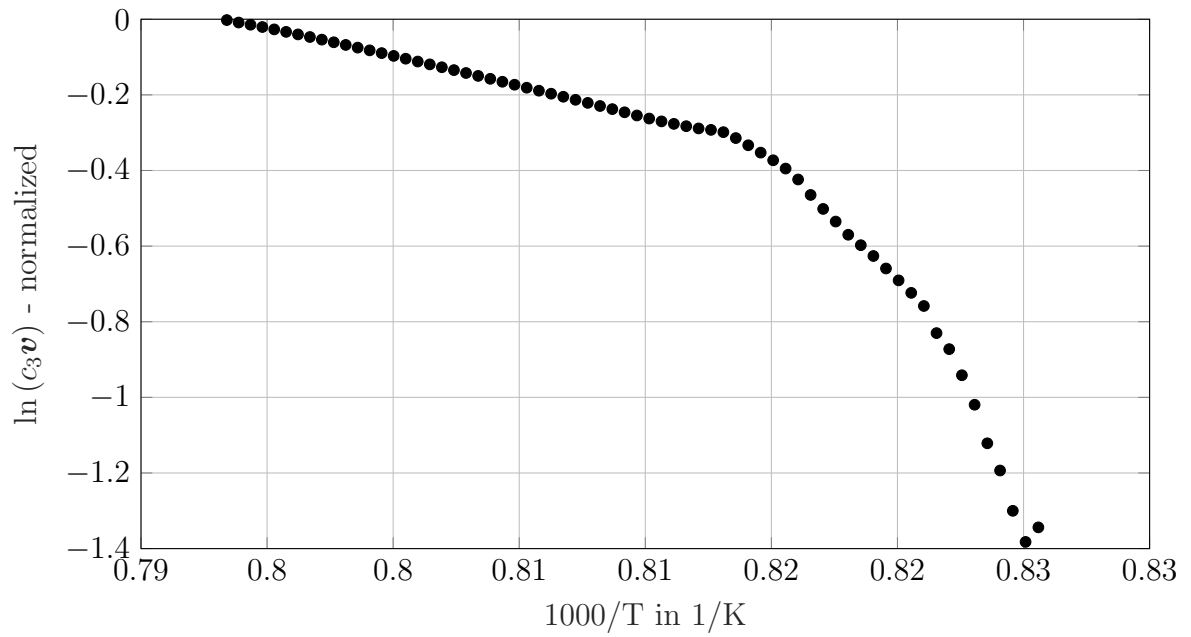


Figure 5.21: Arrhenius plot of \mathbf{v} derived from isothermal measurements of the oxidation of Cu_2O in the reactor

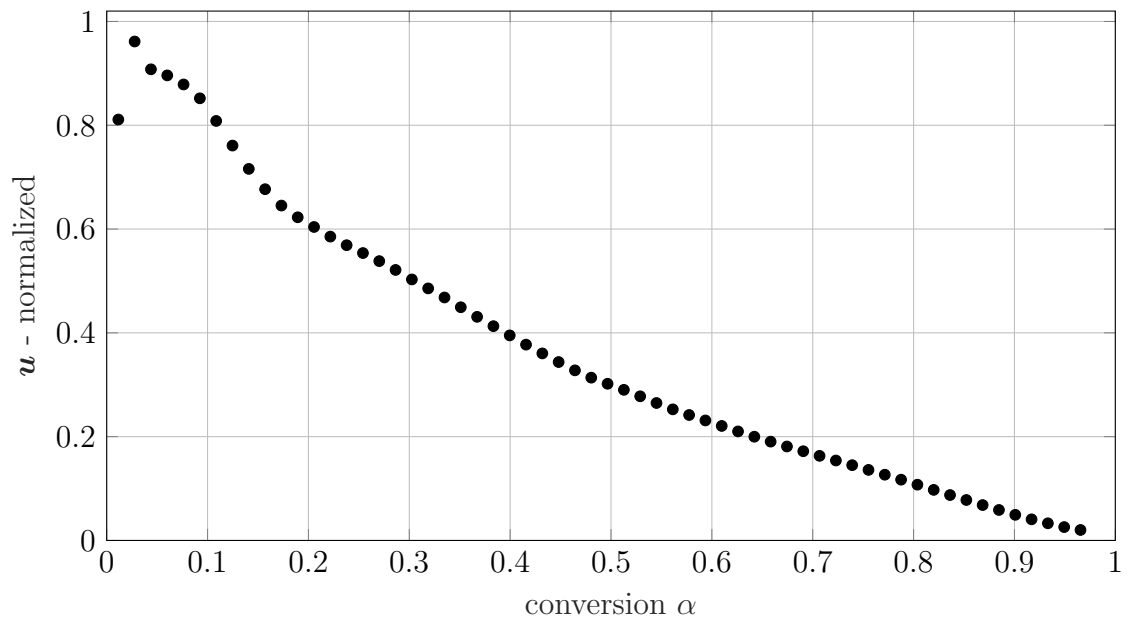


Figure 5.22: Conversion dependency vector \mathbf{u} derived from isothermal measurements of the oxidation of Cu_2O in the reactor

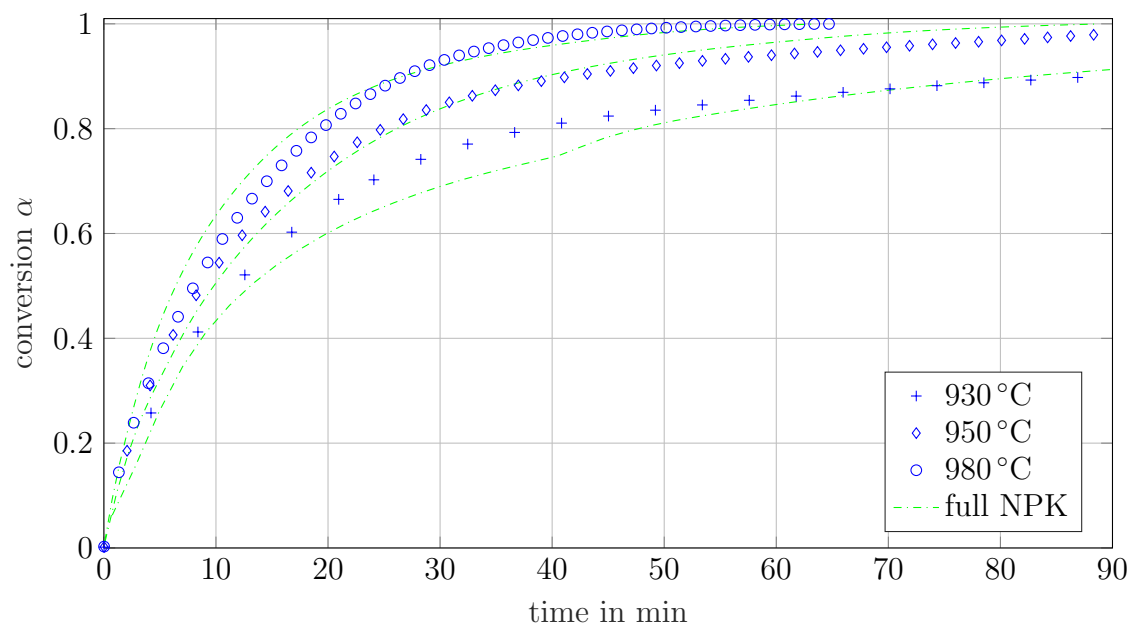


Figure 5.23: Simulation of the isothermal measurements of the oxidation of Cu_2O in the reactor

5.3.5 Cycle test

The cycle stability test in the STA is shown in Figure 5.24. The diagram shows the change of the conversion in the sample and the energy flow over 20 cycles. One can see that the form of the conversion curve changes only minor over the cycles. There is no sign of chemical degradation, in fact after 10 cycles the system reaches nearly theoretical conversion.

An equivalent cycle test was performed in the reactor, with the result that the granular material sintered together, blocking the reaction after a few cycles. Figure 5.25 shows the sintering of the material after the first and the last cycle. Additionally, the sintered material was cut in half (Figure 5.25D). It can be seen that the surface of the material sintered completely together, while the granular structure is still present in the inner core of the sample. Additionally, cavities of Cu_2O were formed in the edge regions, which was confirmed by a XRD analysis. Based on this behavior, it can be concluded that a fixed bed process is not practical for energy storage. An alternative option would be to use a rotary reactor, as it prevents the sintering due to relative movement of the particles, as suggested by Alonso et al. [127].

5.4 Discussion

The measurements revealed a distinctively different behavior between the oxidation in the STA and the fixed bed reactor. In the STA, the oxidation slowed down with increased temperature as described in the literature. This results in a negative apparent activation

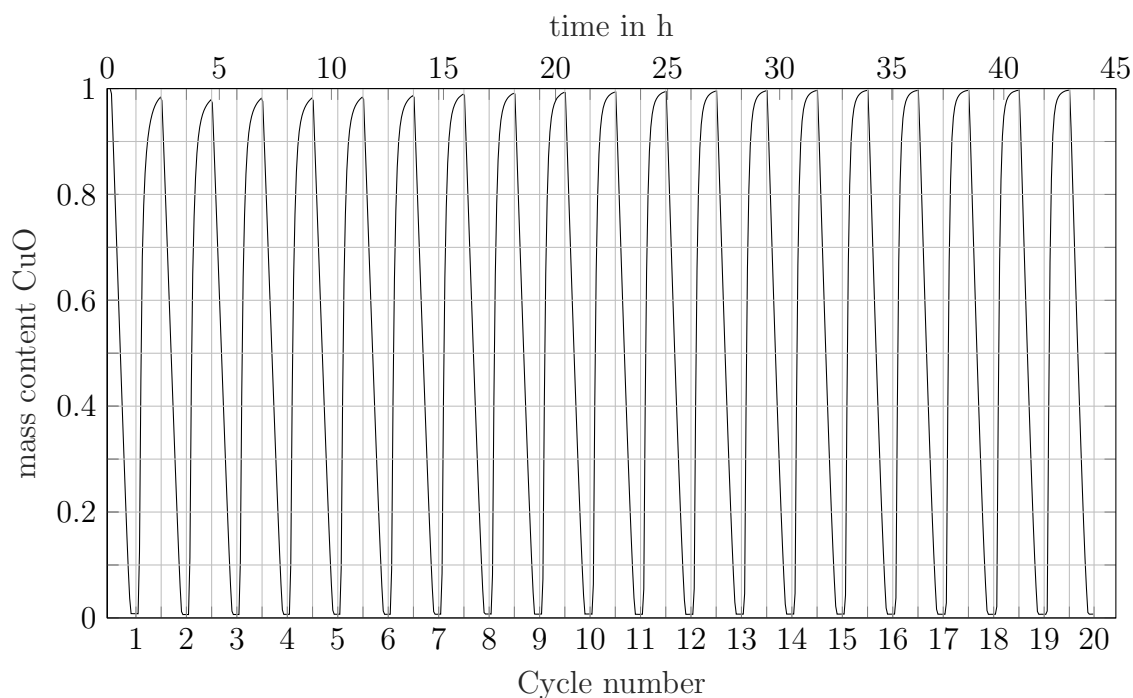


Figure 5.24: CuO reaction behavior over 20 cycles in the STA at 950 °C and changing N_2 /synthetic air atmosphere

energy E_a of -137.10 kJ/mol. Such behavior was not observed in the fixed bed reactor, where a mechanistic change was detected, through a change of E_a , but no negative E_a has been found. A comparison between the available literature [101, 130, 134] and this work show significant differences in the kinetics of the reaction system. Clayton et al. [130] presented conversion times around 1 to 2 min for the reduction, Hu et al. [134] reported the reaction occur within 10 min while the reaction in this work took around 40 min for full conversion. All three publications conducted their measurements in a TGA or STA. The main difference between all publication is the sample material.

While Clayton et al. [130] used copper based oxygen carriers with TiO_2 and ZrO as support material, Hu et al. [134] used an oxygen carrier based Al_2O_3 . The support material reduces the CuO content to around 40 %, which directly reduced the energy density. Thus, this work used granular CuO. Johansson et al. [135] reported that different support materials have different effects on the reactivity of the system Mn_3O_4/MnO . A similar effect could explain the different kinetic behavior. Further examinations are needed to identify the decisive factor behind this different behavior.

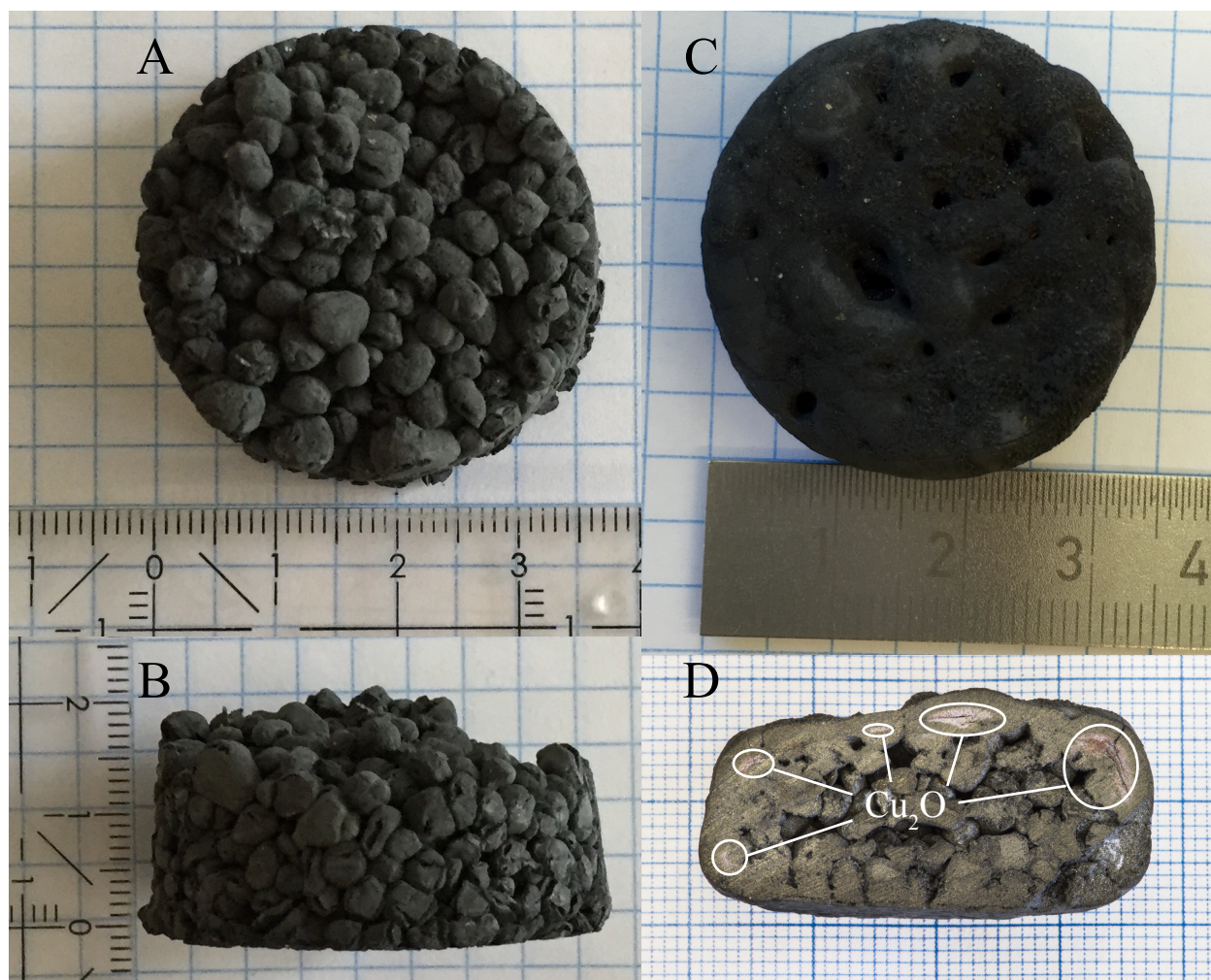


Figure 5.25: Sintering of the granulate material in the fixed bed reactor - A & B: top and side view after 1 cycle, C: top view after 20 cycles, D: inside view of the material after 20 cycles

Chapter 6

Conclusion

The increased perception of TCES materials witnessed in the recent years stimulated a look for a novel, systematic approach to this topic. Due to the so far limited number of investigated reactions the provision of a database was considered, allowing for a broader overview on principally suitable TCES systems, as well as for a quick identification of the corresponding parameters and experimental data. This could offer advantages for researchers and future industrial users as a variety of reactions, covering different temperature and reactive gas profiles are easily searchable.

By the use of a systematic search algorithm potentially suitable candidates for TCES systems were identified. As a source for the needed thermodynamic data the HSC database was used. The algorithm screens for reaction couples, where both educts and products have a database entry and can be matched via mathematical analysis of the corresponding elemental coefficients. Nevertheless, a control eliminating stoichiometric correct couples, where a reaction cannot occur, has to avoid chemically nonsense entries. In a first approach the search was limited to gas-solid reactions. It led to 1012 principally suitable TCES systems for five different reactive gases (H₂O 553 hits, CO₂ 40 hits, NH₃ 39 hits, SO₂ 28 hits and O₂ 352 hits). A full description of the algorithm and more details on the found systems are found in Chapter 3.

Those systems were filtered based on their equilibrium temperature, energy density and manageability.

To further assess their potential as TCES material and distinguish between possible candidates for an application, a novel method to analyze the kinetics of a TCES system was developed. The method extends the NPK method to also identify a pressure dependency in addition to the temperature and conversion dependencies. It does so by splitting a three-dimensional problem (α , T , p) into three one-dimensional problems, thus reducing its complexity. The method is based on the assumption that the effect of α , T and p are linked multiplicatively. By arranging measurement data in special data matrices a singular value

decomposition can be utilized to approximate the underlying dependencies. The resulting vectors can be combined to build a full model or they can be further analyzed to get insight into the underlying physical processes. This gives the opportunity to improve the reaction behavior and optimize the TCES system for an application. The complete method is described in Chapter 4.

Based on the search results, the TCES system $\text{CuO}/\text{Cu}_2\text{O}$ was found to be a potential candidate for the application in CSP. To validate this assessment the kinetic behavior and the cycle stability of the system were analyzed in a STA and a fixed bed reactor. Based on isokinetic and isothermal measurements kinetic models were derived for oxidation and reduction. Therefore, the NPK method was applied and the Arrhenius equation was introduced to expand the applicable temperature range.

In the fixed bed reactor, the system showed a high energy output during oxidation, proofing the capability of CuO as a TCES material. In the STA the reaction system shows an excellent cycle stability over the course of 20 cycles. In the fixed bed reactor, heavy sintering occurred which reduced the reaction to a minimum by blocking most of the reactive surface. This allowed only the outmost layer of the material to react. Further investigations show that the sample in the STA also sintered, but due to the small thickness of the sample in the crucible, no reaction hindering effect was measured. Thus, a fixed bed process is not suitable for application, instead a system with movement of the material to prevent sintering should be considered. Nevertheless, the study shows, that the system $\text{CuO}/\text{Cu}_2\text{O}$ is a valid candidate for TCES in combination with CSP, but further investigations are necessary. The detailed analysis of this system is found in Chapter 5.

In summary, it can be stated that the presented approach supports an efficient identification and analysis of future TCES systems.

Nomenclature

Acronyms

CLC chemical looping combustion

CSP concentrating solar power

DSC differential scanning calorimetry

DTA differential thermal analysis

GEA Global Energy Assessment, <http://www.globalenergyassessment.org/>

HSC thermodynamic database by Outotec, stands for enthalpy, entropy and heat capacity

IEA International Energy Agency

NPK non-parametric kinetics

OFW Ozawa, Flynn and Wall kinetic identification

PCM phase change material

SSE sum of squared errors

STA simultaneous thermal analysis

SVD singular value decomposition

TCES thermochemical energy storage

TES thermal energy storage

TGA thermogravimetric analysis

WBGU Wissenschaftlicher Beirat der Bundesregierung Globale Umweltveränderungen, Germany, <http://www.wbgu.de>

Greek Symbols

α	conversion	-
β	heating or cooling rate	K/s
χ	fitting parameter	system dependent
$\frac{d\alpha}{dT}$	non isothermal conversion rate	1/K
$\frac{d\alpha}{dt}$	conversion rate	1/s
λ	growth dimension	-
μ	chemical potential	J/mol
ν_i	stoichiometric coefficient of substance i	-
ω	fitting parameter	system dependent
ϕ_i	scaling factor of each submatrix in NKP analysis	-
ψ	fitting parameter	system dependent
ρ	density	kg/m ³
σ	shape factor (e.g. $4\pi/3$ for a sphere)	-

Indices

α	at specific conversion α
m	at position of peak maximum
p	for the identification of $h(p)$
R	value calculated for a reaction
T	for the identification of $k(T)$
0	at the beginning, at time t_0
1, 2	different states of a system or variable
f	formation, as in $H_{\{textf\}}$ or S_f
PC	value for/at phase change
s	submatrix

Latin Symbols

ΔH_f	molar enthalpy of formation	J/mol
ΔH_{PC}	molar phase change enthalpy	J/mol
ΔH_R	molar reaction enthalpy	J/mol
ΔS_R	molar reaction entropy	J/(mol · K)
\dot{V}	volume flow	m ³ /s
A	pre-exponential factor for a reaction	1/s
a	linear fitting parameter of the Doyle approximation of the temperature integral	-
a_i	thermodynamic activity of substance i	-
A_{app}	apparent pre-exponential factor	1/s
b	linear fitting parameter of the Doyle approximation of the temperature integral	-
c_1, c_2, c_3, \dots	scaling constants used in the NPK method	-
c_p	specific isobaric heat capacity	J/(kg · K)
c_i	concentration of substance i	mol/m ³
E_a	activation energy	J/mol
F	free energy	J
$f(\alpha)$	differential conversion dependency	-
G	Gibbs energy	J
$g(\alpha)$	integral conversion dependency	-
H	enthalpy	J
$h(p)$	pressure dependency	-
K	equilibrium constant	system dependent
k	constant	system dependent
$k(T)$	temperature dependency	1/s
M	molar mass	kg/mol
m	mass	kg

NOMENCLATURE

N	number of nuclei	-
n_i	molar amount of substance i	mol
p	pressure	Pa
Q	Energy	J
$q(x)$	exponential integral of the temperature integral transformation	-
R	universal gas constant	8.314 J/(mol · K)
r	radius of particle or crystal	m
S	entropy	J/K
s	first singular value of the SVD of matrix \mathbf{A}	1/s
T	temperature	K
t	time	s
T_0	Temperature at standard conditions	298.15 K
T_{mean}	mean temperature of the experiment	K
T_{PC}	temperature of phase change of a material	K
T_{start}	start temperature of temperature program	K
U	inner energy	J
V	volume	m ³
v	specific volume	m ³ /kg
v_i	molar volume of substance i	m ³ /mol
$w(t)$	mass content	-
x	integration variable in the transformed temperature integral with the transformation $x = E/(RT)$	-
z	igeneral reaction process	-
\mathbf{A}	data matrix or tensor	1/s
\mathbf{a}	vector of activities a_i	-

<i>f</i>	vector representation of conversion dependency according (4.8)	-
<i>k</i>	vector representation of temperature dependency according (4.9)	-
<i>n</i>	vector of molar amounts n_i	mol
<i>u</i>	conversion dependency vector derived by NPK method	-
<i>v</i>	temperature dependency vector derived by NPK method	-
<i>w</i>	pressure dependency vector derived by NPK method	-
<i>x</i>	vector of molar fractions x_i	-

Superscripts

0	value at standard conditions ($T^0 = 273.15 \text{ K}$, $p^0 = 1 \times 10^5 \text{ Pa}$)
---	--

Bibliography

- [1] NOAA National Centers for Environmental Information. State of the climate: Global analysis for annual 2016, January 2017.
- [2] NOAA National Centers for Environmental Information. State of the climate: Global analysis for annual 2015, January 2016.
- [3] Ch. D. Keeling, St. C. Piper, R. B. Bacastow, M. Wahlen, T. P. Whorf, M. Heimann, and H. A. Meijer. Atmospheric CO₂ and 13 CO₂ exchange with the terrestrial biosphere and oceans from 1978 to 2000: Observations and carbon cycle implications. In I.T Baldwin, M.M Caldwell, G. Heldmaier, R. B. Jackson, O.L Lange, H.A Mooney, E.-D Schulze, U. Sommer, J. R. Ehleringer, M. Denise Dearing, and T. E. Cerling, editors, *A History of Atmospheric CO₂ and Its Effects on Plants, Animals, and Ecosystems*, pages 83–113. Springer New York, New York and NY, 2005.
- [4] R. Wrangham. *Catching fire. How cooking made us Human*. Perseus Books Group, New York, 2009.
- [5] Food and Agriculture Organisation of the United Nations. *Energy for sustainable rural development projects: A reader*, volume 23 of *Training materials for agricultural planning*. FAO, Rome, 1991.
- [6] E. Cook. Flow of energy in an industrial society. *Scientific American (United States)*, 1971.
- [7] IEA. *Key World Energy Statistics 2016*. IEA, 2016.
- [8] O. Ellabban, H. Abu-Rub, and F. Blaabjerg. Renewable energy resources: Current status, future prospects and their enabling technology. *Renewable and Sustainable Energy Reviews*, 39:748–764, 2014.
- [9] Bull, S. R. Renewable energy today and tomorrow. *Proceedings of the IEEE*, 89(8):1216–1226, 2001.

- [10] Wissenschaftlicher Beirat der Bundesregierung Globale Umweltveränderungen. *Welt im Wandel: Gesellschaftsvertrag für eine große Transformation: Hauptgutachten*. WGBU, Berlin and Deutschland, 2011.
- [11] IEA. *Co-generation and Renewables: Solutions for a low-carbon energy future*. IEA, 2011.
- [12] Q. Ma, L. Luo, R. Z. Wang, and G. Sauce. A review on transportation of heat energy over long distance: Exploratory development. *Renewable and Sustainable Energy Reviews*, 13(6–7):1532–1540, 2009.
- [13] P. Arce, M. Medrano, A. Gil, E. Oró, and L. F. Cabeza. Overview of thermal energy storage (tes) potential energy savings and climate change mitigation in spain and europe. *Applied Energy*, 88(8):2764–2774, 2011.
- [14] IEA. *Heating without global warming: Market Developments and Policy Considerations for Renewable Heat*. IEA, 2014.
- [15] H. Kerskes, F. Bertsch, B. Mette, A. Wörner, and F. Schaube. Thermochemische energiespeicher: Thermochemical energy storage. *Chemie Ingenieur Technik*, 83(11):2014–2026, 2011.
- [16] D. Stitou, N. Mazet, and S. Mauran. Experimental investigation of a solid/gas thermochemical storage process for solar air-conditioning. *23rd International Conference on Efficiency, Cost, Optimization, Simulation and Environmental Impact of Energy Systems, ECOS 2010*, 41(1):261–270, 2012.
- [17] C. W. Chan, J. Ling-Chin, and A. P. Roskilly. A review of chemical heat pumps, thermodynamic cycles and thermal energy storage technologies for low grade heat utilisation. *Applied Thermal Engineering*, 50(1):1257–1273, 2013.
- [18] J. Cot-Gores, A. Castell, and L. F. Cabeza. Thermochemical energy storage and conversion: A-state-of-the-art review of the experimental research under practical conditions. *Renewable and Sustainable Energy Reviews*, 16(7):5207–5224, 2012.
- [19] Brandstätter, R. Industrielle Abwärmenutzung, Beispiel & Technologien, 2008.
- [20] R. Kuder. Technology orientated analysis of the emission reduction potentials in the industrial sector in the EU-27, 23.06.2010.
- [21] J. Widhalm, T. Fellner, M. Deutsch, A. Werner, and F. Winter. Thermochemical energy storage as a way to increase the sustainability of energy generation. In *The*

- International Academic Forum, editor, *ACSEE2015 - Official Conference Proceedings*, pages 579–593, 2015.
- [22] Y. Kato, R. Takahashi, T. Sekiguchi, and J. Ryu. Study on medium-temperature chemical heat storage using mixed hydroxides: Progress in sorptive cooling systems. *International Journal of Refrigeration*, 32(4):661–666, 2009.
- [23] M. Jakobi, P. Hoffmann, and B. Geringer. Chemical heat storage for automotive heating and cooling applications. 3rd IAV Conference: Thermoelectrics goes Automotive. expert Verlag, 2012.
- [24] California Independent System Operator. What the duck curve tells us about managing a green grid: Fast facts, 2016.
- [25] M. Romero and A. Steinfeld. Concentrating solar thermal power and thermochemical fuels. *Energy Environmental Science*, 5(11):9234–9245, 2012.
- [26] F. Zaversky, J. García-Barberena, M. Sánchez, and D. Astrain. Transient molten salt two-tank thermal storage modeling for CSP performance simulations. *Solar Energy*, 93:294–311, 2013.
- [27] T. Kousksou, P. Bruel, A. Jamil, T. El Rhafiki, and Y. Zeraouli. Energy storage: Applications and challenges. *Solar Energy Materials and Solar Cells*, 120(0):59–80, 2014.
- [28] M. Sterner and I. Stadler. *Energiespeicher-Bedarf, Technologien, Integration*. Springer-Verlag, 2014.
- [29] N. Fisch, M. Bodmann, L. Kühl, C. Saße, and H. Schnürer. *Wärmespeicher: Bine-Informationspaket, 4*. Solarpraxis AG, Berlin and Deutschland, 4 edition, 2005.
- [30] M. Deutsch, D. Müller, C. Aumeyr, C. Jordan, C. Gierl-Mayer, P. Weinberger, F. Winter, and A. Werner. Systematic search algorithm for potential thermochemical energy storage systems. *Applied Energy*, 183:113–120, 2016.
- [31] K. E. N’Tsoukpoe, H. Liu, N. Le Pierrès, and L. Luo. A review on long-term sorption solar energy storage. *Renewable and Sustainable Energy Reviews*, 13(9):2385–2396, 2009.
- [32] Y. Kato. Thermal energy storage in vehicles for fuel efficiency improvement. *Proceedings of the Effstock Conference*, pages 14–17, 2009.

- [33] A. H. Abedin and M. A. Rosen. A critical review of thermochemical energy storage systems. *Open Renewable Energy Journal*, 4:42–46, 2011.
- [34] P. Pardo, Z. Anxionnaz-Minvielle, S. Rougé, P. Cognet, and M. Cabassud. Ca(OH)₂/CaO reversible reaction in a fluidized bed reactor for thermochemical heat storage. *Solar Energy*, 107(0):605–616, 2014.
- [35] Felderhoff M., Urbanczyk R., and Peil S. Thermochemical heat storage for high temperature applications – a review, 2013.
- [36] L. Thorndike. *A History of Magic and Experimental Science*. Columbia University Press, 1923.
- [37] C. B. Heiatt and R. F. Jones. Two anglo-norman culinary collections edited from british library manuscripts additional 32085 and royal 12.C.XII. *Speculum*, 61(4):859–882, 1986.
- [38] G. Beckmann and P.V. Gilli. *Thermal Energy Storage*. Topics in Energy. Springer-Verlag, Wien, 1984.
- [39] D. Aydin, S. P. Casey, and S. Riffat. The latest advancements on thermochemical heat storage systems. *Renewable and Sustainable Energy Reviews*, 41:356–367, 2015.
- [40] K. Korhammer, M. Druske, A. Fopah-Lele, H. U. Rammelberg, N. Wegscheider, O. Opel, T. Osterland, and W. Ruck. Sorption and thermal characterization of composite materials based on chlorides for thermal energy storage. *Applied Energy*, 162:1462–1472, 2016.
- [41] A. Fopah Lele, F. Kuznik, H. U. Rammelberg, T. Schmidt, and W. K. L. Ruck. Thermal decomposition kinetic of salt hydrates for heat storage systems. *Applied Energy*, 154:447–458, 2015.
- [42] S. Hongois, P. Kuznik, F. Stevens, and J. Roux. Development and characterisation of a new MgSO₄–zeolite composite for long-term thermal energy storage. *Solar Energy Materials and Solar Cells*, 95(7):1831–1837, 2011.
- [43] P. A. J. Donkers, S. Beckert, L. Pel, F. Stallmach, M. Steiger, and O. C. G. Adan. Water transport in MgSO₄·7H₂O during dehydration in view of thermal storage. *Journal of Physical Chemistry C*, 119(52):28711–28720, 2015.
- [44] T. Nagel, H. Shao, C. Roßkopf, M. Linder, A. Wörner, and O. Kolditz. The influence of gas–solid reaction kinetics in models of thermochemical heat storage under monotonic and cyclic loading. *Applied Energy*, 136:289–302, 2014.

- [45] Y. Kato, N. Harada, and Y. Yoshizawa. Kinetic feasibility of a chemical heat pump for heat utilization of high-temperature processes. *Applied Thermal Engineering*, 19(3):239–254, 1999.
- [46] K. J. Albrecht, G. S. Jackson, and R. J. Braun. Thermodynamically consistent modeling of redox-stable perovskite oxides for thermochemical energy conversion and storage. *Applied Energy*, 165:285–296, 2016.
- [47] A.J. Carrillo, J. Moya, A. Bayón, P. Jana, V. A. de La Peña O’Shea, M. Romero, J. Gonzalez-Aguilar, D. P. Serrano, P. Pizarro, and J. M. Coronado. Thermochemical energy storage at high temperature via redox cycles of Mn and Co oxides: Pure oxides versus mixed ones. *Solar Energy Materials and Solar Cells*, 123(0):47–57, 2014.
- [48] B. Wong, L. Brown, F. Schaube, R. Tamme, and C. Sattler. Oxide based thermochemical heat storage. In *Proceedings of the 16th SolarPACES Conference, Perpignan, France*, pages 21–24, 2010.
- [49] B. Wong. Thermochemical heat storage for concentrated solar power: Thermochemical system reactor design for thermal energy storage: Phase II final report for the period September 30, 2008 through April 30, 2011, 2011.
- [50] M. Neises, S. Tescari, L. de Oliveira, M. Roeb, C. Sattler, and B. Wong. Solar-heated rotary kiln for thermochemical energy storage. *Solar Energy*, 86(10):3040–3048, 2012.
- [51] T. Block, N. Knoblauch, and M. Schmücker. The cobalt-oxide/iron-oxide binary system for use as high temperature thermochemical energy storage material. *Thermochimica Acta*, 577(0):25–32, 2014.
- [52] C. Agrafiotis, M. Roeb, M. Schmücker, and C. Sattler. Exploitation of thermochemical cycles based on solid oxide redox systems for thermochemical storage of solar heat. part 1: Testing of cobalt oxide-based powders. *Solar Energy*, 102:189–211, 2014.
- [53] A. J. Carrillo, D. P. Serrano, P. Pizarro, and J. M. Coronado. Thermochemical heat storage based on the $\text{Mn}_2\text{O}_3/\text{Mn}_3\text{O}_4$ redox couple: influence of the initial particle size on the morphological evolution and cyclability. *Journal of Material Chemistry A*, 2(45):19435–19443, 2014.
- [54] K. E. N’Tsoukpoe, T. Schmidt, H. U. Rammelberg, B. A. Watts, and W. K. L. Ruck. A systematic multi-step screening of numerous salt hydrates for low temperature thermochemical energy storage. *Applied Energy*, 124:1–16, 2014.

- [55] S. L. S. Stipp, G. A. Parks, D. K. Nordstrom, and J. O. Leckie. Solubility-product constant and thermodynamic properties for synthetic otavite, $\text{CdCO}_3(\text{s})$, and aqueous association constants for the $\text{Cd}(\text{II})\text{-CO}_2\text{-H}_2\text{O}$ system. *Geochimica et Cosmochimica Acta*, 57(12):2699–2713, 1993.
- [56] J. Gmehling, B. Kolbe, M. Kleiber, and J. Rarey. *Chemical Thermodynamics for Process Simulation*. Wiley-VCH Verlag GmbH, Weinheim and Germany, 2012.
- [57] S. Vyazovkin, A. K. Burnham, J. M. Criado, L. A. Pérez-Maqueda, C. Popescu, and N. Sbirrazzuoli. ICTAC kinetics committee recommendations for performing kinetic computations on thermal analysis data. *Thermochimica Acta*, 520(1–2):1–19, 2011.
- [58] K. Darkwa, A. Ianakiev, and P. W. O’Callaghan. Modelling and simulation of adsorption process in a fluidised bed thermochemical energy reactor. *Applied Thermal Engineering*, 26(8–9):838–845, 2006.
- [59] S. Arrhenius. Über die Reaktionsgeschwindigkeit bei der Inversion von Rohrzucker durch Säuren. *Zeitschrift für physikalische Chemie*, 4:226–248, 1889.
- [60] M. E. Brown, D. Dollimore, and A. K. Galwey. *Reactions in the solid state*, volume 22. Elsevier, 1980.
- [61] J. H. Flynn. The ‘temperature integral’ — its use and abuse. *A Collection of Invited Papers in Celebration of Volume 300*, 300(1):83–92, 1997.
- [62] J. H. Flynn and L. A. Wall. General treatment of the thermogravimetry of polymers. *Journal of Research of the National Bureau of Standards*, 70(6):487–523, 1966.
- [63] E. Segal. Non-isothermal kinetics with non-linear temperature programme. V. non-linear heating programmes with exact solutions for the temperature integral. *Thermochimica Acta*, 55(1):43–47, 1982.
- [64] S. Vyazovkin. Evaluation of activation energy of thermally stimulated solid-state reactions under arbitrary variation of temperature. *Journal of Computational Chemistry*, 18(3):393–402, 1997.
- [65] A. W. Coats and J. P. Redfern. Kinetic parameters from thermogravimetric data. *Nature*, 201(4914):68–69, 1964.
- [66] G. I. Senum and R. T. Yang. Rational approximations of the integral of the arrhenius function. *Journal of thermal analysis*, 11(3):445–447, 1977.

- [67] V. M. Gorbachev. A solution of the exponential integral in the non-isothermal kinetics for linear heating. *Journal of Thermal Analysis and Calorimetry*, 8(2):349–350, 1975.
- [68] V. M. Gorbachev. Algorithm for the solution of the exponential integral in non-isothermal kinetics at linear heating. *Journal of Thermal Analysis and Calorimetry*, 10(3):447–449, 1976.
- [69] T. V. Lee and S. R. Beck. A new integral approximation formula for kinetic analysis of nonisothermal TGA data. *AIChE Journal*, 30(3):517–519, 1984.
- [70] R. K. Agrawal and M. S. Sivasubramanian. Integral approximations for nonisothermal kinetics. *AIChE Journal*, 33(7):1212–1214, 1987.
- [71] T. Wanjun, L. Yuwen, Z. Hen, W. Zhiyong, and W. Cunxin. New temperature integral approximate formula for non-isothermal kinetic analysis. *Journal of Thermal Analysis and Calorimetry*, 74(1):309–315, 2003.
- [72] J. Cai, F. Yao, W. Yi, and F. He. New temperature integral approximation for non-isothermal kinetics. *AIChE Journal*, 52(4):1554–1557, 2006.
- [73] L. Pérez-Maqueda and J. Criado. The accuracy of Senum and Yang’s approximations to the Arrhenius integral. *Journal of Thermal Analysis and Calorimetry*, 60(3):909–915, 2000.
- [74] C. D. Doyle. Estimating isothermal life from thermogravimetric data. *Journal of Applied Polymer Science*, 6(24):639–642, 1962.
- [75] C. D. Doyle. Kinetic analysis of thermogravimetric data. *Journal of Applied Polymer Science*, 5(15):285–292, 1961.
- [76] C. D. Doyle. Series approximations to the equation of thermogravimetric data. *Nature*, 207(4994):290–291, 1965.
- [77] J. H. Flynn and L. A. Wall. A quick, direct method for the determination of activation energy from thermogravimetric data. *Journal of Polymer Science Part B: Polymer Letters*, 4(5):323–328, 1966.
- [78] C. F. Dickinson and G. R. Heal. Solid–liquid diffusion controlled rate equations. *Thermochimica Acta*, 340–341:89–103, 1999.
- [79] A. Khawam and D. R. Flanagan. Solid-state kinetic models: Basics and mathematical fundamentals. *Journal of Physical Chemistry B*, 110(35):17315–17328, 2006.

- [80] J. Sesták and G. Berggren. Study of the kinetics of the mechanism of solid-state reactions at increasing temperatures. *Thermochimica Acta*, 3(1):1–12, 1971.
- [81] J. Graetz and J. J. Reilly. Decomposition kinetics of the alh3 polymorphs. *Journal of Physical Chemistry B*, 109(47):22181–22185, 2005.
- [82] S. Wang, Q. Gao, and J. Wang. Thermodynamic analysis of decomposition of thiourea and thiourea oxides. *Journal of Physical Chemistry B*, 109(36):17281–17289, 2005.
- [83] M. Hromadová, R. Sokolová, L. Pospíšil, and N. Fanelli. Surface interactions of s-triazine-type pesticides. An electrochemical impedance study. *Journal of Physical Chemistry B*, 110(10):4869–4874, 2006.
- [84] C. Wu, P. Wang, X. Yao, C. Liu, D. Chen, G. Q. Lu, and H. Cheng. Effects of SWNT and metallic catalyst on hydrogen absorption/desorption performance of MgH₂. *Journal of Physical Chemistry B*, 109(47):22217–22221, 2005.
- [85] V. K. Peterson, D. A. Neumann, and R. A. Livingston. Hydration of tricalcium and dicalcium silicate mixtures studied using quasielastic neutron scattering. *Journal of Physical Chemistry B*, 109(30):14449–14453, 2005.
- [86] A. Khawam and D. R. Flanagan. Complementary use of model-free and modelistic methods in the analysis of solid-state kinetics. *Journal of Physical Chemistry B*, 109(20):10073–10080, 2005.
- [87] J. Yang, B. J. McCoy, and G. Madras. Distribution kinetics of polymer crystallization and the Avrami equation. *The Journal of Chemical Physics*, 122(6):064901, 2005.
- [88] J. Yang, B. J. McCoy, and G. Madras. Kinetics of nonisothermal polymer crystallization. *Journal of Physical Chemistry B*, 109(39):18550–18557, 2005.
- [89] J. Liu, J. Wang, H. Li, D. Shen, J. Zhang, Y. Ozaki, and S. Yan. Epitaxial crystallization of isotactic poly(methyl methacrylate) on highly oriented polyethylene. *Journal of Physical Chemistry B*, 110(2):738–742, 2006.
- [90] A. K. Burnham, R. K. Weese, and B. L. Weeks. A distributed activation energy model of thermodynamically inhibited nucleation and growth reactions and its application to the β – δ phase transition of HMX, url = <http://dx.doi.org/10.1021/jp0483167>, pages = 19432–19441, volume = 108, number = 50, issn = 1520-6106, journal = Journal of Physical Chemistry B, doi = 10.1021/jp0483167. 2004.
- [91] V. V. Boldyrev. Topochemistry of thermal decompositions of solids. *Thermochimica Acta*, 100(1):315–338, 1986.

- [92] W. E. Garner. *Chemistry of the solid state*. Academic press, New York, 1955.
- [93] A. K. Galwey and M. E. Brown. *Thermal decomposition of ionic solids: chemical properties and reactivities of ionic crystalline phases*, volume 86. Elsevier, Amsterdam, 1999.
- [94] L. Guo, A. Radisic, and P. C. Searson. Kinetic Monte Carlo simulations of nucleation and growth in electrodeposition. *Journal of Physical Chemistry B*, 109(50):24008–24015, 2005.
- [95] M. Avrami. Kinetics of phase change. II transformation–time relations for random distribution of nuclei. *The Journal of Chemical Physics*, 8(2):212–224, 1940.
- [96] B. V. Erofeyev. Generalized equation of chemical kinetics and its application to reactions involving solid phase components. In *Doklady AN USSR*, volume 12, pages 515–8, 1946.
- [97] J. T. Carstensen. Stability of solids and solid dosage forms. *Journal of Pharmaceutical Sciences*, 63(1):1–14, 1974.
- [98] W. Jander. Reaktionen im festen Zustande bei höheren Temperaturen. Reaktionsgeschwindigkeiten endotherm verlaufender Umsetzungen. *Zeitschrift für anorganische und allgemeine Chemie*, 163(1):1–30, 1927.
- [99] F. Schaube, L. Koch, A. Wörner, and H. Müller-Steinhagen. A thermodynamic and kinetic study of the de- and rehydration of $\text{Ca}(\text{OH})_2$ at high H_2O partial pressures for thermo-chemical heat storage. *Thermochimica Acta*, 538(0):9–20, 2012.
- [100] A. K. Burnham, R. K. Weese, A. P. Wemhoff, and J. L. Maienschein. A historical and current perspective on predicting thermal cookoff behavior. *Journal of Thermal Analysis and Calorimetry*, 89(2):407–415, 2007.
- [101] C. K. Clayton and K. J. Whitty. Measurement and modeling of decomposition kinetics for copper oxide-based chemical looping with oxygen uncoupling. *Applied Energy*, 116:416–423, 2014.
- [102] J. Khinast, G. F. Krammer, Ch Brunner, and G. Staudinger. Decomposition of limestone: The influence of CO_2 and particle size on the reaction rate. *Chemical Engineering Science*, 51(4):623–634, 1996.
- [103] J. H. Sharp and S. A. Wentworth. Kinetic analysis of thermogravimetric data. *Anal. Chem.*, 41(14):2060–2062, 1969.

- [104] A. W. Coats and J. P. Redfern. Kinetic parameters from thermogravimetric data. ii. *Journal of Polymer Science Part B: Polymer Letters*, 3(11):917–920, 1965.
- [105] H. E. Kissinger. Variation of peak temperature with heating rate in differential thermal analysis. *Journal of research of the National Bureau of Standards*, 57(4):217–221, 1956.
- [106] H. E. Kissinger. Reaction kinetics in differential thermal analysis. *Analytical Chemistry*, 29(11):1702–1706, 1957.
- [107] D. Chen, X. Gao, and D. Dollimore. A generalized form of the Kissinger equation. *Thermochimica Acta*, 215:109–117, 1993.
- [108] P. Simon. Isoconversional methods. *Journal of Thermal Analysis and Calorimetry*, 76(1):123, 2004.
- [109] J. Zsakó. Kinetic analysis of thermogravimetric data, VI. *Journal of Thermal Analysis and Calorimetry*, 5(2-3):239–251, 1973.
- [110] J. Zsakó. Kinetic analysis of thermogravimetric data. *Journal of Thermal Analysis and Calorimetry*, 46(6):1845–1864, 1996.
- [111] H. L. Friedman. Kinetics of thermal degradation of char-forming plastics from thermogravimetry. Application to a phenolic plastic. In *Journal of Polymer Science Part C: Polymer Symposia*, volume 6, pages 183–195. Wiley Online Library, 1964.
- [112] T. Ozawa. A new method of analyzing thermogravimetric data. *Bulletin of the chemical society of Japan*, 38(11):1881–1886, 1965.
- [113] A. K. Burnham and R. L. Braun. Global kinetic analysis of complex materials. *Energy Fuels*, 13(1):1–22, 1999.
- [114] A. Solé, X. Fontanet, C. Barreneche, A. Fernández, I. Martorell, and L. F. Cabeza. Requirements to consider when choosing a thermochemical material for solar energy storage. *Solar Energy*, 97:398–404, 2013.
- [115] A. Roine. HSC chemistry, 2007.
- [116] J. A. Hartigan and M. A. Wong. Algorithm as 136: A k-means clustering algorithm. *Journal of the Royal Statistical Society. Series C (Applied Statistics)*, 28(1):100–108, 1979.
- [117] R. Serra, J. Sempere, and R. Nomen. A new method for the kinetic study of thermoanalytical data:: The non-parametric kinetics method. *Thermochimica Acta*, 316(1):37–45, 1998.

- [118] R. Serra, R. Nomen, and J. Sempere. The non-parametric kinetics a new method for the kinetic study of thermoanalytical data. *Journal of Thermal Analysis and Calorimetry*, 52(3):933–943, 1998.
- [119] J. Sempere, R. Nomen, and R. Serra. Progress in non-parametric kinetics. *Journal of Thermal Analysis and Calorimetry*, 56(2):843–849, 1999.
- [120] J. Sempere, R. Nomen, R. Serra, and J. Soravilla. The NPK method: An innovative approach for kinetic analysis of data from thermal analysis and calorimetry. *Thermochimica Acta*, 388(1–2):407–414, 2002.
- [121] G. R. Heal. A generalisation of the non-parametric, NPK (SVD) kinetic analysis method: Part 1. Isothermal experiments. *Thermochimica Acta*, 426(1–2):15–21, 2005.
- [122] G. R. Heal. A generalisation of the non-parametric, NPK (SVD) kinetic analysis method: Part 2. Non-isothermal experiments. *Thermochimica Acta*, 426(1–2):23–31, 2005.
- [123] G. H. Golub and C. Reinsch. Singular value decomposition and least squares solutions. *Numerische Mathematik*, 14(5):403–420, 1970.
- [124] J. M. Criado, M. González, and M. Macias. Influence of CO₂ pressure on the kinetics of thermal decomposition of CdCO₃. *Thermochimica Acta*, 113:31–38, 1987.
- [125] J. Mu and D. D. Perlmutter. Thermal decomposition of carbonates, carboxylates, oxalates, acetates, formates, and hydroxides. *Thermochimica Acta*, 49(2):207–218, 1981.
- [126] B. V. L’vov. Mechanism and kinetics of thermal decomposition of carbonates. *Thermochimica Acta*, 386(1):1–16, 2002.
- [127] E. Alonso, C. Pérez-Rábago, J. Licurgo, E. Fuentealba, and C. A. Estrada. First experimental studies of solar redox reactions of copper oxides for thermochemical energy storage. *Solar Energy*, 115:297–305, 2015.
- [128] A. Abad, T. Mattisson, A. Lyngfelt, and M. Rydén. Chemical-looping combustion in a 300 w continuously operating reactor system using a manganese-based oxygen carrier. *Fuel*, 85(9):1174–1185, 2006.
- [129] E. M. Eyring, G. Konya, J. S. Lighty, A. H. Sahir, A. F. Sarofim, and K. Whitty. Chemical looping with copper oxide as carrier and coal as fuel. *Oil and Gas Science and Technologies – Rev. IFP Energies nouvelles*, 66(2):209–221, 2011.

- [130] C. K. Clayton, H. Y. Sohn, and K. J. Whitty. Oxidation kinetics of Cu_2O in oxygen carriers for chemical looping with oxygen uncoupling. *Industrial and Engineering Chemistry Research*, 53(8):2976–2986, 2014.
- [131] Y. Zhu, K. Mimura, and M. Isshiki. Oxidation mechanism of Cu_2O to CuO at 600 °C–1050 °C. *Oxidation of Metals*, 62(3):207–222, 2004.
- [132] S. Brunauer, P. H. Emmett, and E. Teller. Adsorption of gases in multimolecular layers. *Journal of the American Chemical Society*, 60(2):309–319, 1938.
- [133] J. Szekeley. *Gas-solid reactions*. Elsevier, 2012.
- [134] W. Hu, F. Donat, S. A. Scott, and J. S. Dennis. Kinetics of oxygen uncoupling of a copper based oxygen carrier. *Applied Energy*, 161:92–100, 2016.
- [135] M. Johansson, T. Mattisson, and A. Lyngfelt. Investigation of mn_3o_4 with stabilized zr_2o_2 for chemical-looping combustion. *Carbon Capture and Storage*, 84(9):807–818, 2006.

Appendix

A1 Asymptotic series expansion

$$p(x) = \frac{e^{-x}}{x^2} \left[1 - \frac{2!}{x} + \frac{3!}{x^2} - \frac{4!}{x^3} + \dots + (-1)^n \frac{(n+1)!}{x^n} + \dots \right] \quad (6.1)$$

A2 Schlömich series expansion

The Schlömich series expansion is one often used method of approximating the temperature integral $p(x)$.

$$p(x) = \frac{e^{-x}}{x(x+1)} \left[1 - \frac{1}{x+2} + \frac{2}{(x+2)(x+3)} - \frac{4}{(x+2)(x+3)(x+4)} + \dots \right] \quad (6.2)$$

A3 Reaction systems found by the algorithm

The reactions found by the search algorithm for the reactive gases H₂O, CO₂, O₂, NH₃ and SO₂. The storage capacity is calculated for 1 kg of educt. The energy density is calculated for 1 m³ of educt. A missing energy density means the density of the educt was not available in the database.

Table 6.1: Reactions with H₂O as reactive gas

ID	reaction system	T_{equ} °C	storage capacity kJ/kg	storage density MJ/m^3
A1	$2 \text{Ac}(\text{OH})_3 \longleftrightarrow 3 \text{H}_2\text{O} + \text{Ac}_2\text{O}_3$	341	286	-
A2	$\text{AgF} \cdot \text{H}_2\text{O} \longleftrightarrow \text{H}_2\text{O} + \text{AgF}$	371	409	-
A3	$\text{AgF} \cdot 2 \text{H}_2\text{O} \longleftrightarrow \text{H}_2\text{O} + \text{AgF} \cdot \text{H}_2\text{O}$	335	333	-
A4	$\text{AgF} \cdot 2 \text{H}_2\text{O} \longleftrightarrow 2 \text{H}_2\text{O} + \text{AgF}$	375	696	-
A5	$\text{AgF} \cdot 4 \text{H}_2\text{O} \longleftrightarrow 2 \text{H}_2\text{O} + \text{AgF} \cdot 2 \text{H}_2\text{O}$	392	529	-
A6	$\text{AgF} \cdot 4 \text{H}_2\text{O} \longleftrightarrow 3 \text{H}_2\text{O} + \text{AgF} \cdot \text{H}_2\text{O}$	351	801	-
A7	$\text{AgF} \cdot 4 \text{H}_2\text{O} \longleftrightarrow 4 \text{H}_2\text{O} + \text{AgF}$	383	1099	-
A8	$\text{Al}_4\text{C}_3 \cdot 6 \text{H}_2\text{O} \longleftrightarrow 6 \text{H}_2\text{O} + \text{Al}_4\text{C}_3$	1000	4068	9763

Continued on next page

Table 6.1: Reactions with H₂O as reactive gas – continued

ID	reaction system	T_{equ} °C	storage capacity kJ/kg	storage density MJ/m^3
A9	$\text{AlCl}_3 \cdot 6 \text{H}_2\text{O} \longleftrightarrow 6 \text{H}_2\text{O} + \text{AlCl}_3$	570	2216	5314
A10	$2 \text{AlCl}_3 \cdot 6 \text{H}_2\text{O} \longleftrightarrow 12 \text{H}_2\text{O} + \text{Al}_2\text{Cl}_6$	496	2222	5329
A12	$2 \text{Al}(\text{OH})_3 \longleftrightarrow 3 \text{H}_2\text{O} + \text{Al}_2\text{O}_3$	318	968	2343
A13	$\text{Al}_2\text{O}_3 \cdot \text{H}_2\text{O} \longleftrightarrow \text{H}_2\text{O} + \text{Al}_2\text{O}_3$	479	680	2047
A14	$\text{Al}_2\text{O}_3 \cdot 3 \text{H}_2\text{O} \longleftrightarrow 2 \text{H}_2\text{O} + \text{Al}_2\text{O}_3 \cdot \text{H}_2\text{O}$	333	665	1610
A15	$\text{Al}_2\text{O}_3 \cdot 3 \text{H}_2\text{O} \longleftrightarrow 3 \text{H}_2\text{O} + \text{Al}_2\text{O}_3$	386	1188	2876
A16	$\text{Al}_2\text{O}_3 \cdot 2 \text{SiO}_2 \cdot 2 \text{H}_2\text{O} \longleftrightarrow 2 \text{H}_2\text{O} + \text{Al}_2\text{O}_3 \cdot 2 \text{SiO}_2$	947	1142	-
A18	$\text{Al}_2(\text{SO}_4)_3 \cdot 6 \text{H}_2\text{O} \longleftrightarrow 6 \text{H}_2\text{O} + \text{Al}_2(\text{SO}_4)_3$	702	1363	-
A19	$\text{Al}_2\text{Si}_2\text{O}_5(\text{OH})_4 \longleftrightarrow 2 \text{H}_2\text{O} + \text{Al}_2\text{O}_3 \cdot 2 \text{SiO}_2$	889	1071	-
A20	$2 \text{Am}(\text{OH})_3 \longleftrightarrow 3 \text{H}_2\text{O} + \text{Am}_2\text{O}_3$	649	494	-
A21	$\text{As}_2\text{O}_5 \cdot 4 \text{H}_2\text{O} \longleftrightarrow 4 \text{H}_2\text{O} + \text{As}_2\text{O}_5$	335	666	-
A22	$\text{AuCl}_3 \cdot 2 \text{H}_2\text{O} \longleftrightarrow 2 \text{H}_2\text{O} + \text{AuCl}_3$	355	333	-
A23	$2 \text{Au}(\text{OH})_3 \longleftrightarrow 3 \text{H}_2\text{O} + \text{Au}_2\text{O}_3$	379	243	-
A24	$2 \text{B}(\text{OH})_3 \longleftrightarrow 3 \text{H}_2\text{O} + \text{B}_2\text{O}_3$	438	1554	2238
A25	$\text{BaAl}_2\text{O}_4 \cdot \text{H}_2\text{O} \longleftrightarrow \text{H}_2\text{O} + \text{BaO} \cdot \text{Al}_2\text{O}_3$	385	253	-
A26	$\text{BaBr}_2 \cdot \text{H}_2\text{O} \longleftrightarrow \text{H}_2\text{O} + \text{BaBr}_2$	377	183	-
A27	$\text{BaBr}_2 \cdot 2 \text{H}_2\text{O} \longleftrightarrow \text{H}_2\text{O} + \text{BaBr}_2 \cdot \text{H}_2\text{O}$	358	202	723
A28	$\text{BaBr}_2 \cdot 2 \text{H}_2\text{O} \longleftrightarrow 2 \text{H}_2\text{O} + \text{BaBr}_2$	406	375	1344
A30	$\text{BaCl}_2 \cdot \text{H}_2\text{O} \longleftrightarrow \text{H}_2\text{O} + \text{BaCl}_2$	469	300	-
A31	$\text{BaCl}_2 \cdot 2 \text{H}_2\text{O} \longleftrightarrow \text{H}_2\text{O} + \text{BaCl}_2 \cdot \text{H}_2\text{O}$	349	219	679
A32	$\text{BaCl}_2 \cdot 2 \text{H}_2\text{O} \longleftrightarrow 2 \text{H}_2\text{O} + \text{BaCl}_2$	407	496	1539
A33	$\text{Ba}(\text{ClO}_4)_2 \cdot 3 \text{H}_2\text{O} \longleftrightarrow 3 \text{H}_2\text{O} + \text{Ba}(\text{ClO}_4)_2$	712	1127	3088
A34	$\text{BaI}_2 \cdot \text{H}_2\text{O} \longleftrightarrow \text{H}_2\text{O} + \text{BaI}_2$	483	189	-
A35	$\text{BaI}_2 \cdot 2 \text{H}_2\text{O} \longleftrightarrow \text{H}_2\text{O} + \text{BaI}_2 \cdot \text{H}_2\text{O}$	328	129	666
A36	$\text{BaI}_2 \cdot 2 \text{H}_2\text{O} \longleftrightarrow 2 \text{H}_2\text{O} + \text{BaI}_2$	435	311	1599
A37	$\text{Ba}(\text{IO}_3)_2 \cdot \text{H}_2\text{O} \longleftrightarrow \text{H}_2\text{O} + \text{Ba}(\text{IO}_3)_2$	365	105	-
A38	$\text{Ba}(\text{N}_3)_2 \cdot \text{H}_2\text{O} \longleftrightarrow \text{H}_2\text{O} + \text{Ba}(\text{N}_3)_2$	352	185	-
A39	$\text{Ba}(\text{OH})_2 \longleftrightarrow \text{H}_2\text{O} + \text{BaO}$	1283	880	3960
A40	$\text{Ba}(\text{OH})_2 \cdot \text{H}_2\text{O} \longleftrightarrow \text{H}_2\text{O} + \text{Ba}(\text{OH})_2$	397	314	-
A41	$\text{Ba}(\text{OH})_2 \cdot \text{H}_2\text{O} \longleftrightarrow 2 \text{H}_2\text{O} + \text{BaO}$	645	1110	-
A42	$\text{Ba}(\text{OH})_2 \cdot 3 \text{H}_2\text{O} \longleftrightarrow 2 \text{H}_2\text{O} + \text{Ba}(\text{OH})_2 \cdot \text{H}_2\text{O}$	345	511	-
A43	$\text{Ba}(\text{OH})_2 \cdot 3 \text{H}_2\text{O} \longleftrightarrow 3 \text{H}_2\text{O} + \text{Ba}(\text{OH})_2$	384	774	-
A44	$\text{Ba}(\text{OH})_2 \cdot 3 \text{H}_2\text{O} \longleftrightarrow 4 \text{H}_2\text{O} + \text{BaO}$	520	1443	-
A45	$\text{Ba}(\text{OH})_2 \cdot 8 \text{H}_2\text{O} \longleftrightarrow 5 \text{H}_2\text{O} + \text{Ba}(\text{OH})_2 \cdot 3 \text{H}_2\text{O}$	359	927	2021
A46	$\text{Ba}(\text{OH})_2 \cdot 8 \text{H}_2\text{O} \longleftrightarrow 7 \text{H}_2\text{O} + \text{Ba}(\text{OH})_2 \cdot \text{H}_2\text{O}$	363	1292	2817
A47	$\text{Ba}(\text{OH})_2 \cdot 8 \text{H}_2\text{O} \longleftrightarrow 8 \text{H}_2\text{O} + \text{Ba}(\text{OH})_2$	388	1480	3227
A48	$\text{Ba}(\text{OH})_2 \cdot 8 \text{H}_2\text{O} \longleftrightarrow 9 \text{H}_2\text{O} + \text{BaO}$	451	1958	4269

Continued on next page

Table 6.1: Reactions with H₂O as reactive gas – continued

ID	reaction system	T_{equ} °C	storage capacity kJ/kg	storage density MJ/m^3
A49	$\text{Be}(\text{OH})_2 \longleftrightarrow \text{H}_2\text{O} + \text{BeO}$	347	1201	-
A50	$\text{BeSO}_4 \cdot \text{H}_2\text{O} \longleftrightarrow \text{H}_2\text{O} + \text{BeSO}_4$	472	556	952
A51	$\text{BeSO}_4 \cdot 2\text{H}_2\text{O} \longleftrightarrow \text{H}_2\text{O} + \text{BeSO}_4 \cdot \text{H}_2\text{O}$	476	497	-
A52	$\text{BeSO}_4 \cdot 2\text{H}_2\text{O} \longleftrightarrow 2\text{H}_2\text{O} + \text{BeSO}_4$	474	982	-
A53	$\text{BeSO}_4 \cdot 3\text{H}_2\text{O} \longleftrightarrow \text{H}_2\text{O} + \text{BeSO}_4 \cdot 2\text{H}_2\text{O}$	352	350	-
A54	$\text{BeSO}_4 \cdot 3\text{H}_2\text{O} \longleftrightarrow 2\text{H}_2\text{O} + \text{BeSO}_4 \cdot \text{H}_2\text{O}$	405	790	-
A55	$\text{BeSO}_4 \cdot 3\text{H}_2\text{O} \longleftrightarrow 3\text{H}_2\text{O} + \text{BeSO}_4$	423	1220	-
A56	$\text{BeSO}_4 \cdot 4\text{H}_2\text{O} \longleftrightarrow \text{H}_2\text{O} + \text{BeSO}_4 \cdot 3\text{H}_2\text{O}$	341	347	594
A57	$\text{BeSO}_4 \cdot 4\text{H}_2\text{O} \longleftrightarrow 2\text{H}_2\text{O} + \text{BeSO}_4 \cdot 2\text{H}_2\text{O}$	380	661	1131
A58	$\text{BeSO}_4 \cdot 4\text{H}_2\text{O} \longleftrightarrow 3\text{H}_2\text{O} + \text{BeSO}_4 \cdot \text{H}_2\text{O}$	412	1057	1808
A59	$\text{BeSO}_4 \cdot 4\text{H}_2\text{O} \longleftrightarrow 4\text{H}_2\text{O} + \text{BeSO}_4$	426	1443	2468
A60	$\text{BeSeO}_4 \cdot 4\text{H}_2\text{O} \longleftrightarrow 2\text{H}_2\text{O} + \text{BeSeO}_4 \cdot 2\text{H}_2\text{O}$	353	542	-
A62	$\text{CaAl}_2\text{Si}_4\text{O}_{12} \cdot 4\text{H}_2\text{O} \longleftrightarrow 2\text{H}_2\text{O} + \text{CaAl}_2\text{Si}_4\text{O}_{12} \cdot 2\text{H}_2\text{O}$	358	223	-
A63	$\text{CaAl}_2\text{Si}_7\text{O}_{18} \cdot 7\text{H}_2\text{O} \longleftrightarrow \text{H}_2\text{O} + \text{CaAl}_2\text{Si}_7\text{O}_{18} \cdot 6\text{H}_2\text{O}$	309	73	-
A65	$\text{Ca}_2\text{Al}_2\text{SiO}_6(\text{OH})_2 \cdot 2\text{CaO} \cdot \text{Al}_2\text{O}_3 \cdot \text{SiO}_2 \longleftrightarrow \text{H}_2\text{O} + \text{Ca}_2\text{Al}_2\text{SiO}_6(\text{OH})_2 \cdot \text{CaO} \cdot \text{Al}_2\text{O}_3 \cdot 2\text{SiO}_2$	609	363	-
A66	$\text{CaAl}_2\text{Si}_2\text{O}_7(\text{OH})_2 \cdot \text{H}_2\text{O} \cdot \text{CaO} \cdot \text{Al}_2\text{O}_3 \cdot 2\text{SiO}_2 \longleftrightarrow 2\text{H}_2\text{O} + \text{CaAl}_2\text{Si}_2\text{O}_7(\text{OH})_2 \cdot \text{CaO} \cdot \text{Al}_2\text{O}_3 \cdot 2\text{SiO}_2$	431	468	-
A67	$\text{CaB}_3\text{O}_3(\text{OH})_5 \cdot 4\text{H}_2\text{O} \cdot \text{CaB}_3\text{O}_4(\text{OH})_3 \cdot \text{H}_2\text{O} \longleftrightarrow 4\text{H}_2\text{O} + \text{CaB}_3\text{O}_3(\text{OH})_5 \cdot 3\text{H}_2\text{O} \cdot \text{CaB}_3\text{O}_4(\text{OH})_3 \cdot \text{H}_2\text{O}$	326	757	1415
A68	$2\text{CaB}_3\text{O}_3(\text{OH})_5 \cdot 4\text{H}_2\text{O} \cdot 2\text{CaO} \cdot 3\text{B}_2\text{O}_3 \longleftrightarrow 13\text{H}_2\text{O} + 2\text{CaB}_3\text{O}_3(\text{OH})_5 \cdot 3\text{H}_2\text{O} \cdot 2\text{CaO} \cdot 3\text{B}_2\text{O}_3$	355	1365	2552
A69	$2\text{CaB}_3\text{O}_4(\text{OH})_3 \cdot \text{H}_2\text{O} \cdot 2\text{CaO} \cdot 3\text{B}_2\text{O}_3 \longleftrightarrow 5\text{H}_2\text{O} + 2\text{CaB}_3\text{O}_4(\text{OH})_3 \cdot \text{CaO} \cdot 3\text{B}_2\text{O}_3$	382	821	-
A70	$\text{CaBr}_2 \cdot 6\text{H}_2\text{O} \longleftrightarrow 6\text{H}_2\text{O} + \text{CaBr}_2$	427	1205	2760
A72	$\text{CaCl}_2 \cdot \text{H}_2\text{O} \longleftrightarrow \text{H}_2\text{O} + \text{CaCl}_2$	480	561	-
A73	$\text{CaCl}_2 \cdot 2\text{H}_2\text{O} \longleftrightarrow \text{H}_2\text{O} + \text{CaCl}_2 \cdot \text{H}_2\text{O}$	305	307	-
A74	$\text{CaCl}_2 \cdot 2\text{H}_2\text{O} \longleftrightarrow 2\text{H}_2\text{O} + \text{CaCl}_2$	404	800	-
A75	$\text{CaCl}_2 \cdot 4\text{H}_2\text{O} \longleftrightarrow 2\text{H}_2\text{O} + \text{CaCl}_2 \cdot 2\text{H}_2\text{O}$	363	704	-
A76	$\text{CaCl}_2 \cdot 4\text{H}_2\text{O} \longleftrightarrow 3\text{H}_2\text{O} + \text{CaCl}_2 \cdot \text{H}_2\text{O}$	353	951	-
A77	$\text{CaCl}_2 \cdot 4\text{H}_2\text{O} \longleftrightarrow 4\text{H}_2\text{O} + \text{CaCl}_2$	410	1346	-
A78	$\text{CaCl}_2 \cdot 6\text{H}_2\text{O} \longleftrightarrow 2\text{H}_2\text{O} + \text{CaCl}_2 \cdot 4\text{H}_2\text{O}$	381	517	884
A79	$\text{CaCl}_2 \cdot 6\text{H}_2\text{O} \longleftrightarrow 4\text{H}_2\text{O} + \text{CaCl}_2 \cdot 2\text{H}_2\text{O}$	364	1105	1890
A80	$\text{CaCl}_2 \cdot 6\text{H}_2\text{O} \longleftrightarrow 5\text{H}_2\text{O} + \text{CaCl}_2 \cdot \text{H}_2\text{O}$	357	1312	2243
A81	$\text{CaCl}_2 \cdot 6\text{H}_2\text{O} \longleftrightarrow 6\text{H}_2\text{O} + \text{CaCl}_2$	401	1642	2808
A82	$\text{Ca}(\text{ClO}_4)_2 \cdot 4\text{H}_2\text{O} \longleftrightarrow 4\text{H}_2\text{O} + \text{Ca}(\text{ClO}_4)_2$	424	816	-
A83	$\text{CaHPO}_4 \cdot 2\text{H}_2\text{O} \longleftrightarrow 2\text{H}_2\text{O} + \text{CaHPO}_4$	412	715	1650

Continued on next page

Table 6.1: Reactions with H₂O as reactive gas – continued

ID	reaction system	T_{equ} °C	storage capacity kJ/kg	storage density MJ/m^3
A84	$2 \text{CaHPO}_4 \cdot 2 \text{H}_2\text{O} \longleftrightarrow 5 \text{H}_2\text{O} + \text{Ca}_2\text{P}_2\text{O}_7$	391	855	1973
A85	$\text{Ca}(\text{H}_2\text{PO}_4)_2 \cdot \text{H}_2\text{O} \longleftrightarrow \text{H}_2\text{O} + \text{Ca}(\text{H}_2\text{PO}_4)_2$	456	301	669
A86	$\text{Ca}(\text{H}_2\text{PO}_4)_2 \cdot \text{H}_2\text{O} \longleftrightarrow 3 \text{H}_2\text{O} + \text{Ca}(\text{PO}_3)_2$	472	849	1885
A87	$\text{Ca}(\text{IO}_3)_2 \cdot \text{H}_2\text{O} \longleftrightarrow \text{H}_2\text{O} + \text{Ca}(\text{IO}_3)_2$	421	234	-
A88	$\text{Ca}(\text{IO}_3)_2 \cdot 6 \text{H}_2\text{O} \longleftrightarrow 5 \text{H}_2\text{O} + \text{Ca}(\text{IO}_3)_2 \cdot \text{H}_2\text{O}$	302	466	-
A89	$\text{Ca}(\text{IO}_3)_2 \cdot 6 \text{H}_2\text{O} \longleftrightarrow 6 \text{H}_2\text{O} + \text{Ca}(\text{IO}_3)_2$	339	657	-
A90	$\text{Ca}(\text{NO}_3)_2 \cdot 2 \text{H}_2\text{O} \longleftrightarrow 2 \text{H}_2\text{O} + \text{Ca}(\text{NO}_3)_2$	400	601	-
A91	$\text{Ca}(\text{NO}_3)_2 \cdot 3 \text{H}_2\text{O} \longleftrightarrow \text{H}_2\text{O} + \text{Ca}(\text{NO}_3)_2 \cdot 2 \text{H}_2\text{O}$	399	254	-
A92	$\text{Ca}(\text{NO}_3)_2 \cdot 3 \text{H}_2\text{O} \longleftrightarrow 3 \text{H}_2\text{O} + \text{Ca}(\text{NO}_3)_2$	399	806	-
A93	$\text{Ca}(\text{NO}_3)_2 \cdot 4 \text{H}_2\text{O} \longleftrightarrow \text{H}_2\text{O} + \text{Ca}(\text{NO}_3)_2 \cdot 3 \text{H}_2\text{O}$	396	222	405
A94	$\text{Ca}(\text{NO}_3)_2 \cdot 4 \text{H}_2\text{O} \longleftrightarrow 2 \text{H}_2\text{O} + \text{Ca}(\text{NO}_3)_2 \cdot 2 \text{H}_2\text{O}$	397	457	832
A95	$\text{Ca}(\text{NO}_3)_2 \cdot 4 \text{H}_2\text{O} \longleftrightarrow 4 \text{H}_2\text{O} + \text{Ca}(\text{NO}_3)_2$	399	966	1759
A96	$3 \text{CaO} \cdot \text{Al}_2\text{O}_3 \cdot 6 \text{H}_2\text{O} \longleftrightarrow 6 \text{H}_2\text{O} + 3 \text{CaO} \cdot \text{Al}_2\text{O}_3$	495	1253	3158
A97	$\text{Ca}(\text{OH})_2 \longleftrightarrow \text{H}_2\text{O} + \text{CaO}$	791	1473	3300
A100	$\text{CaSO}_3 \cdot 2 \text{H}_2\text{O} \longleftrightarrow 2 \text{H}_2\text{O} + \text{CaSO}_3$	405	764	-
A101	$\text{CaSO}_4 \cdot 2 \text{H}_2\text{O} \longleftrightarrow 2 \text{H}_2\text{O} + \text{CaSO}_4$	349	589	1366
A102	$\text{CaSeO}_4 \cdot 2 \text{H}_2\text{O} \longleftrightarrow 2 \text{H}_2\text{O} + \text{CaSeO}_4$	441	565	1555
A103	$\text{CaSiF}_6 \cdot 2 \text{H}_2\text{O} \longleftrightarrow 2 \text{H}_2\text{O} + \text{CaSiF}_6$	446	688	-
A104	$\text{CaTeO}_3 \cdot \text{H}_2\text{O} \longleftrightarrow \text{H}_2\text{O} + \text{CaTeO}_3$	385	303	-
A105	$\text{CdBr}_2 \cdot 4 \text{H}_2\text{O} \longleftrightarrow 4 \text{H}_2\text{O} + \text{CdBr}_2$	356	602	-
A106	$\text{CdCl}_2 \cdot \text{H}_2\text{O} \longleftrightarrow \text{H}_2\text{O} + \text{CdCl}_2$	389	265	-
A107	$\text{Cd}(\text{NO}_3)_2 \cdot 2 \text{H}_2\text{O} \longleftrightarrow 2 \text{H}_2\text{O} + \text{Cd}(\text{NO}_3)_2$	391	422	-
A108	$\text{Cd}(\text{NO}_3)_2 \cdot 4 \text{H}_2\text{O} \longleftrightarrow 2 \text{H}_2\text{O} + \text{Cd}(\text{NO}_3)_2 \cdot 2 \text{H}_2\text{O}$	342	369	909
A109	$\text{Cd}(\text{NO}_3)_2 \cdot 4 \text{H}_2\text{O} \longleftrightarrow 4 \text{H}_2\text{O} + \text{Cd}(\text{NO}_3)_2$	402	742	1826
A110	$\text{Cd}(\text{OH})_2 \longleftrightarrow \text{H}_2\text{O} + \text{CdO}$	401	414	1985
A111	$\text{CdSO}_4 \cdot \text{H}_2\text{O} \longleftrightarrow \text{H}_2\text{O} + \text{CdSO}_4$	410	285	1081
A112	$\text{CeCl}_3 \cdot 7 \text{H}_2\text{O} \longleftrightarrow 7 \text{H}_2\text{O} + \text{CeCl}_3$	402	1146	-
A113	$\text{CePO}_4 \cdot 2 \text{H}_2\text{O} \longleftrightarrow 2 \text{H}_2\text{O} + \text{CePO}_4$	320	373	-
A114	$\text{Ce}(\text{SO}_4)_2 \cdot 5 \text{H}_2\text{O} \longleftrightarrow 5 \text{H}_2\text{O} + \text{Ce}(\text{SO}_4)_2$	1617	4548	-
A115	$\text{CoBr}_2 \cdot 6 \text{H}_2\text{O} \longleftrightarrow 6 \text{H}_2\text{O} + \text{CoBr}_2$	391	1081	2659
A116	$\text{CoCl}_2 \cdot \text{H}_2\text{O} \longleftrightarrow \text{H}_2\text{O} + \text{CoCl}_2$	446	414	-
A117	$\text{CoCl}_2 \cdot 2 \text{H}_2\text{O} \longleftrightarrow \text{H}_2\text{O} + \text{CoCl}_2 \cdot \text{H}_2\text{O}$	339	363	-
A118	$\text{CoCl}_2 \cdot 2 \text{H}_2\text{O} \longleftrightarrow 2 \text{H}_2\text{O} + \text{CoCl}_2$	418	732	-

Continued on next page

Table 6.1: Reactions with H₂O as reactive gas – continued

ID	reaction system	T_{equ} °C	storage capacity kJ/kg	storage density MJ/m^3
A119	$\text{CoCl}_2 \cdot 6 \text{H}_2\text{O} \longleftrightarrow 4 \text{H}_2\text{O} + \text{CoCl}_2 \cdot 2 \text{H}_2\text{O}$	347	967	1861
A120	$\text{CoCl}_2 \cdot 6 \text{H}_2\text{O} \longleftrightarrow 5 \text{H}_2\text{O} + \text{CoCl}_2 \cdot \text{H}_2\text{O}$	353	1221	2348
A121	$\text{CoCl}_2 \cdot 6 \text{H}_2\text{O} \longleftrightarrow 6 \text{H}_2\text{O} + \text{CoCl}_2$	387	1478	2843
A123	$\text{Co}(\text{NO}_3)_2 \cdot 6 \text{H}_2\text{O} \longleftrightarrow 6 \text{H}_2\text{O} + \text{Co}(\text{NO}_3)_2$	396	1155	2159
A124	$\text{Co}(\text{OH})_2 \longleftrightarrow \text{H}_2\text{O} + \text{CoO}$	395	671	2412
A125	$\text{CoSO}_4 \cdot 6 \text{H}_2\text{O} \longleftrightarrow 6 \text{H}_2\text{O} + \text{CoSO}_4$	392	1311	2621
A126	$\text{CoSO}_4 \cdot 7 \text{H}_2\text{O} \longleftrightarrow \text{H}_2\text{O} + \text{CoSO}_4 \cdot 6 \text{H}_2\text{O}$	360	193	366
A127	$\text{CoSO}_4 \cdot 7 \text{H}_2\text{O} \longleftrightarrow 7 \text{H}_2\text{O} + \text{CoSO}_4$	387	1419	2697
A129	$\text{CrCl}_2 \cdot 2 \text{H}_2\text{O} \longleftrightarrow 2 \text{H}_2\text{O} + \text{CrCl}_2$	408	783	-
A130	$\text{CrCl}_2 \cdot 3 \text{H}_2\text{O} \longleftrightarrow \text{H}_2\text{O} + \text{CrCl}_2 \cdot 2 \text{H}_2\text{O}$	345	352	-
A131	$\text{CrCl}_2 \cdot 3 \text{H}_2\text{O} \longleftrightarrow 3 \text{H}_2\text{O} + \text{CrCl}_2$	410	1056	-
A132	$\text{CrCl}_2 \cdot 4 \text{H}_2\text{O} \longleftrightarrow \text{H}_2\text{O} + \text{CrCl}_2 \cdot 3 \text{H}_2\text{O}$	332	299	-
A133	$\text{CrCl}_2 \cdot 4 \text{H}_2\text{O} \longleftrightarrow 2 \text{H}_2\text{O} + \text{CrCl}_2 \cdot 2 \text{H}_2\text{O}$	354	619	-
A134	$\text{CrCl}_2 \cdot 4 \text{H}_2\text{O} \longleftrightarrow 4 \text{H}_2\text{O} + \text{CrCl}_2$	404	1258	-
A136	$\text{Cr}_2(\text{SO}_4)_3 \cdot 8 \text{H}_2\text{O} \longleftrightarrow 8 \text{H}_2\text{O} + \text{Cr}_2(\text{SO}_4)_3$	687	1486	-
A137	$\text{Cr}_2(\text{SO}_4)_3 \cdot 14 \text{H}_2\text{O} \longleftrightarrow 6 \text{H}_2\text{O} + \text{Cr}_2(\text{SO}_4)_3 \cdot 8 \text{H}_2\text{O}$	388	537	-
A138	$\text{Cr}_2(\text{SO}_4)_3 \cdot 14 \text{H}_2\text{O} \longleftrightarrow 14 \text{H}_2\text{O} + \text{Cr}_2(\text{SO}_4)_3$	556	1774	-
A142	$\text{CsAl}(\text{SO}_4)_2 \cdot 12 \text{H}_2\text{O} \longleftrightarrow 12 \text{H}_2\text{O} + \text{CsAl}(\text{SO}_4)_2$	347	1158	-
A143	$\text{CsF} \cdot \text{H}_2\text{O} \longleftrightarrow \text{H}_2\text{O} + \text{CsF}$	445	388	-
A144	$2 \text{CsF} \cdot 3 \text{H}_2\text{O} \longleftrightarrow \text{H}_2\text{O} + 2 \text{CsF} \cdot \text{H}_2\text{O}$	322	152	-
A145	$2 \text{CsF} \cdot 3 \text{H}_2\text{O} \longleftrightarrow 3 \text{H}_2\text{O} + 2 \text{CsF}$	420	520	-
A147	$\text{CuBr}_2 \cdot 4 \text{H}_2\text{O} \longleftrightarrow 4 \text{H}_2\text{O} + \text{CuBr}_2$	366	738	-
A148	$\text{CuCl}_2 \cdot 2 \text{H}_2\text{O} \longleftrightarrow 2 \text{H}_2\text{O} + \text{CuCl}_2$	371	701	1759
A149	$\text{CuF}_2 \cdot 2 \text{H}_2\text{O} \longleftrightarrow 2 \text{H}_2\text{O} + \text{CuF}_2$	435	988	2899
A150	$\text{CuHPO}_4 \cdot \text{H}_2\text{O} \longleftrightarrow \text{H}_2\text{O} + \text{CuHPO}_4$	548	198	-
A152	$\text{Cu}(\text{IO}_3)_2 \cdot \text{H}_2\text{O} \longleftrightarrow \text{H}_2\text{O} + \text{Cu}(\text{IO}_3)_2$	334	139	-
A153	$\text{Cu}(\text{NO}_3)_2 \cdot 6 \text{H}_2\text{O} \longleftrightarrow 6 \text{H}_2\text{O} + \text{Cu}(\text{NO}_3)_2$	387	1203	2491
A154	$\text{Cu}(\text{OH})_2 \longleftrightarrow \text{H}_2\text{O} + \text{CuO}$	429	541	1822
A155	$\text{Cu}_3(\text{PO}_4)_2 \cdot 3 \text{H}_2\text{O} \longleftrightarrow 3 \text{H}_2\text{O} + \text{Cu}_3(\text{PO}_4)_2$	627	319	-
A156	$\text{CuSO}_4 \cdot \text{H}_2\text{O} \longleftrightarrow \text{H}_2\text{O} + \text{CuSO}_4$	455	392	-
A157	$\text{CuSO}_4 \cdot 3 \text{H}_2\text{O} \longleftrightarrow 2 \text{H}_2\text{O} + \text{CuSO}_4 \cdot \text{H}_2\text{O}$	382	537	-
A158	$\text{CuSO}_4 \cdot 3 \text{H}_2\text{O} \longleftrightarrow 3 \text{H}_2\text{O} + \text{CuSO}_4$	406	862	-
A159	$\text{CuSO}_4 \cdot 5 \text{H}_2\text{O} \longleftrightarrow 2 \text{H}_2\text{O} + \text{CuSO}_4 \cdot 3 \text{H}_2\text{O}$	374	447	1023
A160	$\text{CuSO}_4 \cdot 5 \text{H}_2\text{O} \longleftrightarrow 4 \text{H}_2\text{O} + \text{CuSO}_4 \cdot \text{H}_2\text{O}$	378	907	2073
A161	$\text{CuSO}_4 \cdot 5 \text{H}_2\text{O} \longleftrightarrow 5 \text{H}_2\text{O} + \text{CuSO}_4$	394	1185	2710
A162	$\text{CuSeO}_3 \cdot 2 \text{H}_2\text{O} \longleftrightarrow 2 \text{H}_2\text{O} + \text{CuSeO}_3$	387	389	1289
A163	$\text{DyCl}_3 \cdot 6 \text{H}_2\text{O} \longleftrightarrow 6 \text{H}_2\text{O} + \text{DyCl}_3$	495	1123	-

Continued on next page

Table 6.1: Reactions with H₂O as reactive gas – continued

ID	reaction system	T_{equ} °C	storage capacity kJ/kg	storage density MJ/m^3
A164	$2 \text{Dy}(\text{OH})_3 \longleftrightarrow 3 \text{H}_2\text{O} + \text{Dy}_2\text{O}_3$	783	909	-
A165	$\text{DyPO}_4 \cdot 2 \text{H}_2\text{O} \longleftrightarrow 2 \text{H}_2\text{O} + \text{DyPO}_4$	531	733	-
A166	$\text{ErCl}_3 \cdot 6 \text{H}_2\text{O} \longleftrightarrow 6 \text{H}_2\text{O} + \text{ErCl}_3$	489	1124	-
A167	$2 \text{Er}(\text{OH})_3 \longleftrightarrow 3 \text{H}_2\text{O} + \text{Er}_2\text{O}_3$	487	520	-
A168	$\text{ErPO}_4 \cdot 2 \text{H}_2\text{O} \longleftrightarrow 2 \text{H}_2\text{O} + \text{ErPO}_4$	501	665	-
A169	$\text{EuCl}_3 \cdot 6 \text{H}_2\text{O} \longleftrightarrow 6 \text{H}_2\text{O} + \text{EuCl}_3$	456	1077	5267
A170	$\text{Eu}(\text{IO}_3)_3 \cdot 2 \text{H}_2\text{O} \longleftrightarrow 2 \text{H}_2\text{O} + \text{Eu}(\text{IO}_3)_3$	1250	65	-
A171	$2 \text{Eu}(\text{OH})_3 \longleftrightarrow 3 \text{H}_2\text{O} + \text{Eu}_2\text{O}_3$	637	713	-
A172	$\text{EuPO}_4 \cdot 2 \text{H}_2\text{O} \longleftrightarrow 2 \text{H}_2\text{O} + \text{EuPO}_4$	319	346	-
A173	$\text{FeCl}_2 \cdot 2 \text{H}_2\text{O} \longleftrightarrow 2 \text{H}_2\text{O} + \text{FeCl}_2$	401	808	1931
A174	$\text{FeCl}_2 \cdot 4 \text{H}_2\text{O} \longleftrightarrow 2 \text{H}_2\text{O} + \text{FeCl}_2 \cdot 2 \text{H}_2\text{O}$	341	564	1089
A175	$\text{FeCl}_2 \cdot 4 \text{H}_2\text{O} \longleftrightarrow 4 \text{H}_2\text{O} + \text{FeCl}_2$	390	1226	2366
A176	$\text{FeCl}_3 \cdot 6 \text{H}_2\text{O} \longleftrightarrow 6 \text{H}_2\text{O} + \text{FeCl}_3$	401	1394	-
A179	$2 \text{FeO} \cdot \text{OH} \longleftrightarrow \text{H}_2\text{O} + \text{Fe}_2\text{O}_3$	355	310	1323
A180	$\text{FePO}_4 \cdot 2 \text{H}_2\text{O} \longleftrightarrow 2 \text{H}_2\text{O} + \text{FePO}_4$	361	576	1554
A183	$\text{FeSO}_4 \cdot \text{H}_2\text{O} \longleftrightarrow \text{H}_2\text{O} + \text{FeSO}_4$	472	419	1243
A184	$\text{FeSO}_4 \cdot 4 \text{H}_2\text{O} \longleftrightarrow 3 \text{H}_2\text{O} + \text{FeSO}_4 \cdot \text{H}_2\text{O}$	363	716	-
A185	$\text{FeSO}_4 \cdot 4 \text{H}_2\text{O} \longleftrightarrow 4 \text{H}_2\text{O} + \text{FeSO}_4$	391	1033	-
A186	$\text{FeSO}_4 \cdot 7 \text{H}_2\text{O} \longleftrightarrow 3 \text{H}_2\text{O} + \text{FeSO}_4 \cdot 4 \text{H}_2\text{O}$	368	581	1104
A187	$\text{FeSO}_4 \cdot 7 \text{H}_2\text{O} \longleftrightarrow 6 \text{H}_2\text{O} + \text{FeSO}_4 \cdot \text{H}_2\text{O}$	366	1158	2199
A188	$\text{FeSO}_4 \cdot 7 \text{H}_2\text{O} \longleftrightarrow 7 \text{H}_2\text{O} + \text{FeSO}_4$	381	1413	2685
A189	$2 \text{FrOH} \longleftrightarrow \text{H}_2\text{O} + \text{Fr}_2\text{O}$	881	481	-
A191	$2 \text{GaOOH} \longleftrightarrow \text{H}_2\text{O} + \text{Ga}_2\text{O}_3$	457	379	-
A192	$\text{GdCl}_3 \cdot 6 \text{H}_2\text{O} \longleftrightarrow 6 \text{H}_2\text{O} + \text{GdCl}_3$	454	1097	2660
A193	$2 \text{Gd}(\text{OH})_3 \longleftrightarrow 3 \text{H}_2\text{O} + \text{Gd}_2\text{O}_3$	949	1036	-
A194	$\text{GdPO}_4 \cdot 2 \text{H}_2\text{O} \longleftrightarrow 2 \text{H}_2\text{O} + \text{GdPO}_4$	548	775	-
A195	$\text{H}_2\text{SO}_4 \cdot \text{H}_2\text{O} \longleftrightarrow \text{H}_2\text{O} + \text{H}_2\text{SO}_4$	564	619	-
A196	$\text{H}_2\text{SO}_4 \cdot 2 \text{H}_2\text{O} \longleftrightarrow \text{H}_2\text{O} + \text{H}_2\text{SO}_4 \cdot \text{H}_2\text{O}$	473	430	-
A197	$\text{H}_2\text{SO}_4 \cdot 2 \text{H}_2\text{O} \longleftrightarrow 2 \text{H}_2\text{O} + \text{H}_2\text{SO}_4$	518	965	-
A198	$\text{H}_2\text{SO}_4 \cdot 3 \text{H}_2\text{O} \longleftrightarrow \text{H}_2\text{O} + \text{H}_2\text{SO}_4 \cdot 2 \text{H}_2\text{O}$	435	338	-
A199	$\text{H}_2\text{SO}_4 \cdot 3 \text{H}_2\text{O} \longleftrightarrow 2 \text{H}_2\text{O} + \text{H}_2\text{SO}_4 \cdot \text{H}_2\text{O}$	454	717	-
A200	$\text{H}_2\text{SO}_4 \cdot 3 \text{H}_2\text{O} \longleftrightarrow 3 \text{H}_2\text{O} + \text{H}_2\text{SO}_4$	490	1189	-
A201	$\text{H}_2\text{SO}_4 \cdot 4 \text{H}_2\text{O} \longleftrightarrow \text{H}_2\text{O} + \text{H}_2\text{SO}_4 \cdot 3 \text{H}_2\text{O}$	415	288	-
A202	$\text{H}_2\text{SO}_4 \cdot 4 \text{H}_2\text{O} \longleftrightarrow 2 \text{H}_2\text{O} + \text{H}_2\text{SO}_4 \cdot 2 \text{H}_2\text{O}$	425	590	-
A203	$\text{H}_2\text{SO}_4 \cdot 4 \text{H}_2\text{O} \longleftrightarrow 3 \text{H}_2\text{O} + \text{H}_2\text{SO}_4 \cdot \text{H}_2\text{O}$	441	929	-
A204	$\text{H}_2\text{SO}_4 \cdot 4 \text{H}_2\text{O} \longleftrightarrow 4 \text{H}_2\text{O} + \text{H}_2\text{SO}_4$	472	1351	-
A205	$\text{HoCl}_3 \cdot 6 \text{H}_2\text{O} \longleftrightarrow 6 \text{H}_2\text{O} + \text{HoCl}_3$	477	1110	-
A206	$2 \text{Ho}(\text{OH})_3 \longleftrightarrow 3 \text{H}_2\text{O} + \text{Ho}_2\text{O}_3$	570	632	-
A207	$\text{HoPO}_4 \cdot 2 \text{H}_2\text{O} \longleftrightarrow 2 \text{H}_2\text{O} + \text{HoPO}_4$	537	741	-

Continued on next page

Table 6.1: Reactions with H₂O as reactive gas – continued

ID	reaction system	T_{equ} °C	storage capacity kJ/kg	storage density MJ/m^3
A208	$2 \text{In}(\text{OH})_3 \longleftrightarrow 3 \text{H}_2\text{O} + \text{In}_2\text{O}_3$	310	429	1887
A210	$\text{KAl}(\text{SO}_4)_2 \cdot 3 \text{H}_2\text{O} \longleftrightarrow 3 \text{H}_2\text{O} + \text{KAl}(\text{SO}_4)_2$	406	594	-
A211	$\text{KAl}(\text{SO}_4)_2 \cdot 12 \text{H}_2\text{O} \longleftrightarrow 9 \text{H}_2\text{O} + \text{KAl}(\text{SO}_4)_2 \cdot 3 \text{H}_2\text{O}$	382	1063	1828
A212	$\text{KAl}(\text{SO}_4)_2 \cdot 12 \text{H}_2\text{O} \longleftrightarrow 12 \text{H}_2\text{O} + \text{KAl}(\text{SO}_4)_2$	389	1454	2501
A214	$\text{K}_2\text{CuCl}_4 \cdot 2 \text{H}_2\text{O} \longleftrightarrow 2 \text{H}_2\text{O} + \text{K}_2\text{CuCl}_4$	343	374	-
A215	$\text{K}_2\text{CuCl}_2(\text{H}_2\text{O})_2 \cdot \text{Cl}_2 \longleftrightarrow 2 \text{H}_2\text{O} + \text{K}_2\text{CuCl}_4$	323	330	-
A216	$\text{KF} \cdot 2 \text{H}_2\text{O} \longleftrightarrow 2 \text{H}_2\text{O} + \text{KF}$	362	1134	2835
A217	$\text{K}_4\text{Fe}(\text{CN})_6 \cdot 3 \text{H}_2\text{O} \longleftrightarrow 3 \text{H}_2\text{O} + \text{K}_4\text{Fe}(\text{CN})_6$	415	356	659
A218	$\text{K}_2\text{Mg}(\text{SO}_4)_2 \cdot 6 \text{H}_2\text{O} \longleftrightarrow 2 \text{H}_2\text{O} + \text{K}_2\text{Mg}(\text{SO}_4)_2 \cdot 4 \text{H}_2\text{O}$	320	265	-
A220	$\text{KOH} \cdot \text{H}_2\text{O} \longleftrightarrow \text{H}_2\text{O} + \text{KOH}$	560	1176	-
A221	$2 \text{KOH} \cdot \text{H}_2\text{O} \longleftrightarrow 3 \text{H}_2\text{O} + \text{K}_2\text{O}$	978	2822	-
A222	$\text{KOH} \cdot 2 \text{H}_2\text{O} \longleftrightarrow \text{H}_2\text{O} + \text{KOH} \cdot \text{H}_2\text{O}$	340	615	-
A223	$\text{KOH} \cdot 2 \text{H}_2\text{O} \longleftrightarrow 2 \text{H}_2\text{O} + \text{KOH}$	477	1561	-
A224	$2 \text{KOH} \cdot 2 \text{H}_2\text{O} \longleftrightarrow 5 \text{H}_2\text{O} + \text{K}_2\text{O}$	736	2886	-
A225	$\text{K}_3\text{PO}_4 \cdot 7 \text{H}_2\text{O} \longleftrightarrow 7 \text{H}_2\text{O} + \text{K}_3\text{PO}_4$	337	1033	-
A226	$\text{K}_4\text{P}_2\text{O}_7 \cdot 3 \text{H}_2\text{O} \longleftrightarrow 3 \text{H}_2\text{O} + \text{K}_4\text{P}_2\text{O}_7$	349	402	-
A227	$\text{K}_2\text{SO}_3 \cdot \text{H}_2\text{O} \longleftrightarrow \text{H}_2\text{O} + \text{K}_2\text{SO}_3$	310	259	-
A228	$\text{LaCl}_3 \cdot 7 \text{H}_2\text{O} \longleftrightarrow 7 \text{H}_2\text{O} + \text{LaCl}_3$	418	1117	-
A229	$2 \text{La}(\text{OH})_3 \longleftrightarrow 3 \text{H}_2\text{O} + \text{La}_2\text{O}_3$	681	798	-
A230	$\text{LaPO}_4 \cdot 2 \text{H}_2\text{O} \longleftrightarrow 2 \text{H}_2\text{O} + \text{LaPO}_4$	690	843	-
A232	$\text{LiBr} \cdot \text{H}_2\text{O} \longleftrightarrow \text{H}_2\text{O} + \text{LiBr}$	456	663	-
A233	$\text{LiBr} \cdot 2 \text{H}_2\text{O} \longleftrightarrow \text{H}_2\text{O} + \text{LiBr} \cdot \text{H}_2\text{O}$	309	469	-
A234	$\text{LiBr} \cdot 2 \text{H}_2\text{O} \longleftrightarrow 2 \text{H}_2\text{O} + \text{LiBr}$	371	1035	-
A235	$\text{LiCl} \cdot \text{H}_2\text{O} \longleftrightarrow \text{H}_2\text{O} + \text{LiCl}$	436	1041	1874
A236	$2 \text{LiCl} \cdot \text{H}_2\text{O} \longleftrightarrow 2 \text{H}_2\text{O} + \text{Li}_2\text{Cl}_2$	613	2785	5013
A237	$\text{LiClO}_4 \cdot \text{H}_2\text{O} \longleftrightarrow \text{H}_2\text{O} + \text{LiClO}_4$	400	515	-
A238	$\text{LiClO}_4 \cdot 3 \text{H}_2\text{O} \longleftrightarrow 2 \text{H}_2\text{O} + \text{LiClO}_4 \cdot \text{H}_2\text{O}$	362	759	-
A239	$\text{LiClO}_4 \cdot 3 \text{H}_2\text{O} \longleftrightarrow 3 \text{H}_2\text{O} + \text{LiClO}_4$	411	1158	-
A240	$\text{LiI} \cdot \text{H}_2\text{O} \longleftrightarrow \text{H}_2\text{O} + \text{LiI}$	500	497	-
A241	$\text{LiI} \cdot 2 \text{H}_2\text{O} \longleftrightarrow \text{H}_2\text{O} + \text{LiI} \cdot \text{H}_2\text{O}$	421	347	-
A242	$\text{LiI} \cdot 2 \text{H}_2\text{O} \longleftrightarrow 2 \text{H}_2\text{O} + \text{LiI}$	483	792	-
A243	$\text{LiI} \cdot 3 \text{H}_2\text{O} \longleftrightarrow \text{H}_2\text{O} + \text{LiI} \cdot 2 \text{H}_2\text{O}$	422	313	1096
A244	$\text{LiI} \cdot 3 \text{H}_2\text{O} \longleftrightarrow 2 \text{H}_2\text{O} + \text{LiI} \cdot \text{H}_2\text{O}$	431	627	2194
A245	$\text{LiI} \cdot 3 \text{H}_2\text{O} \longleftrightarrow 3 \text{H}_2\text{O} + \text{LiI}$	483	1029	3601
A246	$\text{LiNO}_2 \cdot \text{H}_2\text{O} \longleftrightarrow \text{H}_2\text{O} + \text{LiNO}_2$	438	929	-
A247	$\text{LiNO}_3 \cdot 3 \text{H}_2\text{O} \longleftrightarrow 3 \text{H}_2\text{O} + \text{LiNO}_3$	352	1356	-

Continued on next page

Table 6.1: Reactions with H₂O as reactive gas – continued

ID	reaction system	T_{equ} °C	storage capacity kJ/kg	storage density MJ/m^3
A248	$2 \text{LiOH} \longleftrightarrow \text{H}_2\text{O} + \text{Li}_2\text{O}$	1337	2716	3966
A249	$\text{LiOH} \cdot \text{H}_2\text{O} \longleftrightarrow \text{H}_2\text{O} + \text{LiOH}$	400	1503	2270
A250	$2 \text{LiOH} \cdot \text{H}_2\text{O} \longleftrightarrow 3 \text{H}_2\text{O} + \text{Li}_2\text{O}$	561	3053	4611
A251	$\text{Li}_2\text{SO}_4 \cdot \text{H}_2\text{O} \longleftrightarrow \text{H}_2\text{O} + \text{Li}_2\text{SO}_4$	359	438	903
A252	$\text{LuCl}_3 \cdot 6 \text{H}_2\text{O} \longleftrightarrow 6 \text{H}_2\text{O} + \text{LuCl}_3$	424	1009	-
A253	$2 \text{Lu}(\text{OH})_3 \longleftrightarrow 3 \text{H}_2\text{O} + \text{Lu}_2\text{O}_3$	383	380	-
A254	$\text{LuPO}_4 \cdot 2 \text{H}_2\text{O} \longleftrightarrow 2 \text{H}_2\text{O} + \text{LuPO}_4$	446	539	-
A255	$\text{MgBr}_2 \cdot 6 \text{H}_2\text{O} \longleftrightarrow 6 \text{H}_2\text{O} + \text{MgBr}_2$	493	1488	2976
A256	$\text{MgCO}_3 \cdot 3 \text{H}_2\text{O} \longleftrightarrow 3 \text{H}_2\text{O} + \text{MgCO}_3$	347	1126	2083
A257	$\text{MgCO}_3 \cdot 5 \text{H}_2\text{O} \longleftrightarrow 2 \text{H}_2\text{O} + \text{MgCO}_3 \cdot 3 \text{H}_2\text{O}$	358	608	-
A258	$\text{MgCO}_3 \cdot 5 \text{H}_2\text{O} \longleftrightarrow 5 \text{H}_2\text{O} + \text{MgCO}_3$	357	1501	-
A259	$\text{MgCl}_2 \cdot \text{H}_2\text{O} \longleftrightarrow \text{H}_2\text{O} + \text{MgCl}_2$	583	711	-
A260	$\text{MgCl}_2 \cdot 2 \text{H}_2\text{O} \longleftrightarrow \text{H}_2\text{O} + \text{MgCl}_2 \cdot \text{H}_2\text{O}$	491	543	-
A261	$\text{MgCl}_2 \cdot 2 \text{H}_2\text{O} \longleftrightarrow 2 \text{H}_2\text{O} + \text{MgCl}_2$	535	1156	-
A262	$\text{MgCl}_2 \cdot 4 \text{H}_2\text{O} \longleftrightarrow 2 \text{H}_2\text{O} + \text{MgCl}_2 \cdot 2 \text{H}_2\text{O}$	464	811	-
A263	$\text{MgCl}_2 \cdot 4 \text{H}_2\text{O} \longleftrightarrow 3 \text{H}_2\text{O} + \text{MgCl}_2 \cdot \text{H}_2\text{O}$	473	1237	-
A264	$\text{MgCl}_2 \cdot 4 \text{H}_2\text{O} \longleftrightarrow 4 \text{H}_2\text{O} + \text{MgCl}_2$	499	1718	-
A265	$\text{MgCl}_2 \cdot 6 \text{H}_2\text{O} \longleftrightarrow 2 \text{H}_2\text{O} + \text{MgCl}_2 \cdot 4 \text{H}_2\text{O}$	423	572	898
A266	$\text{MgCl}_2 \cdot 6 \text{H}_2\text{O} \longleftrightarrow 4 \text{H}_2\text{O} + \text{MgCl}_2 \cdot 2 \text{H}_2\text{O}$	444	1240	1945
A267	$\text{MgCl}_2 \cdot 6 \text{H}_2\text{O} \longleftrightarrow 5 \text{H}_2\text{O} + \text{MgCl}_2 \cdot \text{H}_2\text{O}$	454	1590	2495
A268	$\text{MgCl}_2 \cdot 6 \text{H}_2\text{O} \longleftrightarrow 6 \text{H}_2\text{O} + \text{MgCl}_2$	474	1986	3116
A269	$\text{Mg}(\text{ClO}_4)_2 \cdot 6 \text{H}_2\text{O} \longleftrightarrow 6 \text{H}_2\text{O} + \text{Mg}(\text{ClO}_4)_2$	458	1282	2308
A270	$\text{Mg}(\text{NO}_3)_2 \cdot 2 \text{H}_2\text{O} \longleftrightarrow 2 \text{H}_2\text{O} + \text{Mg}(\text{NO}_3)_2$	447	743	-
A271	$\text{Mg}(\text{NO}_3)_2 \cdot 6 \text{H}_2\text{O} \longleftrightarrow 4 \text{H}_2\text{O} + \text{Mg}(\text{NO}_3)_2 \cdot 2 \text{H}_2\text{O}$	367	914	1499
A272	$\text{Mg}(\text{NO}_3)_2 \cdot 6 \text{H}_2\text{O} \longleftrightarrow 6 \text{H}_2\text{O} + \text{Mg}(\text{NO}_3)_2$	429	1448	2375
A273	$\text{Mg}(\text{OH})_2 \longleftrightarrow \text{H}_2\text{O} + \text{MgO}$	538	1393	3287
A274	$\text{MgSO}_3 \cdot 3 \text{H}_2\text{O} \longleftrightarrow 3 \text{H}_2\text{O} + \text{MgSO}_3$	354	1011	-
A275	$\text{MgSO}_3 \cdot 6 \text{H}_2\text{O} \longleftrightarrow 3 \text{H}_2\text{O} + \text{MgSO}_3 \cdot 3 \text{H}_2\text{O}$	330	752	-
A276	$\text{MgSO}_3 \cdot 6 \text{H}_2\text{O} \longleftrightarrow 6 \text{H}_2\text{O} + \text{MgSO}_3$	353	1506	-
A277	$\text{MgSO}_4 \cdot \text{H}_2\text{O} \longleftrightarrow \text{H}_2\text{O} + \text{MgSO}_4$	773	769	1976
A278	$\text{MgSO}_4 \cdot 2 \text{H}_2\text{O} \longleftrightarrow \text{H}_2\text{O} + \text{MgSO}_4 \cdot \text{H}_2\text{O}$	303	286	-
A279	$\text{MgSO}_4 \cdot 2 \text{H}_2\text{O} \longleftrightarrow 2 \text{H}_2\text{O} + \text{MgSO}_4$	507	967	-
A280	$\text{MgSO}_4 \cdot 4 \text{H}_2\text{O} \longleftrightarrow 2 \text{H}_2\text{O} + \text{MgSO}_4 \cdot 2 \text{H}_2\text{O}$	392	607	-
A281	$\text{MgSO}_4 \cdot 4 \text{H}_2\text{O} \longleftrightarrow 3 \text{H}_2\text{O} + \text{MgSO}_4 \cdot \text{H}_2\text{O}$	362	839	-
A282	$\text{MgSO}_4 \cdot 4 \text{H}_2\text{O} \longleftrightarrow 4 \text{H}_2\text{O} + \text{MgSO}_4$	449	1392	-
A283	$\text{MgSO}_4 \cdot 5 \text{H}_2\text{O} \longleftrightarrow \text{H}_2\text{O} + \text{MgSO}_4 \cdot 4 \text{H}_2\text{O}$	396	270	-
A284	$\text{MgSO}_4 \cdot 5 \text{H}_2\text{O} \longleftrightarrow 3 \text{H}_2\text{O} + \text{MgSO}_4 \cdot 2 \text{H}_2\text{O}$	394	825	-
A285	$\text{MgSO}_4 \cdot 5 \text{H}_2\text{O} \longleftrightarrow 4 \text{H}_2\text{O} + \text{MgSO}_4 \cdot \text{H}_2\text{O}$	373	1038	-

Continued on next page

Table 6.1: Reactions with H₂O as reactive gas – continued

ID	reaction system	T_{equ} °C	storage capacity kJ/kg	storage density MJ/m^3
A286	$\text{MgSO}_4 \cdot 5 \text{H}_2\text{O} \longleftrightarrow 5 \text{H}_2\text{O} + \text{MgSO}_4$	434	1544	-
A287	$\text{MgSO}_4 \cdot 6 \text{H}_2\text{O} \longleftrightarrow \text{H}_2\text{O} + \text{MgSO}_4 \cdot 5 \text{H}_2\text{O}$	313	218	-
A288	$\text{MgSO}_4 \cdot 6 \text{H}_2\text{O} \longleftrightarrow 2 \text{H}_2\text{O} + \text{MgSO}_4 \cdot 4 \text{H}_2\text{O}$	387	467	-
A289	$\text{MgSO}_4 \cdot 6 \text{H}_2\text{O} \longleftrightarrow 4 \text{H}_2\text{O} + \text{MgSO}_4 \cdot 2 \text{H}_2\text{O}$	390	978	-
A290	$\text{MgSO}_4 \cdot 6 \text{H}_2\text{O} \longleftrightarrow 5 \text{H}_2\text{O} + \text{MgSO}_4 \cdot \text{H}_2\text{O}$	372	1174	-
A291	$\text{MgSO}_4 \cdot 6 \text{H}_2\text{O} \longleftrightarrow 6 \text{H}_2\text{O} + \text{MgSO}_4$	430	1639	-
A292	$\text{MgSO}_4 \cdot 7 \text{H}_2\text{O} \longleftrightarrow \text{H}_2\text{O} + \text{MgSO}_4 \cdot 6 \text{H}_2\text{O}$	364	243	408
A293	$\text{MgSO}_4 \cdot 7 \text{H}_2\text{O} \longleftrightarrow 2 \text{H}_2\text{O} + \text{MgSO}_4 \cdot 5 \text{H}_2\text{O}$	325	445	747
A294	$\text{MgSO}_4 \cdot 7 \text{H}_2\text{O} \longleftrightarrow 3 \text{H}_2\text{O} + \text{MgSO}_4 \cdot 4 \text{H}_2\text{O}$	379	676	1135
A295	$\text{MgSO}_4 \cdot 7 \text{H}_2\text{O} \longleftrightarrow 5 \text{H}_2\text{O} + \text{MgSO}_4 \cdot 2 \text{H}_2\text{O}$	384	1149	1931
A296	$\text{MgSO}_4 \cdot 7 \text{H}_2\text{O} \longleftrightarrow 6 \text{H}_2\text{O} + \text{MgSO}_4 \cdot \text{H}_2\text{O}$	370	1331	2236
A297	$\text{MgSO}_4 \cdot 7 \text{H}_2\text{O} \longleftrightarrow 7 \text{H}_2\text{O} + \text{MgSO}_4$	419	1763	2961
A298	$\text{MgSeO}_3 \cdot 6 \text{H}_2\text{O} \longleftrightarrow 6 \text{H}_2\text{O} + \text{MgSeO}_3$	381	1351	2824
A299	$\text{MgSeO}_4 \cdot \text{H}_2\text{O} \longleftrightarrow \text{H}_2\text{O} + \text{MgSeO}_4$	617	477	-
A300	$\text{MgSeO}_4 \cdot 4 \text{H}_2\text{O} \longleftrightarrow 3 \text{H}_2\text{O} + \text{MgSeO}_4 \cdot \text{H}_2\text{O}$	351	706	-
A301	$\text{MgSeO}_4 \cdot 4 \text{H}_2\text{O} \longleftrightarrow 4 \text{H}_2\text{O} + \text{MgSeO}_4$	453	1076	-
A302	$\text{MgSeO}_4 \cdot 6 \text{H}_2\text{O} \longleftrightarrow 2 \text{H}_2\text{O} + \text{MgSeO}_4 \cdot 4 \text{H}_2\text{O}$	326	383	-
A303	$\text{MgSeO}_4 \cdot 6 \text{H}_2\text{O} \longleftrightarrow 5 \text{H}_2\text{O} + \text{MgSeO}_4 \cdot \text{H}_2\text{O}$	349	997	-
A304	$\text{MgSeO}_4 \cdot 6 \text{H}_2\text{O} \longleftrightarrow 6 \text{H}_2\text{O} + \text{MgSeO}_4$	425	1318	-
A305	$\text{MgTeO}_3 \cdot 5 \text{H}_2\text{O} \longleftrightarrow 5 \text{H}_2\text{O} + \text{MgTeO}_3$	378	1052	-
A306	$\text{MgTeO}_3 \cdot 6 \text{H}_2\text{O} \longleftrightarrow \text{H}_2\text{O} + \text{MgTeO}_3 \cdot 5 \text{H}_2\text{O}$	317	171	-
A307	$\text{MgTeO}_3 \cdot 6 \text{H}_2\text{O} \longleftrightarrow 6 \text{H}_2\text{O} + \text{MgTeO}_3$	373	1162	-
A308	$\text{MnBr}_2 \cdot 4 \text{H}_2\text{O} \longleftrightarrow 4 \text{H}_2\text{O} + \text{MnBr}_2$	358	756	-
A309	$\text{MnBr}_2 \cdot 6 \text{H}_2\text{O} \longleftrightarrow 2 \text{H}_2\text{O} + \text{MnBr}_2 \cdot 4 \text{H}_2\text{O}$	416	381	-
A310	$\text{MnBr}_2 \cdot 6 \text{H}_2\text{O} \longleftrightarrow 6 \text{H}_2\text{O} + \text{MnBr}_2$	384	1053	-
A311	$\text{MnCl}_2 \cdot \text{H}_2\text{O} \longleftrightarrow \text{H}_2\text{O} + \text{MnCl}_2$	468	464	-
A312	$\text{MnCl}_2 \cdot 2 \text{H}_2\text{O} \longleftrightarrow \text{H}_2\text{O} + \text{MnCl}_2 \cdot \text{H}_2\text{O}$	347	372	-
A313	$\text{MnCl}_2 \cdot 2 \text{H}_2\text{O} \longleftrightarrow 2 \text{H}_2\text{O} + \text{MnCl}_2$	462	785	-
A314	$\text{MnCl}_2 \cdot 4 \text{H}_2\text{O} \longleftrightarrow 2 \text{H}_2\text{O} + \text{MnCl}_2 \cdot 2 \text{H}_2\text{O}$	372	563	1076
A315	$\text{MnCl}_2 \cdot 4 \text{H}_2\text{O} \longleftrightarrow 3 \text{H}_2\text{O} + \text{MnCl}_2 \cdot \text{H}_2\text{O}$	354	867	1659
A316	$\text{MnCl}_2 \cdot 4 \text{H}_2\text{O} \longleftrightarrow 4 \text{H}_2\text{O} + \text{MnCl}_2$	411	1205	2305
A317	$\text{MnF}_2 \cdot 4 \text{H}_2\text{O} \longleftrightarrow 4 \text{H}_2\text{O} + \text{MnF}_2$	341	1218	-
A318	$\text{MnI}_2 \cdot 4 \text{H}_2\text{O} \longleftrightarrow 4 \text{H}_2\text{O} + \text{MnI}_2$	396	598	-
A319	$\text{Mn(OH)}_2 \longleftrightarrow \text{H}_2\text{O} + \text{MnO}$	464	775	2527
A320	$2 \text{MnO} \cdot \text{OH} \longleftrightarrow \text{H}_2\text{O} + \text{Mn}_2\text{O}_3$	445	427	-
A321	$\text{MnSO}_4 \cdot \text{H}_2\text{O} \longleftrightarrow \text{H}_2\text{O} + \text{MnSO}_4$	480	411	1212
A322	$\text{MnSO}_4 \cdot 4 \text{H}_2\text{O} \longleftrightarrow 3 \text{H}_2\text{O} + \text{MnSO}_4 \cdot \text{H}_2\text{O}$	348	700	1582
A323	$\text{MnSO}_4 \cdot 4 \text{H}_2\text{O} \longleftrightarrow 4 \text{H}_2\text{O} + \text{MnSO}_4$	379	1011	2285

Continued on next page

Table 6.1: Reactions with H₂O as reactive gas – continued

ID	reaction system	T_{equ} °C	storage capacity kJ/kg	storage density MJ/m^3
A327	$\text{MnSO}_4 \cdot 7 \text{H}_2\text{O} \longleftrightarrow 2 \text{H}_2\text{O} + \text{MnSO}_4 \cdot 5 \text{H}_2\text{O}$	864	1888	3965
A328	$\text{MnSO}_4 \cdot 7 \text{H}_2\text{O} \longleftrightarrow 3 \text{H}_2\text{O} + \text{MnSO}_4 \cdot 4 \text{H}_2\text{O}$	349	561	1178
A329	$\text{MnSO}_4 \cdot 7 \text{H}_2\text{O} \longleftrightarrow 6 \text{H}_2\text{O} + \text{MnSO}_4 \cdot \text{H}_2\text{O}$	348	1124	2361
A330	$\text{MnSO}_4 \cdot 7 \text{H}_2\text{O} \longleftrightarrow 7 \text{H}_2\text{O} + \text{MnSO}_4$	367	1375	2887
A331	$\text{MnSeO}_4 \cdot \text{H}_2\text{O} \longleftrightarrow \text{H}_2\text{O} + \text{MnSeO}_4$	562	362	-
A332	$\text{MoO}_2\text{Cl}_2 \cdot \text{H}_2\text{O} \longleftrightarrow \text{H}_2\text{O} + \text{MoCl}_2\text{O}_2$	416	290	-
A333	$\text{MoO}_3 \cdot \text{H}_2\text{O} \longleftrightarrow \text{H}_2\text{O} + \text{MoO}_3$	447	342	-
A334	$\text{NH}_4 \cdot \text{Al}(\text{SO}_4)_2 \cdot 12 \text{H}_2\text{O} \longleftrightarrow 12 \text{H}_2\text{O} + \text{NH}_4 \cdot \text{Al}(\text{SO}_4)_2$	386	1518	2490
A335	$\text{NH}_4(\text{UO}_2)_2\text{F}_5 \cdot 3 \text{H}_2\text{O} \longleftrightarrow 3 \text{H}_2\text{O} + \text{NH}_4(\text{UO}_2)_2\text{F}_5$	336	73	-
A336	$\text{NH}_4(\text{UO}_2)_2\text{F}_5 \cdot 4 \text{H}_2\text{O} \longleftrightarrow \text{H}_2\text{O} + \text{NH}_4(\text{UO}_2)_2\text{F}_5 \cdot 3 \text{H}_2\text{O}$	309	67	-
A337	$\text{NH}_4(\text{UO}_2)_2\text{F}_5 \cdot 4 \text{H}_2\text{O} \longleftrightarrow 4 \text{H}_2\text{O} + \text{NH}_4(\text{UO}_2)_2\text{F}_5$	338	138	-
A338	$2 \text{NaAl}(\text{OH})_4 \longleftrightarrow 4 \text{H}_2\text{O} + \text{Na}_2\text{O} \cdot \text{Al}_2\text{O}_3$	464	965	-
A339	$\text{Na}_2\text{B}_4\text{O}_7 \cdot 10 \text{H}_2\text{O} \longleftrightarrow 10 \text{H}_2\text{O} + \text{Na}_2\text{B}_4\text{O}_7$	373	1458	2522
A340	$\text{NaBr} \cdot 2 \text{H}_2\text{O} \longleftrightarrow 2 \text{H}_2\text{O} + \text{NaBr}$	364	764	1666
A341	$\text{NaCH}_3\text{COO} \cdot 3 \text{H}_2\text{O} \longleftrightarrow 3 \text{H}_2\text{O} + \text{NaC}_2\text{H}_3\text{O}_2$	389	1241	-
A342	$\text{NaCHOO} \cdot 2 \text{H}_2\text{O} \longleftrightarrow 2 \text{H}_2\text{O} + \text{NaCHO}_2$	363	1046	-
A344	$\text{NaCHOO} \cdot 3 \text{H}_2\text{O} \longleftrightarrow 3 \text{H}_2\text{O} + \text{NaCHO}_2$	333	1228	-
A345	$\text{NaCN} \cdot 2 \text{H}_2\text{O} \longleftrightarrow 2 \text{H}_2\text{O} + \text{NaCN}$	352	1241	-
A346	$\text{Na}_2\text{CO}_3 \cdot \text{H}_2\text{O} \longleftrightarrow \text{H}_2\text{O} + \text{Na}_2\text{CO}_3$	372	479	1083
A347	$\text{Na}_2\text{CO}_3 \cdot 7 \text{H}_2\text{O} \longleftrightarrow 6 \text{H}_2\text{O} + \text{Na}_2\text{CO}_3 \cdot \text{H}_2\text{O}$	351	1335	2002
A348	$\text{Na}_2\text{CO}_3 \cdot 7 \text{H}_2\text{O} \longleftrightarrow 7 \text{H}_2\text{O} + \text{Na}_2\text{CO}_3$	354	1591	2386
A349	$\text{Na}_2\text{CO}_3 \cdot 10 \text{H}_2\text{O} \longleftrightarrow 3 \text{H}_2\text{O} + \text{Na}_2\text{CO}_3 \cdot 7 \text{H}_2\text{O}$	400	572	824
A350	$\text{Na}_2\text{CO}_3 \cdot 10 \text{H}_2\text{O} \longleftrightarrow 9 \text{H}_2\text{O} + \text{Na}_2\text{CO}_3 \cdot \text{H}_2\text{O}$	364	1655	2383
A351	$\text{Na}_2\text{CO}_3 \cdot 10 \text{H}_2\text{O} \longleftrightarrow 10 \text{H}_2\text{O} + \text{Na}_2\text{CO}_3$	365	1863	2682
A352	$\text{NaClO}_2 \cdot 3 \text{H}_2\text{O} \longleftrightarrow 3 \text{H}_2\text{O} + \text{NaClO}_2$	348	1160	-
A353	$\text{NaClO}_4 \cdot \text{H}_2\text{O} \longleftrightarrow \text{H}_2\text{O} + \text{NaClO}_4$	325	340	-
A354	$\text{Na}_2\text{CrO}_4 \cdot 4 \text{H}_2\text{O} \longleftrightarrow 4 \text{H}_2\text{O} + \text{Na}_2\text{CrO}_4$	376	932	-
A355	$\text{Na}_2\text{HPO}_4 \cdot 2 \text{H}_2\text{O} \longleftrightarrow 2 \text{H}_2\text{O} + \text{Na}_2\text{HPO}_4$	373	643	-
A356	$2 \text{Na}_2\text{HPO}_4 \cdot 2 \text{H}_2\text{O} \longleftrightarrow 5 \text{H}_2\text{O} + \text{Na}_4\text{P}_2\text{O}_7$	410	889	-
A357	$\text{Na}_2\text{HPO}_4 \cdot 7 \text{H}_2\text{O} \longleftrightarrow 5 \text{H}_2\text{O} + \text{Na}_2\text{HPO}_4 \cdot 2 \text{H}_2\text{O}$	339	993	1687
A358	$\text{Na}_2\text{HPO}_4 \cdot 7 \text{H}_2\text{O} \longleftrightarrow 7 \text{H}_2\text{O} + \text{Na}_2\text{HPO}_4$	367	1419	2413
A359	$2 \text{Na}_2\text{HPO}_4 \cdot 7 \text{H}_2\text{O} \longleftrightarrow 15 \text{H}_2\text{O} + \text{Na}_4\text{P}_2\text{O}_7$	380	1583	2691

Continued on next page

Table 6.1: Reactions with H₂O as reactive gas – continued

ID	reaction system	T_{equ} °C	storage capacity kJ/kg	storage density MJ/m^3
A360	$\text{Na}_2\text{HPO}_4 \cdot 12 \text{H}_2\text{O} \longleftrightarrow 5 \text{H}_2\text{O} + \text{Na}_2\text{HPO}_4 \cdot 7 \text{H}_2\text{O}$	361	750	1125
A361	$\text{Na}_2\text{HPO}_4 \cdot 12 \text{H}_2\text{O} \longleftrightarrow 10 \text{H}_2\text{O} + \text{Na}_2\text{HPO}_4 \cdot 2 \text{H}_2\text{O}$	343	1493	2239
A362	$\text{Na}_2\text{HPO}_4 \cdot 12 \text{H}_2\text{O} \longleftrightarrow 12 \text{H}_2\text{O} + \text{Na}_2\text{HPO}_4$	364	1812	2719
A363	$2 \text{Na}_2\text{HPO}_4 \cdot 12 \text{H}_2\text{O} \longleftrightarrow 25 \text{H}_2\text{O} + \text{Na}_4\text{P}_2\text{O}_7$	372	1935	2902
A364	$\text{NaHSO}_4 \cdot \text{H}_2\text{O} \longleftrightarrow \text{H}_2\text{O} + \text{NaHSO}_4$	339	379	-
A365	$2 \text{NaHSO}_4 \cdot \text{H}_2\text{O} \longleftrightarrow 3 \text{H}_2\text{O} + \text{Na}_2\text{S}_2\text{O}_7$	424	689	-
A366	$\text{NaH}_2\text{SiO}_4 \cdot 8 \text{H}_2\text{O} \longleftrightarrow \text{H}_2\text{O} + \text{NaH}_2\text{SiO}_4 \cdot 7 \text{H}_2\text{O}$	301	203	-
A367	$\text{NaI} \cdot 2 \text{H}_2\text{O} \longleftrightarrow 2 \text{H}_2\text{O} + \text{NaI}$	309	600	1470
A368	$\text{NaIO}_3 \cdot \text{H}_2\text{O} \longleftrightarrow \text{H}_2\text{O} + \text{NaIO}_3$	419	317	-
A369	$\text{NaIO}_3 \cdot 5 \text{H}_2\text{O} \longleftrightarrow 4 \text{H}_2\text{O} + \text{NaIO}_3 \cdot \text{H}_2\text{O}$	328	714	-
A370	$\text{NaIO}_3 \cdot 5 \text{H}_2\text{O} \longleftrightarrow 5 \text{H}_2\text{O} + \text{NaIO}_3$	365	951	-
A373	$\text{NaOH} \cdot \text{H}_2\text{O} \longleftrightarrow \text{H}_2\text{O} + \text{NaOH}$	387	1125	-
A374	$2 \text{NaOH} \cdot \text{H}_2\text{O} \longleftrightarrow 3 \text{H}_2\text{O} + \text{Na}_2\text{O}$	689	2803	-
A375	$\text{Na}_3\text{PO}_4 \cdot 12 \text{H}_2\text{O} \longleftrightarrow 12 \text{H}_2\text{O} + \text{Na}_3\text{PO}_4$	372	1740	2819
A376	$2 \text{Na}_3\text{PO}_4 \cdot 12 \text{H}_2\text{O} \longleftrightarrow 24 \text{H}_2\text{O} + \text{Na}_6\text{P}_2\text{O}_8$	372	1740	2819
A377	$\text{Na}_4\text{P}_2\text{O}_7 \cdot 10 \text{H}_2\text{O} \longleftrightarrow 10 \text{H}_2\text{O} + \text{Na}_4\text{P}_2\text{O}_7$	368	1212	-
A378	$\text{Na}_2\text{SO}_3 \cdot 7 \text{H}_2\text{O} \longleftrightarrow 7 \text{H}_2\text{O} + \text{Na}_2\text{SO}_3$	360	1447	-
A379	$\text{Na}_2\text{SO}_4 \cdot 7 \text{H}_2\text{O} \longleftrightarrow 7 \text{H}_2\text{O} + \text{Na}_2\text{SO}_4$	355	1403	-
A380	$\text{Na}_2\text{SO}_4 \cdot 10 \text{H}_2\text{O} \longleftrightarrow 3 \text{H}_2\text{O} + \text{Na}_2\text{SO}_4 \cdot 7 \text{H}_2\text{O}$	329	450	659
A381	$\text{Na}_2\text{SO}_4 \cdot 10 \text{H}_2\text{O} \longleftrightarrow 10 \text{H}_2\text{O} + \text{Na}_2\text{SO}_4$	361	1617	2368
A382	$\text{Na}_2\text{S}_2\text{O}_3 \cdot 5 \text{H}_2\text{O} \longleftrightarrow 5 \text{H}_2\text{O} + \text{Na}_2\text{S}_2\text{O}_3$	372	1087	1838
A383	$\text{Na}_2\text{SiO}_3 \cdot 5 \text{H}_2\text{O} \longleftrightarrow 5 \text{H}_2\text{O} + \text{Na}_2\text{SiO}_3$	389	1239	-
A384	$\text{Na}_2\text{SiO}_3 \cdot 6 \text{H}_2\text{O} \longleftrightarrow \text{H}_2\text{O} + \text{Na}_2\text{SiO}_3 \cdot 5 \text{H}_2\text{O}$	318	225	-
A385	$\text{Na}_2\text{SiO}_3 \cdot 6 \text{H}_2\text{O} \longleftrightarrow 6 \text{H}_2\text{O} + \text{Na}_2\text{SiO}_3$	386	1367	-
A386	$\text{Na}_2\text{SiO}_3 \cdot 8 \text{H}_2\text{O} \longleftrightarrow 2 \text{H}_2\text{O} + \text{Na}_2\text{SiO}_3 \cdot 6 \text{H}_2\text{O}$	323	404	-
A387	$\text{Na}_2\text{SiO}_3 \cdot 8 \text{H}_2\text{O} \longleftrightarrow 3 \text{H}_2\text{O} + \text{Na}_2\text{SiO}_3 \cdot 5 \text{H}_2\text{O}$	331	599	-
A388	$\text{Na}_2\text{SiO}_3 \cdot 8 \text{H}_2\text{O} \longleftrightarrow 8 \text{H}_2\text{O} + \text{Na}_2\text{SiO}_3$	382	1586	-
A389	$\text{Na}_2\text{SiO}_3 \cdot 9 \text{H}_2\text{O} \longleftrightarrow \text{H}_2\text{O} + \text{Na}_2\text{SiO}_3 \cdot 8 \text{H}_2\text{O}$	301	187	-
A390	$\text{Na}_2\text{SiO}_3 \cdot 9 \text{H}_2\text{O} \longleftrightarrow 3 \text{H}_2\text{O} + \text{Na}_2\text{SiO}_3 \cdot 6 \text{H}_2\text{O}$	320	565	-
A391	$\text{Na}_2\text{SiO}_3 \cdot 9 \text{H}_2\text{O} \longleftrightarrow 4 \text{H}_2\text{O} + \text{Na}_2\text{SiO}_3 \cdot 5 \text{H}_2\text{O}$	326	748	-
A392	$\text{Na}_2\text{SiO}_3 \cdot 9 \text{H}_2\text{O} \longleftrightarrow 9 \text{H}_2\text{O} + \text{Na}_2\text{SiO}_3$	371	1673	-

Continued on next page

Table 6.1: Reactions with H₂O as reactive gas – continued

ID	reaction system	T_{equ} °C	storage capacity kJ/kg	storage density MJ/m^3
A393	$\text{Na}_2\text{WO}_4 \cdot 2 \text{H}_2\text{O} \longleftrightarrow 2 \text{H}_2\text{O} + \text{Na}_2\text{WO}_4$	369	335	-
A394	$\text{NdCl}_3 \cdot 6 \text{H}_2\text{O} \longleftrightarrow 6 \text{H}_2\text{O} + \text{NdCl}_3$	409	1024	2355
A395	$2 \text{Nd}(\text{OH})_3 \longleftrightarrow 3 \text{H}_2\text{O} + \text{Nd}_2\text{O}_3$	1230	1219	-
A396	$\text{NdPO}_4 \cdot 2 \text{H}_2\text{O} \longleftrightarrow 2 \text{H}_2\text{O} + \text{NdPO}_4$	691	812	-
A397	$\text{Nd}_2(\text{SO}_4)_3 \cdot 8 \text{H}_2\text{O} \longleftrightarrow 8 \text{H}_2\text{O} + \text{Nd}_2(\text{SO}_4)_3$	593	920	-
A398	$\text{NiCl}_2 \cdot 2 \text{H}_2\text{O} \longleftrightarrow 2 \text{H}_2\text{O} + \text{NiCl}_2$	433	804	2075
A399	$\text{NiCl}_2 \cdot 4 \text{H}_2\text{O} \longleftrightarrow 2 \text{H}_2\text{O} + \text{NiCl}_2 \cdot 2 \text{H}_2\text{O}$	332	550	-
A400	$\text{NiCl}_2 \cdot 4 \text{H}_2\text{O} \longleftrightarrow 4 \text{H}_2\text{O} + \text{NiCl}_2$	395	1210	-
A401	$\text{NiCl}_2 \cdot 6 \text{H}_2\text{O} \longleftrightarrow 2 \text{H}_2\text{O} + \text{NiCl}_2 \cdot 4 \text{H}_2\text{O}$	331	432	-
A402	$\text{NiCl}_2 \cdot 6 \text{H}_2\text{O} \longleftrightarrow 4 \text{H}_2\text{O} + \text{NiCl}_2 \cdot 2 \text{H}_2\text{O}$	340	898	-
A403	$\text{NiCl}_2 \cdot 6 \text{H}_2\text{O} \longleftrightarrow 6 \text{H}_2\text{O} + \text{NiCl}_2$	387	1459	-
A404	$\text{Ni}(\text{IO}_3)_2 \cdot 2 \text{H}_2\text{O} \longleftrightarrow 2 \text{H}_2\text{O} + \text{Ni}(\text{IO}_3)_2$	323	238	-
A405	$\text{Ni}(\text{NO}_3)_2 \cdot 6 \text{H}_2\text{O} \longleftrightarrow 6 \text{H}_2\text{O} + \text{Ni}(\text{NO}_3)_2$	419	1200	2461
A406	$\text{Ni}(\text{OH})_2 \longleftrightarrow \text{H}_2\text{O} + \text{NiO}$	347	520	2130
A407	$\text{NiSO}_4 \cdot \text{H}_2\text{O} \longleftrightarrow \text{H}_2\text{O} + \text{NiSO}_4$	1210	812	-
A408	$\text{NiSO}_4 \cdot 4 \text{H}_2\text{O} \longleftrightarrow 3 \text{H}_2\text{O} + \text{NiSO}_4 \cdot \text{H}_2\text{O}$	387	764	-
A409	$\text{NiSO}_4 \cdot 4 \text{H}_2\text{O} \longleftrightarrow 4 \text{H}_2\text{O} + \text{NiSO}_4$	527	1382	-
A412	$\text{NiSO}_4 \cdot 6 \text{H}_2\text{O} \longleftrightarrow 6 \text{H}_2\text{O} + \text{NiSO}_4$	399	1365	2825
A413	$\text{NiSO}_4 \cdot 7 \text{H}_2\text{O} \longleftrightarrow \text{H}_2\text{O} + \text{NiSO}_4 \cdot 6 \text{H}_2\text{O}$	358	184	364
A415	$\text{NiSO}_4 \cdot 7 \text{H}_2\text{O} \longleftrightarrow 6 \text{H}_2\text{O} + \text{NiSO}_4 \cdot \text{H}_2\text{O}$	303	962	1904
A416	$\text{NiSO}_4 \cdot 7 \text{H}_2\text{O} \longleftrightarrow 7 \text{H}_2\text{O} + \text{NiSO}_4$	394	1461	2893
A419	$\text{Pb}(\text{OH})_2 \longleftrightarrow \text{H}_2\text{O} + \text{PbO}$	331	233	1766
A421	$\text{PrCl}_3 \cdot 6 \text{H}_2\text{O} \longleftrightarrow 6 \text{H}_2\text{O} + \text{PrCl}_3$	403	1041	-
A422	$\text{PrCl}_3 \cdot 7 \text{H}_2\text{O} \longleftrightarrow \text{H}_2\text{O} + \text{PrCl}_3 \cdot 6 \text{H}_2\text{O}$	367	147	-
A423	$\text{PrCl}_3 \cdot 7 \text{H}_2\text{O} \longleftrightarrow 7 \text{H}_2\text{O} + \text{PrCl}_3$	398	1138	-
A424	$2 \text{Pr}(\text{OH})_3 \longleftrightarrow 3 \text{H}_2\text{O} + \text{Pr}_2\text{O}_3$	659	789	-
A425	$\text{PtCl}_4 \cdot 5 \text{H}_2\text{O} \longleftrightarrow 5 \text{H}_2\text{O} + \text{PtCl}_4$	381	736	-
A427	$\text{PuCl}_3 \cdot 6 \text{H}_2\text{O} \longleftrightarrow 6 \text{H}_2\text{O} + \text{PuCl}_3$	409	792	-
A428	$2 \text{Pu}(\text{OH})_3 \longleftrightarrow 3 \text{H}_2\text{O} + \text{Pu}_2\text{O}_3$	362	335	-
A429	$\text{PuO}_2(\text{OH})_2 \cdot \text{H}_2\text{O} \longleftrightarrow \text{H}_2\text{O} + \text{PuO}_2(\text{OH})_2$	332	104	-
A430	$\text{RaBr}_2 \cdot 2 \text{H}_2\text{O} \longleftrightarrow 2 \text{H}_2\text{O} + \text{RaBr}_2$	415	311	-
A431	$\text{Ra}(\text{BrO}_3)_2 \cdot \text{H}_2\text{O} \longleftrightarrow \text{H}_2\text{O} + \text{Ra}(\text{BrO}_3)_2$	405	120	-
A432	$\text{RaCl}_2 \cdot 2 \text{H}_2\text{O} \longleftrightarrow 2 \text{H}_2\text{O} + \text{RaCl}_2$	314	282	-
A433	$\text{Ra}(\text{IO}_3)_2 \cdot \text{H}_2\text{O} \longleftrightarrow \text{H}_2\text{O} + \text{Ra}(\text{IO}_3)_2$	333	86	-
A434	$\text{Ra}(\text{OH})_2 \longleftrightarrow \text{H}_2\text{O} + \text{RaO}$	1326	712	-
A435	$\text{RbAl}(\text{SO}_4)_2 \cdot 12 \text{H}_2\text{O} \longleftrightarrow 12 \text{H}_2\text{O} + \text{RbAl}(\text{SO}_4)_2$	362	1330	-
A436	$\text{Rb}_2\text{CO}_3 \cdot \text{H}_2\text{O} \longleftrightarrow \text{H}_2\text{O} + \text{Rb}_2\text{CO}_3$	450	281	-
A437	$\text{RbF} \cdot \text{H}_2\text{O} \longleftrightarrow \text{H}_2\text{O} + \text{RbF}$	443	541	-

Continued on next page

Table 6.1: Reactions with H₂O as reactive gas – continued

ID	reaction system	T_{equ} °C	storage capacity kJ/kg	storage density MJ/m^3
A438	$2 \text{RbF} \cdot 3 \text{H}_2\text{O} \longleftrightarrow \text{H}_2\text{O} + 2 \text{RbF} \cdot \text{H}_2\text{O}$	308	181	-
A439	$2 \text{RbF} \cdot 3 \text{H}_2\text{O} \longleftrightarrow 3 \text{H}_2\text{O} + 2 \text{RbF}$	404	685	-
A441	$\text{RbOH} \cdot \text{H}_2\text{O} \longleftrightarrow \text{H}_2\text{O} + \text{RbOH}$	568	733	-
A442	$2 \text{RbOH} \cdot \text{H}_2\text{O} \longleftrightarrow 3 \text{H}_2\text{O} + \text{Rb}_2\text{O}$	995	1803	-
A443	$\text{RbOH} \cdot 2 \text{H}_2\text{O} \longleftrightarrow \text{H}_2\text{O} + \text{RbOH} \cdot \text{H}_2\text{O}$	356	453	-
A444	$\text{RbOH} \cdot 2 \text{H}_2\text{O} \longleftrightarrow 2 \text{H}_2\text{O} + \text{RbOH}$	501	1091	-
A445	$2 \text{RbOH} \cdot 2 \text{H}_2\text{O} \longleftrightarrow 5 \text{H}_2\text{O} + \text{Rb}_2\text{O}$	770	2021	-
A447	$\text{ScCl}_3 \cdot 6 \text{H}_2\text{O} \longleftrightarrow 6 \text{H}_2\text{O} + \text{ScCl}_3$	464	1647	-
A451	$\text{SmCl}_3 \cdot 6 \text{H}_2\text{O} \longleftrightarrow 6 \text{H}_2\text{O} + \text{SmCl}_3$	435	1071	2550
A452	$2 \text{Sm}(\text{OH})_3 \longleftrightarrow 3 \text{H}_2\text{O} + \text{Sm}_2\text{O}_3$	532	618	-
A453	$\text{SmPO}_4 \cdot 2 \text{H}_2\text{O} \longleftrightarrow 2 \text{H}_2\text{O} + \text{SmPO}_4$	558	824	-
A454	$\text{Sn}(\text{OH})_2 \longleftrightarrow \text{H}_2\text{O} + \text{SnO}$	408	253	-
A456	$\text{SrBr}_2 \cdot \text{H}_2\text{O} \longleftrightarrow \text{H}_2\text{O} + \text{SrBr}_2$	481	274	-
A457	$\text{SrBr}_2 \cdot 6 \text{H}_2\text{O} \longleftrightarrow 5 \text{H}_2\text{O} + \text{SrBr}_2 \cdot \text{H}_2\text{O}$	402	814	1945
A458	$\text{SrBr}_2 \cdot 6 \text{H}_2\text{O} \longleftrightarrow 6 \text{H}_2\text{O} + \text{SrBr}_2$	417	1018	2434
A459	$\text{Sr}(\text{BrO}_3)_2 \cdot \text{H}_2\text{O} \longleftrightarrow \text{H}_2\text{O} + \text{Sr}(\text{BrO}_3)_2$	516	384	1449
A460	$\text{SrCl}_2 \cdot \text{H}_2\text{O} \longleftrightarrow \text{H}_2\text{O} + \text{SrCl}_2$	333	346	-
A461	$\text{SrCl}_2 \cdot 2 \text{H}_2\text{O} \longleftrightarrow \text{H}_2\text{O} + \text{SrCl}_2 \cdot \text{H}_2\text{O}$	462	305	-
A462	$\text{SrCl}_2 \cdot 2 \text{H}_2\text{O} \longleftrightarrow 2 \text{H}_2\text{O} + \text{SrCl}_2$	441	619	-
A463	$\text{SrCl}_2 \cdot 6 \text{H}_2\text{O} \longleftrightarrow 4 \text{H}_2\text{O} + \text{SrCl}_2 \cdot 2 \text{H}_2\text{O}$	371	820	1582
A464	$\text{SrCl}_2 \cdot 6 \text{H}_2\text{O} \longleftrightarrow 5 \text{H}_2\text{O} + \text{SrCl}_2 \cdot \text{H}_2\text{O}$	403	1042	2012
A465	$\text{SrCl}_2 \cdot 6 \text{H}_2\text{O} \longleftrightarrow 6 \text{H}_2\text{O} + \text{SrCl}_2$	391	1271	2454
A466	$\text{Sr}(\text{IO}_3)_2 \cdot \text{H}_2\text{O} \longleftrightarrow \text{H}_2\text{O} + \text{Sr}(\text{IO}_3)_2$	333	108	-
A467	$\text{Sr}(\text{IO}_3)_2 \cdot 6 \text{H}_2\text{O} \longleftrightarrow 5 \text{H}_2\text{O} + \text{Sr}(\text{IO}_3)_2 \cdot \text{H}_2\text{O}$	333	496	-
A468	$\text{Sr}(\text{IO}_3)_2 \cdot 6 \text{H}_2\text{O} \longleftrightarrow 6 \text{H}_2\text{O} + \text{Sr}(\text{IO}_3)_2$	349	586	-
A469	$\text{Sr}(\text{NO}_3)_2 \cdot 4 \text{H}_2\text{O} \longleftrightarrow 4 \text{H}_2\text{O} + \text{Sr}(\text{NO}_3)_2$	351	723	1591
A470	$\text{Sr}(\text{OH})_2 \longleftrightarrow \text{H}_2\text{O} + \text{SrO}$	1020	1110	4025
A471	$\text{SrTeO}_3 \cdot \text{H}_2\text{O} \longleftrightarrow \text{H}_2\text{O} + \text{SrTeO}_3$	359	228	-
A472	$\text{TbCl}_3 \cdot 6 \text{H}_2\text{O} \longleftrightarrow 6 \text{H}_2\text{O} + \text{TbCl}_3$	460	1123	-
A474	$\text{TbPO}_4 \cdot 2 \text{H}_2\text{O} \longleftrightarrow 2 \text{H}_2\text{O} + \text{TbPO}_4$	516	713	-
A475	$\text{Tc}_2\text{O}_7 \cdot \text{H}_2\text{O} \longleftrightarrow \text{H}_2\text{O} + \text{Tc}_2\text{O}_7$	400	141	-
A476	$\text{Th}(\text{NO}_3)_4 \cdot 4 \text{H}_2\text{O} \longleftrightarrow 4 \text{H}_2\text{O} + \text{Th}(\text{NO}_3)_4$	459	553	-
A477	$\text{Th}(\text{NO}_3)_4 \cdot 5 \text{H}_2\text{O} \longleftrightarrow \text{H}_2\text{O} + \text{Th}(\text{NO}_3)_4 \cdot 4 \text{H}_2\text{O}$	304	83	-
A478	$\text{Th}(\text{NO}_3)_4 \cdot 5 \text{H}_2\text{O} \longleftrightarrow 5 \text{H}_2\text{O} + \text{Th}(\text{NO}_3)_4$	446	619	-
A480	$2 \text{TlOH} \longleftrightarrow \text{H}_2\text{O} + \text{Tl}_2\text{O}$	410	151	1125
A481	$2 \text{Tm}(\text{OH})_3 \longleftrightarrow 3 \text{H}_2\text{O} + \text{Tm}_2\text{O}_3$	511	540	-
A482	$\text{TmPO}_4 \cdot 2 \text{H}_2\text{O} \longleftrightarrow 2 \text{H}_2\text{O} + \text{TmPO}_4$	516	689	-
A483	$\text{UO}_2\text{Br}_2 \cdot \text{H}_2\text{O} \longleftrightarrow \text{H}_2\text{O} + \text{UO}_2\text{Br}_2$	482	171	-

Continued on next page

Table 6.1: Reactions with H₂O as reactive gas – continued

ID	reaction system	T_{equ} °C	storage capacity kJ/kg	storage density MJ/m^3
A484	$\text{UO}_2\text{Br}_2 \cdot 3 \text{H}_2\text{O} \longleftrightarrow 2 \text{H}_2\text{O} + \text{UO}_2\text{Br}_2 \cdot \text{H}_2\text{O}$	354	245	-
A485	$\text{UO}_2\text{Br}_2 \cdot 3 \text{H}_2\text{O} \longleftrightarrow 3 \text{H}_2\text{O} + \text{UO}_2\text{Br}_2$	438	403	-
A486	$\text{UO}_2\text{Cl}_2 \cdot \text{H}_2\text{O} \longleftrightarrow \text{H}_2\text{O} + \text{UO}_2\text{Cl}_2$	467	208	-
A487	$\text{UO}_2\text{Cl}_2 \cdot 3 \text{H}_2\text{O} \longleftrightarrow 2 \text{H}_2\text{O} + \text{UO}_2\text{Cl}_2 \cdot \text{H}_2\text{O}$	355	307	-
A488	$\text{UO}_2\text{Cl}_2 \cdot 3 \text{H}_2\text{O} \longleftrightarrow 3 \text{H}_2\text{O} + \text{UO}_2\text{Cl}_2$	428	496	-
A489	$\text{UOF}_2 \cdot \text{H}_2\text{O} \longleftrightarrow \text{H}_2\text{O} + \text{UOF}_2$	371	179	-
A490	$\text{UO}_2\text{F}_2 \cdot 3 \text{H}_2\text{O} \longleftrightarrow 3 \text{H}_2\text{O} + \text{UO}_2\text{F}_2$	357	429	-
A492	$\text{UO}_2\text{FOH} \cdot 3 \text{H}_2\text{O} \longleftrightarrow \text{H}_2\text{O} + \text{UO}_2\text{OHF} \cdot 2 \text{H}_2\text{O}$	423	313	-
A493	$\text{UO}_2\text{FOH} \cdot 3 \text{H}_2\text{O} \longleftrightarrow 2 \text{H}_2\text{O} + \text{UO}_2\text{OHF} \cdot \text{H}_2\text{O}$	387	426	-
A494	$\text{UO}_3 \cdot \text{H}_2\text{O} \longleftrightarrow \text{H}_2\text{O} + \text{UO}_3$	480	237	1669
A495	$\text{UO}_3 \cdot 2 \text{H}_2\text{O} \longleftrightarrow \text{H}_2\text{O} + \text{UO}_3 \cdot \text{H}_2\text{O}$	351	147	-
A496	$\text{UO}_3 \cdot 2 \text{H}_2\text{O} \longleftrightarrow 2 \text{H}_2\text{O} + \text{UO}_3$	419	370	-
A497	$2 \text{UO}_2\text{HPO}_4 \cdot 4 \text{H}_2\text{O} \longleftrightarrow 8 \text{H}_2\text{O} + \text{H}_2(\text{UO}_2)_2(\text{PO}_4)_2$	443	626	-
A498	$2 \text{UO}_2\text{HPO}_4 \cdot 4 \text{H}_2\text{O} \longleftrightarrow 9 \text{H}_2\text{O} + (\text{UO}_2)_2\text{P}_2\text{O}_7$	400	606	-
A499	$\text{UO}_2(\text{NO}_3)_2 \cdot \text{H}_2\text{O} \longleftrightarrow \text{H}_2\text{O} + \text{UO}_2(\text{NO}_3)_2$	445	173	-
A500	$\text{UO}_2(\text{NO}_3)_2 \cdot 2 \text{H}_2\text{O} \longleftrightarrow \text{H}_2\text{O} + \text{UO}_2(\text{NO}_3)_2 \cdot \text{H}_2\text{O}$	360	169	-
A501	$\text{UO}_2(\text{NO}_3)_2 \cdot 2 \text{H}_2\text{O} \longleftrightarrow 2 \text{H}_2\text{O} + \text{UO}_2(\text{NO}_3)_2$	498	335	-
A502	$\text{UO}_2(\text{NO}_3)_2 \cdot 3 \text{H}_2\text{O} \longleftrightarrow \text{H}_2\text{O} + \text{UO}_2(\text{NO}_3)_2 \cdot 2 \text{H}_2\text{O}$	400	134	-
A503	$\text{UO}_2(\text{NO}_3)_2 \cdot 3 \text{H}_2\text{O} \longleftrightarrow 2 \text{H}_2\text{O} + \text{UO}_2(\text{NO}_3)_2 \cdot \text{H}_2\text{O}$	366	296	-
A504	$\text{UO}_2(\text{NO}_3)_2 \cdot 3 \text{H}_2\text{O} \longleftrightarrow 3 \text{H}_2\text{O} + \text{UO}_2(\text{NO}_3)_2$	466	455	-
A505	$\text{UO}_2(\text{NO}_3)_2 \cdot 6 \text{H}_2\text{O} \longleftrightarrow 3 \text{H}_2\text{O} + \text{UO}_2(\text{NO}_3)_2 \cdot 3 \text{H}_2\text{O}$	334	322	904
A506	$\text{UO}_2(\text{NO}_3)_2 \cdot 6 \text{H}_2\text{O} \longleftrightarrow 4 \text{H}_2\text{O} + \text{UO}_2(\text{NO}_3)_2 \cdot 2 \text{H}_2\text{O}$	385	441	1240
A507	$\text{UO}_2(\text{NO}_3)_2 \cdot 6 \text{H}_2\text{O} \longleftrightarrow 5 \text{H}_2\text{O} + \text{UO}_2(\text{NO}_3)_2 \cdot \text{H}_2\text{O}$	362	586	1647
A508	$\text{UO}_2(\text{NO}_3)_2 \cdot 6 \text{H}_2\text{O} \longleftrightarrow 6 \text{H}_2\text{O} + \text{UO}_2(\text{NO}_3)_2$	423	728	2046
A509	$\text{UO}_2(\text{OH})_2 \longleftrightarrow \text{H}_2\text{O} + \text{UO}_3$	470	224	-
A511	$\text{UO}_2(\text{OH})_2 \cdot \text{H}_2\text{O} \longleftrightarrow \text{H}_2\text{O} + \text{UO}_2(\text{OH})_2$	338	156	-
A512	$\text{UO}_2(\text{OH})_2 \cdot \text{H}_2\text{O} \longleftrightarrow 2 \text{H}_2\text{O} + \text{UO}_3$	402	368	-
A513	$(\text{UO}_2)_3(\text{PO}_4)_2 \cdot 4 \text{H}_2\text{O} \longleftrightarrow 4 \text{H}_2\text{O} + (\text{UO}_2)_3(\text{PO}_4)_2$	456	262	-

Continued on next page

Table 6.1: Reactions with H₂O as reactive gas – continued

ID	reaction system	T_{equ} °C	storage capacity kJ/kg	storage density MJ/m^3
A514	$(\text{UO}_2)_3(\text{PO}_4)_2 \cdot 6 \text{H}_2\text{O} \longleftrightarrow 2 \text{H}_2\text{O} +$ $(\text{UO}_2)_3(\text{PO}_4)_2 \cdot 4 \text{H}_2\text{O}$	317	95	-
A515	$(\text{UO}_2)_3(\text{PO}_4)_2 \cdot 6 \text{H}_2\text{O} \longleftrightarrow 6 \text{H}_2\text{O} +$ $(\text{UO}_2)_3(\text{PO}_4)_2$	426	348	-
A517	$\text{UO}_2\text{SO}_4 \cdot 3 \text{H}_2\text{O} \longleftrightarrow 2 \text{H}_2\text{O} + \text{UO}_2\text{SO}_4 \cdot \text{H}_2\text{O}$	399	331	1085
A518	$\text{UO}_2\text{SO}_4 \cdot 3 \text{H}_2\text{O} \longleftrightarrow 3 \text{H}_2\text{O} + \text{UO}_2\text{SO}_4$	407	431	1412
A519	$\text{U}(\text{SO}_4)_2 \cdot 4 \text{H}_2\text{O} \longleftrightarrow 4 \text{H}_2\text{O} + \text{U}(\text{SO}_4)_2$	355	411	-
A520	$\text{U}(\text{SO}_4)_2 \cdot 8 \text{H}_2\text{O} \longleftrightarrow 4 \text{H}_2\text{O} +$ $\text{U}(\text{SO}_4)_2 \cdot 4 \text{H}_2\text{O}$	335	369	-
A521	$\text{U}(\text{SO}_4)_2 \cdot 8 \text{H}_2\text{O} \longleftrightarrow 8 \text{H}_2\text{O} + \text{U}(\text{SO}_4)_2$	361	729	-
A522	$\text{V}_2\text{O}_5 \cdot \text{H}_2\text{O} \longleftrightarrow \text{H}_2\text{O} + \text{V}_2\text{O}_5$	349	261	-
A523	$\text{VOSO}_4 \cdot \text{H}_2\text{O} \longleftrightarrow \text{H}_2\text{O} + \text{VOSO}_4$	971	744	-
A524	$\text{VOSO}_4 \cdot 3 \text{H}_2\text{O} \longleftrightarrow 2 \text{H}_2\text{O} + \text{VOSO}_4 \cdot \text{H}_2\text{O}$	433	592	-
A525	$\text{VOSO}_4 \cdot 3 \text{H}_2\text{O} \longleftrightarrow 3 \text{H}_2\text{O} + \text{VOSO}_4$	600	1213	-
A526	$\text{VOSO}_4 \cdot 6 \text{H}_2\text{O} \longleftrightarrow 3 \text{H}_2\text{O} + \text{VOSO}_4 \cdot 3 \text{H}_2\text{O}$	371	612	-
A527	$\text{VOSO}_4 \cdot 6 \text{H}_2\text{O} \longleftrightarrow 5 \text{H}_2\text{O} + \text{VOSO}_4 \cdot \text{H}_2\text{O}$	396	1086	-
A528	$\text{VOSO}_4 \cdot 6 \text{H}_2\text{O} \longleftrightarrow 6 \text{H}_2\text{O} + \text{VOSO}_4$	483	1583	-
A529	$\text{YCl}_3 \cdot 6 \text{H}_2\text{O} \longleftrightarrow 6 \text{H}_2\text{O} + \text{YCl}_3$	479	1457	-
A530	$2 \text{Y}(\text{OH})_3 \longleftrightarrow 3 \text{H}_2\text{O} + \text{Y}_2\text{O}_3$	412	695	-
A531	$\text{YPO}_4 \cdot 2 \text{H}_2\text{O} \longleftrightarrow 2 \text{H}_2\text{O} + \text{YPO}_4$	338	461	-
A532	$\text{YbCl}_3 \cdot 6 \text{H}_2\text{O} \longleftrightarrow 6 \text{H}_2\text{O} + \text{YbCl}_3$	493	1120	2883
A533	$2 \text{Yb}(\text{OH})_3 \longleftrightarrow 3 \text{H}_2\text{O} + \text{Yb}_2\text{O}_3$	541	570	-
A534	$\text{YbPO}_4 \cdot 2 \text{H}_2\text{O} \longleftrightarrow 2 \text{H}_2\text{O} + \text{YbPO}_4$	556	749	-
A535	$\text{ZnBr}_2 \cdot 2 \text{H}_2\text{O} \longleftrightarrow 2 \text{H}_2\text{O} + \text{ZnBr}_2$	399	427	-
A536	$\text{ZnF}_2 \cdot 4 \text{H}_2\text{O} \longleftrightarrow 4 \text{H}_2\text{O} + \text{ZnF}_2$	366	1270	-
A537	$\text{Zn}(\text{NO}_3)_2 \cdot 2 \text{H}_2\text{O} \longleftrightarrow 2 \text{H}_2\text{O} + \text{Zn}(\text{NO}_3)_2$	384	634	-
A538	$\text{Zn}(\text{NO}_3)_2 \cdot 4 \text{H}_2\text{O} \longleftrightarrow 2 \text{H}_2\text{O} +$ $\text{Zn}(\text{NO}_3)_2 \cdot 2 \text{H}_2\text{O}$	360	402	-
A539	$\text{Zn}(\text{NO}_3)_2 \cdot 4 \text{H}_2\text{O} \longleftrightarrow 4 \text{H}_2\text{O} + \text{Zn}(\text{NO}_3)_2$	390	949	-
A540	$\text{Zn}(\text{NO}_3)_2 \cdot 6 \text{H}_2\text{O} \longleftrightarrow 2 \text{H}_2\text{O} +$ $\text{Zn}(\text{NO}_3)_2 \cdot 4 \text{H}_2\text{O}$	322	417	863
A541	$\text{Zn}(\text{NO}_3)_2 \cdot 6 \text{H}_2\text{O} \longleftrightarrow 4 \text{H}_2\text{O} +$ $\text{Zn}(\text{NO}_3)_2 \cdot 2 \text{H}_2\text{O}$	355	771	1594
A542	$\text{Zn}(\text{NO}_3)_2 \cdot 6 \text{H}_2\text{O} \longleftrightarrow 6 \text{H}_2\text{O} + \text{Zn}(\text{NO}_3)_2$	378	1252	2587
A543	$\text{Zn}(\text{OH})_2 \longleftrightarrow \text{H}_2\text{O} + \text{ZnO}$	329	499	1523
A544	$\text{ZnSO}_4 \cdot \text{H}_2\text{O} \longleftrightarrow \text{H}_2\text{O} + \text{ZnSO}_4$	520	444	1419
A545	$\text{ZnSO}_4 \cdot 2 \text{H}_2\text{O} \longleftrightarrow \text{H}_2\text{O} + \text{ZnSO}_4 \cdot \text{H}_2\text{O}$	372	267	-
A546	$\text{ZnSO}_4 \cdot 2 \text{H}_2\text{O} \longleftrightarrow 2 \text{H}_2\text{O} + \text{ZnSO}_4$	449	670	-
A547	$\text{ZnSO}_4 \cdot 6 \text{H}_2\text{O} \longleftrightarrow 4 \text{H}_2\text{O} + \text{ZnSO}_4 \cdot 2 \text{H}_2\text{O}$	365	800	1658

Continued on next page

Table 6.1: Reactions with H₂O as reactive gas – continued

ID	reaction system	T_{equ} °C	storage capacity kJ/kg	storage density MJ/m^3
A548	$\text{ZnSO}_4 \cdot 6 \text{H}_2\text{O} \longleftrightarrow 5 \text{H}_2\text{O} + \text{ZnSO}_4 \cdot \text{H}_2\text{O}$	366	996	2063
A549	$\text{ZnSO}_4 \cdot 6 \text{H}_2\text{O} \longleftrightarrow 6 \text{H}_2\text{O} + \text{ZnSO}_4$	393	1291	2675
A550	$\text{ZnSO}_4 \cdot 7 \text{H}_2\text{O} \longleftrightarrow \text{H}_2\text{O} + \text{ZnSO}_4 \cdot 6 \text{H}_2\text{O}$	369	201	393
A551	$\text{ZnSO}_4 \cdot 7 \text{H}_2\text{O} \longleftrightarrow 5 \text{H}_2\text{O} + \text{ZnSO}_4 \cdot 2 \text{H}_2\text{O}$	365	951	1861
A552	$\text{ZnSO}_4 \cdot 7 \text{H}_2\text{O} \longleftrightarrow 6 \text{H}_2\text{O} + \text{ZnSO}_4 \cdot \text{H}_2\text{O}$	367	1134	2219
A553	$\text{ZnSO}_4 \cdot 7 \text{H}_2\text{O} \longleftrightarrow 7 \text{H}_2\text{O} + \text{ZnSO}_4$	389	1411	2761
A554	$\text{Zr}(\text{OH})_4 \longleftrightarrow \text{H}_2\text{O} + \text{ZrO}(\text{OH})_2$	370	409	-
A555	$\text{Zr}(\text{OH})_4 \longleftrightarrow 2 \text{H}_2\text{O} + \text{ZrO}_2$	443	854	-
A556	$\text{ZrO}(\text{OH})_2 \longleftrightarrow \text{H}_2\text{O} + \text{ZrO}_2$	458	502	-
A558	$\text{BaC}_2\text{O}_4 \cdot 3.5 \text{H}_2\text{O} \longleftrightarrow 3 \text{H}_2\text{O} + \text{BaC}_2\text{O}_4 \cdot 0.5 \text{H}_2\text{O}$	338	566	-
A559	$2 \text{BaC}_2\text{O}_4 \cdot 3.5 \text{H}_2\text{O} \longleftrightarrow 3 \text{H}_2\text{O} + 2 \text{BaC}_2\text{O}_4 \cdot 2 \text{H}_2\text{O}$	328	271	-
A560	$25 \text{CaO} \cdot 6 \text{SiO}_2 \cdot 5.5 \text{H}_2\text{O} \longleftrightarrow 5 \text{H}_2\text{O} + 25 \text{CaO} \cdot 6 \text{SiO}_2 \cdot 3 \text{H}_2\text{O}$	392	198	-
A561	$5 \text{CaO} \cdot 6 \text{SiO}_2 \cdot 10.5 \text{H}_2\text{O} \longleftrightarrow 5 \text{H}_2\text{O} + 5 \text{CaO} \cdot 6 \text{SiO}_2 \cdot 5.5 \text{H}_2\text{O}$	380	342	-
A562	$25 \text{CaO} \cdot 6 \text{SiO}_2 \cdot 10.5 \text{H}_2\text{O} \longleftrightarrow 15 \text{H}_2\text{O} + 25 \text{CaO} \cdot 6 \text{SiO}_2 \cdot 3 \text{H}_2\text{O}$	384	518	-
A563	$2 \text{CaSO}_3 \cdot 0.5 \text{H}_2\text{O} \longleftrightarrow \text{H}_2\text{O} + 2 \text{CaSO}_3$	423	243	-
A565	$2 \text{CdCl}_2 \cdot 2.5 \text{H}_2\text{O} \longleftrightarrow 3 \text{H}_2\text{O} + 2 \text{CdCl}_2 \cdot \text{H}_2\text{O}$	360	351	1167
A566	$2 \text{CdCl}_2 \cdot 2.5 \text{H}_2\text{O} \longleftrightarrow 5 \text{H}_2\text{O} + 2 \text{CdCl}_2$	372	584	1943
A567	$2 \text{Cs}_2\text{CO}_3 \cdot 3.5 \text{H}_2\text{O} \longleftrightarrow 7 \text{H}_2\text{O} + 2 \text{Cs}_2\text{CO}_3$	419	581	-
A568	$2 \text{H}_2\text{O} \longleftrightarrow \text{H}_2\text{O} + \text{H}_2\text{O}$	373	1221	1120
A569	$3 \text{H}_2\text{O} \longleftrightarrow \text{H}_2\text{O} + 2 \text{H}_2\text{O}$	373	814	747
A570	$3 \text{H}_2\text{O} \longleftrightarrow 2 \text{H}_2\text{O} + \text{H}_2\text{O}$	373	1628	1493
A571	$4 \text{H}_2\text{O} \longleftrightarrow \text{H}_2\text{O} + 3 \text{H}_2\text{O}$	373	611	560
A572	$4 \text{H}_2\text{O} \longleftrightarrow 3 \text{H}_2\text{O} + \text{H}_2\text{O}$	373	1832	1680
A573	$5 \text{H}_2\text{O} \longleftrightarrow \text{H}_2\text{O} + 4 \text{H}_2\text{O}$	373	489	448
A574	$5 \text{H}_2\text{O} \longleftrightarrow 2 \text{H}_2\text{O} + 3 \text{H}_2\text{O}$	373	977	896
A575	$5 \text{H}_2\text{O} \longleftrightarrow 3 \text{H}_2\text{O} + 2 \text{H}_2\text{O}$	373	1466	1344
A576	$5 \text{H}_2\text{O} \longleftrightarrow 4 \text{H}_2\text{O} + \text{H}_2\text{O}$	373	1954	1792
A577	$6 \text{H}_2\text{O} \longleftrightarrow \text{H}_2\text{O} + 5 \text{H}_2\text{O}$	373	407	373
A578	$6 \text{H}_2\text{O} \longleftrightarrow 5 \text{H}_2\text{O} + \text{H}_2\text{O}$	373	2036	1867
A579	$2 \text{H}_3\text{PO}_4 \cdot 0.5 \text{H}_2\text{O} \longleftrightarrow \text{H}_2\text{O} + 2 \text{H}_3\text{PO}_4$	377	293	-
A580	$2 \text{H}_3\text{PO}_4 \cdot 0.5 \text{H}_2\text{O} \longleftrightarrow 4 \text{H}_2\text{O} + \text{P}_2\text{O}_5$	634	1824	-
A581	$4 \text{H}_3\text{PO}_4 \cdot 0.5 \text{H}_2\text{O} \longleftrightarrow 8 \text{H}_2\text{O} + \text{P}_4\text{O}_{10}$	635	1824	-
A582	$2 \text{H}_2\text{SO}_4 \cdot 6.5 \text{H}_2\text{O} \longleftrightarrow 5 \text{H}_2\text{O} + 2 \text{H}_2\text{SO}_4 \cdot 4 \text{H}_2\text{O}$	398	546	-

Continued on next page

Table 6.1: Reactions with H₂O as reactive gas – continued

ID	reaction system	T_{equ} °C	storage capacity kJ/kg	storage density MJ/m^3
A583	$2 \text{H}_2\text{SO}_4 \cdot 6.5 \text{H}_2\text{O} \longleftrightarrow 7 \text{H}_2\text{O} + 2 \text{H}_2\text{SO}_4 \cdot 3 \text{H}_2\text{O}$	403	774	-
A584	$2 \text{H}_2\text{SO}_4 \cdot 6.5 \text{H}_2\text{O} \longleftrightarrow 9 \text{H}_2\text{O} + 2 \text{H}_2\text{SO}_4 \cdot 2 \text{H}_2\text{O}$	410	1013	-
A585	$2 \text{H}_2\text{SO}_4 \cdot 6.5 \text{H}_2\text{O} \longleftrightarrow 11 \text{H}_2\text{O} + 2 \text{H}_2\text{SO}_4 \cdot \text{H}_2\text{O}$	422	1281	-
A586	$2 \text{H}_2\text{SO}_4 \cdot 6.5 \text{H}_2\text{O} \longleftrightarrow 13 \text{H}_2\text{O} + 2 \text{H}_2\text{SO}_4$	444	1615	-
A587	$2 \text{K}_2\text{CO}_3 \cdot 0.5 \text{H}_2\text{O} \longleftrightarrow \text{H}_2\text{O} + 2 \text{K}_2\text{CO}_3$	444	238	-
A588	$\text{K}_2\text{CO}_3 \cdot 1.5 \text{H}_2\text{O} \longleftrightarrow \text{H}_2\text{O} + \text{K}_2\text{CO}_3 \cdot 0.5 \text{H}_2\text{O}$	346	385	-
A589	$2 \text{K}_2\text{CO}_3 \cdot 1.5 \text{H}_2\text{O} \longleftrightarrow 3 \text{H}_2\text{O} + 2 \text{K}_2\text{CO}_3$	421	597	-
A590	$2 \text{NaCN} \cdot 0.5 \text{H}_2\text{O} \longleftrightarrow \text{H}_2\text{O} + 2 \text{NaCN}$	317	420	-
A591	$2 \text{RaI}_2 \cdot 0.5 \text{H}_2\text{O} \longleftrightarrow \text{H}_2\text{O} + 2 \text{RaI}_2$	420	72	-
A592	$2 \text{Rb}_2\text{CO}_3 \cdot 1.5 \text{H}_2\text{O} \longleftrightarrow \text{H}_2\text{O} + 2 \text{Rb}_2\text{CO}_3 \cdot \text{H}_2\text{O}$	338	135	-
A593	$2 \text{Rb}_2\text{CO}_3 \cdot 1.5 \text{H}_2\text{O} \longleftrightarrow 3 \text{H}_2\text{O} + 2 \text{Rb}_2\text{CO}_3$	453	406	-
A594	$\text{Rb}_2\text{CO}_3 \cdot 3.5 \text{H}_2\text{O} \longleftrightarrow 2 \text{H}_2\text{O} + \text{Rb}_2\text{CO}_3 \cdot 1.5 \text{H}_2\text{O}$	317	349	-
A595	$2 \text{Rb}_2\text{CO}_3 \cdot 3.5 \text{H}_2\text{O} \longleftrightarrow 5 \text{H}_2\text{O} + 2 \text{Rb}_2\text{CO}_3 \cdot \text{H}_2\text{O}$	332	467	-
A596	$2 \text{Rb}_2\text{CO}_3 \cdot 3.5 \text{H}_2\text{O} \longleftrightarrow 7 \text{H}_2\text{O} + 2 \text{Rb}_2\text{CO}_3$	386	705	-
A597	$2 \text{ThF}_4 \cdot 2.5 \text{H}_2\text{O} \longleftrightarrow 5 \text{H}_2\text{O} + 2 \text{ThF}_4$	387	429	-
A599	$2 \text{UOFOH} \cdot 0.5 \text{H}_2\text{O} \longleftrightarrow \text{H}_2\text{O} + 2 \text{UOFOH}$	331	95	-
A600	$2 \text{UO}_2\text{SO}_4 \cdot 2.5 \text{H}_2\text{O} \longleftrightarrow 3 \text{H}_2\text{O} + 2 \text{UO}_2\text{SO}_4 \cdot \text{H}_2\text{O}$	412	281	-
A601	$2 \text{UO}_2\text{SO}_4 \cdot 2.5 \text{H}_2\text{O} \longleftrightarrow 5 \text{H}_2\text{O} + 2 \text{UO}_2\text{SO}_4$	403	383	-
A602	$\text{UO}_2\text{SO}_4 \cdot 3.5 \text{H}_2\text{O} \longleftrightarrow \text{H}_2\text{O} + \text{UO}_2\text{SO}_4 \cdot 2.5 \text{H}_2\text{O}$	319	123	-
A603	$2 \text{UO}_2\text{SO}_4 \cdot 3.5 \text{H}_2\text{O} \longleftrightarrow \text{H}_2\text{O} + 2 \text{UO}_2\text{SO}_4 \cdot 3 \text{H}_2\text{O}$	343	68	-
A604	$2 \text{UO}_2\text{SO}_4 \cdot 3.5 \text{H}_2\text{O} \longleftrightarrow 5 \text{H}_2\text{O} + 2 \text{UO}_2\text{SO}_4 \cdot \text{H}_2\text{O}$	392	392	-
A605	$2 \text{UO}_2\text{SO}_4 \cdot 3.5 \text{H}_2\text{O} \longleftrightarrow 7 \text{H}_2\text{O} + 2 \text{UO}_2\text{SO}_4$	390	490	-

Table 6.2: Reactions with CO₂ as reactive gas

ID	reaction system	T_{equ} °C	storage capacity kJ/kg	storage density MJ/m^3
B1	$\text{AgCO}_3 \longleftrightarrow \text{CO}_2 + \text{AgO}$	584	602	-
B2	$2 \text{AgCO}_3 \longleftrightarrow 2 \text{CO}_2 + \text{Ag}_2\text{O}_2$	632	599	-
B3	$\text{Ag}_2\text{CO}_3 \longleftrightarrow \text{CO}_2 + \text{Ag}_2\text{O}$	523	309	1879
B5	$\text{Am}_2(\text{CO}_3)_3 \longleftrightarrow 3 \text{CO}_2 + \text{Am}_2\text{O}_3$	716	526	-
B6	$\text{BaCO}_3 \longleftrightarrow \text{CO}_2 + \text{BaO}$	1831	1381	6117
B8	$\text{CaCO}_3 \longleftrightarrow \text{CO}_2 + \text{CaO}$	1159	1780	4824
B10	$\text{CaMg}(\text{CO}_3)_2 \longleftrightarrow 2 \text{CO}_2 + \text{CaO} \cdot \text{MgO}$	879	1602	4601
B11	$\text{Ca}_3\text{Si}_2\text{O}_7 \cdot 2 \text{CaCO}_3 \longleftrightarrow \text{CO}_2 + 2 \text{Ca}_2\text{SiO}_4 \cdot \text{CaCO}_3$	706	232	-
B12	$\text{CdCO}_3 \longleftrightarrow \text{CO}_2 + \text{CdO}$	567	576	2454
B13	$\text{CoCO}_3 \longleftrightarrow \text{CO}_2 + \text{CoO}$	455	686	2880
B15	$\text{CsHCO}_3 \longleftrightarrow \text{CO}_2 + \text{CsOH}$	710	806	-
B17	$\text{Eu}_2(\text{CO}_3)_3 \cdot 3 \text{H}_2\text{O} \longleftrightarrow 3 \text{CO}_2 + 2 \text{Eu}(\text{OH})_3$	338	273	-
B18	$\text{FeCO}_3 \longleftrightarrow \text{CO}_2 + \text{FeO}$	447	689	2686
B19	$\text{Fr}_2\text{CO}_3 \longleftrightarrow \text{CO}_2 + \text{Fr}_2\text{O}$	1234	802	-
B20	$\text{HgCO}_3 \longleftrightarrow \text{CO}_2 + \text{HgO}$	592	264	-
B21	$\text{Hg}_2\text{CO}_3 \longleftrightarrow \text{CO}_2 + \text{Hg}_2\text{O}$	421	149	-
B23	$\text{K}_2\text{C}_2\text{O}_4 \longleftrightarrow 2 \text{CO}_2 + 2 \text{K}$	1138	3339	-
B24	$\text{KHCO}_3 \longleftrightarrow \text{CO}_2 + \text{KOH}$	783	1466	3181
B25	$\text{Li}_2\text{CO}_3 \longleftrightarrow \text{CO}_2 + \text{Li}_2\text{O}$	1879	3040	6415
B26	$\text{MgCO}_3 \longleftrightarrow \text{CO}_2 + \text{MgO}$	577	1197	3650
B27	$\text{Mg}_5(\text{OH})_2(\text{CO}_3)_4 \cdot 4 \text{H}_2\text{O} \longleftrightarrow 4 \text{CO}_2 + 5 \text{Mg}(\text{OH})_2$	507	679	-
B28	$\text{MnCO}_3 \longleftrightarrow \text{CO}_2 + \text{MnO}$	617	894	3308
B29	$\text{NH}_4\text{HCO}_3 \longleftrightarrow \text{CO}_2 + \text{NH}_4\text{OH}$	457	1675	2647
B31	$\text{Na}_2\text{C}_2\text{O}_4 \longleftrightarrow 2 \text{CO}_2 + 2 \text{Na}$	951	3940	9220
B32	$\text{Na}_2\text{CO}_3 \cdot \text{H}_2\text{O} \longleftrightarrow \text{CO}_2 + 2 \text{NaOH}$	856	1507	3406
B33	$\text{NaHCO}_3 \longleftrightarrow \text{CO}_2 + \text{NaOH}$	741	1565	3380
B34	$\text{NiCO}_3 \longleftrightarrow \text{CO}_2 + \text{NiO}$	381	532	2333
B35	$\text{PbCO}_3 \longleftrightarrow \text{CO}_2 + \text{PbO}$	584	328	2162
B36	$2 \text{PbCO}_3 \longleftrightarrow \text{CO}_2 + \text{PbO} \cdot \text{PbCO}_3$	576	155	1026
B37	$3 \text{PbCO}_3 \longleftrightarrow 2 \text{CO}_2 + \cdot 2 \text{PbO} \cdot \text{PbCO}_3$	465	210	1384
B39	$\text{PbO} \cdot \text{PbCO}_3 \longleftrightarrow \text{CO}_2 + 2 \text{PbO}$	591	188	-
B40	$3 \text{PbO} \cdot \text{PbCO}_3 \longleftrightarrow \text{CO}_2 + 2 \cdot 2 \text{PbO} \cdot \text{PbCO}_3$	427	59	-
B41	$2 \text{PbO} \cdot \text{PbCO}_3 \longleftrightarrow \text{CO}_2 + 3 \text{PbO}$	541	132	-
B42	$\text{RaCO}_3 \longleftrightarrow \text{CO}_2 + \text{RaO}$	1772	1068	-
B44	$\text{Rb}_2\text{CO}_3 \cdot \text{H}_2\text{O} \longleftrightarrow \text{CO}_2 + 2 \text{RbOH}$	950	856	-
B45	$\text{RbHCO}_3 \longleftrightarrow \text{CO}_2 + \text{RbOH}$	665	981	-
B46	$\text{SrCO}_3 \longleftrightarrow \text{CO}_2 + \text{SrO}$	1488	1629	6027

Continued on next page

Table 6.2: Reactions with CO₂ as reactive gas – continued

ID	reaction system	T_{equ} °C	storage capacity kJ/kg	storage density MJ/m^3
B47	$Tl_2CO_3 \longleftrightarrow CO_2 + Tl_2O$	698	293	2085
B48	$UO_2CO_3 \longleftrightarrow CO_2 + UO_3$	447	224	-
B51	$ZnCO_3 \longleftrightarrow CO_2 + ZnO$	394	548	2412

Table 6.3: Reactions with NH₃ as reactive gas

ID	reaction system	T_{equ} °C	storage capacity kJ/kg	storage density MJ/m^3
D1	$AgCl \cdot NH_3 \longleftrightarrow NH_3 + AgCl$	340	318	-
D2	$CdCl_2 \cdot 6NH_3 \longleftrightarrow 6NH_3 + CdCl_2$	379	1334	-
D6	$CeCl_3 \cdot 8NH_3 \longleftrightarrow 4NH_3 + CeCl_3 \cdot 4NH_3$	306	375	-
D9	$CeCl_3 \cdot 12NH_3 \longleftrightarrow 4NH_3 + CeCl_3 \cdot 8NH_3$	325	258	-
D10	$CeCl_3 \cdot 12NH_3 \longleftrightarrow 8NH_3 + CeCl_3 \cdot 4NH_3$	318	576	-
D11	$CeCl_3 \cdot 12NH_3 \longleftrightarrow 10NH_3 + CeCl_3 \cdot 2NH_3$	304	865	-
D13	$CeCl_3 \cdot 20NH_3 \longleftrightarrow 8NH_3 + CeCl_3 \cdot 12NH_3$	321	317	-
D14	$CeCl_3 \cdot 20NH_3 \longleftrightarrow 12NH_3 + CeCl_3 \cdot 8NH_3$	327	515	-
D15	$CeCl_3 \cdot 20NH_3 \longleftrightarrow 16NH_3 + CeCl_3 \cdot 4NH_3$	324	759	-
D16	$CeCl_3 \cdot 20NH_3 \longleftrightarrow 18NH_3 + CeCl_3 \cdot 2NH_3$	315	981	-
D17	$CeCl_3 \cdot 20NH_3 \longleftrightarrow 20NH_3 + CeCl_3$	306	1267	-
D20	$2NH_4F \longleftrightarrow NH_3 + NH_4HF_2$	434	1058	1074
D21	$NH_4 \cdot H_2PO_4 \longleftrightarrow NH_3 + H_3PO_4$	641	1049	1891
D22	$NH_4HSO_4 \longleftrightarrow NH_3 + H_2SO_4$	567	1429	2543
D23	$NH_4I \cdot NH_3 \longleftrightarrow NH_3 + NH_4I$	323	251	-
D25	$NH_4I \cdot 2NH_3 \longleftrightarrow 2NH_3 + NH_4I$	304	452	-
D26	$NH_4NO_3 \longleftrightarrow NH_3 + HNO_3$	542	1818	3136
D28	$NH_4ReO_4 \longleftrightarrow NH_3 + HReO_4$	579	512	2033
D29	$(NH_4)_2SO_4 \longleftrightarrow NH_3 + NH_4HSO_4$	666	837	1481
D30	$(NH_4)_2SO_4 \longleftrightarrow 2NH_3 + H_2SO_4$	846	2081	3683
D32	$(NH_4)_2SO_4 \cdot 3NH_3 \longleftrightarrow 4NH_3 + NH_4HSO_4$	442	1209	-
D33	$(NH_4)_2SO_4 \cdot 3NH_3 \longleftrightarrow 5NH_3 + H_2SO_4$	493	2107	-
D34	$NaNH_3 \longleftrightarrow NH_3 + Na$	424	1821	-
D35	$Ni(NH_3)_2I_2 \longleftrightarrow 2NH_3 + NiI_2$	532	424	-
D36	$Ni(NH_3)_4I_2 \longleftrightarrow 2NH_3 + Ni(NH_3)_2I_2$	879	977	-
D37	$Ni(NH_3)_4I_2 \longleftrightarrow 4NH_3 + NiI_2$	1649	1362	-
D38	$Pd(NH_3)_4Cl_2 \longleftrightarrow 4NH_3 + PdCl_2$	492	1202	-
D39	$Pt(NH_3)_2Br_2 \longleftrightarrow 2NH_3 + PtBr_2$	888	592	-
D40	$Pt(NH_3)_4Cl_2 \longleftrightarrow 4NH_3 + PtCl_2$	621	1311	-

Continued on next page

Table 6.3: Reactions with NH₃ as reactive gas – continued

ID	reaction system	T_{equ} °C	storage capacity kJ/kg	storage density MJ/m^3
D41	$\text{Pt}(\text{NH}_3)_2\text{I}_2 \longleftrightarrow 2 \text{NH}_3 + \text{PtI}_2$	484	377	-
D42	$\text{Pt}(\text{NH}_3)_4\text{I}_2 \longleftrightarrow 2 \text{NH}_3 + \text{Pt}(\text{NH}_3)_2\text{I}_2$	398	233	-
D43	$\text{Pt}(\text{NH}_3)_4\text{I}_2 \longleftrightarrow 4 \text{NH}_3 + \text{PtI}_2$	437	586	-
D44	$\text{ScCl}_3 \cdot 4 \text{NH}_3 \longleftrightarrow 4 \text{NH}_3 + \text{ScCl}_3$	485	1392	-
D45	$\text{ScCl}_3 \cdot 5 \text{NH}_3 \longleftrightarrow \text{NH}_3 + \text{ScCl}_3 \cdot 4 \text{NH}_3$	324	230	-
D46	$\text{ScCl}_3 \cdot 5 \text{NH}_3 \longleftrightarrow 5 \text{NH}_3 + \text{ScCl}_3$	466	1522	-
D47	$\text{ScCl}_3 \cdot 7 \text{NH}_3 \longleftrightarrow 2 \text{NH}_3 + \text{ScCl}_3 \cdot 5 \text{NH}_3$	309	341	-
D48	$\text{ScCl}_3 \cdot 7 \text{NH}_3 \longleftrightarrow 3 \text{NH}_3 + \text{ScCl}_3 \cdot 4 \text{NH}_3$	321	542	-
D49	$\text{ScCl}_3 \cdot 7 \text{NH}_3 \longleftrightarrow 7 \text{NH}_3 + \text{ScCl}_3$	429	1671	-
D50	$\text{ZnCl}_2 \cdot 6 \text{NH}_3 \longleftrightarrow 6 \text{NH}_3 + \text{ZnCl}_2$	433	1637	-

Table 6.4: Reactions with SO₂ as reactive gas

ID	reaction system	T_{equ} °C	storage capacity kJ/kg	storage density MJ/m^3
E1	$\text{Ag}_2\text{SO}_3 \longleftrightarrow \text{SO}_2 + \text{Ag}_2\text{O}$	676	551	-
E2	$\text{Ag}_2\text{SO}_4 \longleftrightarrow \text{SO}_2 + \text{Ag}_2\text{O}_2$	1122	1270	6922
E3	$\text{Ag}_2\text{SO}_4 \longleftrightarrow \text{SO}_2 + 2 \text{AgO}$	1085	1274	6941
E4	$\text{BaSO}_4 \longleftrightarrow \text{SO}_2 + \text{BaO}_2$	1601	2262	10156
E5	$\text{CaSO}_3 \longleftrightarrow \text{SO}_2 + \text{CaO}$	1269	1895	-
E6	$\text{CaSO}_4 \longleftrightarrow \text{SO}_2 + \text{CaO}_2$	1262	3539	10476
E7	$\text{Cr}_2(\text{SO}_4)_3 \longleftrightarrow 3 \text{SO}_2 + 2 \text{CrO}_3$	981	2188	6783
E10	$\text{Cu}_2\text{SO}_4 \longleftrightarrow \text{SO}_2 + 2 \text{CuO}$	923	642	2316
E11	$\text{Hg}_2\text{SO}_4 \longleftrightarrow \text{SO}_2 + 2 \text{HgO}$	1517	532	4022
E14	$\text{K}_2\text{SO}_3 \cdot \text{H}_2\text{O} \longleftrightarrow \text{SO}_2 + 2 \text{KOH}$	1115	1522	-
E15	$\text{Li}_2\text{SO}_3 \longleftrightarrow \text{SO}_2 + \text{Li}_2\text{O}$	1178	3076	-
E16	$\text{Li}_2\text{SO}_4 \longleftrightarrow \text{SO}_2 + \text{Li}_2\text{O}_2$	1630	4613	10195
E17	$\text{MgSO}_3 \longleftrightarrow \text{SO}_2 + \text{MgO}$	712	1406	-
E18	$\text{MgSO}_4 \longleftrightarrow \text{SO}_2 + \text{MgO}_2$	979	2845	7567
E19	$\text{MnSO}_4 \longleftrightarrow \text{SO}_2 + \text{MnO}_2$	1029	1631	5302
E22	$\text{PbO} \cdot \text{PbSO}_4 \longleftrightarrow \text{SO}_2 + \text{Pb}_2\text{O}_3$	1284	701	4850
E24	$\text{PbSO}_4 \longleftrightarrow \text{SO}_2 + \text{PbO}_2$	1469	1122	7059
E25	$\text{Pr}_2(\text{SO}_3)_3 \longleftrightarrow 3 \text{SO}_2 + \text{Pr}_2\text{O}_3$	848	840	-
E26	$\text{RaSO}_3 \longleftrightarrow \text{SO}_2 + \text{RaO}$	1907	1177	-
E27	$\text{RaSO}_4 \longleftrightarrow \text{SO}_2 + \text{RaO}_2$	1783	1789	-
E29	$\text{SnSO}_4 \longleftrightarrow \text{SO}_2 + \text{SnO}_2$	864	638	2647
E31	$\text{SrSO}_4 \longleftrightarrow \text{SO}_2 + \text{SrO}_2$	1392	2868	11356

Continued on next page

Table 6.4: Reactions with SO₂ as reactive gas – continued

ID	reaction system	T_{equ} °C	storage capacity kJ/kg	storage density MJ/m^3
E32	$\text{UO}_2\text{SO}_3 \longleftrightarrow \text{SO}_2 + \text{UO}_3$	644	401	-
E33	$\text{U}(\text{SO}_3)_2 \longleftrightarrow 2\text{SO}_2 + \text{UO}_2$	477	513	-
E34	$\text{U}(\text{SO}_4)_2 \longleftrightarrow \text{SO}_2 + \text{UO}_2\text{SO}_4$	751	390	-
E35	$\text{U}(\text{SO}_4)_2 \cdot 4\text{H}_2\text{O} \longleftrightarrow 2\text{SO}_2 + \text{UO}_4 \cdot 4\text{H}_2\text{O}$	818	1007	-

Table 6.5: Reactions with O₂ as reactive gas

ID	reaction system	T_{equ} °C	storage capacity kJ/kg	storage density MJ/m^3
C2	$\text{AgBrO}_2 \longleftrightarrow \text{O}_2 + \text{AgBr}$	371	267	-
C3	$2\text{AgBrO}_3 \longleftrightarrow \text{O}_2 + 2\text{AgBrO}_2$	639	444	2311
C4	$2\text{AgBrO}_3 \longleftrightarrow 3\text{O}_2 + 2\text{AgBr}$	632	692	3606
C5	$2\text{AgCNO} \longleftrightarrow \text{O}_2 + 2\text{AgCN}$	1163	1608	-
C6	$2\text{AgCO}_3 \longleftrightarrow \text{O}_2 + \text{Ag}_2\text{C}_2\text{O}_4$	1094	1010	-
C8	$2\text{AgClO}_3 \longleftrightarrow \text{O}_2 + 2\text{AgClO}_2$	402	204	905
C13	$2\text{AgIO}_3 \longleftrightarrow 3\text{O}_2 + 2\text{AgI}$	399	386	2137
C14	$2\text{AgNO}_2 \longleftrightarrow \text{O}_2 + \text{Ag}_2\text{N}_2\text{O}_2$	651	572	2546
C15	$2\text{AgNO}_3 \longleftrightarrow \text{O}_2 + 2\text{AgNO}_2$	619	444	1932
C16	$2\text{AgNO}_3 \longleftrightarrow 2\text{O}_2 + \text{Ag}_2\text{N}_2\text{O}_2$	683	962	4184
C19	$\text{AgO}_2 \longleftrightarrow \text{O}_2 + \text{Ag}$	444	215	-
C20	$2\text{AgO}_2 \longleftrightarrow \text{O}_2 + \text{Ag}_2\text{O}_2$	630	128	-
C21	$2\text{AgO}_2 \longleftrightarrow \text{O}_2 + 2\text{AgO}$	542	132	-
C22	$4\text{AgO}_2 \longleftrightarrow \text{O}_2 + 2\text{Ag}_2\text{O}_3$	1134	336	-
C23	$4\text{AgO}_2 \longleftrightarrow 3\text{O}_2 + 2\text{Ag}_2\text{O}$	429	103	-
C24	$2\text{Ag}_2\text{O} \longleftrightarrow \text{O}_2 + 4\text{Ag}$	467	134	959
C31	$2\text{Ag}_2\text{SO}_3 \longleftrightarrow 3\text{O}_2 + 2\text{Ag}_2\text{S}$	1200	1549	-
C33	$2\text{Ag}_2\text{SO}_4 \longleftrightarrow \text{O}_2 + 2\text{Ag}_2\text{SO}_3$	1062	725	3952
C34	$2\text{Ag}_2\text{SeO}_3 \longleftrightarrow 3\text{O}_2 + 2\text{Ag}_2\text{Se}$	1233	845	-
C35	$\text{Ag}_2\text{SeO}_4 \longleftrightarrow 2\text{O}_2 + \text{Ag}_2\text{Se}$	961	1052	6015
C36	$2\text{Ag}_2\text{SeO}_4 \longleftrightarrow \text{O}_2 + 2\text{Ag}_2\text{SeO}_3$	699	244	1398
C50	$2\text{As}_2\text{O}_3 \longleftrightarrow 3\text{O}_2 + 4\text{As}$	1840	3310	12372
C51	$\text{As}_2\text{O}_4 \longleftrightarrow 2\text{O}_2 + 2\text{As}$	1752	3739	-
C52	$2\text{As}_2\text{O}_4 \longleftrightarrow \text{O}_2 + \text{As}_4\text{O}_6$	917	667	-
C53	$2\text{As}_2\text{O}_4 \longleftrightarrow \text{O}_2 + 2\text{As}_2\text{O}_3$	939	677	-
C54	$\text{As}_2\text{O}_5 \longleftrightarrow \text{O}_2 + \text{As}_2\text{O}_3$	933	1175	5076
C55	$2\text{As}_2\text{O}_5 \longleftrightarrow \text{O}_2 + 2\text{As}_2\text{O}_4$	899	545	2355
C56	$2\text{As}_2\text{O}_5 \longleftrightarrow 2\text{O}_2 + \text{As}_4\text{O}_6$	918	1166	5035

Continued on next page

Table 6.5: Reactions with O₂ as reactive gas – continued

ID	reaction system	T_{equ} °C	storage capacity kJ/kg	storage density MJ/m^3
C57	$2 \text{As}_2\text{O}_5 \longleftrightarrow 5 \text{O}_2 + 4 \text{As}$	1641	4024	17384
C58	$\text{As}_4\text{O}_6 \longleftrightarrow 3 \text{O}_2 + 4 \text{As}$	1825	3321	-
C62	$\text{B}_3\text{O}_3\text{H}_3 \longleftrightarrow \text{O}_2 + \text{B}(\text{OH})_3$	869	2007	-
C63	$4 \text{B}_3\text{O}_3\text{H}_3 \longleftrightarrow 3 \text{O}_2 + 3 \text{B}_2(\text{OH})_4$	1654	2454	-
C67	$\text{Ba}(\text{ClO}_4)_2 \longleftrightarrow 2 \text{O}_2 + \text{Ba}(\text{ClO}_2)_2$	310	345	1104
C69	$\text{Ba}(\text{IO}_3)_2 \longleftrightarrow 3 \text{O}_2 + \text{BaI}_2$	817	866	4528
C70	$\text{Ba}(\text{IO}_3)_2 \cdot \text{H}_2\text{O} \longleftrightarrow 3 \text{O}_2 + \text{BaI}_2 \cdot \text{H}_2\text{O}$	581	787	-
C75	$2 \text{BaO}_2 \longleftrightarrow \text{O}_2 + 2 \text{BaO}$	1158	510	2528
C76	$4 \text{BaO}_2 \longleftrightarrow 3 \text{O}_2 + 2 \text{Ba}_2\text{O}$	1711	1929	9566
C79	$2 \text{BaO} \cdot \text{UO}_3 \longleftrightarrow \text{O}_2 + 2 \text{BaO} \cdot \text{UO}_2$	1084	691	-
C80	$4 \text{BaO} \cdot \text{UO}_3 \longleftrightarrow \text{O}_2 + 2 \text{Ba}_2\text{U}_2\text{O}_7$	840	282	-
C81	$2 \text{BaO} \cdot \text{UO}_2 \cdot \text{UO}_3 \longleftrightarrow \text{O}_2 + 4 \text{BaO} \cdot \text{UO}_2$	903	417	-
C84	$2 \text{BaSeO}_3 \longleftrightarrow 3 \text{O}_2 + 2 \text{BaSe}$	1624	2530	-
C85	$\text{BaSeO}_4 \longleftrightarrow 2 \text{O}_2 + \text{BaSe}$	1500	2763	13124
C86	$2 \text{BaSeO}_4 \longleftrightarrow \text{O}_2 + 2 \text{BaSeO}_3$	582	377	1793
C87	$2 \text{BaTeO}_3 \longleftrightarrow 3 \text{O}_2 + 2 \text{BaTe}$	1965	2506	-
C88	$2 \text{Ba}_2\text{U}_2\text{O}_7 \longleftrightarrow \text{O}_2 + 4 \text{BaO} \cdot \text{UO}_2$	893	417	-
C92	$\text{BiAsO}_4 \longleftrightarrow 2 \text{O}_2 + \text{BiAs}$	1856	2885	-
C94	$2 \text{Bi}_2\text{O}_3 \longleftrightarrow \text{O}_2 + 4 \text{BiO}$	1346	343	3049
C96	$2 \text{BiOCl} \longleftrightarrow \text{O}_2 + 2 \text{BiCl}$	1318	983	7591
C97	$2 \text{BiOI} \longleftrightarrow \text{O}_2 + 2 \text{BiI}$	1100	607	-
C98	$\text{Bi}_2\text{O}_2\text{Se} \longleftrightarrow \text{O}_2 + \text{Bi}_2\text{Se}$	1091	707	-
C99	$2 \text{Bi}_2\text{O}_3 \cdot \text{SeO}_2 \longleftrightarrow 3 \text{O}_2 + 2 \text{Bi}_2\text{O}_2\text{Se}$	1202	775	-
C100	$2 \text{Bi}_2\text{O}_3 \cdot \text{SeO}_2 \longleftrightarrow 5 \text{O}_2 + 2 \text{Bi}_2\text{Se}$	1217	1423	-
C101	$2 \text{Bi}_2\text{O}_3 \cdot 3 \text{SeO}_2 \longleftrightarrow 9 \text{O}_2 + 2 \text{Bi}_2\text{Se}_3$	1346	1564	-
C102	$\text{Bi}_2\text{O}_2\text{Te} \longleftrightarrow \text{O}_2 + \text{Bi}_2\text{Te}$	1168	677	-
C103	$2 \text{Bi}_2\text{O}_3 \cdot \text{TeO}_2 \longleftrightarrow 3 \text{O}_2 + 2 \text{Bi}_2\text{O}_2\text{Te}$	1268	821	-
C104	$2 \text{Bi}_2\text{O}_3 \cdot \text{TeO}_2 \longleftrightarrow 5 \text{O}_2 + 2 \text{Bi}_2\text{Te}$	1337	1446	-
C105	$2 \text{Bi}_2\text{O}_3 \cdot 2 \text{TeO}_2 \longleftrightarrow 7 \text{O}_2 + 4 \text{BiTe}$	1335	1665	-
C106	$\text{Bi}_2(\text{SO}_4)_3 \longleftrightarrow 6 \text{O}_2 + \text{Bi}_2\text{S}_3$	1701	3400	17274
C107	$2 \text{CH}_4\text{N}_2\text{O}_2 \longleftrightarrow \text{O}_2 + 2 \text{CH}_4\text{N}_2\text{O}$	1279	4097	-
C108	$6 \text{CH}_4\text{N}_2\text{O}_2 \longleftrightarrow 3 \text{O}_2 + 2 \text{C}_2\text{N}_6\text{H}_{12} \cdot \text{CO}_3$	1394	4227	-
C109	$2 \text{C}_2\text{H}_5\text{NO}_2 \longleftrightarrow \text{O}_2 + 2 \text{C}_2\text{H}_5\text{NO}$	945	2951	3426
C118	$\text{Ca}(\text{IO}_3)_2 \longleftrightarrow 3 \text{O}_2 + \text{CaI}_2$	789	1195	-
C122	$2 \text{CaO}_2 \longleftrightarrow \text{O}_2 + 2 \text{CaO}$	434	334	976
C132	$2 \text{CaSO}_4 \longleftrightarrow \text{O}_2 + 2 \text{CaSO}_3$	1481	2044	6050
C133	$2 \text{CaSO}_4 \cdot 2 \text{H}_2\text{O} \longleftrightarrow \text{O}_2 + 2 \text{CaSO}_3 \cdot 2 \text{H}_2\text{O}$	913	1512	3508
C135	$\text{CaSeO}_4 \longleftrightarrow 2 \text{O}_2 + \text{CaSe}$	1680	4052	11669
C136	$2 \text{CaSeO}_4 \cdot 2 \text{H}_2\text{O} \longleftrightarrow \text{O}_2 + 2 \text{CaSeO}_3 \cdot 2 \text{H}_2\text{O}$	542	492	1352

Continued on next page

Table 6.5: Reactions with O₂ as reactive gas – continued

ID	reaction system	T_{equ} °C	storage capacity kJ/kg	storage density MJ/m^3
C140	$2 \text{CaTeO}_3 \longleftrightarrow 3 \text{O}_2 + 2 \text{CaTe}$	1983	3595	-
C141	$\text{Cd}_3(\text{AsO}_4)_2 \longleftrightarrow 4 \text{O}_2 + \text{Cd}_3\text{As}_2$	1819	3083	-
C145	$\text{CdSeO}_4 \longleftrightarrow 2 \text{O}_2 + \text{CdSe}$	1484	1912	-
C146	$2 \text{CdSeO}_4 \longleftrightarrow \text{O}_2 + 2 \text{CdSeO}_3$	699	226	-
C147	$2 \text{Ce}(\text{IO}_3)_3 \longleftrightarrow 9 \text{O}_2 + 2 \text{CeI}_3$	813	1179	-
C151	$\text{Ce}(\text{SO}_4)_2 \longleftrightarrow 4 \text{O}_2 + \text{CeS}_2$	1761	5191	20247
C154	$4 \text{CmO}_2 \longleftrightarrow \text{O}_2 + 2 \text{Cm}_2\text{O}_3$	717	251	-
C156	$\text{Co}(\text{AsO}_2)_2 \longleftrightarrow 2 \text{O}_2 + \text{CoAs}_2$	1713	3285	-
C159	$2 \text{Co}_3\text{O}_4 \longleftrightarrow \text{O}_2 + 6 \text{CoO}$	1206	815	4978
C164	$4 \text{CrO}_2 \longleftrightarrow \text{O}_2 + 2 \text{Cr}_2\text{O}_3$	366	169	828
C169	$\text{Cr}_5\text{O}_{12} \longleftrightarrow \text{O}_2 + 5 \text{CrO}_2$	408	120	-
C171	$4 \text{Cr}_5\text{O}_{12} \longleftrightarrow 9 \text{O}_2 + 10 \text{Cr}_2\text{O}_3$	380	278	-
C176	$2 \text{CsAsO}_3 \longleftrightarrow \text{O}_2 + 2 \text{CsAsO}_2$	461	274	-
C182	$2 \text{CsClO}_4 \longleftrightarrow \text{O}_2 + 2 \text{CsClO}_3$	463	220	731
C183	$2 \text{CsIO}_3 \longleftrightarrow 3 \text{O}_2 + 2 \text{CsI}$	768	647	-
C184	$2 \text{CsNO}_3 \longleftrightarrow \text{O}_2 + 2 \text{CsNO}_2$	1206	695	2565
C186	$2 \text{CsO}_2 \longleftrightarrow \text{O}_2 + \text{Cs}_2\text{O}_2$	1668	401	1513
C187	$4 \text{CsO}_2 \longleftrightarrow \text{O}_2 + 2 \text{Cs}_2\text{O}_3$	748	159	598
C188	$4 \text{CsO}_2 \longleftrightarrow 3 \text{O}_2 + 2 \text{Cs}_2\text{O}$	1531	685	2583
C189	$2 \text{CsO}_3 \longleftrightarrow \text{O}_2 + \text{Cs}_2\text{O}_4$	305	61	-
C191	$2 \text{CsO}_3 \longleftrightarrow 2 \text{O}_2 + \text{Cs}_2\text{O}_2$	316	282	-
C192	$2 \text{CsO}_3 \longleftrightarrow 3 \text{O}_2 + 2 \text{Cs}$	1039	1498	-
C194	$4 \text{CsO}_3 \longleftrightarrow 5 \text{O}_2 + 2 \text{Cs}_2\text{O}$	501	540	-
C197	$2 \text{Cs}_2\text{O}_2 \longleftrightarrow \text{O}_2 + 2 \text{Cs}_2\text{O}$	1389	314	1336
C198	$\text{Cs}_2\text{O}_3 \longleftrightarrow \text{O}_2 + \text{Cs}_2\text{O}$	1485	553	2352
C199	$2 \text{Cs}_2\text{O}_3 \longleftrightarrow \text{O}_2 + 2 \text{Cs}_2\text{O}_2$	1595	255	1084
C201	$\text{Cs}_2\text{O}_4 \longleftrightarrow \text{O}_2 + \text{Cs}_2\text{O}_2$	313	242	-
C202	$\text{Cs}_2\text{O}_4 \longleftrightarrow 2 \text{O}_2 + 2 \text{Cs}$	995	1576	-
C204	$2 \text{Cs}_2\text{O}_4 \longleftrightarrow 3 \text{O}_2 + 2 \text{Cs}_2\text{O}$	512	525	-
C206	$2 \text{Cs}_2\text{SO}_3 \longleftrightarrow 3 \text{O}_2 + 2 \text{Cs}_2\text{S}$	1938	2301	-
C208	$2 \text{Cs}_2\text{SO}_4 \longleftrightarrow \text{O}_2 + 2 \text{Cs}_2\text{SO}_3$	964	842	3571
C209	$2 \text{Cs}_2\text{SeO}_4 \longleftrightarrow \text{O}_2 + 2 \text{Cs}_2\text{SeO}_3$	701	408	-
C212	$2 \text{Cs}_2\text{TeO}_4 \longleftrightarrow \text{O}_2 + 2 \text{Cs}_2\text{TeO}_3$	1052	275	-
C213	$2 \text{Cs}_2\text{Te}_4\text{O}_{12} \longleftrightarrow 3 \text{O}_2 + 2 \text{Cs}_2\text{O} \cdot 4 \text{TeO}_2$	846	325	-
C214	$\text{Cu}_3\text{AsO}_4 \longleftrightarrow 2 \text{O}_2 + \text{Cu}_3\text{As}$	1594	2120	-
C215	$\text{Cu}(\text{IO}_3)_2 \longleftrightarrow 3 \text{O}_2 + \text{CuI}_2$	562	921	4828
C216	$2 \text{CuO} \longleftrightarrow \text{O}_2 + 2 \text{Cu}$	1928	1959	12359
C217	$4 \text{CuO} \longleftrightarrow \text{O}_2 + 2 \text{Cu}_2\text{O}$	1392	886	5592
C219	$2 \text{CuO} \cdot \text{CuSO}_4 \longleftrightarrow \text{O}_2 + 2 \text{Cu}_2\text{SO}_4$	1122	735	-

Continued on next page

Table 6.5: Reactions with O₂ as reactive gas – continued

ID	reaction system	T_{equ} °C	storage capacity kJ/kg	storage density MJ/m^3
C220	$2 \text{CuO} \cdot \text{CuSO}_4 \longleftrightarrow 5 \text{O}_2 + 2 \text{Cu}_2\text{S}$	1792	3546	-
C221	$\text{CuSO}_4 \longleftrightarrow 2 \text{O}_2 + \text{CuS}$	1538	4482	16150
C222	$\text{Cu}_2\text{SO}_4 \longleftrightarrow 2 \text{O}_2 + \text{Cu}_2\text{S}$	1829	3013	10861
C223	$2 \text{CuSeO}_3 \longleftrightarrow 3 \text{O}_2 + 2 \text{CuSe}$	1207	2045	-
C224	$\text{CuSeO}_4 \longleftrightarrow 2 \text{O}_2 + \text{CuSe}$	952	2198	-
C225	$2 \text{CuSeO}_4 \longleftrightarrow \text{O}_2 + 2 \text{CuSeO}_3$	445	312	-
C226	$\text{Cu}_2\text{SeO}_4 \longleftrightarrow 2 \text{O}_2 + \text{Cu}_2\text{Se}$	828	1436	-
C227	$2 \text{Dy}(\text{IO}_3)_3 \longleftrightarrow 9 \text{O}_2 + 2 \text{DyI}_3$	741	1151	-
C234	$2 \text{Er}(\text{IO}_3)_3 \longleftrightarrow 9 \text{O}_2 + 2 \text{ErI}_3$	748	1158	-
C239	$2 \text{Eu}(\text{IO}_3)_3 \longleftrightarrow 9 \text{O}_2 + 2 \text{EuI}_3$	607	1173	-
C243	$6 \text{Eu}_2\text{O}_3 \longleftrightarrow \text{O}_2 + 4 \text{Eu}_3\text{O}_4$	1137	410	3041
C245	$2 \text{Eu}_3\text{O}_4 \longleftrightarrow \text{O}_2 + 6 \text{EuO}$	1701	963	-
C247	$\text{EuSO}_4 \longleftrightarrow 2 \text{O}_2 + \text{EuS}$	1938	4244	-
C249	$\text{FeAsO}_4 \longleftrightarrow 2 \text{O}_2 + \text{FeAs}$	1873	4353	-
C253	$6 \text{Fe}_2\text{O}_3 \longleftrightarrow \text{O}_2 + 4 \text{Fe}_3\text{O}_4$	1675	497	2603
C259	$6 \text{FeO} \cdot \text{OH} \longleftrightarrow 5 \text{O}_2 + 2 \text{Fe}(\text{OH})_3$	1454	3179	13543
C260	$2 \text{Fe}_2\text{O}_3 \cdot 2 \text{SeO}_2 \longleftrightarrow 7 \text{O}_2 + 4 \text{FeSe}$	1328	3316	-
C266	$\text{Fe}_2(\text{SO}_4)_3 \longleftrightarrow 6 \text{O}_2 + \text{Fe}_2\text{S}_3$	1537	5765	17871
C270	$2 \text{Fe}_2\text{TiO}_5 \longleftrightarrow \text{O}_2 + 2 \text{Fe}_2\text{TiO}_4$	1698	997	4367
C277	$2 \text{Fr}_2\text{O} \longleftrightarrow \text{O}_2 + 4 \text{Fr}$	1595	734	-
C280	$\text{Ga}_2\text{O}_3 \longleftrightarrow \text{O}_2 + \text{Ga}_2\text{O}$	1783	3921	25253
C282	$6 \text{GaOOH} \longleftrightarrow 5 \text{O}_2 + 2 \text{Ga}(\text{OH})_3$	1568	3738	-
C283	$\text{Ga}_2(\text{SeO}_4)_3 \longleftrightarrow 6 \text{O}_2 + \text{Ga}_2\text{Se}_3$	1378	2762	-
C284	$2 \text{Gd}(\text{IO}_3)_3 \longleftrightarrow 9 \text{O}_2 + 2 \text{GdI}_3$	861	1187	-
C293	$2 \text{HfOCl}_2 \longleftrightarrow \text{O}_2 + 2 \text{HfCl}_2$	1872	2144	-
C294	$2 \text{Hg}_2\text{CO}_3 \longleftrightarrow 2 \text{O}_2 + \text{Hg}_2(\text{COO})_2$	1070	587	-
C295	$2 \text{HgO} \longleftrightarrow \text{O}_2 + 2 \text{Hg}$	856	420	4674
C296	$4 \text{HgO} \longleftrightarrow \text{O}_2 + 2 \text{Hg}_2\text{O}$	673	209	2329
C297	$2 \text{Hg}_2\text{O} \longleftrightarrow \text{O}_2 + 4 \text{Hg}$	686	219	2143
C299	$\text{Hg}_2\text{SO}_4 \longleftrightarrow 2 \text{O}_2 + \text{Hg}_2\text{S}$	1378	1431	10821
C301	$2 \text{HgSO}_4 \cdot \text{HgO} \longleftrightarrow 5 \text{O}_2 + 2 \text{Hg}_2\text{S}$	1237	1329	-
C302	$2 \text{HgSeO}_3 \longleftrightarrow 3 \text{O}_2 + 2 \text{HgSe}$	1154	929	-
C303	$\text{HgSeO}_4 \longleftrightarrow 2 \text{O}_2 + \text{HgSe}$	776	1004	-
C305	$2 \text{Ho}(\text{IO}_3)_3 \longleftrightarrow 9 \text{O}_2 + 2 \text{HoI}_3$	740	1175	-
C308	$2 \text{I}_2\text{O}_5 \longleftrightarrow 5 \text{O}_2 + 2 \text{I}_2$	308	474	2358
C309	$2 \text{I}_2\text{O}_5 \longleftrightarrow 5 \text{O}_2 + 4 \text{I}$	308	474	2358
C312	$\text{In}_2(\text{SO}_4)_3 \longleftrightarrow 6 \text{O}_2 + \text{In}_2\text{S}_3$	1835	4695	16143
C313	$\text{IrO}_2 \longleftrightarrow \text{O}_2 + \text{Ir}$	1371	1112	12973
C314	$4 \text{IrO}_2 \longleftrightarrow \text{O}_2 + 2 \text{Ir}_2\text{O}_3$	1780	478	5573

Continued on next page

Table 6.5: Reactions with O₂ as reactive gas – continued

ID	reaction system	T_{equ} °C	storage capacity kJ/kg	storage density MJ/m^3
C315	$2 \text{Ir}_2\text{O}_3 \longleftrightarrow 3 \text{O}_2 + 4 \text{Ir}$	1119	658	-
C317	$2 \text{K}_2\text{As}_4\text{O}_{11} \longleftrightarrow 11 \text{O}_2 + 4 \text{KAs}_2$	1927	5227	-
C325	$2 \text{KClO}_4 \longleftrightarrow \text{O}_2 + 2 \text{KClO}_3$	434	296	746
C326	$2 \text{KHCO}_3 \longleftrightarrow \text{O}_2 + 2 \text{KCHO}_2$	1533	3034	6584
C328	$2 \text{KIO}_3 \longleftrightarrow 3 \text{O}_2 + 2 \text{KI}$	661	804	3128
C329	$\text{KIO}_4 \longleftrightarrow 2 \text{O}_2 + \text{KI}$	406	600	2170
C331	$2 \text{KNO}_3 \longleftrightarrow \text{O}_2 + 2 \text{KNO}_2$	1196	1273	2685
C334	$4 \text{KO}_2 \longleftrightarrow \text{O}_2 + 2 \text{K}_2\text{O}_3$	1261	311	668
C340	$4 \text{KO}_3 \longleftrightarrow 5 \text{O}_2 + 2 \text{K}_2\text{O}$	478	893	-
C341	$2 \text{K}_2\text{O}_2 \longleftrightarrow \text{O}_2 + 2 \text{K}_2\text{O}$	1597	1203	-
C342	$\text{K}_2\text{O}_3 \longleftrightarrow \text{O}_2 + \text{K}_2\text{O}$	756	1266	-
C345	$2 \text{K}_2\text{O}_4 \longleftrightarrow \text{O}_2 + 2 \text{K}_2\text{O}_3$	393	267	-
C346	$2 \text{K}_2\text{O}_4 \longleftrightarrow 3 \text{O}_2 + 2 \text{K}_2\text{O}$	596	1391	-
C347	$2 \text{K}_2\text{O} \cdot \text{Cr}_2\text{O}_6 \longleftrightarrow 3 \text{O}_2 + 4 \text{KCrO}_2$	1581	1022	2761
C351	$2 \text{K}_2\text{SO}_4 \longleftrightarrow \text{O}_2 + 2 \text{K}_2\text{SO}_3$	1353	1785	4752
C352	$2 \text{K}_2\text{S}_2\text{O}_7 \longleftrightarrow 7 \text{O}_2 + 2 \text{K}_2\text{S}_2$	1684	6096	-
C353	$\text{K}_2\text{S}_2\text{O}_8 \longleftrightarrow 4 \text{O}_2 + \text{K}_2\text{S}_2$	1464	5472	13571
C355	$\text{K}_2\text{S}_4\text{O}_6 \longleftrightarrow 3 \text{O}_2 + \text{K}_2\text{S}_4$	1611	4275	12653
C356	$2 \text{K}_2\text{SeO}_3 \longleftrightarrow 3 \text{O}_2 + 2 \text{K}_2\text{Se}$	1377	2910	-
C357	$\text{K}_2\text{SeO}_4 \longleftrightarrow 2 \text{O}_2 + \text{K}_2\text{Se}$	1360	3279	10066
C358	$2 \text{K}_2\text{SeO}_4 \longleftrightarrow \text{O}_2 + 2 \text{K}_2\text{SeO}_3$	647	579	1777
C360	$2 \text{La}(\text{IO}_3)_3 \longleftrightarrow 9 \text{O}_2 + 2 \text{LaI}_3$	760	1105	-
C364	$2 \text{La}_2(\text{SeO}_3)_3 \longleftrightarrow 9 \text{O}_2 + 2 \text{La}_2\text{Se}_3$	1840	2955	-
C373	$2 \text{LiClO}_4 \longleftrightarrow 3 \text{O}_2 + 2 \text{LiClO}$	701	3445	8364
C376	$2 \text{LiIO}_3 \longleftrightarrow 3 \text{O}_2 + 2 \text{LiI}$	757	1351	-
C377	$2 \text{LiNO}_3 \longleftrightarrow \text{O}_2 + 2 \text{LiNO}_2$	1599	1659	3982
C379	$2 \text{LiO}_3 \longleftrightarrow 3 \text{O}_2 + 2 \text{Li}$	911	4798	-
C383	$2 \text{Li}_2\text{O}_2 \longleftrightarrow \text{O}_2 + 2 \text{Li}_2\text{O}$	415	755	1743
C385	$2 \text{Li}_2\text{SO}_3 \longleftrightarrow 3 \text{O}_2 + 2 \text{Li}_2\text{S}$	1923	7901	-
C387	$2 \text{Li}_2\text{SO}_4 \longleftrightarrow \text{O}_2 + 2 \text{Li}_2\text{SO}_3$	1268	2300	5082
C388	$\text{Li}_2\text{SeO}_4 \longleftrightarrow 2 \text{O}_2 + \text{Li}_2\text{Se}$	1408	4631	-
C389	$2 \text{Lu}(\text{IO}_3)_3 \longleftrightarrow 9 \text{O}_2 + 2 \text{LuI}_3$	742	1107	-
C396	$2 \text{MgMoO}_4 \longleftrightarrow \text{O}_2 + 2 \text{MgMoO}_3$	1268	1131	-
C399	$2 \text{MgO}_2 \longleftrightarrow \text{O}_2 + 2 \text{MgO}$	478	373	1118
C402	$2 \text{MgSO}_3 \longleftrightarrow 3 \text{O}_2 + 2 \text{MgS}$	1919	6702	-
C404	$2 \text{MgSO}_4 \longleftrightarrow \text{O}_2 + 2 \text{MgSO}_3$	1230	1800	4788
C405	$2 \text{MgSO}_4 \cdot 6 \text{H}_2\text{O} \longleftrightarrow \text{O}_2 + 2 \text{MgSO}_3 \cdot 6 \text{H}_2\text{O}$	871	1187	-
C408	$\text{MgSeO}_4 \longleftrightarrow 2 \text{O}_2 + \text{MgSe}$	1316	4039	-
C409	$2 \text{MgSeO}_4 \longleftrightarrow \text{O}_2 + 2 \text{MgSeO}_3$	410	408	-

Continued on next page

Table 6.5: Reactions with O₂ as reactive gas – continued

ID	reaction system	T_{equ} °C	storage capacity kJ/kg	storage density MJ/m^3
C410	$2 \text{MgSeO}_4 \cdot 6 \text{H}_2\text{O} \longleftrightarrow \text{O}_2 + 2 \text{MgSeO}_3 \cdot 6 \text{H}_2\text{O}$	522	293	-
C412	$2 \text{MgTeO}_3 \longleftrightarrow 3 \text{O}_2 + 2 \text{MgTe}$	1889	3646	-
C413	$\text{Mn}(\text{IO}_3)_2 \longleftrightarrow 3 \text{O}_2 + \text{MnI}_2$	812	1124	-
C416	$2 \text{MnO}_2 \longleftrightarrow \text{O}_2 + 2 \text{MnO}$	1273	1574	7998
C417	$3 \text{MnO}_2 \longleftrightarrow \text{O}_2 + \text{Mn}_3\text{O}_4$	895	684	3477
C418	$4 \text{MnO}_2 \longleftrightarrow \text{O}_2 + 2 \text{Mn}_2\text{O}_3$	802	490	2489
C419	$2 \text{Mn}_2\text{O}_3 \longleftrightarrow \text{O}_2 + 4 \text{MnO}$	1759	1194	5375
C421	$6 \text{Mn}_2\text{O}_3 \longleftrightarrow \text{O}_2 + 4 \text{Mn}_3\text{O}_4$	1273	214	963
C423	$2 \text{Mn}_3\text{O}_4 \longleftrightarrow \text{O}_2 + 6 \text{MnO}$	1974	1015	4910
C424	$4 \text{MnO} \cdot \text{OH} \longleftrightarrow 3 \text{O}_2 + 2 \text{Mn}(\text{OH})_2$	1510	3298	-
C425	$2 \text{MnO} \cdot \text{TiO}_2 \longleftrightarrow \text{O}_2 + 2 \text{MnTiO}_2$	307	-0	-0
C428	$2 \text{MnSeO}_3 \longleftrightarrow 3 \text{O}_2 + 2 \text{MnSe}$	1689	3381	-
C429	$\text{MnSeO}_4 \longleftrightarrow 2 \text{O}_2 + \text{MnSe}$	1210	3097	-
C433	$\text{MnTeO}_4 \longleftrightarrow 2 \text{O}_2 + \text{MnTe}$	1711	3452	-
C438	$2 \text{MoCl}_2\text{O}_2 \longleftrightarrow \text{O}_2 + 2 \text{MoCl}_2\text{O}$	1771	976	3229
C439	$2 \text{MoCl}_3\text{O} \longleftrightarrow \text{O}_2 + 2 \text{MoCl}_3$	1267	879	-
C440	$2 \text{MoCl}_4\text{O} \longleftrightarrow \text{O}_2 + 2 \text{MoCl}_4$	1529	702	-
C446	$2 \text{Mo}_4\text{O}_{11} \longleftrightarrow 3 \text{O}_2 + 8 \text{MoO}_2$	1264	814	-
C449	$\text{Mo}_9\text{O}_{26} \longleftrightarrow 4 \text{O}_2 + 9 \text{MoO}_2$	1209	969	-
C452	$2 \text{MoOBr}_3 \longleftrightarrow \text{O}_2 + 2 \text{MoBr}_3$	1118	512	-
C453	$\text{MoO}_2\text{Br}_2 \longleftrightarrow \text{O}_2 + \text{MoBr}_2$	1536	1505	-
C454	$2 \text{MoOF}_4 \longleftrightarrow \text{O}_2 + 2 \text{MoF}_4$	1102	1165	-
C457	$\text{NH}_4\text{HSO}_4 \longleftrightarrow 2 \text{O}_2 + \text{NH}_4\text{HS}$	1587	7515	13376
C458	$\text{NH}_4\text{IO}_4 \longleftrightarrow 2 \text{O}_2 + \text{NH}_4\text{I}$	429	655	2001
C466	$\text{Na}_2\text{C}_2\text{O}_4 \longleftrightarrow 2 \text{O}_2 + \text{Na}_2\text{C}_2$	1952	9963	23314
C468	$2 \text{NaClO}_3 \longleftrightarrow \text{O}_2 + 2 \text{NaClO}_2$	426	505	1258
C470	$\text{NaClO}_4 \longleftrightarrow \text{O}_2 + \text{NaClO}_2$	382	643	1596
C473	$2 \text{Na}_2\text{Cr}_2\text{O}_7 \longleftrightarrow 3 \text{O}_2 + 2 \text{Na}_2\text{Cr}_2\text{O}_4$	1068	1304	-
C474	$2 \text{NaHCO}_3 \longleftrightarrow \text{O}_2 + 2 \text{NaCHO}_2$	1211	3384	7307
C475	$2 \text{NaIO}_3 \longleftrightarrow 3 \text{O}_2 + 2 \text{NaI}$	703	971	4156
C476	$\text{NaIO}_4 \longleftrightarrow 2 \text{O}_2 + \text{NaI}$	399	653	2521
C480	$4 \text{NaO}_2 \longleftrightarrow 3 \text{O}_2 + 2 \text{Na}_2\text{O}$	756	966	2125
C484	$2 \text{Na}_2\text{O}_2 \longleftrightarrow \text{O}_2 + 2 \text{Na}_2\text{O}$	1433	1258	3529
C489	$2 \text{Na}_2\text{S}_2\text{O}_3 \longleftrightarrow 3 \text{O}_2 + 2 \text{Na}_2\text{S}_2$	1806	4591	7654
C490	$2 \text{Na}_2\text{S}_2\text{O}_3 \longleftrightarrow 3 \text{O}_2 + 4 \text{NaS}$	1950	4557	7597
C491	$\text{Na}_2\text{S}_2\text{O}_7 \longleftrightarrow 2 \text{O}_2 + \text{Na}_2\text{S}_2\text{O}_3$	1254	3612	-
C492	$2 \text{Na}_2\text{S}_2\text{O}_7 \longleftrightarrow 7 \text{O}_2 + 2 \text{Na}_2\text{S}_2$	1890	6880	-
C493	$2 \text{Na}_2\text{S}_2\text{O}_7 \longleftrightarrow 7 \text{O}_2 + 4 \text{NaS}$	1977	6856	-
C494	$2 \text{Na}_2\text{SO}_4 \cdot 7 \text{H}_2\text{O} \longleftrightarrow \text{O}_2 + 2 \text{Na}_2\text{SO}_3 \cdot 7 \text{H}_2\text{O}$	650	1134	-

Continued on next page

Table 6.5: Reactions with O₂ as reactive gas – continued

ID	reaction system	T_{equ} °C	storage capacity kJ/kg	storage density MJ/m^3
C496	$2 \text{Na}_2\text{SeO}_3 \longleftrightarrow 3 \text{O}_2 + 2 \text{Na}_2\text{Se}$	1541	3569	-
C497	$\text{Na}_2\text{SeO}_4 \longleftrightarrow 2 \text{O}_2 + \text{Na}_2\text{Se}$	1421	3897	12471
C498	$2 \text{Na}_2\text{SeO}_4 \longleftrightarrow \text{O}_2 + 2 \text{Na}_2\text{SeO}_3$	564	631	2019
C499	$2 \text{Na}_2\text{TeO}_3 \longleftrightarrow 3 \text{O}_2 + 2 \text{Na}_2\text{Te}$	1921	3110	-
C500	$\text{Na}_2\text{TeO}_4 \longleftrightarrow 2 \text{O}_2 + \text{Na}_2\text{Te}$	1846	4028	-
C501	$2 \text{Na}_2\text{TeO}_4 \longleftrightarrow \text{O}_2 + 2 \text{Na}_2\text{TeO}_3$	915	1127	-
C502	$2 \text{Na}_2\text{U}_2\text{O}_7 \longleftrightarrow \text{O}_2 + 4 \text{NaUO}_3$	1171	338	-
C503	$2 \text{Na}_2\text{V}_2\text{O}_7 \longleftrightarrow \text{O}_2 + 2 \text{Na}_2\text{V}_2\text{O}_6$	1669	2061	-
C511	$2 \text{NbOCl}_2 \longleftrightarrow \text{O}_2 + 2 \text{NbCl}_2$	1744	2043	-
C512	$2 \text{NbOCl}_3 \longleftrightarrow \text{O}_2 + 2 \text{NbCl}_3$	1368	1384	5148
C513	$2 \text{Nd}(\text{IO}_3)_3 \longleftrightarrow 9 \text{O}_2 + 2 \text{NdI}_3$	810	1173	-
C516	$\text{Ni}(\text{IO}_3)_2 \longleftrightarrow 3 \text{O}_2 + \text{NiI}_2$	734	1039	5269
C517	$2 \text{NiO} \longleftrightarrow \text{O}_2 + 2 \text{NiH}_0 \cdot 5$	1436	3183	21393
C518	$4 \text{NiO} \cdot \text{OH} \longleftrightarrow 3 \text{O}_2 + 2 \text{Ni}(\text{OH})_2$	908	1365	-
C519	$6 \text{NiO} \cdot \text{OH} \longleftrightarrow 5 \text{O}_2 + 2 \text{Ni}(\text{OH})_3$	893	1787	-
C522	$2 \text{NiSeO}_3 \longleftrightarrow 3 \text{O}_2 + 2 \text{NiSe}$	1558	2617	-
C529	$4 \text{NpO}_3 \cdot \text{H}_2\text{O} \longleftrightarrow 7 \text{O}_2 + 2 \text{NpO}_2(\text{OH})_2$	1446	2317	-
C531	$\text{OsO}_2 \longleftrightarrow \text{O}_2 + \text{Os}$	1687	1328	15095
C533	$2 \text{OsO}_3 \longleftrightarrow 3 \text{O}_2 + 2 \text{Os}$	807	799	-
C536	$2 \text{OsO}_4 \longleftrightarrow \text{O}_2 + 2 \text{OsO}_3$	1106	801	4087
C537	$\text{PO}_2 \longleftrightarrow \text{O}_2 + \text{P}$	1772	4322	-
C538	$2 \text{P}_2\text{O}_5 \longleftrightarrow \text{O}_2 + \text{P}_4\text{O}_8$	1180	2203	5067
C542	$\text{P}_4\text{O}_{10} \longleftrightarrow \text{O}_2 + \text{P}_4\text{O}_8$	1179	2203	5265
C550	$\text{PbO}_2 \longleftrightarrow \text{O}_2 + \text{Pb}$	1480	1182	11397
C551	$2 \text{PbO}_2 \longleftrightarrow \text{O}_2 + 2 \text{PbO}$	676	271	2609
C552	$3 \text{PbO}_2 \longleftrightarrow \text{O}_2 + \text{Pb}_3\text{O}_4$	670	181	1743
C553	$4 \text{PbO}_2 \longleftrightarrow \text{O}_2 + 2 \text{Pb}_2\text{O}_3$	691	154	1489
C554	$2 \text{Pb}_2\text{O}_3 \longleftrightarrow \text{O}_2 + 4 \text{PbO}$	653	120	1208
C555	$2 \text{Pb}_2\text{O}_3 \longleftrightarrow 3 \text{O}_2 + 4 \text{Pb}$	1913	1063	10687
C556	$6 \text{Pb}_2\text{O}_3 \longleftrightarrow \text{O}_2 + 4 \text{Pb}_3\text{O}_4$	547	27	273
C557	$\text{Pb}_3\text{O}_4 \longleftrightarrow 2 \text{O}_2 + 3 \text{Pb}$	1943	1048	9350
C558	$2 \text{Pb}_3\text{O}_4 \longleftrightarrow \text{O}_2 + 6 \text{PbO}$	689	94	839
C559	$2 \text{Pb}_{12}\text{O}_{17} \longleftrightarrow \text{O}_2 + 8 \text{Pb}_3\text{O}_4$	570	57	-
C560	$2 \text{Pb}_{12}\text{O}_{17} \longleftrightarrow 5 \text{O}_2 + 24 \text{PbO}$	611	151	-
C561	$2 \text{Pb}_{12}\text{O}_{17} \longleftrightarrow 17 \text{O}_2 + 24 \text{Pb}$	1357	1099	-
C562	$\text{Pb}_{12}\text{O}_{19} \longleftrightarrow \text{O}_2 + \text{Pb}_{12}\text{O}_{17}$	337	28	-
C563	$2 \text{Pb}_{12}\text{O}_{19} \longleftrightarrow \text{O}_2 + 12 \text{Pb}_2\text{O}_3$	568	58	-
C564	$2 \text{Pb}_{12}\text{O}_{19} \longleftrightarrow 3 \text{O}_2 + 8 \text{Pb}_3\text{O}_4$	564	85	-
C565	$2 \text{Pb}_{12}\text{O}_{19} \longleftrightarrow 7 \text{O}_2 + 24 \text{PbO}$	602	177	-

Continued on next page

Table 6.5: Reactions with O₂ as reactive gas – continued

ID	reaction system	T_{equ} °C	storage capacity kJ/kg	storage density MJ/m^3
C566	$2 \text{Pb}_{12}\text{O}_{19} \longleftrightarrow 19 \text{O}_2 + 24 \text{Pb}$	1309	1115	-
C568	$2 \text{PbSeO}_3 \longleftrightarrow 3 \text{O}_2 + 2 \text{PbSe}$	1491	1311	9176
C569	$\text{PbSeO}_4 \longleftrightarrow 2 \text{O}_2 + \text{PbSe}$	1459	1455	9271
C570	$2 \text{PbSeO}_4 \longleftrightarrow \text{O}_2 + 2 \text{PbSeO}_3$	938	204	1303
C572	$2 \text{PdO} \longleftrightarrow \text{O}_2 + 2 \text{Pd}$	1089	932	7737
C574	$\text{PoO}_2 \longleftrightarrow \text{O}_2 + \text{Po}$	1342	1042	9271
C576	$2 \text{Pr}(\text{IO}_3)_3 \longleftrightarrow 9 \text{O}_2 + 2 \text{PrI}_3$	800	1172	-
C580	$\text{Pr}_6\text{O}_{11} \longleftrightarrow \text{O}_2 + 3 \text{Pr}_2\text{O}_3$	1005	205	-
C586	$2 \text{Pr}_2(\text{SO}_3)_3 \longleftrightarrow 9 \text{O}_2 + 2 \text{Pr}_2\text{S}_3$	1737	3808	-
C587	$2 \text{Pr}_2(\text{TeO}_3)_3 \longleftrightarrow 9 \text{O}_2 + 2 \text{Pr}_2\text{Te}_3$	1906	2546	-
C588	$2 \text{PtO} \longleftrightarrow \text{O}_2 + 2 \text{Pt}$	839	337	4751
C589	$\text{PtO}_2 \longleftrightarrow \text{O}_2 + \text{Pt}$	771	590	6957
C590	$2 \text{PtO}_2 \longleftrightarrow \text{O}_2 + 2 \text{PtO}$	695	276	3261
C591	$3 \text{PtO}_2 \longleftrightarrow \text{O}_2 + \text{Pt}_3\text{O}_4$	799	350	4131
C592	$\text{Pt}_3\text{O}_4 \longleftrightarrow 2 \text{O}_2 + 3 \text{Pt}$	445	251	-
C596	$2 \text{PuO}_2 \longleftrightarrow \text{O}_2 + 2 \text{PuO}_1 \cdot 5$	1339	825	9459
C607	$\text{Ra}(\text{IO}_3)_2 \longleftrightarrow 3 \text{O}_2 + \text{RaI}_2$	603	672	-
C610	$2 \text{RaO}_2 \longleftrightarrow \text{O}_2 + 2 \text{RaO}$	442	291	-
C612	$2 \text{RaSO}_3 \longleftrightarrow 3 \text{O}_2 + 2 \text{RaS}$	1638	2398	-
C613	$\text{RaSO}_4 \longleftrightarrow 2 \text{O}_2 + \text{RaS}$	1795	3182	-
C614	$2 \text{RaSO}_4 \longleftrightarrow \text{O}_2 + 2 \text{RaSO}_3$	1167	903	-
C615	$2 \text{RaSeO}_3 \longleftrightarrow 3 \text{O}_2 + 2 \text{RaSe}$	1538	1907	-
C616	$\text{RaSeO}_4 \longleftrightarrow 2 \text{O}_2 + \text{RaSe}$	1489	2209	-
C617	$2 \text{RaSeO}_4 \longleftrightarrow \text{O}_2 + 2 \text{RaSeO}_3$	698	385	-
C623	$2 \text{RbClO}_4 \longleftrightarrow \text{O}_2 + 2 \text{RbClO}_3$	416	228	638
C625	$2 \text{RbNO}_3 \longleftrightarrow \text{O}_2 + 2 \text{RbNO}_2$	1320	866	2693
C628	$4 \text{RbO}_2 \longleftrightarrow \text{O}_2 + 2 \text{Rb}_2\text{O}_3$	1327	298	1131
C629	$4 \text{RbO}_2 \longleftrightarrow 3 \text{O}_2 + 2 \text{Rb}_2\text{O}$	1719	937	3562
C631	$2 \text{RbO}_3 \longleftrightarrow 2 \text{O}_2 + \text{Rb}_2\text{O}_2$	358	439	-
C632	$2 \text{RbO}_3 \longleftrightarrow 3 \text{O}_2 + 2 \text{Rb}$	988	1975	-
C634	$4 \text{RbO}_3 \longleftrightarrow 5 \text{O}_2 + 2 \text{Rb}_2\text{O}$	480	709	-
C637	$2 \text{Rb}_2\text{O}_2 \longleftrightarrow \text{O}_2 + 2 \text{Rb}_2\text{O}$	1078	355	1348
C638	$\text{Rb}_2\text{O}_3 \longleftrightarrow \text{O}_2 + \text{Rb}_2\text{O}$	665	687	2423
C639	$2 \text{Rb}_2\text{O}_3 \longleftrightarrow \text{O}_2 + 2 \text{Rb}_2\text{O}_2$	494	358	1262
C640	$2 \text{Rb}_2\text{O}_3 \longleftrightarrow 3 \text{O}_2 + 4 \text{Rb}$	1437	2230	7873
C643	$2 \text{Rb}_2\text{SeO}_3 \longleftrightarrow 3 \text{O}_2 + 2 \text{Rb}_2\text{Se}$	1273	1864	-
C644	$\text{Rb}_2\text{SeO}_4 \longleftrightarrow 2 \text{O}_2 + \text{Rb}_2\text{Se}$	1276	2230	-
C645	$2 \text{Rb}_2\text{SeO}_4 \longleftrightarrow \text{O}_2 + 2 \text{Rb}_2\text{SeO}_3$	676	461	-
C647	$4 \text{ReO}_2 \longleftrightarrow \text{O}_2 + 2 \text{Re}_2\text{O}_3$	1668	874	9963

Continued on next page

Table 6.5: Reactions with O₂ as reactive gas – continued

ID	reaction system	T_{equ} °C	storage capacity kJ/kg	storage density MJ/m^3
C648	$2 \text{ReO}_3 \longleftrightarrow \text{O}_2 + 2 \text{ReO}_2$	1967	634	4372
C650	$4 \text{ReO}_3 \longleftrightarrow 3 \text{O}_2 + 2 \text{Re}_2\text{O}_3$	1510	1448	9991
C653	$2 \text{ReO}_4 \longleftrightarrow \text{O}_2 + 2 \text{ReO}_3$	1096	224	-
C654	$4 \text{ReO}_4 \longleftrightarrow \text{O}_2 + 2 \text{Re}_2\text{O}_7$	703	54	-
C655	$4 \text{ReO}_4 \longleftrightarrow 5 \text{O}_2 + 2 \text{Re}_2\text{O}_3$	1260	1579	-
C656	$2 \text{Re}_2\text{O}_3 \longleftrightarrow 3 \text{O}_2 + 4 \text{Re}$	1502	1189	-
C657	$\text{Re}_2\text{O}_7 \longleftrightarrow 2 \text{O}_2 + \text{Re}_2\text{O}_3$	1403	1575	9615
C658	$2 \text{Re}_2\text{O}_7 \longleftrightarrow \text{O}_2 + 4 \text{ReO}_3$	1200	175	1070
C661	$2 \text{RhO} \longleftrightarrow \text{O}_2 + 2 \text{Rh}$	1235	764	-
C662	$4 \text{RhO} \longleftrightarrow \text{O}_2 + 2 \text{Rh}_2\text{O}$	820	364	-
C664	$\text{Rh}_2\text{O}_3 \longleftrightarrow \text{O}_2 + \text{Rh}_2\text{O}$	1108	1027	8421
C665	$2 \text{Rh}_2\text{O}_3 \longleftrightarrow \text{O}_2 + 4 \text{RhO}$	1247	686	5623
C666	$2 \text{Rh}_2\text{O}_3 \longleftrightarrow 3 \text{O}_2 + 4 \text{Rh}$	1413	1401	11490
C667	$\text{RuO}_2 \longleftrightarrow \text{O}_2 + \text{Ru}$	1951	2292	16160
C669	$\text{RuO}_4 \longleftrightarrow 2 \text{O}_2 + \text{Ru}$	1022	1384	4552
C671	$4 \text{SbO}_2 \longleftrightarrow \text{O}_2 + \text{Sb}_4\text{O}_6$	972	670	-
C672	$4 \text{SbO}_2 \longleftrightarrow \text{O}_2 + 2 \text{Sb}_2\text{O}_3$	1445	647	-
C675	$2 \text{Sb}_2\text{O}_4 \longleftrightarrow \text{O}_2 + \text{Sb}_4\text{O}_6$	972	670	4447
C676	$2 \text{Sb}_2\text{O}_4 \longleftrightarrow \text{O}_2 + 2 \text{Sb}_2\text{O}_3$	1409	647	4296
C677	$\text{Sb}_2\text{O}_5 \longleftrightarrow \text{O}_2 + \text{Sb}_2\text{O}_3$	1184	881	3332
C678	$2 \text{Sb}_2\text{O}_5 \longleftrightarrow \text{O}_2 + 2 \text{Sb}_2\text{O}_4$	793	266	1007
C679	$2 \text{Sb}_2\text{O}_5 \longleftrightarrow \text{O}_2 + 4 \text{SbO}_2$	790	266	1007
C680	$2 \text{Sb}_2\text{O}_5 \longleftrightarrow 2 \text{O}_2 + \text{Sb}_4\text{O}_6$	916	903	3413
C681	$2 \text{Sb}_2\text{O}_5 \longleftrightarrow 5 \text{O}_2 + 4 \text{Sb}$	1929	3072	11611
C682	$\text{Sb}_4\text{O}_6 \longleftrightarrow 3 \text{O}_2 + 4 \text{Sb}$	1837	2407	-
C683	$\text{Sb}_2(\text{SO}_4)_3 \longleftrightarrow 6 \text{O}_2 + \text{Sb}_2\text{S}_3$	1613	4133	14983
C685	$\text{SeO}_2 \longleftrightarrow \text{O}_2 + \text{Se}$	1138	2032	8028
C687	$2 \text{SeO}_3 \longleftrightarrow 3 \text{O}_2 + 2 \text{Se}$	708	1341	4614
C690	$2 \text{Se}_2\text{O}_5 \longleftrightarrow 5 \text{O}_2 + 4 \text{Se}$	929	1737	-
C692	$2 \text{Sm}(\text{IO}_3)_3 \longleftrightarrow 9 \text{O}_2 + 2 \text{SmI}_3$	724	1176	-
C701	$\text{Sn}(\text{SO}_4)_2 \longleftrightarrow 4 \text{O}_2 + \text{SnS}_2$	1668	4848	-
C704	$\text{Sr}_6\text{Bi}_2\text{O}_{11} \longleftrightarrow \text{O}_2 + \text{Sr}_6\text{Bi}_2\text{O}_9$	517	164	-
C705	$2 \text{Sr}_6\text{Bi}_2\text{O}_{11} \longleftrightarrow 5 \text{O}_2 + 2 \text{Sr}_6\text{Bi}_2\text{O}_6$	1827	1740	-
C709	$2 \text{SrCrO}_4 \longleftrightarrow \text{O}_2 + 2 \text{SrCrO}_3$	1799	670	-
C711	$\text{Sr}(\text{IO}_3)_2 \longleftrightarrow 3 \text{O}_2 + \text{SrI}_2$	876	1046	5279
C715	$2 \text{SrO}_2 \longleftrightarrow \text{O}_2 + 2 \text{SrO}$	661	347	1657
C718	$\text{SrSeO}_4 \longleftrightarrow 2 \text{O}_2 + \text{SrSe}$	1486	3341	14200
C719	$2 \text{SrTeO}_3 \longleftrightarrow 3 \text{O}_2 + 2 \text{SrTe}$	1827	2864	-
C723	$2 \text{Tb}(\text{IO}_3)_3 \longleftrightarrow 9 \text{O}_2 + 2 \text{TbI}_3$	845	1181	-

Continued on next page

Table 6.5: Reactions with O₂ as reactive gas – continued

ID	reaction system	T_{equ} °C	storage capacity kJ/kg	storage density MJ/m^3
C725	$4 \text{ TbO}_2 \longleftrightarrow \text{O}_2 + 2 \text{ Tb}_2\text{O}_3$	797	204	-
C727	$\text{ Tb}_6\text{O}_{11} \longleftrightarrow \text{O}_2 + 3 \text{ Tb}_2\text{O}_3$	600	109	-
C730	$4 \text{ Tb}_7\text{O}_{12} \longleftrightarrow 3 \text{ O}_2 + 14 \text{ Tb}_2\text{O}_3$	1500	164	-
C732	$4 \text{ Tb}_{11}\text{O}_{20} \longleftrightarrow 7 \text{ O}_2 + 22 \text{ Tb}_2\text{O}_3$	995	173	-
C734	$2 \text{ TcO}_3 \longleftrightarrow \text{O}_2 + 2 \text{ TcO}_2$	1310	561	-
C736	$2 \text{ Tc}_2\text{O}_7 \longleftrightarrow \text{O}_2 + 4 \text{ TcO}_3$	462	153	-
C737	$2 \text{ Tc}_2\text{O}_7 \longleftrightarrow 3 \text{ O}_2 + 4 \text{ TcO}_2$	1349	685	-
C739	$2 \text{ TeO} \longleftrightarrow \text{O}_2 + 2 \text{ Te}$	1923	1632	9271
C740	$\text{ TeO}_2 \longleftrightarrow \text{O}_2 + \text{ Te}$	1712	2011	11867
C741	$2 \text{ TeO}_2 \longleftrightarrow \text{O}_2 + 2 \text{ TeO}$	1045	543	3205
C749	$6 \text{ TiO} \longleftrightarrow \text{O}_2 + 2 \text{ Ti}_3\text{O}_2$	1772	2830	14010
C784	$6 \text{ Ti}_7\text{O}_{13} \longleftrightarrow 25 \text{ O}_2 + 14 \text{ Ti}_3\text{O}_2$	857	1625	-
C789	$6 \text{ Ti}_8\text{O}_{15} \longleftrightarrow \text{O}_2 + 8 \text{ Ti}_6\text{O}_{11}$	639	194	-
C796	$4 \text{ Ti}_9\text{O}_{17} \longleftrightarrow \text{O}_2 + 6 \text{ Ti}_6\text{O}_{11}$	678	258	-
C798	$5 \text{ Ti}_9\text{O}_{17} \longleftrightarrow 2 \text{ O}_2 + 9 \text{ Ti}_5\text{O}_9$	765	415	-
C800	$2 \text{ Ti}_{10}\text{O}_{19} \longleftrightarrow \text{O}_2 + 4 \text{ Ti}_5\text{O}_9$	791	465	-
C803	$3 \text{ Ti}_{10}\text{O}_{19} \longleftrightarrow \text{O}_2 + 5 \text{ Ti}_6\text{O}_{11}$	708	309	-
C808	$2 \text{ Ti}_{20}\text{O}_{39} \longleftrightarrow \text{O}_2 + 4 \text{ Ti}_{10}\text{O}_{19}$	660	228	-
C809	$2 \text{ Ti}_{20}\text{O}_{39} \longleftrightarrow 3 \text{ O}_2 + 8 \text{ Ti}_5\text{O}_9$	894	689	-
C813	$4 \text{ Ti}_{20}\text{O}_{39} \longleftrightarrow 3 \text{ O}_2 + 10 \text{ Ti}_8\text{O}_{15}$	726	343	-
C814	$6 \text{ Ti}_{20}\text{O}_{39} \longleftrightarrow 7 \text{ O}_2 + 20 \text{ Ti}_6\text{O}_{11}$	824	534	-
C818	$2 \text{ ThO}_3 \longleftrightarrow 3 \text{ O}_2 + 2 \text{ Th}$	526	377	-
C819	$2 \text{ ThNO}_3 \longleftrightarrow \text{O}_2 + 2 \text{ ThNO}_2$	588	382	2121
C821	$\text{ Tl}_2\text{O}_3 \longleftrightarrow \text{O}_2 + \text{ Tl}_2\text{O}$	1048	477	4868
C822	$2 \text{ Tl}_2\text{O}_3 \longleftrightarrow 3 \text{ O}_2 + 4 \text{ Tl}$	1511	847	8643
C823	$\text{ Tl}_2\text{SO}_4 \longleftrightarrow 2 \text{ O}_2 + \text{ Tl}_2\text{S}$	1831	1658	11223
C824	$\text{ Tl}_2\text{SeO}_4 \longleftrightarrow 2 \text{ O}_2 + \text{ Tl}_2\text{Se}$	1060	988	6796
C825	$2 \text{ Tm}(\text{IO}_3)_3 \longleftrightarrow 9 \text{ O}_2 + 2 \text{ TmI}_3$	746	1150	-
C827	$2 \text{ UAsO}_5 \longleftrightarrow 5 \text{ O}_2 + 2 \text{ UAs}$	1969	3676	-
C834	$3 \text{ UO}_3 \longleftrightarrow \text{O}_2 + \text{ U}_3\text{O}_7$	694	285	2075
C835	$6 \text{ UO}_3 \longleftrightarrow \text{O}_2 + 2 \text{ U}_3\text{O}_8$	944	113	821
C841	$2 \text{ U}_3\text{O}_8 \longleftrightarrow \text{O}_2 + 2 \text{ U}_3\text{O}_7$	648	175	1470
C846	$\text{ UO}_2(\text{AsO}_3)_2 \longleftrightarrow 4 \text{ O}_2 + \text{ UAs}_2$	1832	3692	-
C847	$2 (\text{UO}_2)_2\text{As}_2\text{O}_7 \longleftrightarrow \text{O}_2 + 4 \text{ UAsO}_5$	819	86	-
C848	$2 (\text{UO}_2)_2\text{As}_2\text{O}_7 \longleftrightarrow 11 \text{ O}_2 + 4 \text{ UAs}$	1886	3688	-
C849	$2 \text{ UOBr}_3 \longleftrightarrow \text{O}_2 + 2 \text{ UBr}_3$	1918	517	-
C850	$2 \text{ UO}_2\text{Br}_2 \longleftrightarrow \text{O}_2 + 2 \text{ UOBr}_2$	1167	381	-
C853	$2 \text{ UO}_2\text{Cl} \longleftrightarrow \text{O}_2 + 2 \text{ UOCl}$	1636	1104	-
C854	$2 \text{ UO}_2\text{Cl}_2 \longleftrightarrow \text{O}_2 + 2 \text{ UOCl}_2$	1066	511	-

Continued on next page

Table 6.5: Reactions with O₂ as reactive gas – continued

ID	reaction system	T _{equi} °C	storage capacity kJ/kg	storage density MJ/m ³
C857	2 UO ₂ F ₂ \longleftrightarrow O ₂ + 2 UOF ₂	1182	484	-
C858	2 U ₂ O ₃ F ₆ \longleftrightarrow 3 O ₂ + 4 UF ₃	1377	903	-
C859	4 UO ₃ · H ₂ O \longleftrightarrow 7 O ₂ + 2 UO ₂ (OH) ₂	1533	2535	17871
C860	UO ₂ (NO ₃) ₂ \longleftrightarrow 4 O ₂ + UN ₂	1009	2335	-
C862	2 (UO ₂) ₂ P ₂ O ₇ \longleftrightarrow O ₂ + 4 UPO ₅	794	146	-
C864	(UO ₂) ₂ (PO ₄) ₂ \longleftrightarrow O ₂ + 2 UPO ₅	1120	615	-
C866	2 (UO ₂) ₂ (PO ₄) ₂ \longleftrightarrow O ₂ + 2 (UO ₂) ₂ P ₂ O ₇	1137	472	-
C868	UO ₂ SO ₃ \longleftrightarrow 2 O ₂ + UOS	1519	2281	-
C869	2 UO ₂ SO ₃ \longleftrightarrow 5 O ₂ + 2 US ₁ · 5	1992	3490	-
C871	2 UO ₂ SO ₄ \longleftrightarrow O ₂ + 2 UO ₂ SO ₃	867	503	-
C872	2 UO ₂ SO ₄ \longleftrightarrow 5 O ₂ + 2 UOS	1529	2685	-
C875	U(SO ₃) ₂ \longleftrightarrow 3 O ₂ + US ₂	1845	3422	-
C876	U(SO ₄) ₂ \longleftrightarrow O ₂ + U(SO ₃) ₂	1248	992	-
C890	4 V ₂ O ₄ \longleftrightarrow O ₂ + 2 V ₄ O ₇	1212	646	2804
C891	5 V ₂ O ₄ \longleftrightarrow O ₂ + 2 V ₅ O ₉	731	458	1986
C892	6 V ₂ O ₄ \longleftrightarrow O ₂ + 2 V ₆ O ₁₁	655	377	1635
C894	2 V ₂ O ₅ \longleftrightarrow O ₂ + 2 V ₂ O ₄	1831	681	2285
C895	2 V ₂ O ₅ \longleftrightarrow O ₂ + 4 VO ₂	1827	681	2286
C898	3 V ₂ O ₅ \longleftrightarrow O ₂ + V ₆ O ₁₃	577	361	1212
C899	3 V ₂ O ₅ \longleftrightarrow 2 O ₂ + V ₆ O ₁₁	891	1024	3439
C900	4 V ₂ O ₅ \longleftrightarrow 3 O ₂ + 2 V ₄ O ₇	1223	1270	4264
C901	6 V ₂ O ₅ \longleftrightarrow 5 O ₂ + 4 V ₃ O ₅	1887	1442	4842
C908	6 V ₄ O ₇ \longleftrightarrow O ₂ + 8 V ₃ O ₅	1084	198	-
C909	V ₅ O ₉ \longleftrightarrow 2 O ₂ + 5 VO	1808	3058	-
C911	3 V ₅ O ₉ \longleftrightarrow O ₂ + 5 V ₃ O ₅	777	393	-
C912	4 V ₅ O ₉ \longleftrightarrow 3 O ₂ + 10 V ₂ O ₃	1049	831	-
C913	V ₆ O ₁₁ \longleftrightarrow O ₂ + 3 V ₂ O ₃	1092	909	-
C914	2 V ₆ O ₁₁ \longleftrightarrow O ₂ + 4 V ₃ O ₅	836	473	-
C915	2 V ₆ O ₁₁ \longleftrightarrow 5 O ₂ + 12 VO	1824	3121	-
C917	4 V ₆ O ₁₁ \longleftrightarrow O ₂ + 6 V ₄ O ₇	760	278	-
C918	V ₆ O ₁₃ \longleftrightarrow O ₂ + V ₆ O ₁₁	857	705	-
C919	V ₆ O ₁₃ \longleftrightarrow 2 O ₂ + 3 V ₂ O ₃	1230	1557	-
C920	2 V ₆ O ₁₃ \longleftrightarrow O ₂ + 6 V ₂ O ₄	718	340	-
C921	2 V ₆ O ₁₃ \longleftrightarrow O ₂ + 12 VO ₂	718	340	-
C922	2 V ₆ O ₁₃ \longleftrightarrow 3 O ₂ + 4 V ₃ O ₅	1058	1149	-
C923	2 V ₆ O ₁₃ \longleftrightarrow 7 O ₂ + 12 VO	1793	3631	-
C925	4 V ₆ O ₁₃ \longleftrightarrow 5 O ₂ + 6 V ₄ O ₇	1037	966	-
C926	V ₇ O ₁₃ \longleftrightarrow 3 O ₂ + 7 VO	1791	3163	-
C928	3 V ₇ O ₁₃ \longleftrightarrow 2 O ₂ + 7 V ₃ O ₅	831	528	-

Continued on next page

Table 6.5: Reactions with O₂ as reactive gas – continued

ID	reaction system	T_{equ} °C	storage capacity kJ/kg	storage density MJ/m^3
C929	$4 V_7O_{13} \longleftrightarrow 5 O_2 + 14 V_2O_3$	1074	961	-
C930	$5 V_7O_{13} \longleftrightarrow O_2 + 7 V_5O_9$	457	140	-
C931	$2 V_8O_{15} \longleftrightarrow O_2 + 4 V_4O_7$	784	374	-
C932	$2 V_8O_{15} \longleftrightarrow 3 O_2 + 8 V_2O_3$	1085	1000	-
C933	$2 V_8O_{15} \longleftrightarrow 7 O_2 + 16 VO$	1789	3194	-
C935	$6 V_8O_{15} \longleftrightarrow O_2 + 8 V_6O_{11}$	397	98	-
C936	$6 V_8O_{15} \longleftrightarrow 5 O_2 + 16 V_3O_5$	849	568	-
C937	$VOCO_3 \longleftrightarrow 2 O_2 + VC$	1740	8264	-
C939	$2 VOCl_3 \longleftrightarrow O_2 + 2 VCl_3$	1453	889	1626
C940	$2 VO_2Cl \longleftrightarrow O_2 + 2 VOCl$	1400	1436	-
C941	$2 VOSO_4 \longleftrightarrow 5 O_2 + 2 VS$	1797	6851	-
C949	$2 W_3O \longleftrightarrow O_2 + 6 W$	1601	557	-
C950	$2 WObR_2 \longleftrightarrow O_2 + 2 WBr_2$	1969	1328	-
C951	$2 WObR_4 \longleftrightarrow O_2 + 2 WBr_4$	1344	552	3033
C952	$WO_2Br_2 \longleftrightarrow O_2 + WBr_2$	1799	1694	-
C953	$2 WO_2Br_2 \longleftrightarrow O_2 + 2 WObR_2$	795	422	-
C955	$2 WOCl_3 \longleftrightarrow O_2 + 2 WCl_3$	1774	1271	-
C959	$2 WOF_4 \longleftrightarrow O_2 + 2 WF_4$	1155	616	3123
C960	$2 Y_2Cu_2O_5 \longleftrightarrow O_2 + 4 YCuO_2$	786	546	-
C961	$2 Y(IO_3)_3 \longleftrightarrow 9 O_2 + 2 YI_3$	844	1332	-
C969	$2 ZnSeO_3 \longleftrightarrow 3 O_2 + 2 ZnSe$	1853	2506	-
C970	$ZnSeO_4 \longleftrightarrow 2 O_2 + ZnSe$	1105	2476	-
C971	$2 ZnSeO_4 \longleftrightarrow O_2 + 2 ZnSeO_3$	300	163	-
C985	$2 KO_3 \longleftrightarrow 3 O_2 + 2 K$	1125	2978	-
C987	$K_2O_4 \longleftrightarrow 2 O_2 + 2 K$	1070	3945	-
C990	$2 NaO_3 \longleftrightarrow 3 O_2 + 2 Na$	721	2720	-

Markus DEUTSCH
Hohe-Wand-Straße 29/9
Austria - 2344 Maria Enzersdorf
☎ +43/680/2082776
✉ markus.deutsch@gmx.at

CURRICULUM VITAE

Personal Information

Name	Markus Deutsch
Date of Birth	13. May 1987
Citizenship	Austria
Native Language	German

Education

Since August 2013	PhD in the field of chemical and process engineering at TU Wien under supervision von Ao.Univ.Prof. Dipl.-Ing. Dr.techn. Franz Winter
Mai 2012	Awarded with the M.Sc. degree for chemical and process engineering from TU Wien with honors
Mai 2012	Master Thesis <i>Model Based Control and Energy Efficiency Optimisation of a Pasteurization Pilot Plant</i> in cooperation with VOIGT+WIPP Engineers under supervision of Univ.Prof. Dipl.-Ing. Dr.techn. Stefan Jakubek
November 2011	Awarded with the B.Sc. degree for chemical and process engineering from TU Wien
September 2011	Bachelor Thesis <i>Modelling of a stratified heat storage tank in Dymola</i> under supervision of Ao.Univ.Prof. Dipl.-Ing. Dr.techn. Andreas Werner

October 2007 – Mai 2012

Student in the field of Chemical and Process Engineering at TU Wien

2001/02 – 2005/06

College of Chemistry specialized in Analytical Chemistry & Environmental Technology
Rosensteingasse 79, 1170 Vienna

Work Experience

Research

Since August 2013

TU Wien, Institute of Chemical, Environmental and Biological Engineering
Getreidemarkt 9/166, 1060 Wien

Solid Heat – Thermochemical energy storage
as project assistant under supervision of Ao.Univ.Prof. Dipl.-Ing. Dr.techn. Franz Winter

May 2012 – June 2013

TU Wien, Institute of Mechanics and Mechatronics, Division of Control and Process Automatisation
Getreidemarkt 9/325, 1060 Wien

Data driven identification of partial differential equations
as project assistant under supervision of Univ.Prof. Dipl.-Ing. Dr.techn. Stefan Jakubek

Industry

Summer 2009

Industrial Alpinists Vienna - Gesellschaft für gerüstfreie Höhenarbeiten GmbH & Co KG
Obachgasse 14 - 1220 Wien
Inspection of structural integrity of the blades of wind turbines

January 2006 – August 2006

ESW Consulting Wruss ZT GmbH
Rosasgasse 25-27; 1120 Wien
Determination of the content of alkenes in soil and water samples

Summer 2004

NUA – Umweltanalytik GmbH
Südstadtzentrum 4, 2344 Ma. Enzersdorf
Control of the water quality in raw and process water

Summer 2003

ISOMAX – Dekorative Laminate AG
Industriezentrum N.Ö.-Süd, 2355 Wr. Neudorf
Inspection and care of an assembly line

Additional Training

July 2006 – January 2007

Military Service

July 2005

Drivers Licence

Journal publications

Markus Deutsch, Danny Müller, Christian Aumeyr, Christian Jordan, Christian Gierl-Mayer, Peter Weinberger, Franz Winter, Andreas Werner

Systematic search algorithm for potential thermochemical energy storage systems

Applied Energy, 183:113-120, 2016 DOI: 10.1016/j.apenergy.2016.08.142

Markus Deutsch, Florian Horvath, Christian Knoll, Daniel Lager, Christian Gierl-Mayer, Peter Weinberger, Franz Winter

High-Temperature Energy Storage: Kinetic Investigations of the CuO/Cu₂O Reaction Cycle

Energy and Fuels, 1 (3), 2324-2334, 2017 DOI: 10.1021/acs.energyfuels.6b02343

Skills and Qualifications

- Awarded the performance gant of the TU Wien at the Faculty of Faculty of Mechanical and Industrial Engineering in the years 2011 and 2012
- excellent command of English language
- excellent knowledge of MatLab/Simulink
- good knowledge of the programming languages Java, C++ and Modelica
- knowledge of the simulation programs Dymola, Aspen Plus as well as the CAD-Tool CATIA V5
- trained skills with Office and LaTeX

Personal Interests

- Sports – hiking, climbing, trail running, mountain biking
- Photography
- Board games
- Music